AGRITECH DAY BY AXEMA

9TH EDITION

2026



INTERNATIONAL CONFERENCE OF TECHNOLOGIES
AND SOLUTIONS FOR EFFICIENT
AND SUSTAINABLE AGRICULTURE

AXEMA

AGRITECH DAY - 9TH EDITION

The International Conference of Technologies and Solutions for Efficient and Sustainable Agriculture

© Published by Axema Promotion & Services, 2026
All rights reserved for all countries.
ISBN: 978-2-491070-08

REPRODUCTION IS STRICTLY PROHIBITED.
Any use of the content of this document, whether retranscribed or reworked to appear in any other print or digital media, must include the following mention: "*Source: AGRITECH DAY 9th Edition – AXEMA*"

APS
Axema Promotion & Services

19 RUE JACQUES BINGEN - 75017 PARIS

Under Article 40 of the Law of March 11, 1957 "Any full or partial representation or reproduction made without the consent of the author or his successors in title is illegal". Article 41 of the same law only authorizes "copies or reproductions strictly reserved for the private use of the copyist and not intended for collective use" and "analyses and short quotations", "provided that the name of the author and the source are clearly indicated".

TABLE OF CONTENTS

TABLE OF CONTENTS 3

FOREWORD 5

SCIENTIFIC COMMITTEE 6

AGENDA 7

SPEAKERS BIOGRAPHIES 8

PAPERS 20

AGRICULTURAL ROBOTICS: RESEARCH FINDINGS AND OPERATIONAL FEEDBACK 20

Rethink its crop system to integrate a robot: a look back at four years of experimentation in sugar beet 20

From agroecological intent to performed work: an open mission-exchange format as a chain of responsibility for light agricultural robots 29

Business Model Patterns in Agricultural Robotics: Evidence from European Firms 41

CROP PROTECTION 59

Development and evaluation of an air confined spraying device to reduce spray drift in viticulture 59

Development of a test protocol to evaluate Droplet Size Distributions (DSD) from nozzles equipped with a spinning disc mounted on unmanned aerial spraying systems 69

A Methodology for Evaluating the Detection Performance of a Spot Spraying System in Field Crops 76

AGRICULTURAL ROBOTICS: TECHNOLOGY AND DEPLOYMENT 87

MTAD: an Unsupervised Method to Identify Obstacles in Complex Agricultural Environments 87

Design and implementation of robotized agroecological cropping systems: challenges and limitations encountered in the Ninsar project 99

MECHANICAL WEED CONTROL SOLUTIONS 111

Research and Testing Bench for Alternative Weed Control Solutions 111

What are the mechanical alternatives to glyphosate for arable crops? 124

ENERGY EFFICIENCY AND DECARBONIZATION OF AGRICULTURAL MACHINERY 135

Evaluation of energy consumption of field operations in a dairy farm 135

Towards an Optimal Model of Energy and Agronomic Performance for Barley Sowing Operations 145

From Diesel to BioCNG and Hydrogen: Transforming Agricultural Mobile Machinery with Internal Combustion Engine 155

PRECISION AGRICULTURE 166

Centrifugal spreading ability of granular products 166

Morphogeometric characterization of fertilizer particles under field conditions: Comparison of an approach based on controlled sampling and expert algorithm with a machine learning approach under bulk conditions 178

RTK autosteering in agriculture: uses, perceptions and implications for the agroecological transition 191

VIRTUAL ENVIRONMENTS AND DIGITAL TWINS 202

High-Fidelity 3D Reconstruction of Potato Tubers from Sparse Unposed RGB Images 202

Scenario Generation and Autonomous Control for High-Precision Vineyard Operations in Virtual Environments 214

SAFETY AND PROTECTION OF AGRICULTURAL MACHINERY 225

Cyber Resilience for Connected Agricultural Machinery: From Digital Transformation to EU CRA Compliance 225

Rollover Prevention Safety Device for Mobile Equipment 236

THANKS 248

OUR SPONSOR – BKT 249

OUR SPONSOR – AMS SOLTECH 250

OUR SPONSOR – SONIC EQUIPMENT 251

OUR SPONSOR – MMT MOVING MAGNET 252

FOREWORD

AXEMA, the French reference association at the service of agricultural equipment.

Building the future

Axema is the French Association for agricultural equipment manufacturers and agricultural environment providers. Its 270 members include both French and foreign manufacturers of agricultural equipment for the various sectors of crop and livestock agricultural production and producers of equipment for the upkeep of green spaces.

A diverse sector

The agricultural equipment sector includes businesses that produce market equipment, fixed and rolling, intended for various users: arable crop farmers, livestock farmers, wine growers, horticultural producers, vegetable farmers, parks and gardens maintenance service providers and home gardeners. Moreover, this sector is increasingly focusing on solutions taking into account the environmental aspects of agriculture, livestock-rearing, parks and gardens, and more generally our territories, thus making it a true Agricultural Environment sector. Agricultural equipment covers a wide range of machines, uses and technical know-how. This diversity is also reflected in the economic organization of the French agricultural equipment industry. The sector is composed of SMEs, French international industrial groups, and importing subsidiaries of foreign groups.

Governance & Operational team

AXEMA is administered by a Board of Directors composed of 18 representatives of active members. The Board of Directors elects a Bureau composed of a Chairman, four Deputy Chairmen and a treasurer who are also appointed for a term of three years. The association's daily activities are carried out by a 15-person team organized by unit and respond to members' requests:

- Technical and Regulation
- Economic and International
- Public Affairs and Communication
- Training and Employment
- Administrative and Accounting

Collective activities of AXEMA are generally conducted through Product Market Group (PMG) meetings, which include active or associate members involved in the same product family or market, and Commissions working on cross-cutting topics.

AXEMA's objective is to show that the sector is innovative, attractive to young talents and offers growth prospects in the context of efficient and sustainable agriculture.

AXEMA is building the future for agricultural equipment & agricultural environment to ensure sustainable agriculture & responsible territorial development.

SCIENTIFIC COMMITTEE

The 9th edition of the AGRITECH DAY gathered all the agroequipment research & innovation actors on October 14, 2026, at Beauvais, France.

Agricultural equipment supports the transformation of agriculture and takes part in developing new agricultural models more respectful of ecosystems. AXEMA created AGRITECH DAY to promote direct exchanges with agricultural equipment research & innovation actors and inform on ongoing developments. The strong mobilization for this ninth edition is a testimony to the sector's vitality and expectations. Agriculture issues challenge many scientific and technological experts. This event spotlighted twenty-one presentations under the form of plenary sessions, selected by a scientific and technical committee to whom we extend our warmest gratitude. It is thanks to the quality and expertise of the industrial, academic and research speakers that AGRITECH DAY has become a key event in France for innovation and research in agricultural equipment.

Composition of the scientific committee

CHAIRMAN – Stéphane LAMPÉRIÈRE - AGCO
Massey Ferguson brand styling Director & Deputy Director, Engineering

Pascal BOUQUET
IN SITU VENSYS GROUP - Technical and R&D Director

Damien CALAIS
INSTITUT AGRO DIJON – Agricultural equipment and precision farming teacher

Dieumet DENIS
SHERPA ENGINEERING – Advanced Autonomous Systems Manager

Jean-Paul DOUZALS
INRAE – Manager of the RéducPol platform (Montpellier)

Julien DURAND-RÉVILLE
PHYTEIS – Health Manager / Digital Agronomy Manager

Yannick GUYOMACH
KEREVAL – Project Manager / ISOBUS consultant

Arnaud JAOUEN
PICHON SAMSON AGRO – Technical Director

Quentin LABOUREY
KUHN – Electronics Group Manager – autonomy and applications

Fabien LEFEBVRE
CETIM – Scientific Advisor

Roland LENAIN
INRAE – Director of the TSCF-INRAE unit Clermont-Auvergne-Rhône-Alpes Centre

Lionel LÉVEILLÉ
BUREL GROUP – Research and Innovation Director

Marine LOUARGANT
CTIFL – Mechanization Automation and Imaging Sensors Unit Manager (MATIC)

Eric LUCET
CEA LIST - Research Engineer in robotics

François PINET
MICHELIN - Manager Test Beyond Road & Trucks

Emmanuel PIRON
INRAE - Head of the Montoldre Technological Research Platform

Philippe POTIER
ROBAGRI - Secretary General

Marilys PRADEL
INRAE - Research engineer in environmental assessment

Xabier REBOUD
INRAE - Director of the Plant Health and Environment Division

Jean-Christophe ROUSSEAU
FRANCE PULVÉ - Product Manager

Cédric SEGUINEAU
GRAND DEFI DE LA ROBOTIQUE AGRICOLE – Director

Carolina UGARTE
UNILASALLE BEAUVAIS - Lecturer and researcher, holder of the Agromachinery and New Technologies Chair Agromachinery and New Technologies Chair – AGHYLE research unit

Florence VERPONT
CTIFL – Research engineer in application techniques

AGENDA

08.30 **CONFERENCE OPENING**

	AGRICULTURAL ROBOTICS: RESEARCH FINDINGS AND OPERATIONAL FEEDBACK	CROP PROTECTION
09.00	**Rethinking Crop Management Practices for Robot Integration: Lessons Learned from Four Years of Sugar Beet Experiments** *Thomas LEBORGNE* – ITB	**How BLISS Ecospray's Air-Confinement Technology Virtually Eliminates Spray Drift?** *Mathilde GUICHARD* – BLISS ECOSPRAY
09.30	**Scalable Agricultural Robotics: Assessing the Operational Maturity of Lightweight Field Robots on Farms as a Foundation for Responsible Innovation Supporting Agroecology** *Alexandre PREVAULT OSMANI* – SABI AGRI	**Development of a Methodology for the Evaluation of Rotary Disc Nozzles Used on Spraying Drones** *Jean-Paul DOUZALS* – INRAE
10.00	**Commercial Strategies of Agricultural Robot Manufacturers in Europe: What Business Models?** *Mohammad NAIM* – UNILASALLE	**A Methodology for Evaluating the Detection Performance of a Spot Spraying System in Field Crops** *Paul MELKI* – EXXACT ROBOTICS

10.30 **BREAK**

	AGRICULTURAL ROBOTICS: TECHNOLOGY AND DEPLOYMENT	MECHANICAL WEED CONTROL SOLUTIONS
11.00	**MTAD: A Novel Obstacle Detection Method for Complex Agricultural Environments** *Théo BIARDEAU* – CYCLAIR	**Experimental Test Bench for Alternative Weed Control Technologies** *Daniel BOFFETY* – INRAE
11.30	**Designing and Managing Robotized Agroecological Cropping Systems: Challenges and Limitations from the Ninsar Project** *Manon BOULET* – INRAE	**What Mechanical Alternatives to Glyphosate Are Available for Arable Cropping Systems?** *Damien BRUN* – ARVALIS

12.00 **LUNCH BREAK**

	ENERGY EFFICIENCY AND DECARBONIZATION OF AGRICULTURAL MACHINERY	PRECISION AGRICULTURE
01.30	**Evaluation of energy consumption of field operations in a dairy farm** *Antti LAJUNEN* – HELSINKI UNIVERSITY	**Evaluating the Spreadability of Granular Products Using Centrifugal Spreaders** *Sylvain VILLETTE* – AGRO DIJON / INRAE
02.00	**Towards an Optimal Model of Energy and Agronomic Performance for Barley Sowing Operations** *Diego URBINA SALAZAR* – UNILASALLE	**Morpho-Geometric Characterization of Fertilizer Particles Under Field Conditions: A Comparison of Controlled Sampling and Expert Vision Methods with Bulk Machine Learning Approaches** *Emeric LECLAIR* – BUREL GROUP
02.30	**From Diesel to BioCNG and Hydrogen: Transforming Agricultural Mobile Machinery with Internal Combustion Engine** *Olivier MARCHAND* – CRMT	**RTK Guidance Systems for Agricultural Vehicles: Applications, User Perceptions, and Implications for the Agroecological Transition** *Damien CALAIS, Eve FAIVRE & Lydiane MARREC – AGRO DIJON / ARVALIS*

03.00 **BREAK**

	VIRTUAL ENVIRONMENTS AND DIGITAL TWINS	SAFETY AND PROTECTION OF AGRICULTURAL MACHINERY
03.30	**Towards Learning Agricultural Product Representations from a Simulated Environment** *Adrien SCHOCKAERT* – DOWNS DUBRULLE	**Securing the Digital Farm: Why Agricultural Machinery Must Be Cyber-Resilient by Design** *Thierry KOLTON* – VICONE
04.00	**Scenario Generation and Autonomous Control for High-Precision Vineyard Operations in Virtual Environments** *Farouk EL FARJI* – IPG AUTOMOTIVE	**Safety device to prevent mobile machinery from overturning** *Bastien LAURENT* – INRAE
04.30	**WORK ORGANISATION AND INNOVATIVE TECHNOLOGIES SUPPORTING NEW AGRICULTURAL MODELS: THE HECTAR FARM EXPERIENCE** *Astrid SPRIET - Director of the HECTAR Pilot Farm*	
05.15	**CONFERENCE CONCLUSION** *Stéphane LAMPERIERE* – MASSEY FERGUSON BRAND STYLING DIRECTOR & DEPUTY DIRECTOR, ENGINEERING AXEMA Technical Committee Chairman	

SPEAKERS BIOGRAPHIES

PLENARY SESSIONS

Astrid SPRIET
Director of the HECTAR Pilot Farm



HEC graduate and granddaughter of a livestock farmer, Astrid Spriet also holds a vocational high school diploma (CGEA) specialising in mixed crop and livestock farming.

After starting her career in project management at one of France's leading real estate companies, she joined Hectar in 2022. She now manages its pilot farm, a 300-hectare organic mixed crop and livestock operation.

The farm includes a herd of 110 dairy and beef cattle, with all milk processed on-site, 200 hectares of organic conservation agriculture, a 75-hive apiary and floriculture activities. A team of 10 people is responsible for its day-to-day operations.

Beyond farming, Hectar is above all a centre dedicated to raising awareness and providing training, with the aim of enhancing the attractiveness of the agricultural sector.

Stéphane LAMPERIERE
Massey Ferguson Brand Styling Director & Deputy Director, Engineering / AGCO
AXEMA Technical Commission Chairman



Stéphane LAMPERIERE holds an engineering degree in mechanical and production engineering from ENIM. After 4 years' experience in earthmover development, he joined the AGCO group as a transmission engineer, where he developed the first range of Massey Ferguson continuously variable tractors. He then defined the vehicle architectures and managed the projects for the various tractor ranges.
From 2013, he held the position of Platform Director and launched AGCO's first common platform with the MF8S and Valtra Q ranges.
Since 2021, with 30 years' experience behind him, he has held the position of Deputy Engineering Director, in charge of the R&D department's support teams.
As part of the "ECOSYSTEM" pillar of Massey Ferguson's growth plan, he manages local technology partnerships and tractor decarbonization activities.

AGRICULTURAL ROBOTICS: RESEARCH FINDINGS AND OPERATIONAL FEEDBACK

Thomas LEBORGNE
Agricultural Engineer – ITB



Thomas LEBORGNE is an agricultural engineer and a graduate of AgroSup Dijon, specializing in agricultural machinery and innovations for the agricultural sector. He works at the French Technical Institute for Sugar Beet (ITB), where he supports industry stakeholders in evaluating and implementing technical solutions designed to improve crop performance and the sustainability of farming practices.

His expertise covers agricultural mechanization, field trials, and the assessment of emerging technologies applied to agriculture. Committed to knowledge sharing, he regularly contributes to technical studies, field trials, and outreach activities for agricultural professionals.

Alexandre PREVAULT OSMANI
President & Chief Technology Officer (CTO) – SABI AGRI



Alexandre PREVAULT OSMANI is Chief Technology Officer and President of SABI AGRI, a French company specializing in the design and manufacture of lightweight electric tractors and agricultural robots.
Since 2017, he has led the technical and industrial development of several generations of electric machines for specialty crops, with a strong focus on practical field applications, technological simplicity, and the industrial deployment of electric and robotic solutions for farmers.
He is also the driving force behind Torque.Works, a platform developed by SABI AGRI to democratize large-scale access to the components, software, and technology building blocks required for the electrification and robotization of agricultural machinery. As part of this initiative, he led the development of the SRBC agricultural robot, a low-cost, modular solution designed to support farmers in implementing agroecological practices.
Throughout his career, Alexandre has developed comprehensive expertise spanning the entire product lifecycle—from concept to operational machine—including vehicle architecture, battery systems, embedded electronics, software, electric hydraulics, type approval, industrialization, field operations, and after-sales support.
His expertise lies at the intersection of engineering, industrial entrepreneurship, and innovation strategy, driven by a clear conviction: making new agricultural technologies accessible, practical, and aligned with the real needs of farmers while supporting the widespread adoption of agroecological practices.

Mohammad NAIM
Lecturer and Researcher – UNILASALLE



Mohammad NAIM is a lecturer and researcher at UniLaSalle Polytechnic Institute, Beauvais, France, and a member of the InTerACT research unit, specialised in agricultural and management sciences. His work is interdisciplinary, situated at the interface of agricultural sciences and management, with a particular interest in the governance and commercialisation of innovative technologies in complex socio-technical systems. Naim's research spans precision agriculture, agroecology, sustainability assessment, behavioural determinants of technology adoption, business model development, all underpinned by a broader emphasis on how innovation processes unfold within agri-food systems and contribute to sustainable transitions. He has authored several scientific publications, demonstrating a strong commitment to advancing innovative, sustainable, and technology-driven solutions across diverse systems.

CROP PROTECTION

Mathilde GUICHARD
CEO – BLISS ECOSPRAY



Mathilde GUICHARD is Chief Executive Officer of Bliss Ecospray. A graduate of Paris Dauphine University and originally from Burgundy, she brings to the company extensive expertise in strategy, business development, and finance, combined with a strong understanding of the agricultural and wine sectors.

Throughout her career, she has supported a wide range of agricultural businesses in their transformation, growth, and investment projects, notably as a strategy consultant at McKinsey & Company. This experience has given her a broad perspective on the economic and environmental challenges facing the agricultural sector.

Convinced that technological innovation is key to reconciling performance with sustainability, she joined Bliss Ecospray in 2024 to accelerate the development of innovative solutions that help reduce agricultural inputs, preserve natural resources, and strengthen the competitiveness of farming businesses.

Jean-Paul DOUZALS
Senior Scientist - INRAE



Jean-Paul DOUZALS is an Agricultural and Environmental Engineer at the ITAP Joint Research Unit (UMR ITAP), INRAE – Institut Agro Montpellier. He coordinates the ReducPol platform, dedicated to the assessment and optimisation of application techniques for plant protection, and contributes to the UMT Ecotech partnership with CTIFL and IFV, focusing on applications in perennial crops.

His work covers applied research and development, often conducted through industrial and international collaborations, as well as expert support for public policy and standardisation. His experimental activities range from droplet size characterisation and the measurement of spray deposits on natural or artificial vegetation to the assessment of spray drift and drift-reduction techniques.

Among his various areas of interest, spray drones represent a particularly challenging field, combining innovative technologies with a highly constrained regulatory framework.
https://www.researchgate.net/profile/Jean-Paul-Douzals

Paul MELKI
Research and Innovation Engineer - EXXACT ROBOTICS



Paul MELKI is currently a Research and Innovation Engineer within the Innovation team at Exxact Robotics. In 2025, he earned a Ph.D. in Machine Learning and Computer Vision from the University of Bordeaux, following the completion of a CIFRE industrial research program conducted jointly at Exxact Robotics and the IMS Laboratory in Bordeaux.

He also holds a Master's degree in Statistics and Econometrics from the Toulouse School of Economics and a Bachelor's degree in Computer Science from the University of Balamand, Lebanon.

At Exxact Robotics, he works closely with the Data, AI/Computer Vision, and Product teams on high-value innovation projects in precision agriculture.

AGRICULTURAL ROBOTICS: TECHNOLOGY AND DEPLOYMENT

Théo BIARDEAU
Doctoral Candidate – CYCLAIR



Théo BIARDEAU is a CIFRE Ph.D. candidate in Signal and Image Processing at the University of Poitiers, conducting his research jointly at the XLIM Laboratory (CNRS) and Cyclair. Holding a Master's degree in the field, he is currently developing unsupervised deep learning algorithms for agricultural obstacle detection.

His research aims to improve the safety of autonomous rover navigation in dynamic agricultural environments. His work focuses primarily on spatiotemporal modeling architectures, as well as the challenges of continuous and online learning.

His broader research interests include the application of artificial intelligence to robotic actuator control, particularly through the study of Vision-Language-Action (VLA) models and reinforcement learning.

Manon BOULET
Research Engineer – INRAE



An agricultural engineer specialising in plant biology, she focuses on agronomic experimentation and the evaluation of agricultural innovations. Since graduating, she has developed expertise at the intersection of agronomy, agricultural machinery and emerging technologies.

After gaining experience in applied research at Limagrain, she joined INRAE within the TSCF research unit, whose work includes the integration of robotics into agroecological farming systems. She has contributed to the evaluation of agricultural robot performance through projects such as the ROSE Challenge, METRICS-ACRE and, more recently, NINSAR.

Her research focuses on assessing technical, energy, agronomic and environmental performance indicators within innovative cropping scenarios and farming systems, including pixel farming.

Through her work, she aims to support the transition towards more precise, efficient and sustainable agriculture.

MECHANICAL WEED CONTROL SOLUTIONS

Daniel BOFFETY
Research Engineer - INRAE



Research Engineer within the Technologies and Information Systems for Agrosystems Research Unit (TSCF), based at INRAE's AgroTechnoPôle in Montoldre. He has extensive experience in managing and implementing projects combining agricultural equipment, new information and communication technologies, sensor networks and connected devices to support precision agriculture techniques and practices, as well as the transition towards agroecological farming systems.

His most recent work has contributed to initiating the development of a research and testing bench for alternative weeding technologies, which is the focus of his presentation at AGRITECH DAY 2026.

Damien BRUN
Agricultural Engineer - ARVALIS



Damien BRUN is an agricultural engineer who graduated from the École Nationale Supérieure d'Agronomie de Nancy (ENSAIA) in 2002. After gaining his first professional experience advising farmers at a company specializing in fresh washed potatoes, he joined ARVALIS in 2008 at the Boigneville experimental station. Damien is a member of the R&D department at ARVALIS, a French technical institute dedicated to applied agricultural research in the field of arable crops. His research focuses on farm machinery, particularly crop establishment: tillage, seeding, mechanical weed control for cereal crops, and potato harvesting. He led AGILE, a project funded by the French Ministry of Agriculture on alternatives to glyphosate in dead-end situations for arable crops, which ran from 2023 to 2026.

ENERGY EFFICIENCY AND DECARBONIZATION OF AGRICULTURAL MACHINERY

Antti LAJUNEN
Associate Professor – HELSINKI UNIVERSITY



Antti LAJUNEN is currently working as an Associate Professor in Agricultural Engineering at the University of Helsinki, Finland. He received the M.Sc. degree in Mechanical Engineering from Helsinki University of Technology by studying Automotive Engineering. After graduation he lived in Paris, France and received the Master of Advanced Studies degree in Industrial Engineering from Ecole Centrale Paris (ECP) in 2007. He received his D.Sc. degree in 2014 from Aalto University, Finland, focusing on the electrification of heavy vehicles and off-road machinery. His main research interests are electrification of agricultural vehicles and machinery, robotics and automation in agriculture, and high-fidelity modelling of off-road vehicles.

Diego URBINA SALAZAR
Scientific Research Officer - UNILASALLE



Scientific Research Officer specialising in agricultural equipm performance at UniLaSalle (France). An Agro-Environmer Engineer who graduated from Universidad del Magdal (Colombia), he holds a Master's degree in Soil Science and Pl Nutrition from ESALQ, University of São Paulo (Brazil), as well a PhD in Environmental Sciences from Université Paris-Sac (France), specialising in remote sensing of organic carbor agricultural soils.

His research focuses on soil remote sensing, digital soil mapp modelling the operating parameters of agricultural equipment, a sensor-based variable-rate agricultural applications. His w aims to develop innovative solutions for more efficie sustainable and data-driven agriculture.

Olivier MARCHAND
Engineer – CRMT



A graduate engineer from the École Nationale Supérieure des Arts et Métiers, he began his career in 1993 at Wärtsilä in Mulhouse, where he contributed to the development of components for multi-megawatt diesel and natural gas engines. He then joined Cummins in the UK in 2000, continuing to work in the field of high-power engines, particularly for biogas cogeneration applications.

Since 2004, he has been based in Lyon at CRMT – Centre de Recherche en Machines Thermiques, an SME specialising in engine innovation. He initially managed technical projects before becoming Technical Director and, in 2023, Director of Innovation and Development.

His core expertise lies in powertrains, from design to testing, both on engine test benches and on heavy-duty machines and vehicles, with a strong focus on low-carbon fuels, on-road vehicles and special-purpose machinery.

PRECISION AGRICULTURE

Sylvain VILLETTE
Lecturer and Researcher – AGRO DIJON



Lecturer and Researcher at Institut Agro Dijon and member of the INRAE TSCF Research Unit, Clermont-Ferrand–Montoldre Centre.

Sylvain VILLETTE graduated as an agricultural engineer from ENITA Dijon in 1994 and earned a Ph.D. in Image Processing from the University of Burgundy in 2006. He is currently a Senior Lecturer at Institut Agro Dijon (France), where he coordinates the advanced specialization in Agricultural Equipment Science and Technology.

His research is conducted within the INRAE TSCF Research Unit (Clermont-Ferrand, France) and at the AgroTechnoPôle platform (Montoldre, France). His current work focuses on studying the centrifugal spreading process using numerical modeling.

Emmanuel PIRON

Engineer, TSCF Research Unit – AGROTECHNOPLE - INRAE



He is an Agricultural and Environmental Engineer specializing in agricultural machinery at INRAE. As Head of the Technological Research Platform within AgroTechnoPôle at the Montoldre site, he conducts research in several areas, including centrifugal spreading of granular materials, spreading of solid and liquid organic fertilizers, agricultural tyre efficiency and its impact on soils, as well as, more recently, seeding and pneumatic conveying of granular materials.

His work is primarily carried out in partnership with manufacturers from the various sectors concerned, leading to the development of test benches and associated methodologies, technical reference data, and technological innovations.

Emeric LECLAIR
Software Engineer – BUREL GROUP



Emeric LECLAIR is a Software Engineer at Burel Production, manufacturer of the Sky Agriculture brand, where he develops embedded algorithms for the management and control systems of seeding and fertilization equipment.
The son of mixed crop and livestock farmers and the partner of a livestock farmer, he has first-hand knowledge of the realities of farming and is committed to developing solutions that address practical needs in the field.
A graduate of Polytech Angers in Automation and Computer Engineering, he joined the Burel Group in 2015. His work notably includes leading the integration of image processing, predictive models, and advanced algorithms into the brand's embedded control units and digital services, with the aim of improving machine performance and ease of use.

Damien CALAIS
Lecturer – INSTITUT AGRO DIJON



Damien CALAIS is a Lecturer in Agricultural Machinery and Precision Agriculture at Institut Agro Dijon. He co-supervised the student project presented at AGRITECH DAY.

His research also focuses on innovation in agricultural machinery for cropping systems transitioning towards conservation agriculture.

Eve FAIVRE
Agricultural Engineering Student – INSTITUT AGRO DIJON



Eve is a final-year agricultural engineering student at Institut Agro Dijon, specializing in agricultural machinery. Her background is grounded in hands-on farming experience, gained both on her family's vineyard and through close involvement with neighboring mixed crop and livestock farms. This experience has given her a practical understanding of production systems and the operational challenges faced by farmers.

She has a particular interest in the role of agricultural machinery in improving farmers' working conditions, optimizing agronomic performance, and addressing labor shortages. Through her studies, she approaches agricultural machinery as a strategic tool for enhancing the efficiency and sustainability of farming systems.

Lydiane MARREC
Agricultural Engineering Student – INSTITUT AGRO DIJON



Lydiane MARREC is an agricultural engineering student at Institut Agro Dijon, specializing in Agricultural Equipment Science and Technology. She contributed to the project presented at AGRITECH DAY in collaboration with the project team.
She has a particular interest in the development of new technologies for precision agriculture, including the creation of prescription maps tailored to crop vegetation and precision inter-row weeding.
Her final-year thesis focuses on the development of a prototype sprayer for viticulture, designed to adapt spraying in real time to the structure of the vegetation through individual nozzle-by-nozzle control.

VIRTUAL ENVIRONMENTS AND DIGITAL TWINS

Adrien SCHOCKAERT
Ph.D. Candidate - DUBRULLE DOWNS



Adrien SCHOCKAERT is a third-year Ph.D. candidate at Dubrulle Downs. His Ph.D. research, jointly supervised by the CERI SN and LaMcube laboratories, focuses on deep learning applied to geometric and physical representations, with the aim of predicting the mechanical behavior of agricultural products.

He is currently developing an innovative model designed to learn the Signed Distance Function (SDF), volume, and inertia directly in latent space. His work has notably led to the development of a Real2Sim2Real approach, enabling the use of digital twins for simulation and synthetic data generation.

His research opens up new perspectives for 3D modeling, simulation, and the development of behavioral models for agricultural products and machinery.

Farouk EL FARJI
Account Manager – IPG AUTOMOTIVE FRANCE



Farouk EL FARJI is an Account Manager at IPG Automotive France, specialising in simulation and virtual validation solutions for the automotive industry. He supports vehicle manufacturers, suppliers and mobility stakeholders in addressing vehicle development, testing and validation challenges, particularly in the fields of ADAS, automated driving and Software-Defined Vehicles.

Working at the intersection of technical challenges and business needs, he is involved in MiL, SiL and HiL simulation projects and contributes to promoting approaches that accelerate development while reducing costs and the need for physical testing. He also takes part in training sessions, webinars and industry events focusing on CarMaker and emerging simulation technologies.

In 2026, his work notably focuses on digital continuity, automotive simulation and generative AI, with an emphasis on new approaches to vehicle development and validation.

SAFETY AND PROTECTION OF AGRICULTURAL MACHINERY

Thierry KOLTON
Director – VICONE



Thierry KOLTON is a Director at VicOne Europe, specializing in crafting cutting-edge solutions for automotive and transportation industry. With over 10 years of experience in the Cybersecurity and Automotive industry, he has honed his expertise in integrating large-scale systems to meet the evolving challenges of cybersecurity. Recently, he has been at the forefront of assisting automotive OEMs and Tier 1 suppliers in establishing robust vulnerability management and exploitation prevention frameworks (CRA and Machine Regulation), ensuring resilience in the face of emerging cyber threats.

Bastien LAURENT
Research Engineer – INRAE



A Research Engineer in Experimental Techniques at INRAE since 2017, he works at the Clermont-Auvergne-Rhône-Alpes Centre within the TSCF Research Unit (Technologies and Information Systems for Agrosystems), which focuses on technological innovation for agriculture.

His work covers the development of agricultural robotics, with the aim of providing automated solutions to address the operational constraints faced by farms, as well as agricultural machinery safety, notably through his involvement in the Secumob project.

Holding a technical degree in Physical Measurements and a Master's degree in Mechatronics, he designs, integrates, and tests prototypes both in the laboratory and under real-world field conditions, combining modeling, electronics, and programming.

This multidisciplinary expertise enables him to support the development of versatile solutions from initial concept through to validation, with the aim of improving the productivity, safety, and sustainability of agricultural systems.

AGRICULTURAL ROBOTICS: RESEARCH FINDINGS AND OPERATIONAL FEEDBACK

Rethink its crop system to integrate a robot: a look back at four years of experimentation in sugar beet

Thomas LEBORGNE*
Institut Technique de la Betterave, 45 rue de Naples, 75008 Paris
* Corresponding author. Email: t.leborgne@itbfr.org 06 09 71 47 53

Abstract

Robotic technology is still not widespread in field crops such as wheat or maize. Sugar beet is one of the few crops that has experienced significant growth in the use of agricultural robots in recent years. In 2025, more than 50 robots were operating in sugar beet fields, with the FarmDroid® robot being the most widely adopted model. This technology can perform both sowing and weeding and is mainly used in organic sugar beet fields. ITB (Institut Technique de la Betterave) has been conducting trials over the last four years using its own robot to identify the strengths and weaknesses of this technology.

The robot enables precise and efficient in-row mechanical weeding, which is difficult to achieve with conventional implements. It can also perform weeding at very early sugar beet growth stages (two-leaf stage) without damaging the crop. Furthermore, in some cases, it can replace manual weeding, which is expensive and time-consuming. Farmers using robots would not go back to a sugar beet cropping system without one.

However, several challenges remain with this technology. First of all, to achieve efficient in-row weeding, the robot must operate at very low speeds, which requires farmers to rethink their work organization and take weather conditions into account. Furthermore, calling this technology an "autonomous machine" can be misleading, as close human supervision is still necessary to ensure proper operation. Despite its numerous advantages, robotics in sugar beet has proven its value. Its future adoption will depend on the willingness of producers, sugar manufacturers, and consumers to support sugarbeet production with reduced herbicide use

KEYWORDS: Robotic / Weeding / Sowing / Agroecology / Precision / Autonomy

Complexity level: 2

1/ INTRODUCTION

The sugar beet sector is the field-crop sector in which agricultural robotics has developed most rapidly. The launch of "made in France" organic sugar beet production in the early 2020s was the

real driver behind this development. In fact, growing organic sugar beet requires a lot of handwork for weeding the fields. Workers who want to do this job are becoming increasingly difficult to find, and a robot makes it possible to significantly reduce this constraint. With about fifty robots now operating across France, most of them being FarmDroid robots, farmers who have adopted this technology have identified clear benefits. Although the organic sugar beet sector is currently facing a slowdown, these robot users would not go back to their previous farming practices.
Figure 1 below presents organic sugar beet production in France in 2025 and the number of FarmDroid® regarding the type of production

Source: Cultures Sucre, Farmdroid®

Figure 1: Surface of sugar beet production regarding the type of production in 2025 in France and number of Farmdroid® robot

However, installing a robot in a sugar beet field is not simply a matter of watching the robot carry out its task. **The entire crop management strategy must be reconsidered**, from sowing to harvesting, and in some cases, this reflection may even extend to the scale of the crop rotation. From an agronomic perspective, many of the farmers' usual benchmarks and decision-making processes need to be reconsidered: When should the robot be deployed? What settings should be used? Which weeds should be targeted?

2023	2024	2025	2026
			
First trial Small surface (4,5 ha) **Conventional farmer** First study of sowing and weeding efficiency in conventional context Recommended robot setting	Big field **(10,5 ha)** **Organic farmer** First study of sowing and weeding efficiency in organic context Recommended robot settings	Big field (10 ha) Organic farmer First study of **the blind seeding** with the robot **Aggressive weeding** setting tested **Multicriterial analysis**	Big field (10 ha) Organic farmer First study of the **'half blind' weeding** with the robot, first study of **early-stage weeding** Multicriterial analysis

Figure 2: Field trials made with the FarmDroid® by ITB through the years

Like farmers, the Institut Technique de la Betterave (ITB) has had to learn through experience when implementing these technologies in the field. The figure 2 above shows how our institute took charge of this technology through the years from trials at small scale to a complete study of the robot at field scale (the words written in bold are the new changes made through the years). Regarding our results and FarmDroid® user's feedback, we adapted our trials through the years to study what seemed interesting to gain work efficiency.

How should the crop management strategy be redesigned to integrate a robot into a sugar beet cropping system, and what are the real challenges and implications of these technologies for this production sector?

2/ MATERIALS AND METHODS

The trials conducted over the years differed considerably from one year to another, but they were all made in farmers' fields, under uncontrolled conditions. Except for the first year (2023), the whole field was managed by the robot. The robot used for our trial was the FarmDroid® robot configured for sugar beet with these specific configurations:

Model name	FD20
Working width	3 m
Weight	900 kg
Inter-row distance	50 cm
In-row distance	18 cm (except in 2026: 19 cm)
Sowing speed	700 m/h
Weeding speed (at early stages)	400 m/h
Weeding speed (at late stages)	900 m/h
In-row knives aggressivity	Normal (except for 2025 trial)

In all our trials, the solar panel on the robot was the only source of energy, we did not use extra battery. Robot settings were managed jointly by the farmer and ITB.

3/ RESULTS AND DISCUSSION

In this part of the article, the results and discussion are divided into different topics to highlight the specificity of the robot and understand how crop systems have to be rethought. The different topics are working time, weeding efficiency and multicriterial analysis with a final chapter dedicated to a crop system comparison.

3.1 Working time

The FarmDroid® robot stands out for its high work precision, enabled by slow workflow rates (sowing at 700 m/h and weeding at 900 m/h). The manufacturer claims a daily sowing capacity of 4 hectares per day. However, our experiments showed an even slower workflow rate for sowing, as illustrated in the figure below (figure 3). Since this operation is carried out in late March/early April, the days are still short with limited sunlight, reducing the robot's autonomy. As a result, the robot stops sowing in the middle of the night and waits for sunrise. Of course, the robot also stopped when the seed hoppers were empty. In this case, the farmer receives an alert notifying them to fill the hoppers (sometimes during the nighttime).

*All times have been recalculated and adjusted to a 10-hectare basis. The days indicated include delays caused by rain during sowing.

Figure 3: Time (in day) to sow* 10 ha with the FarmDroid® each year in our trials

What must be emphasized above all with technologies like robots, which have a low workflow rate, is the need to strongly anticipate, sometimes on a weekly scale, the possibility of carrying out the work under good conditions. In 2023, spring was particularly wet, with regular rainfall that significantly delayed sowing. In subsequent years, sowing was anticipated more precisely based on weekly weather forecasts.

In terms of work organization, farmers who are already used to working with weather forecasts must **be even more attentive to predictions** when using a robot. They must also accept that sowing may sometimes need to be spread out when weather conditions are not ideal. This observation also applies to weeding operations.

3.2 Weeding efficiency

In the different trials, ITB tried to determine whether the robot provided a real advantage in early weeding operations, where traditional mechanical weeding tools cannot intervene. Therefore, we studied the benefits of blind weeding (performing superficial weeding just after sowing, above the sowing depth, to destroy weeds that were just emerging) and weeding at the two-leaf stage of sugar beets.

Figure 4: Effect of the blind weeding on beets and weeds population (2025 trial)

In our 2025 trial (figure 4), a greater number of weeds were recorded in the blind weeding treatments than in the ‘no blind weeding’ control after sowing. The pre-emergence hoeing operation may have created favourable conditions for the germination of previously dormant weed seeds in the soil. However, these results should be interpreted with caution, as it cannot be ruled out that the initial weed seed bank was higher in the blind-weeding plots than in the ‘no blind

weeding' control. In fact, we observe here the same conclusions as in our false seedbed trials: a superficial soil working before or after sowing can have **a rather random effect on weed populations.**

Regarding sugar beet emergence, lower plant populations were observed in the blind weeding modalities. This pre-emergence operation also tends to move soil back onto the row, artificially increasing the sowing depth, which was already relatively deep (3 cm). Plant populations were particularly reduced in the treatment where the row was cultivated to a depth of 2 cm.

Despite these discouraging results, the ITB still recommends performing a weeding operation, if possible, right after sowing by using a kind of "half-blind weeding", where only the inter-row area is superficially worked. By this way, no soil is added to the row, which could otherwise impact the emergence of germinating sugar beets.

In 2026, we conducted a comprehensive study of the weed population before and after the robot weeding, including row and inter-row counting. Above all, the early-stage weeding has been conducted (weeding at 2-leaf stage), where all conventional mechanical weeding implements would severely damage sugar beet plants. The results are presented in the figure 5 below.

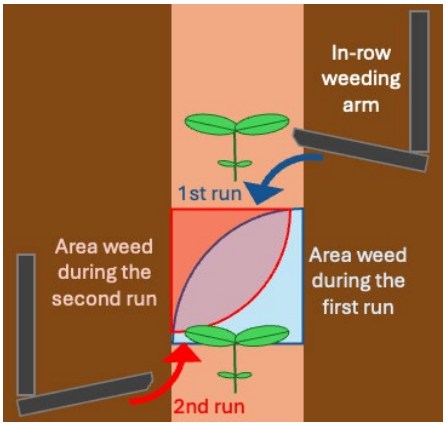


Figure 5: Weeding efficiency (inter-row and in-row) of the FarmDroid® at sugar beet early stages (2026 trial), and in-row weeding principle

It appeared that the in-row weeding enables a weeding efficiency of 67%, which is quite good. This figure can be explained by the movement of the in-row weeding tool of the robot that is doing an arc of a circle in the row to avoid beet damage.

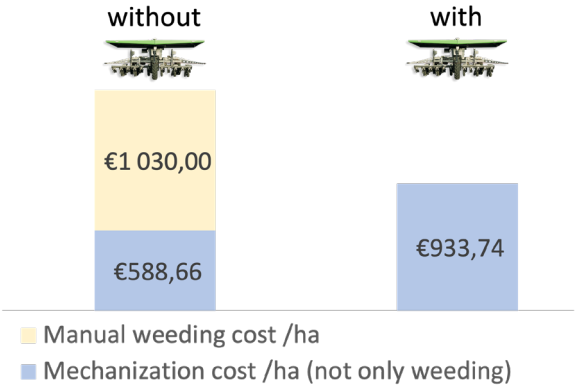
The in-row weeding can be completed with another FarmDroid® hoeing but running in the contrary direction than the first run (as explained in the figure 5). In this way, weeds that were out of reach during the first run can be weed during the second run. ITB experimented 'aggressive setting' with the weeding in-row tool, but it was too destructive for the sugar beet.

Even if it seems to be a good result, weeds remain in the row. In our 2026 trial, we counted at 4 leaves stage after the robot work (in the contrary direction as the first run) 23 weeds/m2 on average which is still a lot, mainly when we know that 1 chenopod per square meter can result in a 3,7-t/ha yield loss. In this context, the in-row weeding should be completed by manual weeding (the time for which will be drastically reduced compared to a non-robot system).

Such as every mechanical weeding tool, the balance has to be found between being efficient enough to destroy the weeds and being selective enough to avoid damage on sugar beet. Robot allows a precise and efficient in-row weeding at very early stage, and FarmDroid® users use this advantage wisely. Tolerance to weeds is then specific to each farmer, the one looking for a really clear field will add manual weeding later, but with a lower time dedicated to this task compared to non-robot users.

3.3 Multicriterial analysis

A multicriterial analysis was also launched in 2025 and continued in 2026 to study the robot beyond technical aspects. One of the main criticisms made to these technologies is that they are expensive, so we did a factchecking regarding this affirmation in an organic sugar beet crop system. The FarmDroid® robot purchase price considered in this study was €75,000, with an annual subscription fee of €995 (2026 price announced by the manufacturer). The cost calculated for manual weeding was €1,030/ha (60 h/ha for the cropping system without the robot).



Source: ARTB, ITB with Systerre ©

Figure 6: Weeding cost with or without FarmDroid® robot in organic sugar beet

Mechanization costs were lower for the cropping system without the robot than for the system incorporating the robot. This difference is mainly explained by the high purchase price of the FarmDroid®, its depreciation being allocated to a single crop (sugar beet only), and its annual subscription fee of €995. However, in our case study, when manual weeding costs are included in the system without the robot, total costs increase sharply and may even exceed those of the FarmDroid-based system. In this context, the robot demonstrates its economic value through its ability to substitute for manual in-row weeding.

It should be noted, however, that although the robot provides effective in-row weed control, it does **not achieve the same level of field cleanliness** as a cropping system completed with manual weeding. During wet spring conditions, the robot may struggle to keep the crop row sufficiently weed-free, which can have a significant negative impact on final yield.

The working time of both the farmer and the robot was also studied in the multicriterial analysis. Manual weeding takes up the majority of the working time without a robot. For sowing and weeding, the robot operates for approximately 23.5 hours per hectare (due to its intervention speed), which is nearly three times less than the time dedicated to manual weeding (60 h/ha). However, these results should be interpreted with some caution. In this study, the robot handles operations that are highly dependent on weather conditions: sowing and mechanical weeding. This means that from April to early June, weather conditions must be optimal over an extended period. This constraint does not apply to the same extent in the traditional organic crop system,

which uses classical sowing implement and mechanical weeding tools with higher workflow rates.

Additionally, an unquantifiable **supervision time** must be added for the robot, involving monitoring various operations, alerts, and potential malfunctions that can occur at any time of the day or night.
What is important to note is that it is not the robot that decides whether the conditions are good or bad for performing the required work. **The decision belongs to the farmer**, who must closely monitor its field and assess the agronomic relevance of the task, which can be time-consuming.

A final focus was done on energy and fuel consumption across the entire sugar beet crop system, from fertilization to harvest. Since the robot operates with a large solar panel that produces electricity, it does not require fuel for its sowing and weeding operations. However, soil preparation, organic fungicide protection, and harvesting remain fuel-dependent in the crop system with robot. As a result, fuel consumption and greenhouse **gas emissions from fuel use are still half** those of the non-robot organic crop system (132 l/ha for the non-robot vs. 63.2 l/ha with FarmDroid®).

3.4 A crop system for the robot

The figure 7 presents 3 different crop systems (conventional, organic with or without FarmDroid®) regarding the sugar beet development stages. A focus was made on the seeding and the weeding, where the robot is involved. These 3 systems were designed with keeping **the same level of field cleanliness** at the end of weeding operations. We assume that the robot's work on the rows was particularly effective and reduced the time required for manual weeding by a factor of 10.

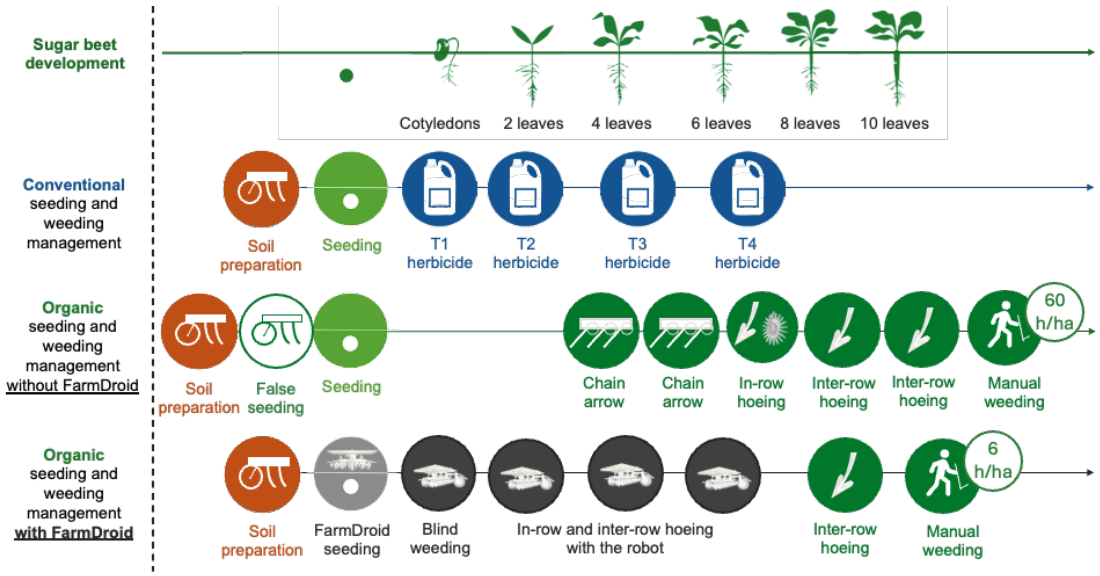


Figure 7: Comparison of 3 crop systems (seeding and weeding) of sugar beet: conventional, organic with and without FarmDroid®

The first difference in the crop system using a robot is noticed before the sowing operation. Since the FarmDroid® is a robot equipped with lightweight sowing and seed-firming tools, the soil must be finely prepared and level to ensure high-quality sowing. While a single preparation pass is generally enough for conventional sowing, two passes are usually required for the robot's sowing to ensure the soil is sufficiently fine and to allow a proper seed placement. The farmer must anticipate this specific soil preparation using the appropriate equipment. Proper levelling of the

field, also recommended in organic farming, is crucial for the success of the next mechanical weeding operations to come.

The shape of the field must also be suited to the robot's operation; fields with triangular headlands or irregular boundaries make the robot's work more challenging. It may therefore be necessary to redesign the field layout, sometimes deciding to take certain areas out of production to ensure optimal robot performance.

Unlike conventional or organic farming methods, where there is a brief delay before the first weeding operations, the robot must begin work immediately after sowing by initiating "blind weeding". Once this step is complete (taking about one week for just over 10 ha), the farmer must prepare to deploy the robot again when the beet plants reach the two-leaf stage for the first in-row weeding pass. As with organic farming, some loss of beet plants during mechanical weeding passes is acceptable; however, total losses across all operations must not exceed 10%.

Farmers must **closely monitor weeding operations**. They need to ensure the robot operates at a stage when weeds can be easily destroyed, taking advantage of the favourable drying conditions that follow the intervention. Since the goal is to effectively eliminate weeds within the crop row, the farmer must take considerable time to fine-tune the tool settings, aiming the right balance between selectivity and efficacy. In fact, just as with a hoe or a chain harrow in organic cropping system, significant time spent on adjustments is essential to ensure the weeding process goes right. Furthermore, no intervention other than the robot is planned between sowing and the six-leaf stage, even though a pass with a hoe or chain harrow could be considered. This is due to the aim of avoiding tractor wheel tracks in the areas worked by the robot; our trials showed that ruts, even shallow ones, could impair the robot's precision.

From the 8-leaf stage, the Farmdroid® can still operate; however, since it now focuses primarily on the area between the rows, it is more efficient in terms of operating speed to prioritize a pass with a hoe.

4/ CONCLUSIONS

Sugar beet, which is a row crop, is particularly well suited to robotization. Since weed competition can cause significant yield losses, weeding is an essential operation in its crop management. With the rise of organic sugar in the 2020s, robots (mainly FarmDroid®) have developed well in this crop, and the ITB has gradually supported their deployment among farmers. Users are satisfied with this technology and its advantages, the main one being the ability to weed sugar beets at an early stage. The robot also drastically reduces the manual weeding, which is painful, expensive and time-consuming. The FarmDroid® can be economically affordable by farmers in this context.

However, many challenges remain with robots in sugar beet. Installing this equipment in a field requires rethinking the overall farming approach: revising soil preparation, field layout, adopting more agronomic decision-making, and being available to troubleshoot the robot 24/7. These technologies are likely to develop further if they can be used not only for one crop but for several crops within the rotation. And it is precisely on this last point that technological progress needs to advance, because, for the moment, few field crops can be managed by a robot.

To take the reflection further, we can try to imagine what **robotic development in sugar beet might look like in 10 years**. We can choose a rather realistic and optimistic premise, which would be as follows: less herbicides are available (government restrictions), sugar producers encourage greener practices with for example financial incentives, organic farming is slowly increasing again.

In this scenario, robots will be no longer targeted for organic sugar beet producers but for all famers. This change will impact various links in the agricultural chain:

- **Agricultural machinery dealers**: sell more robot at affordable prices, mainly ensure a good start-up of these technologies and a very good after-sales service (24/7) such as the example of the milking robot.
- **Farmers:** enhancing agronomic skills and weed identification capabilities, be ready to rely on autonomous machine, rethink the land parcel layout to suit for robots, be available for the robot 24/7 (even during nighttime).
- **Robots' manufacturers:** develop wider robot which can work faster, adapt robot to conventional farmers (spot spray technology for example), support the after-sales service with dealers.
- **Sugars' manufacturers:** financial incentive for greener practices and promote these actions at the consumer's scale.
- **French government:** financial incentive for greener practices.
- **Private and public research:** continue field research and trials, train technical agronomic adviser to make them able to answer to farmer's questions.

References

- A.Jacques (ARTB). *« Robot Farmdroid: quelle place en betterave conventionnelle ? »*. Le Betteravier Français, n° BF1215, 2025, p. 3. [en ligne]. Disponible sur: https://www.itbfr.org/fileadmin/user_upload/PDF/Cahier-central-du-Betteravier-Francais/BF1215-ITB.pdf (Consulté le 11 août 2026).
- ITB. *Webinaire de l'ITB: Comité technique special désherbage* [Vidéo en ligne]. YouTube, 2026. Disponible sur: https://www.youtube.com/watch?v=vPkpJ589u8k&t=3212s (Consulté le 11 août 2026).
- P. Peeters, *« Le robot FarmDroid passe à la moulinette technico-économique »*. La France Agricole. Disponible sur: https://www.lafranceagricole.fr/robot/article/893367/le-robot-farmdroid-passe-a-la-moulinette-technico-economique (Consulté le 11 août 2026)
- T.Leborgne (Institut Technique de la Betterave). *Retour en vidéo sur l'expérimentation 2024 avec le robot FarmDroid* [en ligne]. 2024. Disponible sur: https://www.itbfr.org/tous-les-articles/article/news/retour-en-video-sur-lexperimentation-2024-avec-le-robot-farmdroid (Consulté le 11 août 2026).
- T. Leborgne *« Le binage à l'aveugle avec le robot Farmdroid»*. Le Betteravier Français, n° BF1204, 2024, p. 2. [en ligne]. Disponible sur: https://www.itbfr.org/fileadmin/user_upload/PDF/Cahier-central-du-Betteravier-Francais/BF1204-ITB.pdf (Consulté le 11 août 2026).
- T.Leborgne (Institut Technique de la Betterave). *Retour sur l'expérimentation avec le robot FarmDroid* [en ligne]. 2023. Disponible sur: https://www.itbfr.org/tous-les-articles/article/news/retour-sur-lexperimentation-avec-le-robot-farmdroid (Consulté le 11 août 2026).

From agroecological intent to performed work: an open mission-exchange format as a chain of responsibility for light agricultural robots

Alexandre PREVAULT OSMANI [a,*]

[a] SABI AGRI SAS, Biôpole Clermont-Limagne, Saint-Beauzire, France

* Corresponding author. Email: croissance@sabi-agri.com

Abstract

Robotics can serve agroecology by making precision sowing, early mechanical weeding and repeated interventions with light equipment feasible on small and medium diversified farms. Uptake remains limited by the gap between a performance demonstrated in a trial and a durable service delivered on a farm. Controlled experiments and normative frameworks qualify indispensable functions but document poorly service continuity, residual human workload, conditions actually encountered and the distribution of responsibility. This study instantiates an interoperability architecture intended to make auditable the chain linking an agronomic intent, an authorised mission, a performed work and the associated responsibilities. The open Agri JSON format carries that chain: mission_order states what the robot must do, within which operational design domain (ODD) and with which authorised event strategies; work_performed states what was achieved, under which encountered conditions and under which validation by the farmer. A convergent mixed design combines a retrospective observational cohort with five field cases. 59 missions were linked to a mission_order–work_performed pair; analysis covers the 48 missions performed by light SRBC robots. Coverage reaches 90–98 % depending on the indicator: median clock duration 2.83 h, median effective area 940 m^2, median specific energy 8.2 kWh/ha, median p95 lateral deviation 3.03 cm, median RTK-fix time share 99.1 %, and 39 of 47 missions without any safety stop. These values establish a comparable factual exchange between actors, yet they qualify neither the agronomic service delivered nor the contribution to triple agroecological performance. The five cases document four blind spots that aggregated indicators cannot reveal.

KEYWORDS : light agricultural robotics; agroecology; open mission format; operational design domain; co-responsibility; traceability

Complexity level: 3

1/ INTRODUCTION

Agroecology is used here as the frame of purpose within which the usefulness of a robot is examined. It designates the joint pursuit of a triple performance: environmental and agronomic, through the quality of the service and its measured effects on soils, inputs, crops and living

organisms; social and territorial, through working conditions, the autonomy of the farm system, skills and the local distribution of value; and economic, through accessibility, continuity of service and full cost (Wezel et al., 2009). A robot contributes to that purpose if it enables a practice suited to the cropping system: precise establishment preparing a mechanical weeding operation, repeated passes of a passive implement within a short agronomic window, or substitution for a heavier machine when soil bearing capacity requires it. This contribution has to be demonstrated at the level of the agronomic service delivered; it cannot be inferred from energy consumption alone, nor from an assumed reduction of soil impact.
Small and medium diversified farms concentrate the difficulties of uptake: short production runs, diversity of implements and crops, heterogeneous fields, narrow intervention windows and limited maintenance resources. Beyond centimetre accuracy, the machine must be preparable, supervisable, recoverable after an incident and compatible with the skills available.

1.1 Three levels that must be distinguished

The state of the art has to separate three levels. The first is the **technical capability** of the robot to move and to command an implement safely. The second is the **agronomic service** effectively obtained within a given window. The third is the **agroecological impact**, which requires complementary, macroscopic and retrospective observations: inputs avoided, soil condition, weed pressure, yield and biodiversity; working conditions, farm-system autonomy and territorial effects; full cost and economic viability.

The third level cannot be inferred from the mere success of a mission. Yet it is mainly the first that existing devices document: safety-function testing and normative references (ISO 18497-1:2024), sensor evaluation in controlled environments, simulation and digital twins, and qualification methods based on an explicit operating domain (ISO 34503:2023). Accurate path tracking under sliding, for instance, has been formalised and validated for agricultural vehicles for two decades (Lenain et al., 2006). These works qualify indispensable functions but represent poorly the long run, the variability of implements and the actual organisation of the agricultural service. The present work is positioned downstream, on what happens once the machine is in operation.
Interoperability standards already exist at the implement-control layer: ISO 11783-10:2015 describes the exchange of task and as-applied data between a task controller and a farm management information system. That layer does not carry an explicit operating domain, a bounded vocabulary of authorised reactions to events, or an attestation binding a simulation to one specific version of a mission. The format examined here is therefore complementary to that layer, not a substitute for it.

Following the SMOR white paper (Prevault Osmani, 2026), *diffusability* denotes the capacity of a useful, accessible, safe, maintainable, repairable and appropriable solution to deliver a repeated service across diverse agricultural contexts, with a high degree of autonomy from the farm's point of view.

1.2 Research gap, question and propositions

Publications and industrial reports describe separately guidance performance, safety, work rate, or a single user report. What is missing is a reproducible framework linking, for one and the same unit of analysis: (i) the agronomic service targeted and its link to the agroecological practice; (ii) the authorised operating conditions and those actually encountered; (iii) the planned mission and the recorded events; (iv) the indicators of service, energy, accuracy and human workload; (v) the interventions required to maintain or resume the service; and (vi) the effective responsibilities among farmer, operator, distributor, maintainer and manufacturer. This gap is as much a problem of representation as one of measurement: as long as intent and outcome are not described in the

same versioned vocabulary, field feedback does not aggregate and responsibilities cannot be examined.
The question addressed is therefore: to what extent does an interoperability architecture — explicit operating domain, standardised field records, shared core of indicators — make auditable the chain of intent, execution and responsibility of light agricultural robots, and found a later proof of diffusability serving agroecology?

Four propositions are examined. **P1.** Service availability, residual human workload, recovery after an incident and robot–implement preparation condition uptake more than instantaneous performance. **P2.** Confronting authorised with encountered conditions makes limits, go/no-go decisions and responsibilities explicit. **P3.** A versioned core of metrics allows the same service to be discussed between farmer, distributor and manufacturer. **P4.** Co-responsibility is a condition of broad diffusion: incidents located at the interfaces require an explicit sharing of roles and a verifiable feedback loop.

The article contributes, first, an **open specification carrying a chain of evidence**, in which `mission_order` links the agronomic objective, the robot–implement configuration, the operating domain, the trajectory, the geofencing and the pre-validated strategies, while `work_performed` links that intent to the conditions encountered, the events, the interventions and the results. Second, a **mixed method**, in which the cohort quantifies what can be extracted homogeneously from the logs and five cases explain the mechanisms that aggregates cannot interpret, together with a **co-responsibility matrix** covering the steps from the agronomic choice to the return of experience. Third, **reusable artefacts** — format, parser, Mission Studio preparation software, log schema and indicator catalogue — so that another manufacturer, a technical institute or a cooperative can produce and read these files without depending on a single supplier. Fourth, the identification of the **missing link**: the ergonomic collection of what the machine cannot infer, at the moment and in the place where the farmer can answer.

2/ MATERIALS AND METHODS

2.1 Study design and definitions

A retrospective observational cohort describes what the documentary chain restitutes homogeneously today; five structured field cases analyse the mechanisms linking operating conditions, execution, agronomic service and responsibilities. The cases are not a representative sample and do not enter the cohort statistics: they explain mechanisms that the cohort can subsequently be used to search for.

Four notions structure the study. The **operational design domain (ODD)** designates the conditions under which the robot is authorised to work, described *before* the mission: crop and growth stage, soil condition and bearing capacity, slope, weather, visibility, required localisation quality, presence of people, field geometry, admissible robot and implement, and planned reactions to events. Versioned and attached to `mission_order`, it is a verifiable operational contract. The **conditions observed in the domain (COD)** are the conditions actually encountered, measured by the machine or confirmed by the operator and recorded in `work_performed`; every ODD–COD discrepancy is linked to a detection, a decision, an actor and a piece of evidence. A **safety stop** is an interruption triggered by an emergency stop, a bumper contact, a camera detection or an operator request from the remote control. An **RTK fix** is a satellite localisation in centimetre-level fixed solution; the *RTK-fix time share* measures the fraction of the mission spent in that state.

2.2 The Agri JSON format and the chain of evidence

Agri JSON is an open agricultural mission-exchange format published under a CC BY 4.0 licence (SABI AGRI, 2026). Its version 3 comprises a file type, a vehicle identifier, a geographic origin, point sections, a geofencing description and metadata; trajectories are expressed in a local metric frame attached to a WGS84 origin, and the columns associated with the points may specify speed, working zone and point actions. It contains the following types: `mission_order`, which states what the robot must perform, and `work_performed`, which states what was actually performed.

The proposed enrichment preserves compatibility with version 3: operating domain, robot–implement configuration, event strategies and simulation attestation are placed in the versioned metadata. A strategy written in an open format is not, however, executable for that reason alone: the robot must refuse any instruction that is unknown, incompatible with its configuration, or not pre-validated by the manufacturer.

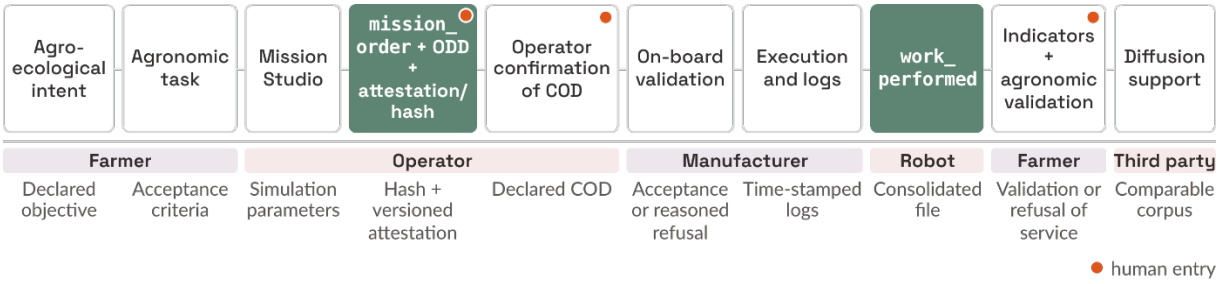


Figure 1. Agri JSON chain from agroecological intent to performed work. Below each link, the responsible actor and the evidence produced. The three human-entry points are marked in orange.

The chain does not turn a technical record into agroecological proof. It preserves the links needed to know what was planned, authorised, observed, executed and validated, along five dimensions: agronomic service, ODD–COD adequacy, operational service, human and organisational workload, and co-responsibility and learning.

2.3 From mission_order to work_performed

Preparation, simulation and attestation. Mission Studio associates with the trajectory the agronomic objective and acceptance criteria, the robot and implement with their dimensions and capabilities, the geofencing, the working zones and authorised paths, the planned operating domain, and a bounded catalogue of reactions to events — a low battery, for instance, calling for a return to a charging area along authorised paths. The software then simulates the trajectory with the digital twin of robot and implement, checking the geofencing, the geometric envelope, the headland manoeuvres and the action zones of the implement. The attestation attached to the mission records the robot and implement profiles, the checks performed and the hash of the `mission_order`: it proves that a given file passed defined checks under identified assumptions, not the absence of real danger.

COD confirmation and on-board validation. On receiving the mission, the interface presents to the operator the dimensions of the operating domain that can be observed: robot and implement actually present, working width, soil condition, crop condition (growth stage and weed cover), moisture or slipperiness, weather, visibility, co-activity and known obstacles. These answers form the first layer of the observed conditions. The robot then verifies locally the hash, the configuration compatibility, the geofencing, the geometric feasibility and the requested strategies; an unknown

or unauthorised policy causes the mission to be refused, even when the file complies with the schema. This second validation is the responsibility of the manufacturer.

Execution and construction of `work_performed`. During the work, the robot complies with the accepted behaviours: stop or degraded mode on loss of localisation, action on the implement, speed limitation and containment within the geofencing. The `work_performed` file automatically aggregates the link to the `mission_order` and its hash, the configuration used, the executed trajectory and worked zones, the measured or confirmed conditions, the events and strategies triggered, and the energy, durations, areas and availability. A short post-mission sequence completes what the machine cannot infer: agronomic satisfaction, perceived complexity, non-observable supervision time and need for a repeat pass — today the main axis for improvement.

2.4 Co-responsibility

Five roles are distinguished. The **farmer** owns the agronomic choice, the knowledge of the field, the working window and the validation of the service delivered. The **operator** prepares and simulates the mission, performs the pre-flight check, confirms the observable conditions, supervises and records events. The **manufacturer** defines the technical limits, the catalogue of accepted strategies, the on-board validation, the instrumentation and the safety rules. The **distributor or maintainer** provides proximity, return to service and structured reporting. A **scientific or sector third party** brings the method, anonymised aggregation, audit and comparability.

Step	Expected information	Entered by	Validated by	Refusal or repeat
Agronomic objective	Target practice, acceptance criteria	Farmer	Farmer	Restatement of expectation
Robot–implement configuration	Model, working width, capabilities	Operator	Manufacturer	Declared incompatibility
ODD	Authorised operating conditions, thresholds	Operator	Manufacturer	Mission outside the domain
Simulation	Geofencing, envelope, manoeuvres	Mission Studio	Operator	Geometric check failure
• COD confirmation	Soil, crop, weather, co-activity, obstacles	Operator	Operator	ODD/COD discrepancy found
On-board validation	Hash, configuration, strategies	Robot	Manufacturer	Unknown policy refused
Execution	Accepted behaviours, events	Robot	Manufacturer	Safety stop, degraded mode
• `work_performed`	Trajectory, COD, indicators	Robot	Operator	Missing field flagged
• Agronomic validation	Delivered service, satisfaction	Farmer	Farmer	Result refused
Feedback	Cause, correction, version	Manufacturer	Third party	Versioned ODD update

Table 1. Co-responsibility matrix. For each step: expected information, actor who enters it, actor who validates it, and mechanism of refusal or repeat. The three human-entry points are marked in orange.

For each step, the matrix in Table 1 states who enters, who validates and on which evidence. A responsibility that is unassigned, or understood differently by two actors, is a result and not a datum to be hidden. This co-responsibility is operational: it neither transfers nor dilutes the regulatory and industrial responsibility of the manufacturer or integrator for the machine placed on the market or put into service.

2.5 Data and cohort construction

The corpus covers ten vehicle identifiers, between December 2025 and June 2026. **59 missions** could be linked to an exploitable `mission_order`–`work_performed` pair; after removal of the eleven missions of the 2 200 kg Zilus robot, treated outside the cohort, the analysis covers **48 missions performed with light SRBC robots**.

That figure calls for an explanation which is itself a result. The machine records automatically what it measures: durations, trajectory, areas, energy, deviation, localisation quality and safety events. The fields that depend on human judgement (conditions actually encountered, agronomic satisfaction, effective supervision time, perceived complexity) have no capture device integrated into the robot interface yet and had to be **reconstructed manually**. It is this data-entry effort that bounds the size of the analysable batch. All `work_performed` files are therefore validated reconstructions: they demonstrate the feasibility of the documentary chain, not a native embedded instrumentation. Coverage ranges from 90 % to 98 % depending on the indicator; a missing value is coded `null` and never assimilated to zero.

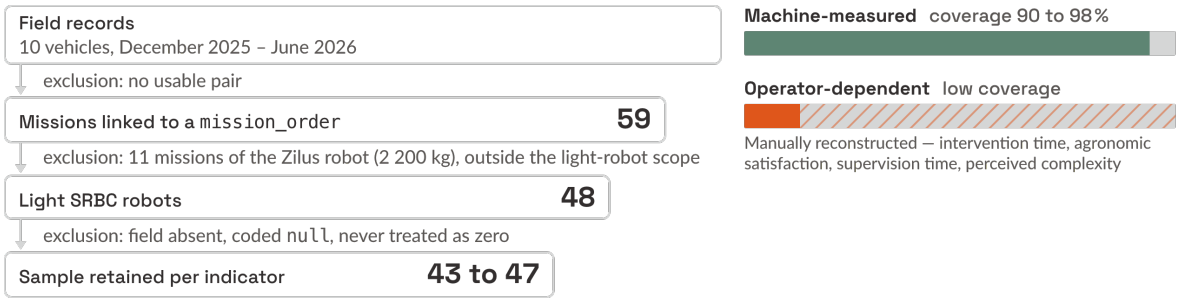


Figure 2. Cohort construction and indicator coverage. The right-hand panel contrasts what the machine measures (green) with what depends on the operator (orange).

2.6 Indicators, conventions and case selection

The families retained are agronomic service, continuity, productivity, energy, human workload, accuracy, localisation, ODD–COD adequacy, safety, economics and user appraisal. A primary result is published only if it carries a metric identifier, a version, a statistical unit, a coverage figure and a quality grade of A or B; the human-workload, economics and user-appraisal families remain at grade C. Two conventions condition the reading. **Lateral deviation is published as a p95**, a statistic that excludes by construction the transient excursions of headland turns and therefore describes trajectory holding during work. The **count of geofence crossings includes mission start-ups**, which explains a median of 1 with no associated safety incident.

The reasoned selection of cases covers five mechanisms, detailed below: accuracy achieved together with continuous human presence (C1); insufficient localisation quality (C2); an obstacle absent from the mission (C3); complete robotic autonomy under imposed supervision (C4); and robotic success with only an average agronomic outcome (C5).

3/ RESULTS AND DISCUSSION

3.1 What the documentary chain restitutes today

Table 2 presents the indicators restituted homogeneously over the 48 SRBC robot missions. Four readings emerge.

Indicator	Unit	n	Coverage	Median	p25–p75	IQR	Mean	Distribution
Clock duration	h	47	98 %	2.83	1.39–3.70	2.31	3.40	0.25 9.23
Active time (implement proxy)	h	47	98 %	1.50	0.92–3.25	2.33	2.34	0.15 7.24
Productive share (active / clock)	0–1	47	98 %	0.76	0.63–0.95	0.33	0.79	0.38 0.99
Effective area	m^2	43	90 %	940	304–1 360	1 056	1 060	110 3 024
Work rate (area / active time)	m^2/h	43	90 %	700	305–937	631	818	98 1 407
Work rate	ha/h	43	90 %	0.070	0.031–0.094	0.063	0.082	0.010 0.141
Lateral deviation (p95)	cm	43	90 %	3.03	2.40–6.29	3.88	3.60	1.55 10.98
RTK-fix time share	%	47	98 %	99.1	93.8–100	6.3	89.8	27.4 100
Mission energy	kWh	44	92 %	1.42	0.82–1.87	1.05	1.81	0.35 4.25
Specific energy	kWh/ha	43	90 %	8.2	5.9–12.7	6.8	9.56	3.5 19.8
Safety stops	count	47	98 %	0	0–0	0	0.21	0 2
Geofence crossings	count	47	98 %	1	0–1	1	0.81	0 5

Table 2. Indicators restituted over the SRBC cohort (n = 48). Each box plot is scaled to its own min–max range; positions are not comparable across rows.

The chain works as an instrument of exchange. Across missions conducted by different robots, on different farms and with different implements, one and the same indicator definition produces comparable values, with a coverage of 90 to 98 %. This is the main result: the factual exchange between actors now rests on a file readable by a third party.

Dispersion is the dominant fact. The interquartile range is of the same order as the median for effective area, 304 to 1 360 m^2 for a median of 940, for work rate, 305 to 937 m^2/h, and for specific energy, 5.9 to 12.7 kWh/ha. Clock duration illustrates the gap between median and mean, 2.83 h against 3.40 h, the signature of a distribution pulled by a few long days. Publishing a mean alone would describe a mission that does not exist.

Localisation is well instrumented, but it is not yet a criterion. The RTK-fix time share is recorded for 47 missions out of 48, with a median of 99.1 % and a first quartile of 93.8 %. One mission nevertheless falls to 27.4 %, and the gap between the mean, 89.8 %, and the median shows that a few missions concentrate the degradation. This quantity is available, comparable and discriminating, yet it is bound to no ODD threshold and to no go/no-go rule. The safety indicators call for the same caution: 39 missions out of 47 proceed without any safety stop, but the count of geofence crossings, of median 1, includes mission start-ups and therefore does not measure a rate of departure from the authorised zone.

What the table does not contain is equally instructive. Human intervention time, agronomic satisfaction and full cost remain `null` over part of the batch. They are often empty because nothing collects them at the moment when the information is available. What the machine measures is covered at 90 to 98 %; what depends on a person is frequently absent.

3.2 What the five cases add

The five cases were documented between late February and late July 2026. Each is confronted with the cohort on one indicator, then on what that indicator does not show.

Case	Signature	Comparison with the cohort	Blind spot	Responsibility
C1 Carrot sowing, SRBC robot	● ● ○	p95 3.4 cm at the median level; 3.89 kWh/ha below p25	12 interventions and continuous presence, agronomically justified but not instrumented	Farmer: seeder operation. Manufacturer: do not equate low autonomy with failure
C2 Tine harrow, SRBC robot	◐ ● ○	p95 18.5 cm above the max, then 4.8 cm within the IQR after changing base	Localisation quality measured but absent from go/no-go; base at 17.8 km then 3.2 km	Manufacturer: localisation threshold in the ODD. Operator: go/no-go
C3 Leeks, SRBC robot	● ● ○	about 2 380 m²/h, above the max, but 1.60 m implement outside the stratum	Temporarily laid hose, absent from `mission_order`	Farmer: field COD. Manufacturer: data-entry safeguard
C4 Rotavator, Zilus robot	● ◐ ○	Outside the cohort; 45.6 kWh/ha against a median of 8.2	Complete autonomy and excellent agronomic result, but operator immobilised by a safety rule; the file reads " 0 intervention "	Manufacturer: usage restriction. Format: distinguish imposed supervision from intervention
C5 Vine, blade hoes, SRBC robot	● ◐ ○	p95 4.9 cm within the IQR; 8.66 kWh/ha close to the median; 0 signal loss	Average satisfaction; weed pressure 20 % against an ODD limit of 10 %	Farmer: timing. Manufacturer: implement effectiveness domain

Signature: robotic execution · agronomic service · human workload and legibility of the format. ● favourable, ◐ partial, ○ unfavourable.

Table 3. Cross-reading of the five cases. The signature column reports, for each case, robotic execution, agronomic service, and human workload and legibility of the format.

C1 — Carrot sowing. The p95 lateral deviation, 3.4 cm, sits at the level of the cohort median and the specific energy, 3.89 kWh/ha, below the first quartile: the robot performed its mission perfectly. The human-workload indicators are nevertheless strongly degraded, with an operator continuously present, four seeder refills and eight setting checks, that is twelve interventions — a normal workload for a sowing operation conducted with a small seeder, whose metering has to be watched. The farmer declares himself very satisfied and the agronomic service is delivered: a straight RTK-guided sowing will allow earlier and automated mechanical weeding, hence durable weed control without herbicide. None of these values is produced by the machine: they come from the user. A purely instrumental reading of `work_performed` would conclude to low autonomy, whereas the agroecological outcome is achieved.

C2 — Tine harrowing on carrots. The area worked, 2 375 m², is close to the cohort maximum and the specific energy, 6.05 kWh/ha, lies within the interquartile range: the mission appears normal. It nevertheless underwent five localisation-related stops and fifteen minutes of unavailability, until an RTK base located 17.8 km away was replaced by a base 3.2 km away. The p95 lateral deviation then falls from 18.5 cm to 4.8 cm. The stability of the corrections is now measured by the RTK-fix time share, so the degradation is indeed visible in `work_performed`. What is missing is not the datum but the criterion: neither a localisation quality threshold nor a maximum distance to the base appears in the `mission_order`. A localisation go/no-go must become an ODD field.

C3 — Leek hoeing. The gross work rate, about 2 380 m²/h with a 1.60 m implement, exceeds the cohort maximum, made up of robots of 0.52 to 0.76 m of useful width: the comparison is meaningful only at constant implement stratum. Above all, a transverse irrigation hose, laid temporarily by the market gardener and therefore absent from the `mission_order`, imposed a seven-minute stop. The interruption is not a guidance error but a **gap in the representation of the field**, bearing on a movable obstacle that only the person present could declare.

C4 — Bed preparation with a rotavator, Zilus robot. Outside the light cohort, this mission consumes 45.6 kWh/ha against an SRBC median of 8.2 kWh/ha: an energy indicator is comparable only at comparable mass and implement. The autonomous phase is faultless, with no intervention at all, the beds being perfectly straight and ready for sowing. This robot is however heavier and fitted with a powered implement that inverts the soil, which is open to criticism within an agroecological itinerary. Above all, the usage restrictions imposed by the manufacturer require an operator to supervise the mission, remote emergency stop in hand. The file therefore records zero intervention, which is exact, while a person was immobilised throughout. The format does not distinguish here a robotic success from an operation that is time-consuming and incompatible with an agroecological practice, and that is the blind spot this case identifies.

C5 — Intra-row vine hoeing. Four thousand square metres worked, a p95 lateral deviation of 4.9 cm within the interquartile range, no signal loss and a specific energy of 8.66 kWh/ha close to the median: execution is nominal on every indicator. The farmer nevertheless declares himself moderately satisfied. The weed pressure observed, 20 %, exceeded the agronomic ODD limit of 10 %, and light spring-mounted blades have only a weak curative capacity on developed weeds, where the expectation was implicitly calibrated on hydraulic intra-row tools. Diffusability here presupposes earlier and more frequent passes.



(a) Temporary obstacle absent from `mission_order`
Case C3 — irrigation hose temporarily laid by the market gardener; 7 min stop; only the person present could report it

(b) Soil tillage with a rotavator, in complete autonomy
Case C4 — the file records 0 intervention; an operator nevertheless remained mobilised for supervision

Figure 3. What the indicators do not show. (a) Case C3, temporary obstacle absent from the mission_order. (b) Case C4, soil tillage with a rotavator in complete autonomy, while an operator remained mobilised for supervision.

3.3 Agri JSON as a thread of evidence, not as sufficient proof

The `mission_order–work_performed` pair makes it possible to situate every decision. A poor description of the equipment or of the context points to operator entry; an incompatible mission accepted on board points to the manufacturer's on-board validation; an accepted behaviour that was not respected points to its implementation; an insufficient agronomic result despite a compliant execution requires the objective, the implement and the acceptance criteria to be examined; a missing datum points to the instrumentation, to the ergonomics of the questionnaire, or to an unassigned data-entry responsibility. The format does not distribute responsibilities in law: it makes auditable the provenance of the decisions and of the evidence needed to discuss them.

Its main contribution is therefore to preserve documentary continuity between the planned and the performed: the hash links the execution to a precise version of the mission, the operating domain and the observed conditions make circumstances discussable, and the events and indicators allow verification that the expected behaviour was observed. This continuity guarantees neither the quality of the content, nor compliance, nor an agroecological benefit. A missing field, an inaccurate declaration or an ignored question can make the interpretation imprecise; conversely, accumulating fields increases the data-entry burden, may reduce effective quality and may slow uptake on farms. The right compromise is to automate technical data, to ask the user only what the user alone can appraise, and to publish the coverage of every indicator.

The chain distinguishes three validations: **preparation**, by Mission Studio on the geometry and the assumptions entered; **operational**, from the confrontation between planned domain, observable conditions and on-board capabilities; and **service**, formulated after the mission from the automatic data and the farmer's agronomic judgement. This separation prevents a simulation

from being taken for a universal authorisation, or a completed mission for a successful agronomic service.

The chain can demonstrate that an identified mission was executed by a given configuration, under confirmed or measured ODD parameters, within its geofencing, with a documented availability, energy and human workload, and that the farmer accepted or refused the result against declared criteria. It cannot demonstrate the evolution of soil structure and soil life, a durable reduction of inputs, effects on yield, biodiversity or resilience, or life-cycle economic viability: those dimensions require complementary protocols, reference situations and multi-year observations at farm scale. The contribution of the format is to make such future observations **attributable** to identified, dated and documented missions.

3.4 The missing link: collecting what only the user knows and perceives

The limit is therefore no longer the specification of indicators but their **collection**. Three capture moments structure the solution, each associated with an actor and a piece of evidence: at the **editing of the `mission_order`**, the agronomic objective, acceptance criteria, known field obstacles and planned operating domain — case C3 shows the cost of an undeclared temporary obstacle; at the **upload to the robot**, confirmation by the operator that the robot, the implement, the crop and the environment present correspond to the described domain — case C2 shows that a localisation quality criterion must appear there; at the **end of the mission**, satisfaction with the work delivered, conditions actually encountered, effective supervision time — including when it results from a safety constraint, as in case C4 — and need for a repeat pass.

The design requirements are joint: pre-fill automatically everything that can be pre-filled, ask few questions, use units the farmer already handles, allow deferred validation, and place the interface where the person actually is. Four recommendations follow: embed in the `mission_order` a versioned operating domain with agronomic acceptance criteria and localisation thresholds; restrict event strategies to an explicit vocabulary, extensible but rejected by default when unsupported; build `work_performed` automatically before soliciting a few targeted human answers, and publish each indicator with its definition, convention, coverage and limits; and, because an open format allows new behaviours to be expressed, keep the machine sovereign in refusing those that fall outside its validated configuration.

3.5 Scope for diffusability, and limitations

The Agri JSON chain contributes to the appropriability, auditability and repairability of evidence, but it does not suffice to establish diffusability, which also depends on price, maintenance, skills and work organisation. As farms, third-party manufacturers, technical institutes and sector organisations produce and read the same files, the chain becomes an instrument of comparison, audit and negotiation. When agroecological benefits become tangible at farm level, the question will no longer be to measure them but to **attribute** them to precise interventions: that is the function the format prepares.

The study bears on a single manufacturer and 48 missions, with a non-random selection of instrumented days. All `work_performed` files are validated reconstructions, and the operator-dependent fields, entered retrospectively, remain incomplete and subject to recall bias. Hardware, software and questionnaire versions evolved over the period; the economic data are insufficient to establish a full cost; and the computation conventions retained preclude direct comparison with values published under other definitions.

4/ CONCLUSION

The Agri JSON format carries a continuous chain between agronomic intent and performed work, from the description of the authorised mission to the validation of the service delivered, by way of the attested simulation, the confrontation of the planned operating domain with the conditions observed, and the on-board verification of what the robot is able to execute safely.

Forty-eight missions suffice to establish that this chain produces a comparable factual exchange between actors, with a coverage of 90 to 98 % on the quantities measured by the machine. They suffice equally to establish what it does not yet produce. The five cases show that the determining variable — an agronomically justified human workload, the distance to the RTK base, an undeclared temporary obstacle, supervision imposed by a safety rule, or the match between implement and weed pressure — is almost never the one that automatic indicators put forward. The case of localisation is instructive: the RTK-fix time share is measured over 47 missions and clearly separates a nominal execution from a degraded one. A measured quantity becomes a criterion only if someone decides on the threshold and writes it into the mission. The priority is therefore twofold: to collect, in the right place, what only the operator knows, and to turn into ODD criteria the quantities the machine already knows how to produce.

This continuity makes responsibilities and gaps visible; it distinguishes a guidance failure, a missing field information, a poor implement–crop match, an underestimated human workload and an ill-formulated agronomic expectation. It cannot, however, turn a successful mission into proof of agroecological diffusability, which will require monitoring at the scale of the cropping system, of the farm and of the long run.

The contribution defended here is therefore a contribution of architecture. For agricultural robotics to spread and to serve the agroecological transition effectively, the performance of machines will not suffice: their actors must be able to describe, exchange and contest facts in a common vocabulary. The `mission_order–work_performed` pair, published under an open licence and implementable by a third party, is proposed as the foundation of that vocabulary.

Acknowledgements
The author thanks the market gardeners and winegrowers who hosted the missions analysed here and accepted that difficulties be documented as precisely as successes, as well as the SABI AGRI field and engineering teams.

Competing interests and status of the study. The author is president and CTO of SABI AGRI, the company that designs the robots studied and produces the software and the data analysed. This work is presented as an exploratory observational study accompanied by a reusable artefact, not as an independent evaluation: the inclusion rules, the computation conventions and the coverage of each indicator are published so that a third party may audit them. The data released are pseudonymised and aggregated.

Data and code availability. The Agri JSON schema, documentation and parser are released under CC BY 4.0, with Mission Studio and the navigation, geofencing and localisation components, in the `Sustainable-Robotics-Base-for-Crops` organisation on GitHub. Aggregated cohort statistics are available from the author; raw logs are not public owing to their volume and sensitivity.

References

- ISO 11783-10:2015. Tractors and machinery for agriculture and forestry — Serial control and communications data network — Part 10: Task controller and management information system data interchange. Geneva: International Organization for Standardization.
- ISO 18497-1:2024. Agricultural machinery and tractors — Safety of partially automated, semi-autonomous and autonomous machinery — Part 1: Machine design principles and vocabulary. Geneva: International Organization for Standardization.
- ISO 34503:2023. Road vehicles — Test scenarios for automated driving systems — Specification for operational design domain. Geneva: International Organization for Standardization.
- Lenain, R., Thuilot, B., Cariou, C., & Martinet, P. (2006). High accuracy path tracking for vehicles in presence of sliding: application to farm vehicle automatic guidance for agricultural tasks. Autonomous Robots, 21(1), 79–97. https://doi.org/10.1007/s10514-006-7806-4
- Prevault Osmani, A. (2025). When open source puts agricultural robotics at the service of agroecology. In Proceedings of the 8th AGRITECH DAY by AXEMA, Clermont-Ferrand, France, 15 October 2025.
- Prevault Osmani, A. (2026). SMOR white paper — Small, Modular, Open & Responsible. SABI AGRI, August 2026. https://github.com/Sustainable-Robotics-Base-for-Crops/ecosystem
- SABI AGRI / Sustainable Robotics Base for Crops. (2026). Agri JSON format, version 3 — schema, documentation and parser. CC BY 4.0. https://github.com/Sustainable-Robotics-Base-for-Crops/json_agri_format
- Wezel, A., Bellon, S., Doré, T., Francis, C., Vallod, D., & David, C. (2009). Agroecology as a science, a movement and a practice. A review. Agronomy for Sustainable Development, 29, 503–515. https://doi.org/10.1051/agro/2009004

Business Model Patterns in Agricultural Robotics: Evidence from European Firms

Mohammad Naim[*,a], Loïc Sauvée[a]
[a] InTerACT (UP 2018.C102), Institut Polytechnique UniLaSalle, Beauvais, France
[*] Corresponding author. Email: mohammad.naim@unilasalle.fr

Abstract

Agricultural robots are increasingly promoted as solutions to labour shortages, input reduction, and sustainability challenges in agriculture. While their technical performance has been widely examined, far less attention has been paid to how these technologies are commercialised and they establish a stable and reliable value proposition. This study addresses this gap by analysing current business models of agricultural robots' firms operating in Europe. Following Eisenhardt's theory-building protocol, the research proceeded through an inductive multiple-case study design, drawing on semi-structured interviews with 11 firms' representatives. Each case was coded using the Business Model Canvas, followed by systematic cross-case comparison.
Findings first reveal convergent patterns across firms, including hybrid revenue models combining robot sales with recurring software and service income, as well as intensive and long-term customer relationships. Building on the commonalities, the analysis identifies three business model archetypes: "tractor-replacement robot", "task-specific robots", and "livestock automation systems", which constitute the main contribution of the study. These archetypes reflect distinct configurations of value creation, customer engagement, and scaling logic. The study contributes to the literature on agricultural robots and servitization by shifting attention from technological feasibility to business model viability. On the practical aspect, the study offers information for manufacturers, policymakers, and researchers seeking to support the responsible and scalable diffusion of agricultural robots in Europe.

KEYWORDS: innovation adoption; servitization; agricultural machinery; precision agriculture; case study

Complexity level: 3

1/ INTRODUCTION

European agriculture is undergoing structural change driven by economic, environmental, and demographic pressures. Farms are expected to increase productivity while reducing chemical inputs and coping with persistent labour shortages (Finger, 2023; Holm et al., 2024). These constraints have accelerated interest in agricultural robots, defined as "mobile, autonomous, decision-making mechatronic devices that perform tasks under human supervision but without direct human labour" (Daum, 2021, p. 774). This definition implies that three types of operations concern agricultural robots: crop and soil management, data collection, and navigation and communication (Naim et al., 2025b). Agricultural robots can perform several key agricultural

tasks, including mechanical weeding, crop monitoring, targeted spraying, and harvesting (Barbosa Júnior et al., 2024; Cheng et al., 2023; Naim et al., 2025a). These capabilities rely on advances in machine vision and machine learning, which allow robots to recognise plants, detect weeds, and make decisions under field conditions characterised by uncertainty and variability of conditions, including weather conditions (Cheng et al., 2023; Hu et al., 2025).

However, engineering studies have emphasised how robots in general still face limitations related to general perception and safe interaction with humans and equipment (Bechar & Vigneault, 2017; Fountas et al., 2020). These constraints affect their reliability, which is a critical determinant of the economic value of an agricultural equipment (Ramin Shamshiri et al., 2018). Consequently, many robotic solutions remain effective only in narrowly defined tasks rather than across whole farming systems (Naim et al., 2025b). As a result, agricultural robots have progressed from experimental prototypes toward commercially trialled machines operating in vineyards, horticulture systems, and open-field crops (Naim et al., 2025a, 2025b).

At this point, the discussion moves from technology performance to market reality. Adoption research shows farmer adoption of agricultural robots is usually studied considering contextual information, like geographical localisation and local conditions, see e.g. (Degieter et al., 2023; Lemay & Boggs, 2024; Rübcke Von Veltheim et al., 2020; Rübcke von Veltheim et al., 2022; Rübcke von Veltheim & Heise, 2021), yet it shows that farmers evaluate innovations not only on technical capability but also on economic risk, operational complexity (i.e. ease of use), and service availability (Degieter et al., 2023; Lemay & Boggs, 2024). In agriculture, investment decisions are strongly influenced by uncertainty because machinery failures directly affect seasonal production outcomes (Lowenberg-DeBoer & Erickson, 2019). Therefore, adoption barriers include as well market-related determinants. On the supply side, addressing this topic requires moving beyond technology assessment toward systematic analysis of how firms organise and commercialise agricultural robots.

In innovation research, the business model is commonly used as an analytical unit to explain how firms create, deliver, and capture value from technological innovations (Teece, 2010). For emerging industries characterised by technological uncertainty and evolving markets such as agricultural robotics, analysing business models helps reveal viable commercial configurations and strategic patterns (Cavazza et al., 2023). At the same time, agricultural robots generate new forms of value beyond labour substitution intensively discussed in the literature and mentioned above. Automatic digital tasks (such as continuous sensing for data collection and monitoring) would offer new profit opportunities for agricultural robots' manufacturers and firms. In contrast, agricultural robots offer additional value through their ability to generate and use data during operation. Hence, this reality implies logically the presence of other value propositions highlighted and commercialised by manufacturers and firms to set agricultural robots on another level in comparison to conventional machinery and make them more attractive to farmers, influencing their decision and perception.

As noted, robotic technologies may require alternative deployment and service models rather than replication of conventional machinery commercialisation pathways. Traditional agricultural equipment markets rely on ownership-based sales of machines and implements distributed through dealer networks, assuming predictable operating environments and continuous large-area use (Al-Amin et al., 2023; Lowenberg-DeBoer et al., 2020). Such strategies function effectively in regions with large and homogeneous farms but become less efficient in fragmented agricultural landscapes where operations must adapt to variable field sizes, crop diversity, and discontinuous workloads (Guiomar et al., 2018; Herman, 2025). Research also shows that economic competitiveness of agricultural robots depends less on agronomic performance alone and more on organisational factors such as fleet management, routing efficiency, supervision

models, and after-sales service (Al-Amin et al., 2023; Lowenberg-DeBoer et al., 2020). Obviously, these elements are controlled primarily by firms' business models rather than by engineering design itself. Very few articles, if any compare in fact how different agricultural robots' firms structure value propositions and customer (in our case, majorly the farmer) access in the market. This poses a major research question:

RQ: What are the main value propositions under the spotlight in agricultural robots' commercialisation in Europe, and what position do firms take with respect to conventional machinery, especially tractors?

2/ MATERIALS AND METHODS

This study adopts the business model framework proposed by Osterwalder and Pigneur, which conceptualises a firm's business logic through interconnected components including, among others, value proposition, customer segments, revenue streams, and cost structure (Osterwalder, 2004; Osterwalder & Pigneur, 2013). Originally developed as a managerial tool, the framework has been widely applied in empirical research to systematically map and compare innovation-driven firms across industries, particularly in digital and technology-based sectors (Joyce & Paquin, 2016; Spieth et al., 2019). This framework, useful to visualise how European agricultural robot manufacturers organise their commercial strategies, was complemented by a multiple case study methodology, which provides a systematic protocol for theory building from comparative case analysis (Eisenhardt, 1989; Eisenhardt & Graebner, 2007). In this way, the identification of industry-level patterns was assured. It is worth noting that the Business Model Canvas (BMC) is employed as an analytical structuring model, not as a normative framework, allowing consistent reconstruction and comparison of firm-level business model logics (Osterwalder et al., 2005; Osterwalder & Pigneur, 2013). The BMC is a structured template that describes how a firm creates, delivers, and captures value through nine interrelated building blocks, enabling comparable, visual analysis across firms and contexts (Joyce & Paquin, 2016; Osterwalder et al., 2005), therefore it is deemed useful to represent the archetypes obtained from the cross-case analysis.

By adopting such a structured approach, it can be possible to identify business model archetypes for agricultural robots, which are recognisable configurations of business model elements shared by firms operating under similar technological and market conditions (Bütikofer et al., 2024; Duparc et al., 2022; Bocken et al., 2014). This study adopts an inductive multiple-case study design aimed at building mid-range theory on business model archetypes in agricultural robots. The methodological approach follows the theory-building logic articulated by Eisenhardt (1989) and further refined by Eisenhardt and Graebner (2007) (Figure 1).

2.1 Research protocol

Cases were selected using theoretical sampling (Eisenhardt, 1989). The sampling logic aimed to capture variation across market segments and commercialisation strategies within agricultural robots' firms.

Three basic inclusion criteria were adopted in this study. First, only companies that actively commercialise agricultural robots were included to exclude prototypes and ensure that the analysis focuses on technologies that have reached the market, in other words, their technology readiness level. Second, companies were required to have their headquarters or primary research and development activities located in Europe to ensure that all cases operate within a similar regulatory and policy context, including EU safety rules, agricultural policy, funding programmes, and sustainability objectives. By incorporating firms from several countries and application domains, the study strengthens analytical transferability and avoids overrepresenting a single

technological paradigm within agricultural robots' research. Third, companies needed at least two years of operational and commercial activity. This requirement ensures that firms have had sufficient time to test their technologies under real farming conditions, refine their products, and respond to customer feedback across more than one growing season, thereby strengthening the reliability of the analysis.

The primary data source consists of semi-structured interviews conducted with key informants directly involved in technology development and commercialisation. Interviewees covered a spectrum of organisational roles, including chief technology officers (CTOs), lead engineers, and managers responsible for commercial or regulatory affairs (Figure 1). For each company, the interview was conducted with the most responsive representative available, facilitating interactive data collection. Such informants are considered appropriate for capturing both technical and business model-related knowledge (Gioia et al., 2013). A common interview guide was used across cases to ensure comparability while retaining flexibility to pursue emergent themes, in line with best practices for inductive qualitative research (Eisenhardt & Graebner, 2007). Interviews were recorded and transcribed to ensure analytical rigor and traceability, and were stopped when no new findings emerged, following the principle of saturation outlined in the protocol. This approach is described in Figure 1.

For ethical and methodological reasons, company names were anonymised. Selective anonymisation is widely recognised in qualitative industry research as a pragmatic balance between transparency and confidentiality, especially when firms operate in small and specialised markets where full anonymisation could undermine analytical clarity (Saunders et al., 2015). In the agricultural robots' sector, publicly identifiable technological profiles and limited numbers of actors increase the risk that naming firms could expose commercially sensitive information or strategic positioning. Removing organisational identifiers reduces potential reputational or competitive harm while still allowing the reporting of meaningful contextual variables such as technological domain, geographic distribution, and innovation focus (Kang & Hwang, 2023).

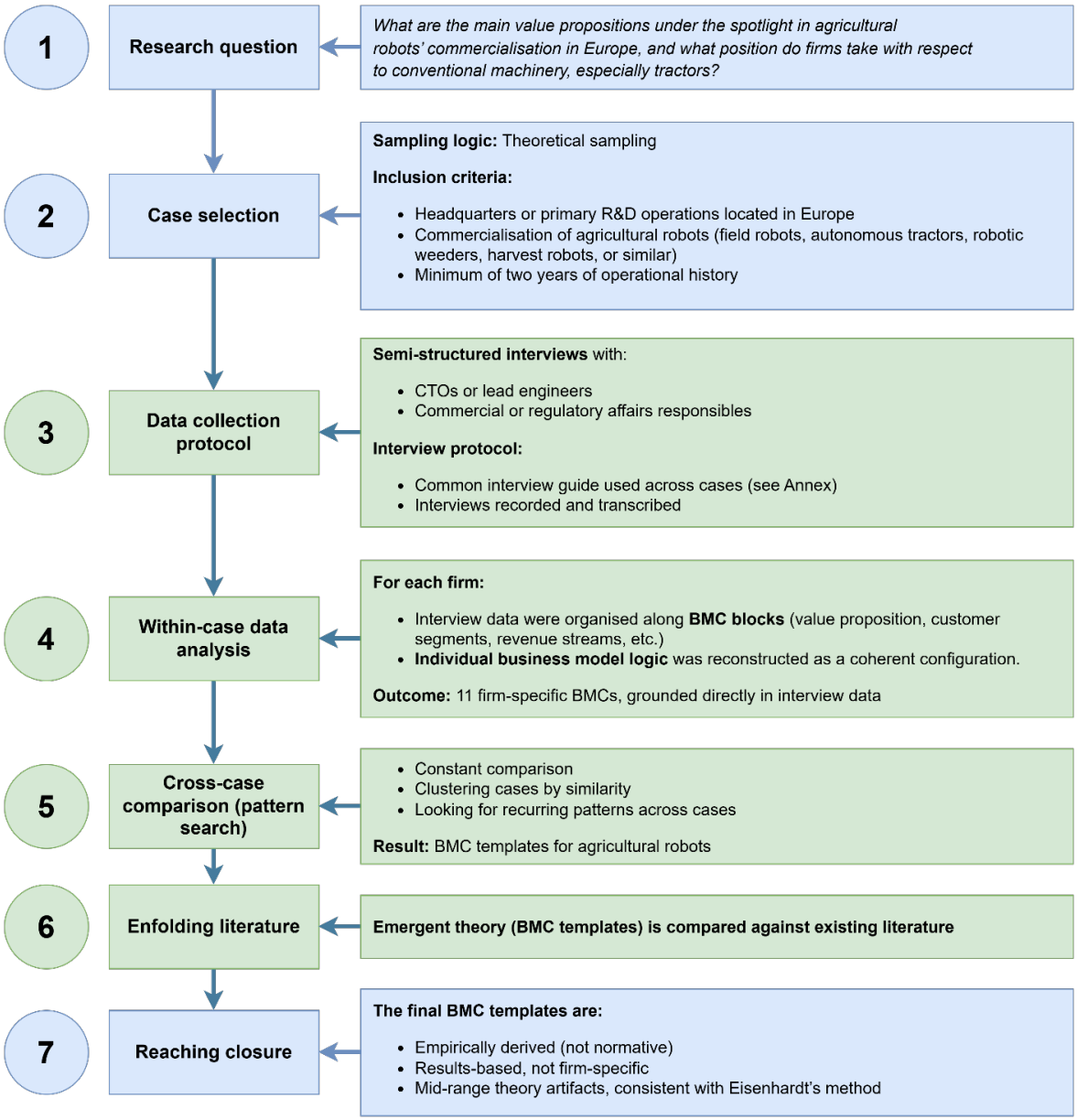


Figure 1: Research design and analytical process. Adapted from (Eisenhardt, 1989).

2.2 Sample description

A total of 11 firms headquartered in France, the Netherlands, Switzerland, Austria, and Denmark were selected (Table 1). This number falls within the range commonly recommended for inductive theory building, balancing analytical depth with cross-case comparability (Eisenhardt, 1989; Yin, 2018). The sample reflects the technological and organisational diversity of the European agricultural robots' sector, covering a broad range of robotic technologies. Such heterogeneity captures multiple innovation trajectories and market niches, which is particularly important in emerging technological sectors where development pathways vary according to agronomic context, regulatory environments, and business models (Klerkx et al., 2019).

The countries selected reflect not only firm-level diversity but also variation in national innovation contexts. They represent leading European contexts for agricultural innovation, characterised by advanced farming systems, strong engineering capabilities, and well-developed research and knowledge infrastructures (Klerkx et al., 2019; Pigford et al., 2018). In particular, the Netherlands

and Denmark are widely recognised for their highly productive and technologically intensive agricultural sectors, with early adoption of precision agriculture and automation technologies driven by high labour costs and strong policy support for digitalisation (Lowenberg-DeBoer & Erickson, 2019; OECD, 2019). France, as one of Europe's largest agricultural producers, combines a diverse agronomic landscape with a rapidly expanding agri-tech ecosystem and increasing investment in robots and digital farming solutions (Bellon-Maurel et al., 2023; OECD, 2019). Switzerland and Austria, while characterised by smaller-scale and more heterogeneous farming systems, contribute strong capabilities in mechanical engineering and niche innovation, particularly in specialised and high-value agricultural applications adapted to complex terrains (OECD, 2022; Petrović et al., 2024).

Case	Country Of Operation	Firm Maturity	Core Offering
C1	**Netherlands**	Growth-stage	Multipurpose autonomous field robots that perform end-to-end soil operations such as tillage, seeding, mowing, and mechanical weeding, enabling continuous operation while reducing reliance on manual labour.
C2	**Switzerland**	Growth-stage	Robot with an ultra-precise spraying system enabling drastic reduction of phytosanitary inputs through plant-level targeting, regulatory compliance, and environmental footprint reduction.
C3	**Netherlands**	Early-stage	Autonomous robots for repetitive manual field tasks (weeding, harrowing, mowing) aimed at reducing labour intensity, improving regularity of work, and operating with low soil impact.
C4	**Austria**	Mature	Offers livestock robotic solutions for automated feeding, feed distribution, and stable management, significantly reducing labour requirements in animal husbandry operations.
C5	**France**	Mature	Robot executing gentle, reliable, and continuous livestock practices with strong emphasis on milk quality, animal welfare, traceability, and long-term operational reliability
C6	**Denmark**	Growth-stage	Develops autonomous implement carriers for precision field operations such as sowing, weeding, and cultivation, enhancing operational accuracy while reducing soil compaction through lightweight automation.
C7	**France**	Growth-stage	Electric autonomous robot for vineyards providing herbicide-free inter-row work, soil preservation, labour relief, and precision operation in constrained environments.
C8	**France**	Growth-stage	Develops multipurpose autonomous field robots in cooperation with other partners and a modular autonomy system adaptable to existing tractors, tools, or robots, enabling safe and evolutive autonomous agricultural operations through software-driven integration.
C9	**France**	Established	Provides robotic systems for spraying and fertilisation combined with crop monitoring, enabling data-driven farming and optimisation of agricultural inputs.

C10	**Netherlands**	Mature	Develops integrated robotics for feeding and herd monitoring, and dairy robots, enabling full farm automation while generating detailed animal-level data for improved decision-making.
C11	**France**	Established	Designs robotic weeding systems focused on inter-row cultivation and soil aeration, reducing dependence on chemical inputs and promoting more sustainable farming practices.

Table 1: Core offerings of each of the firms selected for the analysis. Maturity scale (years since founding): Early-stage: <5 years, Growth-stage: 6–10 years, Established: 11–20 years, Mature: >20 years.

3/ RESULTS AND DISCUSSION

This section presents the findings of the study, offering a structured analysis of the recurring patterns identified across the examined cases. It first distils the key commonalities through subsections 3.1 to 3.3, then assembles these shared patterns into a set of coherent business model archetypes in subsection 3.4.

3.1 Strategic value architecture and market positioning

3.1.1 Convergence of value propositions

Across all cases, value propositions converge around four structural constraints affecting contemporary agriculture: (i) labour substitution, (ii) lower soil compaction, (iii) reduction of chemical inputs, and (iv) process or task stability and consistency.

Labour substitution is the most pervasive value proposition. All firms explicitly address labour shortages, although the framing varies across production systems. C1, C6, and C9 position autonomy as a direct substitute for tractor drivers, allowing continuous operation without dependence on skilled operators. C3, C7, and C11 emphasise the replacement of manual labour in repetitive and physically demanding tasks such as weeding, harrowing, and mowing. Livestock-oriented firms (C4, C5, and C10) adopt a different narrative, framing robots as a means of reallocating human labour from repetitive tasks toward supervision and higher value-added activities.

Across all cases, labour scarcity is therefore treated as a structural driver of adoption rather than as a marginal efficiency issue. Labour reduction is presented as increasingly important to farm continuity.

A second dominant value proposition concerns the reduction of physical externalities, particularly soil compaction. C1 and C6 highlight the lower weight of robots compared with conventional tractors, while C7, C8, and C11 extend this logic to specialised cropping systems where lightweight platforms are better adapted to narrow rows, slopes, and sensitive soils. In livestock systems, C4 and C10 apply a similar argument to feed compaction, linking it to feed quality and animal welfare.

A third value proposition relates to reducing chemical inputs and responding to environmental regulation. C2 most strongly reflects this positioning through precise plant-level targeting and drastic reductions in phytosanitary products. C7, C9, and C11 similarly connect mechanical weeding, precision spraying, and herbicide reduction with environmental certification and regulatory compliance. C8 presents input reduction as a secondary benefit of autonomy and precision, whereas C1 and C6 place comparatively less emphasis on it.

A fourth value proposition concerns task or process stability. Livestock-oriented firms (C4, C5, and C10) emphasise regular feeding or milking and greater predictability of production outcomes. C8 and C11 mobilise similar arguments in crop systems through uniform speed, consistent tool positioning, and repeatable trajectories. Robots are therefore positioned not only as productivity tools but also as assets capable of reducing operational variability and ensuring continuity.

3.1.2 Strategic positioning relative to tractors

Two main positioning strategies emerge: full tractor replacement and task-specific substitution. C1, C9 and, to a lesser extent, C6 adopt a tractor-replacement strategy. Their robots are positioned as functional equivalents to tractors, capable of operating standard implements and performing major field operations. Pricing is consequently benchmarked against conventional tractor economics (see (Naim et al., 2025a). This strategy implies high capital intensity, long sales cycles, and strong expectations regarding reliability, service availability, and residual value.
C8 represents a complementary approach in which autonomy can be added to existing machines. Its autonomy kit reduces switching costs and makes use of farmers' existing capital stock, while shifting part of the firm's value creation from manufacturing toward software, integration, and services.

C2, C3, C4, C5, C7, C10, and C11 instead position their technologies as task-specific systems with no direct tractor equivalent. This allows robots to be presented as new technological categories addressing specific problems, particularly in environments where conventional machinery is poorly adapted.

3.1.3 Software as a key player

All firms emphasise embedded intelligence, including navigation algorithms, perception systems, and decision-support software. C2, C6, C7, C8, and C11 particularly highlight the ability to integrate new crops, tools, or requirements through software updates, transforming robots from fixed assets into evolving technological systems.

Most firms also implement subscription-based models for software or data services. These subscriptions are generally associated with core functionalities such as monitoring, updates, and system optimisation rather than optional services. This generates recurring revenues and establishes longer-term relationships between farmers and firms.

Data generated through robotic systems also represent a strategic resource for algorithm development and differentiation. However, governance approaches differ. Some firms emphasise farmer visibility through remote monitoring interfaces, while others retain greater control over installation, system configuration, and data use. Software therefore contributes simultaneously to value creation, recurring revenue, and customer dependency.

3.2 Market and customer access

3.2.1 Customer relationship models

Customer relationships are substantially more intensive and long-term than those traditionally associated with traditional agricultural machinery (e.g. tractors). Robotic systems require continuous interaction through software platforms (although new tractors also follow this trend), diagnostics, maintenance, training, and technical support. C1, C2, C6, C7, and C8 maintain ongoing relationships through digital services, while livestock-oriented firms (C4, C5, and C10) provide particularly intensive support because feeding and milking systems are critical to daily operations.

Training is consequently an important component of customer relationships. C2, C7, C8, and C11 require initial training for commissioning, calibration, mapping, and configuration. C1 and C6 emphasise simpler "set-and-go" approaches but still provide basic onboarding, particularly for safety and compliance. Training as a result supports both value creation and risk reduction.
Firms also use different mechanisms to reduce farmers' perceived technological and financial risks. C1 employs rent-to-own mechanisms, while C3, C7, and C11 rely heavily on pilot farms, demonstrations, and reference users. Livestock firms reduce risk through preventive maintenance and rapid-response service commitments.

3.2.2 Distribution and channel structures

Distribution strategies balance technological complexity, market reach, and the need for local proximity. C1, C5, C6, and C9 rely strongly on established dealer networks, which provide local sales, installation, maintenance, and customer assurance. This accelerates market penetration but reduces firms' direct control over customer relationships and margins.

C2, C7, and C8 adopt hybrid models, combining direct sales in strategic markets with distributors elsewhere. This allows closer interaction with early adopters while supporting geographic expansion. C3 and C11 rely more heavily on direct sales, demonstrations, and professional fairs, reflecting their smaller scale and more specialised markets.

Across all cases, field demonstrations remain particularly important. Because agricultural robots are still unfamiliar to many farmers, visible proof of functionality plays a central role in adoption. Trade fairs, websites, videos, social media, and other communication channels complement demonstrations by creating awareness and legitimacy.

3.3 Economic structure and scaling logic

3.3.1 Revenue model architectures

Revenue structures reveal a departure from traditional agricultural machinery models. Although all firms derive revenue from initial equipment sales, most combine these with recurring revenues from software, services, maintenance, or consumables. This hybridisation reflects both the technological nature of robotic systems and firms' attempts to stabilise cash flows.
Physical equipment sales remain the dominant initial revenue source, especially for large field robots and livestock systems. C1, C6, and C9 operate at price levels comparable to conventional tractors or specialised machinery, while C4, C5, and C10 rely on substantial upfront investments justified by long service lives and operational centrality. C3, C7, and C11 operate at lower absolute price points because of their smaller and more specialised systems.

Software subscriptions, platform access, and licensing provide recurring revenues for C1, C2, C6, C7, C8, and C11. Livestock firms rely less on explicit software subscriptions but generate recurring revenues through maintenance and service contracts. Across the cases, this combination shifts the business model toward an "equipment-as-a-platform" logic.
Maintenance, spare parts, installation, calibration, training, and technical services provide additional revenues. Their relative importance varies by archetype, but they remain important complements to equipment sales and software-based revenues.

3.3.2 Cost structure characteristics

Despite differences in robot type and firm maturity, three cost categories dominate: research and development, production and assembly, and customer-facing support activities.

R&D represents the largest cost category for most firms. Costs are driven primarily by specialised human resources, software development, testing, prototyping, sensor integration, cybersecurity, and regulatory compliance. Importantly, R&D appears structural rather than transitional: firms do not expect innovation requirements to decline substantially as production volumes increase.

Hardware represents the second major cost block. Large field robots such as those developed by C1, C6, and C9 face high production and assembly costs because of their mechanical complexity and safety requirements. Smaller firms experience lower absolute costs but higher unit costs because of limited production volumes. Standardisation, modular architectures, and off-the-shelf components can reduce costs, although certification and robustness requirements limit these opportunities.

The third major cost category concerns customer-facing activities. Installation, training, maintenance, troubleshooting, and after-sales support remain labour-intensive and difficult to standardise. These costs are especially significant in livestock systems and during the commissioning of technologically complex robots. Customer support scales imperfectly with sales and represents an important constraint on rapid expansion.

3.3.3 Scalability constraints & organisational implications

Scalability emerges as a major structural constraint across most cases.
First, physical production imposes limits on growth. Assembly complexity, supplier availability, quality control, and customisation restrict production capacity. Even C8's kit-based model, which theoretically offers greater scalability, remains constrained by installation and adaptation requirements. Unlike software-only businesses (in general), physical production therefore remains a bottleneck.

Second, human resources constrain scalability. Firms depend on specialised engineers, technicians, agronomists, and AI or computer-vision experts whose recruitment and training are costly and time-consuming. In service-intensive contexts, particularly livestock, expansion is similarly limited by the availability of qualified technical personnel.

Third, demand-side factors affect market scalability. Adoption often requires changes in farming practices, technical competence, and risk tolerance. Interest in robotics does not necessarily translate rapidly into purchases, while mechanisms such as rent-to-own can reduce adoption barriers at the cost of greater financial exposure for firms. Market growth is shaped by both production capacity and farmers' sociotechnical readiness.

These constraints have direct organisational implications. Most firms simultaneously combine manufacturing, software development, and service provision, creating coordination costs that increase with scale. Larger firms develop greater functional specialisation, whereas smaller firms rely on polyvalent teams that increase flexibility but limit scalability.

Finally, several firms rely on public funding, innovation programmes, subsidies, leasing, or customer financing to offset high fixed costs. Such mechanisms support innovation and market entry but do not eliminate the structural cost pressures associated with agricultural robotics.

3.4 Archetypes

The case studies reveal three major business model archetypes clearly based on the commercialised equipment (Table 2): (i) tractor-replacement robots, (ii) task-specific robots, and

(iii) livestock automation systems. Each is characterised by a distinct combination of value creation, revenue and cost structures, customer relationships, and scalability constraints.

	Full Tractor Replacement	Task-Specific Robot	Livestock Automation
Customer Segments	Medium and large farms with high investment capacity	Farms seeking solutions for specific agricultural tasks	Livestock farms requiring reliable daily systems
Value Proposition	Autonomous replacement of conventional tractors	High-precision solutions for specific tasks	Reliability, operational continuity, and animal welfare
Channels	Hybrid direct and dealer distribution	Direct sales, demonstrations, and local networks	Direct or regional sales with strong installation support
Customer Relationships	Long sales cycles; strong reliability and support requirements	Demonstration- and training-intensive relationships	Long-term relationships with high switching costs
Revenue Streams	Equipment sales plus software and digital services	Robot sales plus software and service agreements	Equipment sales plus maintenance and service contracts
Key Resources	Algorithms, industrial hardware, and R&D capabilities	Adaptable software, algorithms, and robust hardware	Skilled service staff and integrated hardware-software infrastructure
Key Activities	R&D, integration, updates, testing, and optimisation	Software development, demonstrations, onboarding, and adaptation	Installation, calibration, monitoring, maintenance, and training
Key Partnerships	Hardware suppliers and dealers/distributors	Technology partners, suppliers, and demonstration farms	Hardware suppliers and regional service networks
Cost Structure	High hardware and R&D costs; limited economies of scale	Moderate hardware costs but high software, support, and customisation costs	High installation and service costs; scalability constrained by skilled labour

Table 2. The three business model archetypes and their corresponding characteristics

3.4.1 Full tractor replacement archetype

The tractor-replacement archetype includes C1, C6, and C9. These firms develop relatively large autonomous machines designed to replace or replicate conventional tractor-based operations. The technology is positioned as a core production asset, strongly shaping the associated business model.

1. Value creation centres on high-cost robotic systems expected to operate continuously and reliably under real farming conditions. Equipment sales constitute the main initial revenue source, complemented by recurring revenues from software, updates, and digital services required to maintain system performance.
2. Costs are dominated by hardware and continuous R&D. Industrial-grade components, sensors, batteries, perception technologies, navigation software, and system integration generate high fixed costs, while limited volumes restrict economies of scale.
3. Adoption is slow and risk-sensitive because farmers evaluate these robots as critical production assets. Reliability, uptime, and service availability therefore strongly influence purchasing decisions and contribute to long sales cycles.
4. Distribution generally follows a hybrid model combining direct sales in strategic markets with dealers or distributors for geographic expansion. Overall, this archetype is characterised by

high capital intensity and limited scalability, with growth constrained by production capacity, service capability, and the need to maintain operational reliability.

3.4.2 Task-specific archetype

The task-specific robot archetype includes C2, C3, C7, and C11. These firms develop specialised robots for dedicated agricultural tasks rather than replacing full-scale machinery. Their business model is therefore based on functional precision and operational specialisation.

1. Value creation centres on solving specific agronomic problems such as weeding or crop treatment, particularly where labour shortages, chemical reduction, or regulatory pressures create strong demand. Because these robots complement rather than replace existing equipment, adoption barriers are generally lower and the value proposition is easier to evaluate.
2. Revenue combines equipment sales with recurring software and service income. Although initial prices are generally lower than for tractor-replacement systems, continued software development, algorithm updates, and technical support remain central to long-term profitability.
3. Hardware costs are moderate, but software development, testing, customisation, onboarding, and support remain significant. Adoption relies strongly on field demonstrations and peer validation, producing gradual and geographically clustered diffusion.
4. Overall, scalability is constrained by customisation and continuing customer interaction. The archetype therefore favours controlled expansion, with success depending on sustained performance improvement, adaptability, and customer trust.

3.4.3 Livestock automation archetype

The livestock automation archetype includes C4, C5, and C10. These technologies are deeply embedded in daily farm operations and function as essential infrastructure, particularly for feeding, milking, and herd management.

1. Value creation is primarily based on reliability and operational continuity. Once installed, systems are difficult and costly to replace, resulting in high switching costs and long-term customer relationships.
2. Revenue combines initial equipment sales with substantial recurring income from maintenance, monitoring, software, and technical support. Service provision is therefore a core component of value capture rather than a secondary activity.
3. The cost structure is particularly labour-intensive. Installation, training, monitoring, and maintenance require skilled personnel and are difficult to automate or standardise. Human resource capacity consequently represents the main constraint on scalability.
4. System failure also carries significant operational risks because it can directly affect animal welfare and farm productivity. Customers therefore place strong emphasis on reliability, response time, and service quality.
5. Overall, this archetype is characterised by deep operational integration, strong customer lock-in, and high dependence on service capacity. Growth is relatively slow but predictable, with success determined primarily by reliability, service quality, and long-term trust.

4/ DISCUSSION

4.1 Boundary case and the limits of archetypal classification

While the analysis revealed three dominant business model archetypes, the case of C8 does not fully conform to any of them. Instead, it occupies an intermediate position that highlights important structural tensions in the commercialisation of agricultural robots. Unlike the full tractor-replacement, task-specific robots, or livestock systems archetypes, C8 does not market

a standalone solution. Rather, it provides a modular autonomy layer designed to be integrated into existing machines, positioning itself as an enabling technology rather than a complete product system.

This positioning fundamentally differentiates C8 from the other cases. Whereas the three archetypes are organised around ownership or operation of a physical robot, C8's value proposition centres on improving existing capital assets, the already owned equipment by the farmers and particularly tractors. This reduces upfront investment for farmers and avoids direct competition with established machinery manufacturers. At the same time, it shifts the firm's core activity away from mechanical production towards software development, systems integration, and safety certification (especially Machinery Directive 2006/42/EC).

From a theoretical perspective, this case aligns with literature on modular innovation and digital complementors rather than with classical servitization models. Prior research on digital platforms and modular technologies shows that firms can create value by embedding intelligence into existing systems, thereby lowering adoption barriers and accelerating diffusion (Gawer & Cusumano, 2014). C8 reflects this logic by decoupling autonomy from hardware ownership. However, unlike pure digital platforms, C8 remains constrained by physical integration, safety validation, and regulatory compliance, which limits scalability and prevents the emergence of network effects typically associated with platform markets.

The case also reveals important tensions in risk allocation and responsibility. By providing autonomy as a layer rather than as a complete system, C8 reduces farmers' capital exposure. Logically, liability, performance accountability, and safety assurance are distributed across multiple actors, including the tractor manufacturer, the autonomy provider, and the end user. This contrasts with the previous archetypes, where responsibility is more clearly concentrated within a single firm. The literature on socio-technical systems suggests that such distributed responsibility structures can slow adoption, as uncertainty over accountability increases perceived risk (Klerkx et al., 2019; Rogers, 2003). C8 illustrates this challenge clearly: while technically attractive, its model requires strong institutional alignment and clear governance mechanisms to scale effectively.

From a business model perspective, C8 also challenges the boundaries of the three archetypes by combining elements of each without fully belonging to any. The presence of such a boundary case has important theoretical implications. It suggests that the three archetypes identified in this study should not be interpreted as rigid categories but as dominant organisational logics within a broader design space. C8 demonstrates that alternative configurations are possible but face higher coordination costs and greater exposure to institutional uncertainty. This finding aligns with recent work on emerging technology markets, which shows that hybrid models often emerge during periods of technological transition but struggle to stabilise without strong ecosystem alignment or standardisation (Adner, 2017; Jacobides et al., 2018). The case of C8 reinforces the central argument of this study, that business model design, rather than technological sophistication alone, determines commercial viability in agricultural robots. It also highlights that future development of the sector may depend not only on improved robot performance, but on clearer interoperability standards that allow hybrid models to operate at scale.

4.2 Limitations and future research

This study has several limitations that should be acknowledged. First, the analysis is limited to firms with headquarters or main R&D activities in Europe. This choice improves comparability by controlling regulatory and policy conditions, but it limits the generalisability of the findings. Agricultural robots' markets outside Europe operate under different labour costs, farm structures,

and regulatory frameworks, which may lead to different business model configurations (OECD, 2021). Therefore, the results should be interpreted as context-specific and not universally applicable. Second, the study relies primarily on data provided by firm representatives. Although interviews were supported by secondary sources and, where and when possible, direct observation, the data may still reflect managerial perspectives and strategic framing. This introduces a potential risk of informant bias, particularly in relation to performance claims, technological maturity, or competitive positioning (Gioia et al., 2013). The absence of systematic input from farmers or end-users further limits knowledge into adoption barriers and real-world use conditions. Third, the research design is cross-sectional. Business models in agricultural robots are likely to evolve rapidly due to technological progress, regulatory change, and market learning. The study therefore captures business models at a single point in time and cannot explain how they develop or adapt over longer periods. Finally, while the BMC provides a clear and consistent analytical structure, it simplifies complex organisational and ecosystem dynamics. In particular, it does not fully capture inter-firm dependencies, platform dynamics, or the role of policy and institutions in shaping innovation trajectories (Osterwalder & Pigneur, 2013).

Nevertheless, our methodological approach enriched some perspectives on business model theory in three main directions. A first point is that it has demonstrated that the BM approach was useful in delineating archetypal forms, which were better understood as the concretisation of specific and transitional organisational forms rather than as enduring structures. Though, these archetypes played a valuable role and carried significant managerial implications: it has been widely shown that the value proposition was idiosyncratic, and this idiosyncrasy, according to our approach, could lead to a deeper understanding of the underlying links between the complexity of industry configurations and customer satisfaction. Next, the trend towards servitization and the definition of what constituted “materiality”, as observed in the agricultural robots’ industry, provided a useful illustration of what could occur and be observed in other industrial sectors, thereby paving the way for intersectoral comparative analysis. The replication of our BM methodology could, for instance, have helped to identify what was sector-specific in this trend towards servitization and what was more generic. Similarly, the respective roles of competitive and institutional environments in this servitization process shed light on the embeddedness of BM evolution in the medium to long term, allowing for the identification of both sector-specific and non-specific factors.

Finally, our approach moved beyond an overly simplistic dichotomy between product-centred and service-centred BMs, instead demonstrating the potential for hybridisation between the two. In line with this reasoning, we suggested that further theoretical investigation was needed regarding the categorisation of services, as proposed by authors such as Frank et al. (2019). Indeed, future research could address the research scope in several ways. Longitudinal studies would allow analysis of how business models evolve as firms scale or face market and regulatory changes. Comparative studies including non-European firms could improve external validity and highlight the role of institutional context. Finally, quantitative or mixed-methods studies could be used to test whether the business model archetypes identified here are associated with performance outcomes such as adoption speed, profitability, or long-term viability.

5/ CONCLUSION

This study examined how agricultural robots’ firms in Europe structure their business models and why commercial outcomes vary despite comparable technological ambitions. Using an inductive multiple-case approach informed by Eisenhardt’s methodology, the analysis identified three recurring business model archetypes and clarified how value creation, revenue logic, and organisational design interact in this sector. The findings indicate that commercial success in agricultural robots is shaped as much by organisational and service-related capabilities as by

technical performance. Across all cases, long-term viability depends on firms' ability to provide reliable support, manage operational risk, and maintain close relationships with users. Manufacturing capacity alone is insufficient; growth is constrained primarily by physical production bottlenecks, demand-offer friction, and human resource availability. By linking business model design to adoption dynamics, the study helps explain the uneven diffusion of agricultural robots across Europe. The resulting business model framework offers practical guidance for firms developing commercial strategies and for policymakers aiming to support effective deployment of robotic technologies. In conclusion, the findings underline that progress in agricultural robots depends as much on business model innovation as on technological advancement.

Acknowledgements

This research was financed in the framework of NINSAR project by ANR under France 2030 (grant n. ANR-22-PEAE-0007). The authors would like to thank the 5th-year Agricultural Machinery students at UniLaSalle Beauvais for their assistance in the investigation process. A CC-BY public copyright license has been applied to the present document and will apply to all subsequent versions up to the author accepted manuscript arising from this submission, under the grant's open access conditions.

References

1. Adner, R. (2017). Ecosystem as Structure: An Actionable Construct for Strategy. Journal of Management, 43(1), 39–58. https://doi.org/10.1177/0149206316678451
2. Al-Amin, A. K. M. A., Lowenberg-DeBoer, J., Franklin, K., & Behrendt, K. (2023). Economics of field size and shape for autonomous crop machines. Precision Agriculture, 24(5), 1738–1765. https://doi.org/10.1007/s11119-023-10016-w
3. Barbosa Júnior, M. R., Santos, R. G. D., Sales, L. D. A., & Oliveira, L. P. D. (2024). Advancements in Agricultural Ground Robots for Specialty Crops: An Overview of Innovations, Challenges, and Prospects. Plants, 13(23). Scopus. https://doi.org/10.3390/plants13233372
4. Bechar, A., & Vigneault, C. (2017). Agricultural robots for field operations. Part 2: Operations and systems. Biosystems Engineering, 153, 110–128. Scopus. https://doi.org/10.1016/j.biosystemseng.2016.11.004
5. Bellon-Maurel, V., Piot-Lepetit, I., Lachia, N., & Tisseyre, B. (2023). Digital agriculture in Europe and in France: Which organisations can boost adoption levels? Crop & Pasture Science, 74(6), 573–585. https://doi.org/10.1071/CP22065
6. Bocken, N. M. P., Short, S. W., Rana, P., & Evans, S. (2014). A literature and practice review to develop sustainable business model archetypes. Journal of Cleaner Production, 65, 42–56. https://doi.org/10.1016/j.jclepro.2013.11.039
7. Bütikofer, L., Goodwin, C. E. D., Varma, V., Evans, P. M., Redhead, J. W., Bullock, J. M., Pywell, R. F., Mead, A., Richter, G. M., & Storkey, J. (2024). Identifying pathways to more sustainable farming using archetypes and multi-objective optimisation. Ecological Indicators, 166, 112433. https://doi.org/10.1016/j.ecolind.2024.112433
8. Cavazza, A., Dal Mas, F., Paoloni, P., & Manzo, M. (2023). Artificial intelligence and new business models in agriculture: A structured literature review and future research agenda. British Food Journal, 125(13), 436–461. https://doi.org/10.1108/BFJ-02-2023-0132
9. Cheng, C., Fu, J., Su, H., & Ren, L. (2023). Recent Advancements in Agriculture Robots: Benefits and Challenges. Machines, 11(1), 48. https://doi.org/10.3390/machines11010048
10. Daum, T. (2021). Farm robots: Ecological utopia or dystopia? Trends in Ecology & Evolution, 36(9), 774–777. https://doi.org/10.1016/j.tree.2021.06.002
11. Degieter, M., De Steur, H., Tran, D., Gellynck, X., & Schouteten, J. J. (2023). Farmers' acceptance of robotics and unmanned aerial vehicles: A systematic review. Agronomy Journal, 115(5), 2159–2173. Scopus. https://doi.org/10.1002/agj2.21427

12. Duparc, E., Möller, F., Jussen, I., Stachon, M., Algac, S., & Otto, B. (2022). Archetypes of open-source business models. Electronic Markets, 32(2), 727–745. https://doi.org/10.1007/s12525-022-00557-9
13. Eisenhardt, K. M. (1989). Building Theories from Case Study Research. The Academy of Management Review, 14(4), 532. https://doi.org/10.2307/258557
14. Eisenhardt, K. M., & Graebner, M. E. (2007). Theory Building From Cases: Opportunities And Challenges. Academy of Management Journal, 50(1), 25–32. https://doi.org/10.5465/amj.2007.24160888
15. Finger, R. (2023). Digital innovations for sustainable and resilient agricultural systems. European Review of Agricultural Economics, 50(4), 1277–1309. https://doi.org/10.1093/erae/jbad021
16. Fountas, S., Mylonas, N., Malounas, I., Rodias, E., Hellmann Santos, C., & Pekkeriet, E. (2020). Agricultural Robotics for Field Operations. Sensors, 20(9), 2672. https://doi.org/10.3390/s20092672
17. Frank, A. G., Mendes, G. H. S., Ayala, N. F., & Ghezzi, A. (2019). Servitization and Industry 4.0 convergence in the digital transformation of product firms: A business model innovation perspective. Technological Forecasting and Social Change, 141, 341–351. https://doi.org/10.1016/j.techfore.2019.01.014
18. Gawer, A., & Cusumano, M. A. (2014). Industry Platforms and Ecosystem Innovation. Journal of Product Innovation Management, 31(3), 417–433. https://doi.org/10.1111/jpim.12105
19. Gioia, D. A., Corley, K. G., & Hamilton, A. L. (2013). Seeking Qualitative Rigor in Inductive Research: Notes on the Gioia Methodology. Organizational Research Methods, 16(1), 15–31. https://doi.org/10.1177/1094428112452151
20. Guiomar, N., Godinho, S., Pinto-Correia, T., Almeida, M., Bartolini, F., Bezák, P., Biró, M., Bjørkhaug, H., Bojnec, Š., Brunori, G., Corazzin, M., Czekaj, M., Davidova, S., Kania, J., Kristensen, S., Marraccini, E., Molnár, Zs., Niedermayr, J., O'Rourke, E., … Wästfelt, A. (2018). Typology and distribution of small farms in Europe: Towards a better picture. Land Use Policy, 75, 784–798. https://doi.org/10.1016/j.landusepol.2018.04.012
21. Herman, E. (2025). Changes and Challenges in EU Agricultural Holdings and Their Impact on Rural Development. Land, 14(5), 1080. https://doi.org/10.3390/land14051080
22. Holm, S., Pedersen, S. M., & Tamirat, T. W. (2024). Robots in agriculture – A case-based discussion of ethical concerns on job loss, responsibility, and data control. Smart Agricultural Technology, 9, 100633. https://doi.org/10.1016/j.atech.2024.100633
23. Hu, F., Wu, F., Gu, H., Abbas, G., Alanazi, M. D., Othmen, S., Wang, J., & Zhang, T. (2025). Transforming Agriculture with Advanced Robotic Decision Systems via Deep Recurrent Learning. Expert Systems with Applications, 259, 125123. https://doi.org/10.1016/j.eswa.2024.125123
24. Jacobides, M. G., Cennamo, C., & Gawer, A. (2018). Towards a theory of ecosystems. Strategic Management Journal, 39(8), 2255–2276. https://doi.org/10.1002/smj.2904
25. Joyce, A., & Paquin, R. L. (2016). The triple layered business model canvas: A tool to design more sustainable business models. Journal of Cleaner Production, 135, 1474–1486. https://doi.org/10.1016/j.jclepro.2016.06.067
26. KANG, E., & HWANG, H.-J. (2023). The Importance of Anonymity and Confidentiality for Conducting Survey Research. Journal of Research and Publication Ethics, 4(1), 1–7. https://doi.org/10.15722/JRPE.4.1.202303.1
27. Klerkx, L., Jakku, E., & Labarthe, P. (2019). A review of social science on digital agriculture, smart farming and agriculture 4.0: New contributions and a future research agenda. NJAS: Wageningen Journal of Life Sciences, 90–91(1), 1–16. https://doi.org/10.1016/j.njas.2019.100315
28. Lemay, M. A., & Boggs, J. (2024). Determinants of adoption of automation and robotics technology in the agriculture sector–A mixed methods, narrative, interpretive knowledge

synthesis. PLOS Sustainability and Transformation, 3(11), e0000110. https://doi.org/10.1371/journal.pstr.0000110
29. Lowenberg-DeBoer, J., & Erickson, B. (2019). Setting the Record Straight on Precision Agriculture Adoption. Agronomy Journal, 111(4), 1552–1569. https://doi.org/10.2134/agronj2018.12.0779
30. Lowenberg-DeBoer, J., Huang, I. Y., Grigoriadis, V., & Blackmore, S. (2020). Economics of robots and automation in field crop production. Precision Agriculture, 21(2), 278–299. https://doi.org/10.1007/s11119-019-09667-5
31. Naim, M., Rizzo, D., Sauvée, L., & Medici, M. (2025a). A systematic classification of agrobots to inform farmers' choice and clarify market development. In J. V. Stafford (Ed.), Precision agriculture 25 (SET TWO VOLUMES) (pp. 991–997). Brill | Wageningen Academic. https://doi.org/10.1163/9789004725232_130
32. Naim, M., Rizzo, D., Sauvée, L., & Medici, M. (2025b). Advancing agroecology and sustainability with agricultural robots at field level: A scoping review. Computers and Electronics in Agriculture, 237, 110650. https://doi.org/10.1016/j.compag.2025.110650
33. OECD. (2019). Digital Opportunities for Better Agricultural Policies. OECD Publishing.
34. OECD. (2021). Agricultural Policy Monitoring and Evaluation 2021 Addressing the Challenges Facing Food Systems. OECD Publishing.
35. OECD. (2022). Enhancing Innovation in Rural Regions of Switzerland (1st ed). Organization for Economic Cooperation & Development.
36. Osterwalder, A. (2004). The business model ontology a proposition in a design science approach. https://doi.org/10.22005/BCU.15985
37. Osterwalder, A., & Pigneur, Y. (2013). Business model generation: A handbook for visionaries, game changers, and challengers. Wiley&Sons.
38. Osterwalder, A., Pigneur, Y., & Tucci, C. L. (2005). Clarifying Business Models: Origins, Present, and Future of the Concept. Communications of the Association for Information Systems, 16. https://doi.org/10.17705/1CAIS.01601
39. Petrović, B., Bumbálek, R., Zoubek, T., Kuneš, R., Smutný, L., & Bartoš, P. (2024). Application of precision agriculture technologies in Central Europe-review. Journal of Agriculture and Food Research, 15, 101048. https://doi.org/10.1016/j.jafr.2024.101048
40. Pigford, A.-A. E., Hickey, G. M., & Klerkx, L. (2018). Beyond agricultural innovation systems? Exploring an agricultural innovation ecosystems approach for niche design and development in sustainability transitions. Agricultural Systems, 164, 116–121. https://doi.org/10.1016/j.agsy.2018.04.007
41. Ramin Shamshiri, R., Weltzien, C., A. Hameed, I., J. Yule, I., E. Grift, T., K. Balasundram, S., Pitonakova, L., Ahmad, D., & Chowdhary, G. (2018). Research and development in agricultural robotics: A perspective of digital farming. International Journal of Agricultural and Biological Engineering, 11(4), 1–11. https://doi.org/10.25165/j.ijabe.20181104.4278
42. Rogers, E. M. (2003). Diffusion of innovations (5th ed). Free Press.
43. Rübcke Von Veltheim, F., Claussen, F., & Heise, H. (2020). Autonomous Field Robots in Agriculture: A Qualitative Analysis of User Acceptance According to Different Agricultural Machinery Companies. https://doi.org/10.22004/AG.ECON.305587
44. Rübcke von Veltheim, F., & Heise, H. (2021). German Farmers' Attitudes on Adopting Autonomous Field Robots: An Empirical Survey. Agriculture, 11(3), 216. https://doi.org/10.3390/agriculture11030216
45. Rübcke von Veltheim, F., Theuvsen, L., & Heise, H. (2022). German farmers' intention to use autonomous field robots: A PLS-analysis. Precision Agriculture, 23(2), 670–697. https://doi.org/10.1007/s11119-021-09854-3
46. Saunders, B., Kitzinger, J., & Kitzinger, C. (2015). Anonymising interview data: Challenges and compromise in practice. Qualitative Research, 15(5), 616–632. https://doi.org/10.1177/1468794114550439

47. Spieth, P., Schneider, S., Clauß, T., & Eichenberg, D. (2019). Value drivers of social businesses: A business model perspective. Long Range Planning, 52(3), 427–444. https://doi.org/10.1016/j.lrp.2018.04.004
48. Teece, D. J. (2010). Business Models, Business Strategy and Innovation. Long Range Planning, 43(2–3), 172–194. https://doi.org/10.1016/j.lrp.2009.07.003
49. Yin, R. K. (2018). Case study research and applications: Design and methods (Sixth edition). SAGE.

Development and evaluation of an air confined spraying device to reduce spray drift in viticulture

Mathilde GUICHARD*, Vincent de RUDNICKI

Contributors: Raphael CHERFAN, INRAE, FLUENT modelling; Jean François BONICEL, INRAE, mechanical design; Eric ZOPPELARI, AIREEDIC, modelling

* Corresponding author. Email: mathilde.guichard@bliss-ecospray.com

Abstract

Reducing spray drift from plant protection products is a major challenge in limiting the environmental and health impacts of vineyard spraying. This study presents the design and evaluation of a face-to-face spraying device based on an air-confined system principle, in which a continuous peripheral air curtain forms an immaterial barrier around the spray jets. The device geometry was developed through an iterative approach combining computational fluid dynamics (CFD) simulations, prototyping and experimental flow characterization. Airborne drift reduction was then evaluated on the French Vine and Wine Institute's EOLEDRIFT test bench at two stages of canopy development, using conventional nozzles and air-induction nozzles.

Compared with the test-bench reference values, the device fitted with conventional nozzles achieved average drift reductions of approximately 70% in early growth and 76% at full canopy. With air-induction nozzles, the corresponding reductions reached 95.5% and 97.5%. These results demonstrate the ability of the complete device to greatly limit off-target losses without the use of physical containment panels. Additional trials combining several air-curtain velocities, application rates and canopy-development stages would make it possible to isolate the specific contribution of air-confined system and optimize its settings.

KEYWORDS: Viticulture, crop protection, drift, environment, air-confined system

Complexity level: 2

1/ INTRODUCTION

"Spray drift is the quantity of plant protection product carried out of the sprayed (treated) area by air currents during application" (ISO 22866, 2005). It depends in particular on the equipment used (sprayer type, pressure and nozzles), the co-formulants and any adjuvants added to the product (F. Griesang et al., 2017), the crop being treated (development, height and porosity), and weather conditions such as temperature and wind at the time of treatment. Product losses are significant, ranging from 10 to 45% on the ground and from 15 to 40% in the air (Bedos C., Douzals J.P. et al., 2020).

The design of the spray downpipes and the types of nozzle used are key factors in reducing drift.

Various technical solutions have been implemented to reduce losses of sprayed products. One example is the face-to-face sprayer with recovery panels and air-induction nozzles, whose droplet ballistics reduce the risk of airborne transport and therefore make them less susceptible to spray drift (Bedos C., Douzals J.P. et al., 2020). Compared with a conventional sprayer, the use of panel sprayers reduces off-target losses without compromising overall application quality (Jamar et al., 2010). Nevertheless, the literature highlights limitations of this technology, including purchase cost, restriction to relatively flat topographies, longer field-operation times and longer cleaning times (Carra M. et al., 2017).

These limitations motivated a research project aimed at developing a solution capable of limiting the transverse dispersion of droplets without using a physical barrier around the row. This paradigm shift seeks not to address the limitations of treatment-equipment designs through an incremental drift-mitigation solution, but to eliminate the source of drift directly. Accordingly, an air-curtain containment system, also referred to as “air-confined system”, was investigated to overcome the limitations of existing technologies for trellised crops, particularly grapevines.
The objective of this research is to develop a prototype using this air-confined spraying system that can effectively reduce drift without physical containment, and to measure the system’s drift-reduction performance on an official French Vine and Wine Institute test bench known as EOLEDRIFT (Codis, S., et al., 2024). The system of downpipes resulting from the study has been named BLISS for “Blade Low Impact Spray System”.

2/ MATERIALS AND METHODS

2.1 Principle selected: air-curtain containment

Air-curtain containment is a technique used in sensitive environments (laboratories, hospitals, the nuclear industry and clean rooms) to control airflow and prevent the spread of particles or contaminants by maintaining specific positive or negative pressures in confined spaces.

It uses one or more laminar air curtains to isolate a volume from external contaminants or, conversely, to protect the outside environment from contamination.

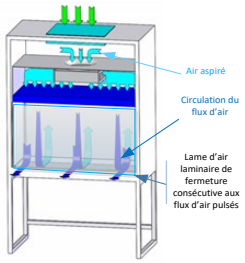


Figure 1 : Vertical laminar-flow hood



Figure 2: Air-curtain principle (KERMAZ)

Air curtains derive much of their effectiveness from the Coandă effect (Kadosch M., 1958). In an air curtain, the primary flow of compressed air expelled at high velocity through a narrow slot entrains the surrounding ambient air, producing an amplified, uniform, dense and powerful jet. In air-curtain systems, a primary chamber of a specific volume pressurises a substantial volume of air upstream of the slot, thereby producing uniform pressure along the entire length of the curtain. An amplification ratio of 30:1 (entrained air/compressed air) is produced (Dong-Won Lee et al., 2007), making it possible to obtain a uniform velocity along the entire curtain.

These properties led to an investigation into whether the air-curtain principle, originally used in laboratories and clean rooms, could be transferred to spraying in order to contain the sprayed product and reduce drift.

2.2 Ring design

Transferring the air-curtain system to a spray downpipe required several technological barriers to be overcome during design: (i) adapting the air-curtain principle to an air ring while avoiding turbulence at the junctions between straight air curtains; (ii) creating sufficient, homogeneous pressure upstream of the slot to generate the desired air curtain; and (iii) obtaining a controlled outlet velocity around the entire ring to ensure containment and application quality. The design was produced using CATIA 5.0 software.

2.2.1 Barrier 1: Adapting the air-curtain principle to face-to-face spraying—how can droplets be enclosed within an immaterial barrier?

The first barrier concerns adapting an air-curtain system, which is normally rectilinear, to the geometry of a vineyard spray downpipe. The aim of the study was to design genuine, complete containment on every relevant face of the treatment device around the vine row: front, rear, top, bottom and the two sides of the row. Enclosing the sprays therefore requires consideration of all six faces of the treatment volume.

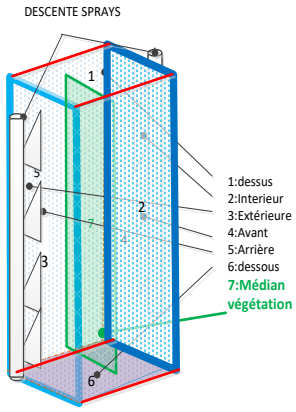


Figure 3: Containment on all six faces of the treatment volume

Closing the air-confined system in this way would have required four horizontally oriented air curtains in a parallelepiped arrangement (Figure 3), and therefore four blower units. In addition, the intersections between the curtains would have created discontinuities and strong turbulence liable to promote local droplet escape.

To overcome this phenomenon, the selected solution connects the curtains using a rounded section with a sufficiently large radius to ensure curtain continuity. This approach led to the design of an oblong ring with rounded ends surrounding the spray nozzles, hereinafter referred to as an “air-curtain tube”.

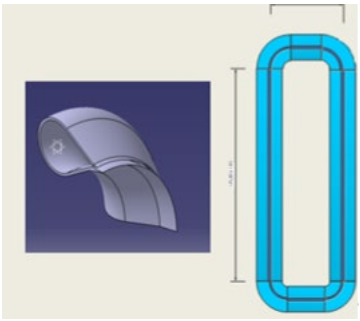


Figure 4: Teardrop profile and rounded ring section

2.2.2 Barrier 2: Creating sufficient pressure upstream of the blowing slot

The second barrier is the need to create sufficient pressure upstream of the air-curtain outlet to generate the Coandă effect and obtain an amplified, uniform, dense and powerful air curtain. This requires a profile that provides a large volume and increases pressure towards the outlet while promoting air circulation around the entire ring.

A specific prototype profile, known as the “teardrop profile” (Figure 5), was designed for this purpose. Its internal cross-section forms a plenum whose volume distributes the air before it passes through the peripheral slot.

The progressive reduction in cross-section towards the outlet then accelerates the flow and converts the available pressure into velocity (Figure 6).

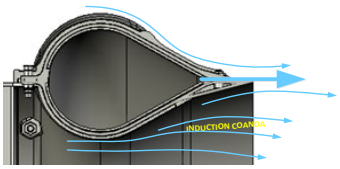


Figure 5: Curtain at the profile tip

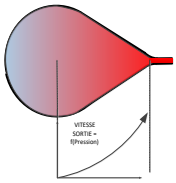


Figure 6: Increase in pressure and velocity through the teardrop profile

2.2.3 Barrier 3: Achieving uniform velocity around the entire perimeter

The third technological barrier associated with the ring design, which remains poorly documented in the scientific literature, concerns the continuity of the air outlet velocity around the entire ring perimeter.

The position of the air generator on the ring influences the pressure distribution and, consequently, the circulation of flow within the ring.

The air generator is positioned longitudinally at the ring’s front vertical curtain. This creates continuous airflow at constant pressure and equal velocity around the entire ring perimeter, and therefore a nearly constant outlet velocity at every point along the air curtain (Figure 7).

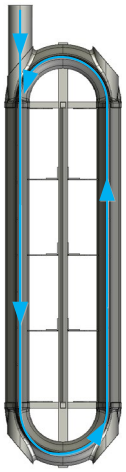


Figure 7: Operating principle of the air-curtain ring

2.3 CFD simulation

The device was designed with the support of several computational fluid dynamics (CFD) studies conducted using Fluent and OpenFOAM. CFD involves numerically solving the equations that describe fluid flow in order to determine, for a given geometry and set of boundary conditions, the pressure and velocity fields, streamlines and turbulent phenomena. The simulations were used to characterize the operation of the peripheral air jet produced—more specifically, to visualize the jet’s shape, expansion and trajectory—and thus to assess the flow’s ability to contain and transport droplets to their target. Several series of iterations guided the sizing of the profile, the ring’s internal layout and the selection of configurations subsequently evaluated on a prototype.

2.4 Prototype production and air-velocity measurements

The simulations were supplemented by prototype manufacture in order to take measurements on a physical ring and verify the air velocity distribution and reach of the air curtain.

The prototype rings were supplied with air by individual turbines and installed on a support frame hitched to a tractor, allowing the rings to be placed in their operating position and the turbines to be run. Velocity measurements to verify the distribution around the ring were taken using a VOLTCRAFT VPT 100 anemometer fitted with a Pitot tube and measuring air velocity in m/s. Because of the shape and narrowness of the slot, direct measurement with the Pitot tube was insufficiently repeatable, and a special tip was required. Designed specifically for the shape of the ring slot, it was produced using a 3D printer. The Pitot tube was thus positioned exactly at the air-curtain outlet and always at the same angle, allowing repeatable measurements regardless of the operator (Figure 9).



Figure 8: Prototype version of the spray downpipes



Figure 9: Positioning the Pitot tube on the slot using the special tip

2.5 EOLEDRIFT protocol

The ability of the air-curtain containment system to reduce airborne drift was evaluated by IFV (French Wine and Vineyard Institute), with support from INRAE (National Institute of Agricultural Research), on the EOLEDRIFT test bench. A Calvet SP Eco+ 2MR face-to-face sprayer fitted with production-version spray downpipes (Figure 10) was tested on an artificial grapevine reproducing two stages of canopy development: early growth and full canopy. Four treatments were studied by combining these two stages with conventional Albuz ATI 80 0075 nozzles or Albuz TVI 80 0075 air-induction nozzles. Travel speed was 5.9 $km \cdot h^{-1}$, and the settings followed the StopDrift project recommendations to reproduce conditions representative of vineyard use (Codis, S., et al., 2024).



Figure 10: Calvet sprayer fitted with BLISS spray downpipes

The results, expressed as a percentage of the full-area application rate, were compared with EOLEDRIFT test-bench reference values established from 15 trials conducted with three pneumatic arch sprayers. Reduction classes of 66, 75, 90 and 95% were determined using two criteria: average drift across the entire collection plane and vertical-profile values between 0 and 3.5 m.

3/ RESULTS AND DISCUSSION

3.1 CFD results: validation of the peripheral air jet

The 2D CFD simulations characterized the flow generated at the outlet of the teardrop-shaped profile. The jet shape, transverse expansion and axial decay were consistent with the general behavior of a free plane jet (i.e. the two-dimensional flow of a fluid escaping through a long, narrow slot into an unconfined ambient space) (Figure 12).

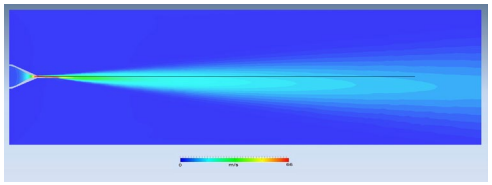


Figure 12: CFD modelling of the BLISS profile principle

The comparison of normalized velocities (U/Umax) also shows that the jet produced by the profile maintained its velocity over a greater distance than estimated from the theoretical relationships used for the reference plane jets (Figure 13). The air curtain therefore retains a high velocity up to several tens of centimetres from the ring.

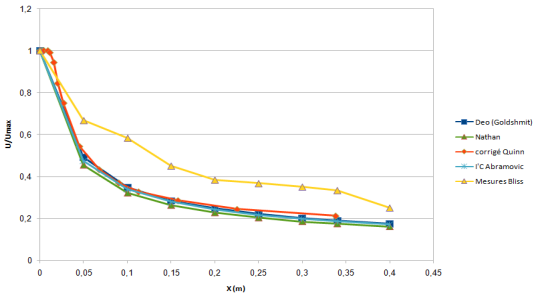


Figure 13: Comparison of literature reference values and BLISS measurements. Change in air velocity as a function of longitudinal position x (m) (AIREEDIC)

These results confirmed that the air-curtain principle could be transferred to a face-to-face spray downpipe. The measured jet reach appears compatible with the distance between the nozzles and the canopy, and maintains flow directed towards the vegetation.

3.2 Selected prototype and main characteristics

Following the modelling, design and aeraulic characterization phases, the selected solution was a spray downpipe consisting of an oblong tubular ring with rounded ends and a teardrop-shaped cross-sectional profile.

The air-curtain tube encloses the opposing sprays as far as the vegetation and carries them deep into the canopy in the same way as a conventional air-assisted jet.

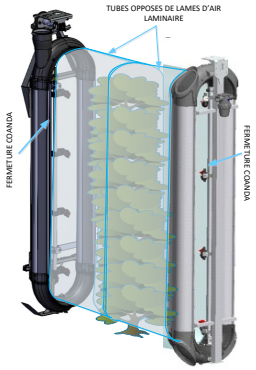


Figure 6. Comparison of driving speed and fuel consumption in the mower cycle.

The design of an oblong tubular form with rounded ends made it possible to connect the different portions of the blowing slot without creating intersections between multiple rectilinear jets. The prototype thus produces a closed, continuous peripheral jet around the nozzles.

While the air-curtain tubes enclose the sprays up to the vegetation, Coandă-induced suction inside each air ring prevents droplets from escaping through the rear (Figure 17a).

The average air velocity induced by the Coandă effect at the center of the ring is approximately 3 m/s (Figure 12b). This corresponds to an average entrained airflow of 2,000 m^3/h, which constrains the droplets within the ring and carries them towards the vegetation.

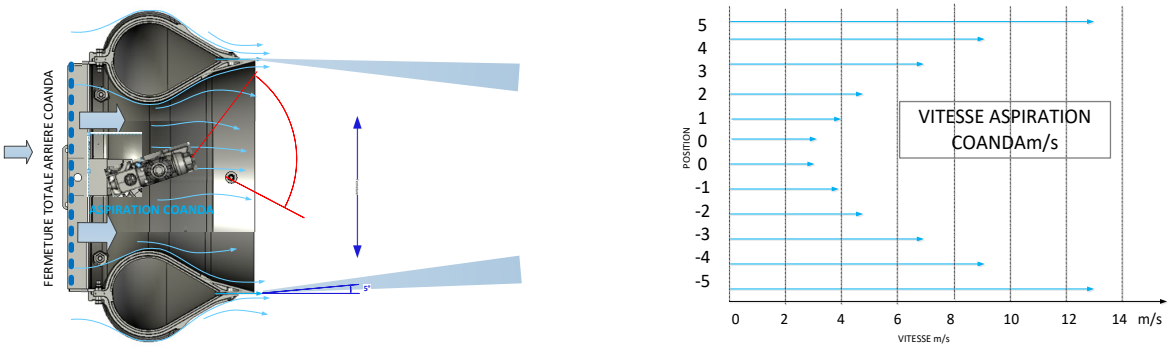


Figure 17 a&b: Internal flow induced by Coandă suction

For a 125 cm spray downpipe with an outlet velocity of 60 m/s, the airflow generated by the laminar curtains is approximately 1,800 m^3/h.

Measurements on the prototype show a nearly uniform outlet velocity around the entire ring perimeter, with the exception of limited variations associated with pressure losses in the curved sections (Figure 18). The geometric continuity of the slot and the uniformity of velocity therefore limit the formation of low-flow areas that could promote droplet escape.

Control of the continuous airflow also makes it possible, by means of internal aeraulics devices, to modulate and reduce the velocity of the rear curtain. In the system, the front curtain therefore carries droplets towards the vegetation, while the rear curtain closes the air-confined system.

Because the BLISS ring forms a homogeneous aeraulics unit, reducing the rear-curtain velocity increases the front-curtain velocity for a constant inlet air velocity at the duct (Figure 19).

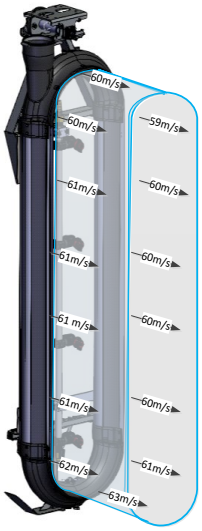


Figure 18: Balanced outlet velocities around the entire ring perimeter

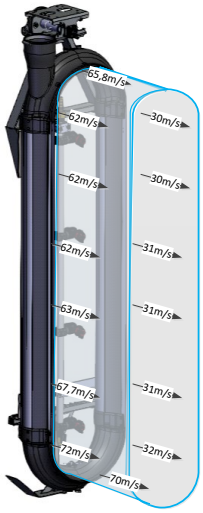


Figure 19: Independent control of rear-curtain velocity

This prototype therefore aims to combine the functions usually provided by an air-assisted jet and a containment system: transporting droplets to the canopy, promoting their penetration and reducing their dispersion outside the application zone. Its performance in terms of deposition on the vegetation and drift reduction was subsequently evaluated experimentally.

3.3 Validation of drift reduction on EOLEDRIFT

The tests conducted on the EOLEDRIFT test bench show that the sprayer fitted with aerodynamically contained spray downpipes reduced airborne drift in all four treatments studied compared with the pneumatic arch sprayer reference.

In early growth, the reference average drift of 0.111% of the full-area application rate was reduced to 0.033% with ATI nozzles and 0.005% with TVI air-induction nozzles, corresponding to reductions of 70% and 95.5%, respectively, and to IFV reduction classes of 66% and 95%.

At full canopy, the reference average drift of 0.080% was reduced to 0.019% with ATI nozzles and 0.002% with TVI nozzles, corresponding to reductions of 76% and 97.5%, respectively, and to average-drift reduction classes of 75% and 95%.

Canopy stage	Nozzles	BLISS drift (% of application	Reference drift	Approximate reduction	Class based on average drift
Early growth	ATI	0.033%	0.111%	70 %	66 %
Early growth	TVI	0.005%	0.111%	95,5 %	95 %
Full canopy	ATI	0.019%	0.080%	76 %	75 %
Full canopy	TVI	0.002%	0.080%	97,5 %	95 %

Analysis of the vertical profiles confirms the effect of nozzle type. In early growth, the ATI treatment attained the 66% reduction class based on average drift, but exceeded this threshold at 1.5 m height. With TVI nozzles, every profile point was below the 90% reduction threshold, but

one point at 1.5 m did not meet the 95% threshold. This treatment was therefore classified at 95% based on average drift and at 90% based on the vertical profile.

3.4 Discussion

The EOLEDRIFT results show that the configuration combining BLISS spray downpipes with TVI air-induction nozzles achieved an average drift reduction greater than 95% at both growth stages studied. At full canopy, this threshold was also met at every height analyzed in the vertical profile. These results demonstrate that a high reduction in airborne drift can be achieved by means of air-confined spraying system without surrounding the vegetation with physical panels. They therefore validate the functional objective defined during design: to create a face-to-face spray downpipe capable of keeping droplets within the treatment zone while transporting them towards the canopy.

Performance nevertheless depends on the complete application configuration. The use of air-induction nozzles greatly improves the results compared with conventional nozzles, while canopy development increases droplet interception. The observed effectiveness must therefore be attributed to the complete system combining aerodynamically contained spray downpipes, nozzles, air-assistance settings and vegetation.

4/ CONCLUSIONS

This study aimed to design a face-to-face spray downpipe capable of limiting drift without physical containment and to evaluate its performance. The approach combining CFD calculations, prototyping and experimental aeraulics characterization resulted in an oblong ring generating a continuous peripheral air curtain whose reach and uniformity are compatible with transporting droplets towards the canopy.

On the EOLEDRIFT test bench, every configuration tested reduced drift compared with the reference; the combination of air-confined spray downpipes and air-induction nozzles attained the 95% reduction class at both growth stages according to the average-drift criterion. These results establish the potential of air-confined system as a means of reducing airborne losses in vineyard spraying.

Further in-depth studies and trials at different air-curtain velocities and canopy-development stages would make it possible to investigate how this parameter should be adjusted in relation to application rates and growth stages, and to isolate the contribution of air-confined system more precisely.

REFERENCES

Bedos, C., Douzals, J.-P., Barriuso, E., Bordes, J.-P., Chantelot, E., Cellier, P., Loubet, B., Mercier, T., Perriot, B., Siné, M., Verjux, N., Verpont, F., & Huyghe, C. (2020). *Application des produits phytopharmaceutiques et protection des riverains : Synthèse des connaissances pour définir les distances de sécurité*. Rapport du groupe de travail INRAE–ANSES–ACTA. https://doi.org/10.15454/8W26-5W57

Carra, M., et al. (2017). *Les panneaux récupérateurs : Atouts et limites*. UMT EcoTechViti, IFV–IRSTEA–Montpellier SupAgro.

Codis, S., et al. (2024). *Mesures de dérive de pulvérisation sur le banc d'essai EoleDrift avec le pulvérisateur Calvet SP Eco+ 2MR équipé de descentes Bliss simples 150* (Contrat no ISVI-22193).

Danton, A., Roux, J.-C., Dance, B., Cariou, C., & Lenain, R. (2020). Development of a spraying robot for precision agriculture: An edge-following approach. In *2020 IEEE Conference on Control Technology and Applications (CCTA)* (pp. 267–272). IEEE. https://doi.org/10.1109/CCTA41146.2020.9206304

Gil, Y., & Sinfort, C. (2005). Emission of pesticides to the air during sprayer application: A bibliographic review. *Atmospheric Environment, 39*(28), 5183–5193.
Griesang, F., et al. (2017). How much do adjuvant and nozzle models reduce spraying drift? *American Journal of Plant Sciences, 8*, 2785–2794.

Jamar, L., Mostade, O., Huyghebaert, B., Pigeon, O., & Lateur, M. (2010). Comparative performance of recycling tunnel and conventional sprayers using standard and drift-mitigating nozzles in dwarf apple orchards. *Crop Protection, 29*(6), 561–566.

Kadosch, M. (1958). Déviation d'un jet par adhérence à une paroi convexe. *Journal de physique et le Radium*, 1–12A

Development of a test protocol to evaluate Droplet Size Distributions (DSD) from nozzles equipped with a spinning disc mounted on unmanned aerial spraying systems

Jean-Paul Douzals[a,*], Cyril Tinet[a], Jean-Philippe Trani[a], Pengchao Chen[b], Emilio Gil[b]

[a] ITAP INRAE-Institut Agro, Université de Montpellier, Montpellier, France
[b] UMA - Universitat Politècnica de Catalunya– Barcelonatech, Castelldefells, Spain
* Corresponding author. Email: jean-paul.douzals@inrae.fr

Abstract

Unmanned aerial spraying systems (UASS) market is developing at a global scale, as they provide potential solutions to plant protection in contexts like steep slope situations, soil portance limitations, etc. Recent generations of drones are now equipped with rotary nozzles fitted with a PWM controlled spinning discs and pumps that deliver a wide range of droplets sizes and flowrates. In order to verify the potential substitution of air inclusion nozzles, an experimental study was conducted at INRAE Montpellier Experiments were held at INRAE facility in Montpellier. A laser diffraction equipment was used for the measurements. An electrically driven rotary nozzle was fed by an electrically driven pump. Both components were controlled using a PWM controller considering duty cycles of 0 to 100% and adjustable frequencies from 50 to 500 Hz. Flowrates were ranged from 3 to 6.0 L/min and revolution speed of spinning disc were ranged from 3 000 to 16 000 rpm.

Results showed a logical decrease in the droplet size with the increasing revolution speed of the spinning disc in a proportion of 60 – 500 µm but results are also influenced by the flowrate. Both droplet size (Dv50) and relative span factor (RSF) showed different patterns depending on the revolution speed. These results will help the practical implementation of EU and national policies and practical advices when using spraying with an UASS both to select on-the-go optimal DSD for the droplet deposition on target and to minimize environmental impact beside sensitive areas.

KEYWORDS : Drones, rotary nozzles, droplet size distribution, PWM control

Complexity level: 3

1/ INTRODUCTION

Drones used for spray protection are called Unmanned Aerial Spraying Systems (UASS), spraying drones or Remotely Piloted Aerial Systems (RPAS) as defined by ISO 23117-1. Originally developed in Asia due to terrain constrains (lack of manpower in paddy rice fields and steep slope areas), the use of UASS is developing worldwide with a certain number of advantages: no dependence to soil wetness, high precision spray possible (ex. precision weeding), reduce labour arduousness in steep slope conditions where only manual application with portable equipment's is possible,

remote control in automated mode and a limited exposure of the operator (ANSES 2022). However, these spray application equipment's also show inconvenient: a payload limited to up to 85 kg and limited application rates/productivity, limited electrical autonomy (20 min), vertical gradient of spray deposition in 3D crops. First generations of UASS (payload from about 10 to 30 kg) were equipped with traditional pressure nozzles (Flat fan or Hollow cone) that can be replaced by air inclusion nozzles when needed in order to comply with local regulation (Chen et al., 2022). One of the limitations of these nozzles is the limited range of flowrate allowed with a low-pressure pump. New generations of UASS (payload from about 50 to 85 kg) are now equipped with spinning disc nozzles and PWM controlled pumps able to generate higher flowrates. Depending on revolution speed of the spinning disc, the droplet size will differ but will remain in a limited range of droplet size span (Dubuis et al., 2026)

Spinning disc atomizers are used for a long time in agriculture (Craig et al., 2014). Among several designs, the principle is based on the spreading of the liquid onto a spinning disc equipped with small radial peaks at the periphery. The liquid sheet is more or less elongated depending to the revolution speed and peaks may help to generate ligaments (first breakup) that rapidly turn to droplets (second breakup). Historical rotary atomizers in agriculture were producing fine droplets (30 – 50 µm) for localized herbicide application using shields, disinfection of livestock buildings or for mosquito control purposes. Aerial or ground application systems can sometimes be equipped with rotary cage atomizers (see Microngroup CDA).
The progressive inclusion of drones for spray application in the European Union is restricted by the ban of aerial spraying imposed by the article 9 of the sustainable use directive (2009/128/EC). In this context, derogations are only possible if using the best solution to reduce spray drift. There is then a need to demonstrate that drones equipped with rotary nozzles are able to minimize spray drift and a first indicator rely on droplet sizes. The current Marie S. Curie project Dynamic Droplet Size Control (DDSC) between UPC Barcelona and INRAE Montpellier aims at better characterizing new generations of drones using rotary nozzles in terms of deposition and spray drift reduction.

2/ MATERIALS AND METHODS

Experiments were held at INRAE ReducPol facility in Montpellier. A laser diffraction Malvern Spraytec (Malvern Panalytical, UK) was used for the measurements. The equipment is equipped with two optics: a laser beam emitter (632 nm - red) and a receiver including 36 photodiods. With an angle function of the droplet size (Mye principle). The measuring range was from 2 to 2000 µm provided a sufficient number of droplets. A complete droplet size distribution (DSD) is provided every second.
Experiments were conducted in a laboratory with temperature control of 20°C +/-2.
An electrically driven rotary nozzle (Hobbywing SPRAY 9L, Haoying, Shenzhen, China) was fed by an electrically driven pump (Hobbywing PUMP 8L, Haoying, Shenzhen China). Both components were connected to a DC power supply 0 - 60 V (JT-PS1440, Joy-it, Germany) and were controlled using a PWM controllers (KPWM, Jixing Electrotronic Co, Shenzhen, China) considering duty cycles of 0 to 100% and variable frequencies from 50 to 500 Hz, adjusted to 415 Hz for the experiments.

The spinning disc nozzle (disc of 60 mm diameter) was placed in a vertical position in order to avoid the contamination of the optics of the Malvern system with droplets. Flowrates were ranged from 1 to 6.0 L min^{-1} and revolution speed of spinning disc were ranged from 3000 to 16000 rpm representing tangential ejection velocities of droplets from 7 to 50 m s^{-1}. Considering two nozzles, a flight speed of 15 km h^{-1} and a flying height of 5m (spray swath 5m), these flowrates correspond to a range of application rates from 18 to 96 l ha^{-1}.

A calibration was operated to directly relate the disc revolution speed with either the pump flowrate or the duty cycle value at a frequency of 415 Hz in both cases (Fig 1). Test liquid was ordinary water as provided by the facility.

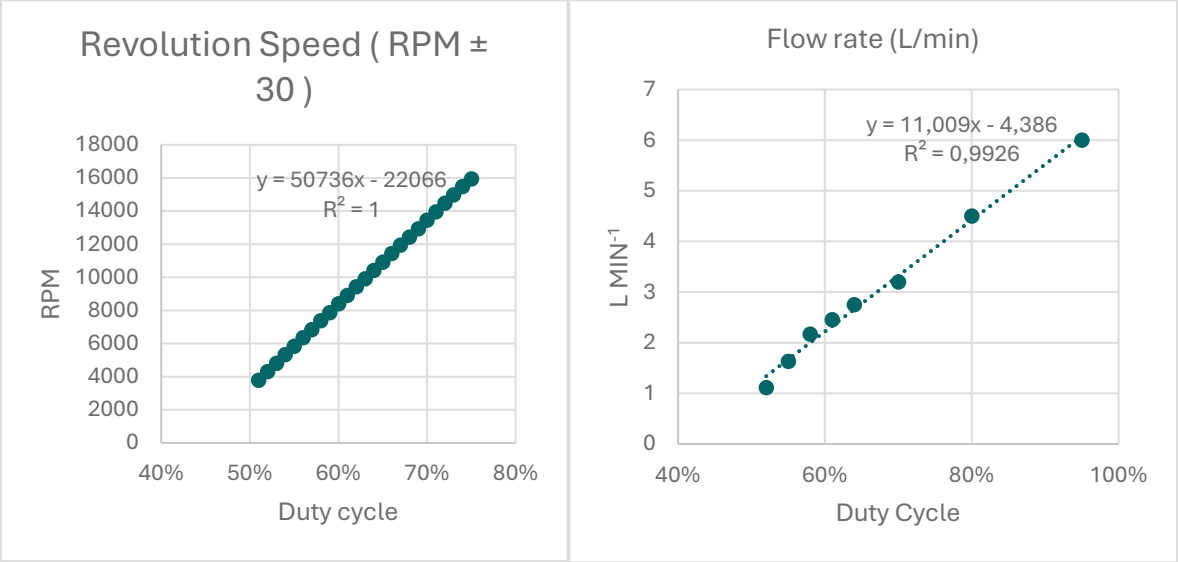


Fig 1 : Calibration of the pump and spinning disc

Droplet size distribution indicators are generally expressed according to the volume occupied by droplets :
Dv0.1 : 10 % of the total volume corresponds to droplets with a diameter that is lower or equal to this value.
Dv0.9 : 10 % of the volume corresponds to droplets with a diameter that is greater of equal to this value.
Dv0.5 or VMD: 50 % of the volume corresponds to droplets with a diameter that is greater of equal to this value. Also named Volume Median Diameter (VMD).
RSF - Relative Span Factor : (Dv0.9 – Dv0.1) / Dv0.5 that indicates the range of the distribution.

3/ RESULTS AND DISCUSSION

Evolution of Dv0.5 with rpm and flowrate
According to Fig 2, the evolution of the Dv0.5 is influenced by the revolution speed of the spinning disc but also by the flowrate. Max Dv0.5 is observed for the lowest rpm value (2200 rpm) and may reach between 350 µm to 500 µm depending on the flowrate. 350 µm is a typical Dv0.5 value for a pre-orifice nozzle with intermediate droplet size distribution and 500 µm is quite comparable to air inclusion nozzles at standard pressure.

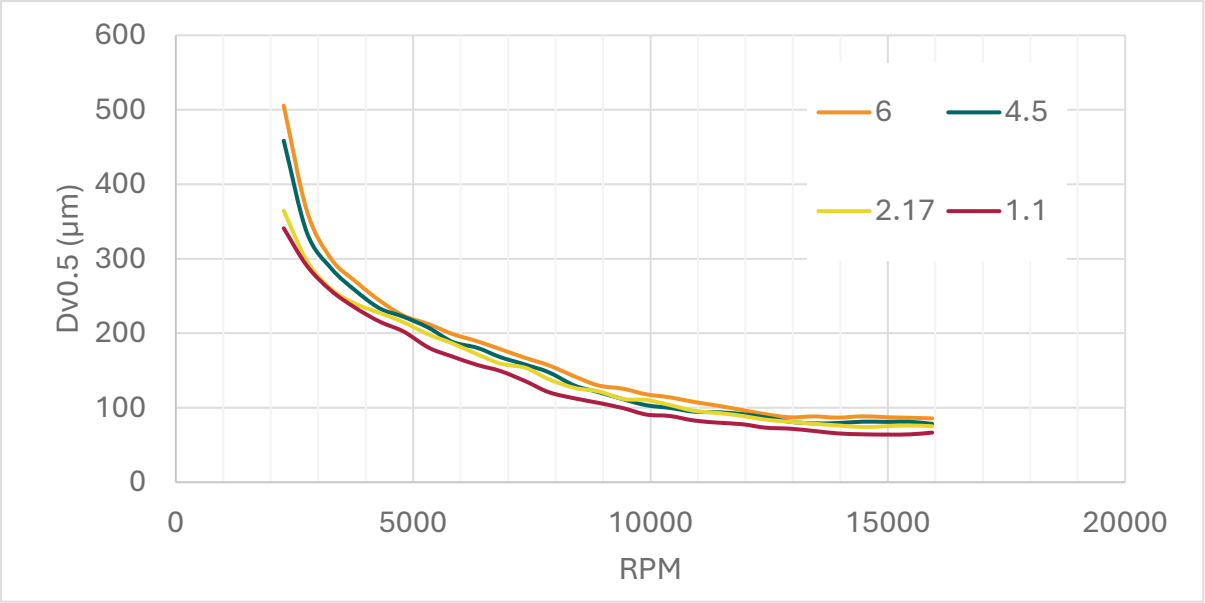


Fig 2: Evolution of the Dv0.5 with different rpm and flowrates from 1.1 to 6 l min^{-1}

Between 2200 and 4000 rpm, all curves show a rapid decrease in Dv0.5 values whereas the decrease appears only slight between 12000 rpm and 16000 rpm. Between 4000 and 16000 rpm, differences between flowrates still remains but with limited impact on droplet size. At maximum rpm, Dv0.5 reaches between 65 µm to 85 µm corresponding to an extra fine (XF) class (ISO 25358 µm). These droplets are highly susceptible to generate spray drift (Alheidary et al., 2014).

Evolution of RSF with flowrate

Fig 3 shows the evolution of the RSF with the flowrate. From 1 to 3 l min^{-1}, the increase in flowrate generates a linear increase of the distribution span. From 3 to 6 l min^{-1}, the increase in the span value is less pronounced.

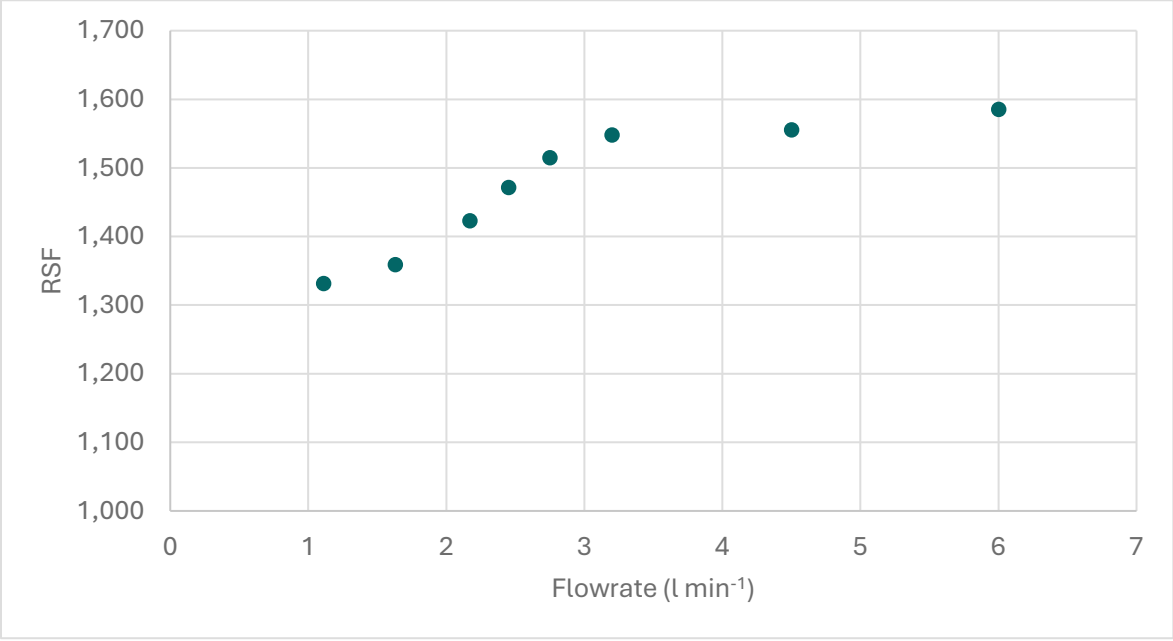


Fig. 3: evolution of the average relative span factor (RSF) with the flowrate.

A close-up on the effect of the rpm on the RSF is given in the following Fig 4. Values were normalized considering the last 16 values of each curve (out of 28). Normalized RSF curves shows 3 main patterns. From 2200 to 4000 rpm, the normalized RSF strongly decreases from 1 to 0.7 in average. This means that distributions become much more homogeneous with the increase in rpm. From 4000 to 8000 rpm, the normalized RSF values increase up to the initial value meaning an increase in the distribution span. Finally, a plateau is observed between 8000 and 16000 rpm where DSD span is stable.

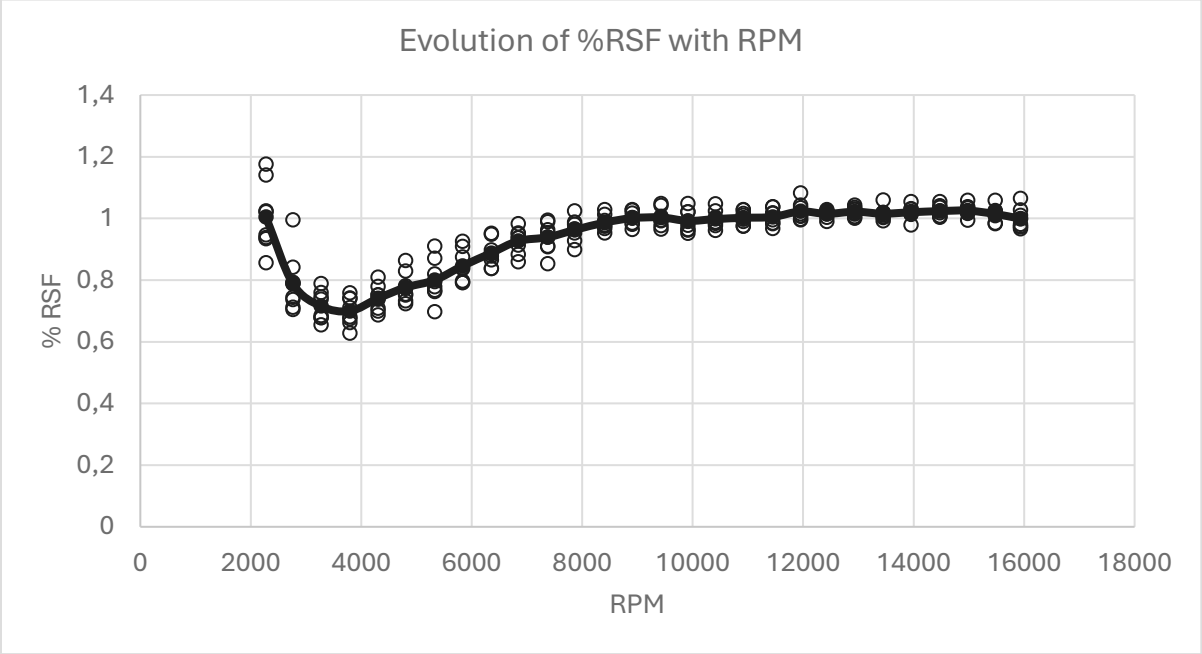


Fig. 4: Evolution of the relative span factor with rpm for different flowrates

Discussion – Comparison with a pressure nozzle

The range of flowrate of a pressure nozzle (Flat Fan) is generally limited by the range of compatible pressure which varies from 1 to about 8 bar. Under these conditions, the range of flowrate is less than 3 times the minimum volume. Similarly, the range of droplet sizes distributions is about 1.5 compared to about 5 to 6 for spinning disc nozzles (Fig 5).

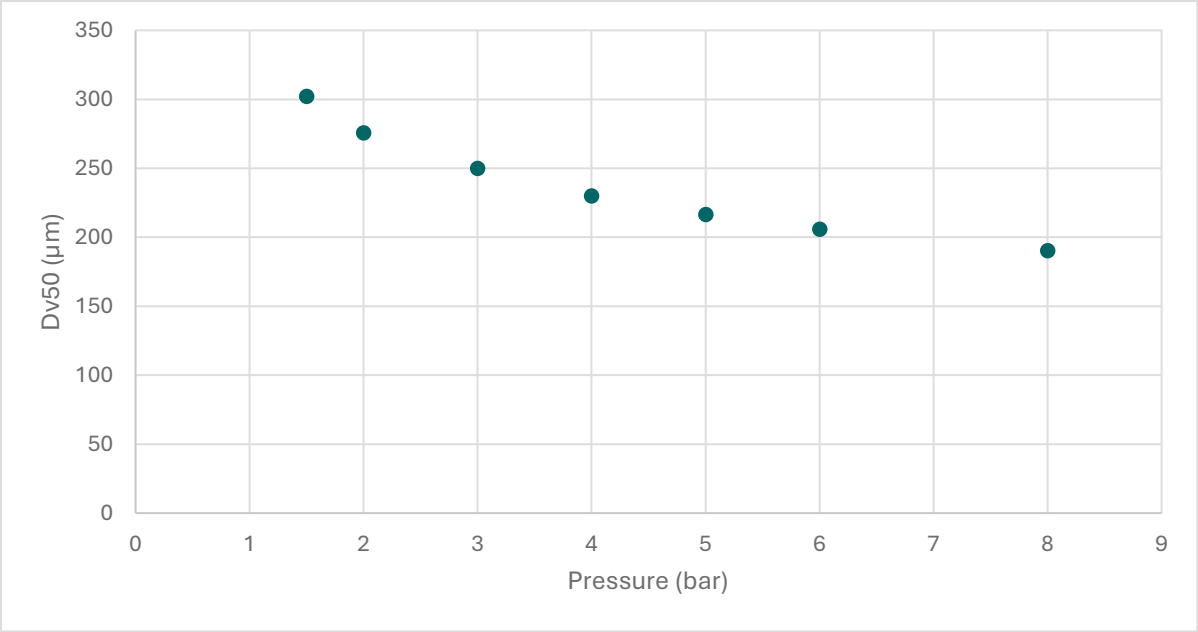


Fig 5: Evolution of Dv50 vs pressure for a Flat Fan nozzle 110 03 (INRAE)

For the Flat Fan nozzle 110 03, the RSF was not significantly modified with the pressure (average 1.15 +/- 0.1).

4/ CONCLUSIONS

This study aimed at better understand how spinning disc nozzles mounted on drones may modify the droplet size according to the revolution speed of the disc and flowrate. As such this technology is able to propose wider ranges of both droplet size distributions and flowrate compared to a traditional flat fan nozzle. The range of Dv50 varies from 350 – 500 µm at maximum (2200 rpm) equivalent to a pre-orifice flat fan nozzle and an air inclusion nozzle respectively. Minimum Dv50 of 65 – 85 µm were observed at 16000 rpm. Interestingly, the evolution the droplet size does not totally follow a linear trend according to rpm but several patterns can be identified at low, intermediate and high revolution speeds. Different patterns are also visible when looking at the relative span factor (RSF) where the span of the distribution appears also dependent on the revolution speed and the flowrate.
These measurements will be completed by drift tests in the field in order to confirm the potential benefit of spinning disc nozzles to prevent environmental exposure to plant protection products.

Acknowledgements
This study was financed by HORIZON-MSCA-2025-PF DDSC project n° 101271124 between the Polytechnic University of Catalogna (UPC) Barcelona, Spain and INRAE ITAP Montpellier

References

- ANSES. 2022. NOTE d'appui scientifique et technique de l'Agence nationale de sécurité sanitaire de l'alimentation, de l'environnement et du travail relative à « l'expérimentation de l'utilisation de drones pour la pulvérisation de produits phytopharmaceutiques», 44p.
- M. Al Heidary, J.P. Douzals, C. Sinfort, A. Vallet, 2014. Influence of spray characteristics on potential spray drift of field crop sprayers: A literature review, Crop Prot, 63, 120-130, https://doi.org/10.1016/j.cropro.2014.05.006.

- Chen P, Douzals JP, Lan Y, Cotteux E, Delpuech X, Pouxviel G and Zhan Y. 2022. Characteristics of unmanned aerial spraying systems and related spray drift: A review. Front. Plant Sci. 13:870956.
- https://doi.org/10.3389/fpls.2022.870956
- Ian P. Craig, Andrew Hewitt, Howard Terry, 2014. Rotary atomiser design requirements for optimum pesticide application efficiency, Crop Prot., 66, 34-39 https://doi.org/10.1016/j.cropro.2014.08.012
- Pierre-Henri Dubuis, Céline Villars-Corbex, M. Clare Butler Ellis, H. Christoph Geiser, Jeremy J. Harwood, Marco C. Knobloch, Andrew G. Lane, Aurélie Melgar, Joel D. Stohler, Clive R. Tuck, Helen C. Wheeler, Jürg A. Zarn, Sebastian L.B. König, 2026. Environmental, resident and bystander exposure from spraying applications with unmanned aerial vehicles equipped with flat-fan nozzles or rotary atomizers, Crop Prot., 209, 107776, https://doi.org/10.1016/j.cropro.2026.107776
- Micron CDA : www.microngroup.com
- ISO 25358:2018. Crop protection equipment — Droplet-size spectra from atomizers — Measurement and classification. 7p.
- ISO 23117-1:2023 Agricultural and forestry machinery — Unmanned aerial spraying systems — Part 1: Environmental requirements, 13p.
- 2009/128/EC: DIRECTIVE 2009/128/EC OF THE EUROPEAN PARLIAMENT AND OF THE COUNCIL of 21 October 2009 establishing a framework for Community action to achieve the sustainable use of pesticides, 26 p.

A Methodology for Evaluating the Detection Performance of a Spot Spraying System in Field Crops

Paul Melki[‡,*], Pierre Soidé[‡], Estelle Millet, Jérôme Dias, Olivier Francart, Vincent Rachet

EXXACT Robotics, 51200 Épernay, France

[‡] Equal contribution Germany

* Corresponding author. Email: paul.melki@exxact-robotics.com

Abstract

The technology behind spot spraying has been manifesting an ever-increasing level of progress over the past few years and has reached a certain level of maturity. In order to achieve the required precision of application, it is crucial for the systems to accurately detect the targets that need to be sprayed. The evaluation of the system's perception should therefore be the first step towards a full assessment of any spot spraying system. In this article, we introduce a methodology for evaluating the detection performance of a precision weeding system on real targets under real-world conditions. The proposed protocol consists of two distinct "episodes." Episode I aims at measuring the spatial imprecision of the detection maps generated by the spot spraying system with respect to accurately mapped artificial targets.

Episode II aims at evaluating the system on real targets by comparing the "ground-truth map," comprising spatially identified weed and control (non-weed) points in the field, and the "detection map" generated by the sprayer. The Episode II protocol is then applied on a number of different sessions that took place in two separate areas of a maize field in post-emergence spraying conditions in the North-East of France. An exploratory statistical methodology is then proposed for the analysis of these sessions, particularly for studying the system's repeatability under the same conditions, and the influence of the sprayer's speed. Finally, the empirical results are presented and discussed.

KEYWORDS: Precision weed spraying, spatial point patterns, statistical methodology, spatial mapping

Complexity level: 4

1/ INTRODUCTION

Weeds have been a challenge to farmers since the earliest days of agriculture. The practices for dealing with these (generally) undesirable plants are multiple and diverse and have evolved over the centuries. The latest in the long series of weeding practices is chemical spraying, which has become the most widely used approach since the mid-20th century (Holm and Johnson 2009). Chemical weeding consists of spraying specialized substances known as herbicides in the field with the aim of killing or reducing the growth of undesirable plants. This approach has proven to be the most efficient for large scale farms (Yu and Marble 2022).

However, chemical spraying has a number of undesirable consequences, some of which can be witnessed on the short term while others manifest themselves only after some period of time. The clearest short term negative effect of chemical spraying, as commonly practiced in its broadcast form, are crop injuries. Indeed, in broadcast spraying, herbicides are applied over all the plants in the field. Some of the chemical products designed to attack the weeds may also injure the crops. This negatively impacts their health and ultimately reduces the yield. On the longer term, the repeated spraying of the same chemical products over time and over large geographical zones has pushed some weed species to develop "herbicide-resistance" (Young et al. 2014; Yu and Marble 2022). Chemical products have thus become less effective on these species. Moreover, the iterated spraying of chemical products has negative impact on the health of the soil and can deteriorate the quality of underground water with negative consequences on the health of the plants, the ecosystem, and eventually on humans (Van Bruggen et al. 2021).

With the aim of minimizing the negative repercussions of broadcast spraying, a new approach to herbicide application has been developed. Precision spraying, also known as spot spraying, is the practice of applying herbicides only where needed, that is, on the weeds. Instead of spreading chemical products over all the parcel, this approach consists of spraying as precisely as possible on the weeds only, thus reducing the surface that receives chemical deposits. The promise of this approach is to reduce crop injuries and increase yields, minimize the pollution of soil and water, reduce the farmers' consumption of costly chemical products, and ultimately create more virtuous agricultural practices without compromising on efficiency and productivity.

Spot spraying technologies are quickly evolving and the number of systems available on the market is increasing (Allmendinger et al. 2022; Vijayakumar et al. 2023). Two modes of spot spraying have emerged: deferred and real-time. The procedure of differed precision spraying is divided into two steps: the first step consists of mapping the weeds in the field using a vision system that detects the weeds and creates a spraying map. This map informs the sprayer of the exact locations of weeds in the field. The second step then consists of the sprayer moving in the field and spraying only where needed. Real-time spot spraying, on the other hand, combines the detection and spraying of weeds in one pass. While the sprayer travels in the field, the spot spraying system detects and automatically sprays the weeds in real-time. Real-time spot sprayers can thus be considered robotic systems since they implement the three core tasks of a robot: (1) perception, (2) decision-making, and (3) action, in real-time (Melki 2025). Therefore, like any robotic system built to be deployed in the real-world, the three core tasks should be evaluated and validated separately and in coordination before the system is deemed ready for deployment.

Unfortunately, the evaluation of spot spraying systems under real-world conditions has not received enough public attention, with the exception of Challenge ROSE (Regnier et al. 2021), which, however, evaluated experimental rather than commercial systems. Now that these systems are reaching a certain level of maturity and are being deployed in farms around the world, it becomes crucial to reliably validate them using well-defined protocols.

In this article, we present a statistical protocol for evaluating the perception task of a spot spraying system (1), on which all the rest of the spraying pipeline is based. This protocol can be used for evaluating deferred and real-time spot spraying systems as it is based on spatial detection maps. The protocol can thus be used to compare multiple detection systems or multiple detection sessions over the same spatial extent. Unlike other protocols that are often conducted in controlled environments, the proposed protocol can be used to evaluate systems in the field under real use case conditions.

The contributions of this articles can be summarized as:

- Development of a scientific methodology for the evaluation of the detection (perception) performance of a spot spraying system under real-world conditions based on detection maps. The methodology consists of two episodes: a first episode (I) that studies the spatial mapping precision of the detection system on artificial targets, and a second episode (II) that evaluates the detection performance of the system with respect to a "ground-truth" map consisting of spatially mapped weed and "control" (non-weed) points.
- Implementation of the presented protocol for the evaluation of Exxact Robotics' Spot Spraying System (3S) under real-world field tests conducted in two zones of a maize parcel in North-East France in June 2025.
- Presentation and discussion of the empirical results obtained.

In section "Materials and Methods" we present in detail the full protocol in its two episodes, starting from the collection of data to the deployment of the system and finally the statistical analysis of the generated maps. Details of the experimental conditions under which the 3S system has been evaluated are also given in this section. In section "Results and Discussion" we present the empirical results obtained. These include the evaluation of the repeatability of the system over different trials conducted under comparable conditions, and the analysis of the possible effect of some intrinsic (the moving speed of the sprayer) and extrinsic (the position of the weed in the row) factors on the performance of the system. We finish the article with some concluding remarks and a call for more efforts for evaluating these systems.

2/ MATERIALS AND METHODS

2.1 Description of the Protocol

The evaluation protocol we propose in this article is composed of two episodes (represented in Figure 1). **Episode I** analyzes the behavior of the system on artificial targets that are placed in real-world conditions. The goal of this episode is to study the spatial dispersion error of the generated detection points with respect to the ground-truth points. Indeed, it would be unrealistic to suppose that the detection points produced by the system should perfectly overlap with the ground-truth points in space. Multiple factors may play a role in generating such noise: for example, an unreliable GNSS signal, a small synchronization lag, etc. Therefore, it is crucial to quantify the spatial error before analyzing the performance of the system on real targets. Without such a prior quantification, it would be impossible to associate a detection point generated by the system to a weed in the ground-truth map (especially in parcels that are particularly dense with weeds).

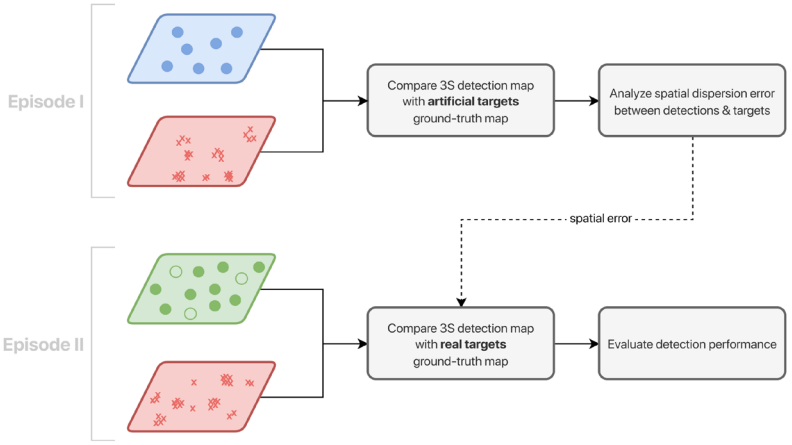


Figure 2 – High-level representation of the proposed protocol in two episodes. Episode I compares the detection maps (red) to the ground-truth map of artificial targets (blue) in order to analyze the spatial error between the two. Episode II evaluates the performance of the system under real-world conditions by comparing the detection maps (red) to the ground-truth map (green) on real targets while taking into the consideration the spatial error computed in Episode I.

Episode II is the actual evaluation phase whereby we analyze the performance of the system on a sample of real weeds in the field while taking into consideration the spatial error measured in Episode I. By comparing the detection and ground-truth maps, we can derive a confusion matrix from which we can compute a number of evaluation metrics that give us a clear picture of the behavior of the system *under real-world conditions*. In the following subsections, we will start by discussing the different steps required for Episode II, which would clarify the need for Episode I that will be discussed at the end of "Materials and Methods."

2.2 Creation of the Ground-Truth Map

The ground-truth map constitutes the "standard truth" against which the detection map generated by the system will be compared. It is a critical element for the evaluation procedure conducted in Episode II. It is essential that the ground-truth map be as faithful as possible to the reality of the studied parcel, otherwise the quantitative evaluation of the system would not reflect its real performance. Great care has been taken towards the construction of the ground-truth map, starting with the choice of the data collectors. Indeed, they need to be professional agronomists who can reliably identify and visually distinguish between different varieties of weed. Four families of weeds have been defined, each with its own "weed identification sheet" for helping the data collectors and an assigned color. The data collectors are divided into groups of two, with each group being responsible for one family of weeds. They are instructed to travel freely in the parcel in search for a fixed number of weeds belonging to their assigned family. This approach leads to a random sampling of points in the parcel, which avoids statistical bias that may result from sampling only in a small spatial region of the parcel. A fifth group is responsible for the collection of a fixed number of "control" points, which are spots where the data collectors are sure that no weed is present in a radius of 50 cm.

For each family of weeds, and for control points, 50 points are retrieved, creating a total sample of size 250 out of which 200 points correspond to weeds and 50 to points where there is no weed. The studied sample thus contains 4 times more weed points than non-weed points, which is a prevalence that is not completely realistic. In a typical parcel, a spot spraying system is expected to encounter more non-weed scenes than otherwise. However, such a design choice has been made to put more weight on the evaluation of the system's performance for weed detection rather than on non-detection of clean points. Indeed, we would like to study the system's behavior when

it should be “activated” (when there is a weed) rather than when it should be “inactive” (when there is anything else).



Figure 3 – Diagram showing the steps towards the creation of the ground-truth map. Whenever the data collectors identify a weed, (1) they signal it with a colored marker corresponding to the weeds’ species. (2) The weed’s spatial coordinated are then retrieved using a RTK stick and a photo of the weed is taken. (3) Different characteristics of the weed are noted in a predefined weed identification sheet. (4) At the end of the collection campaign, we obtain a ground-truth map with all the collected weed points.

Figure 2 shows the data collection procedure. (a) Whenever a duo of annotators identifies a weed (or a “control” point), they place a numbered marker as close as possible to the point of interest (without damaging it) and the spot is photographed with the marker. Each type of weed is assigned a marker color: red for bindweed, blue for rapeseed, orange for chenopodium, and yellow for all other types. (b) Some metadata about the identified weed are collected using a predefined form. The information collected include the ID (same as the marker’s number), the weed’s position relative to the row, the number of leaves, etc. (c) The object of interest’s location is then registered using a GNSS stick with the same RTK correction as the sprayer. This procedure allows us to (d) create a ground-truth map where each spatial point has its own associated metadata. The ground-truth map thus includes both weed and “control” points (assigned white markers). These serve as “witnesses” to the performance of the system in cases where we are sure that no weed exists.

2.3 Generation of the Detection Map

After the weed and the control points have been identified in the parcel, the colored markers are removed to clear the field for the sprayer. A “detection map” is generated for each spraying session wherein each spatial point corresponds to a “weed prediction” generated by the system’s vision-based predictive model. Whenever a “weed prediction” is generated by the model, its exact spatial locations is saved locally in the spraying system’s processing unit and can be retrieved at the end of the session to constitute the detection map (Figure 3).

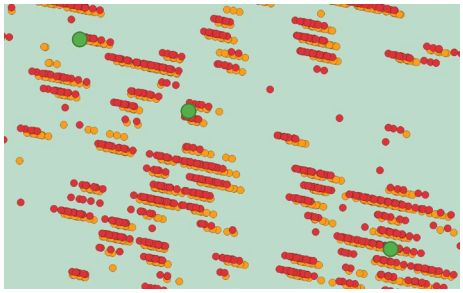


Figure 4 - Zoom on a portion of a parcel showing two detection maps for two different sessions (red and orange). The

2.4 Definition of a “Detection”

The predictive system may generate many prediction points in the neighbourhood of a given weed as can be seen in Figure 3. It is not realistic to expect a weed prediction point to overlap exactly with a weed due to a multitude of physical factors that may influence the exactitude of the registered spatial location. Such factors may be: the oscillations of the spraying boom, a connection latency between the detection system and the GNSS sensor or an unstable GNSS signal, among others. This poses the question of *how to define a “detection.”* In other words, in

our experimental setup to evaluate the performance of the spot spraying system based on ground-truth and detection maps, *how exactly do we decide whether a weed has been detected or not?*

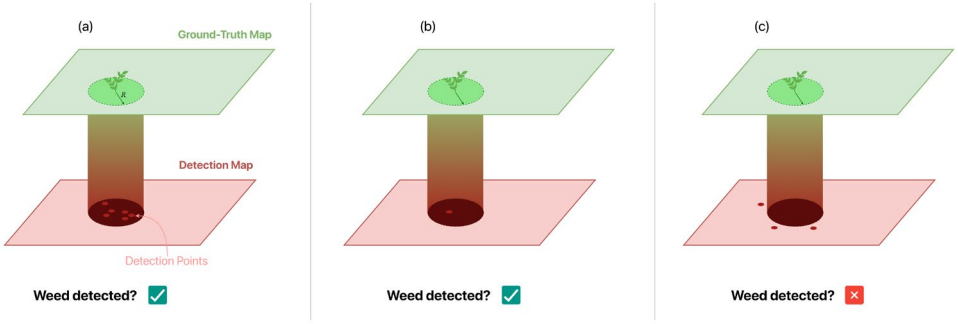


Figure 5 – Representation of what constitutes a "detection." A circle of radius *R* centered on the weed is considered. If there are any detection points that fall in this circle, then the weed is considered as "detected" (True Positive), as is the case in (a) and (b). If there are no detection points that fall in the circle, then the weed is "not detected" (False Negative). The same logic is followed for "control" points: (a) and (b) would be considered a "detection" of a clean point (False Positive), while (c) would be a correct "non-detection" (True Negative).

To take into account all the noise that enters into the generation of the maps for the definition of a "detection," we consider a buffer area of radius R around each weed in the ground-truth map and count the number of "weed prediction" points that fall into this buffer area, as shown in Figure 4. If there is at least one prediction point that falls into this buffer area, we consider that the system has detected the weed (cases (a) and (b) in Figure 4). However, if no detection point falls into this area, then the object of interest is considered as "not detected", as in case (c).

The introduction of this buffer zone allows to solve the problem of the definition of a "detection" but requires the definition of the buffer radius *R*. This is precisely why Episode I conducted on artificial targets is a required step in the proposed evaluation methodology: it allows us to empirically define the radius *R* by studying the average observed dispersion of detection points around the artificial targets based on multiple sessions. This analysis is conducted on artificial targets in order to control for other stochastic factors that may influence the precision of the maps, in particular the predictive performance of the vision-based weed detection model.

2.5 Evaluation Metrics

The above definition of a "detection" can be applied to both "weed" and "control" points in the ground-truth map. Indeed, any of the points in the ground-truth map can be either "detected" or "not detected." However, the relationship of these two types of points to detection is different: we do want to detect weed points, but we do not want to detect control points. This distinction allows us to derive the confusion matrix, classically used to evaluate classification tasks in machine learning and shown in Figure 5. From this confusion matrix, a large number of evaluation metrics can be derived, each shedding light on a certain aspect of the predictive performance of the model and presenting distinct mathematical characteristics (Foulle 2025). Two of the most commonly used metrics are the sensitivity (recall, True Positive Rate) and the specificity (True Negative Rate) defined as follows:

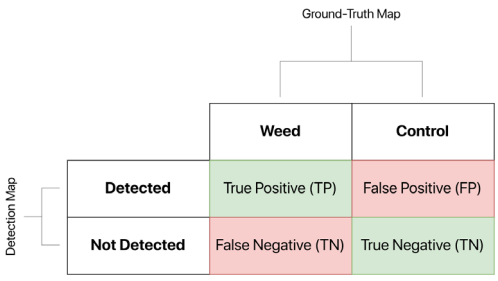


Figure 6 – Confusion matrix adapted for the task of spot spraying evaluation. Green corresponds

$$\text{sensitivity} = \text{True Positive Rate} = \frac{\text{TP}}{\text{FN} + \text{TP}} \quad ; \quad \text{specificity} = \text{True Negative Rate} = \frac{\text{TN}}{\text{TN} + \text{TP}}.$$

Another metric that combines the above two is Youden's *J* index (Youden 1950), which is particularly adapted to summarizing the model's performance using one value:

$$J = \frac{\mathrm{TP} \times \mathrm{TN} - \mathrm{FP} \times \mathrm{FN}}{(\mathrm{TP} + \mathrm{FN})(\mathrm{TN} + \mathrm{FP})} = \text{sensitivity} + \text{specificity} - 1.$$

The *J* index takes values between -1 and 1, with 0 corresponding to a random predictive model that cannot distinguish between the elements that should be detected and those that should not, and 1 corresponding to the "perfect" model that does not make any mistake.

2.6 Experimental Setup

2.6.1 Episode I – Analysis of Spatial Error

The first episode is used to define the detection radius based on the empirical scatter of detection points around ground-truth points. It is a required step in the analysis since we are working under real-world, imperfect conditions. The experimental setup for this episode consists of deploying the sprayer in the parcel to detect 9 artificial targets (blue plastic markers) placed on the ground (Figure 6). To do this, the weed detection model has been replaced with a deterministic algorithm for detecting blue targets. This allows us to reduce the measured uncertainty only to that due to spatial error, without being influenced by the inherent uncertainty of predictive models (Hüllermeier and Waegeman 2021). The sprayer is then deployed over the targets once in each direction as shown in Figure 6, that and over 2 sessions (which provides us with 36 sample points).

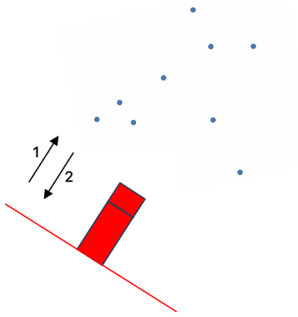


Figure 7 - Representation of the experimental setup on artificial targets represented by blue dots. The sprayer and

2.6.2 Episode II – Deployment under Real-World Conditions

The developed protocol has been deployed to test the performance of a 3S spraying system under real-world conditions. The experiments were conducted in a 21 ha maize parcel located in the Marne department in the North-East of France in June 2025. The maize plants were at a growth stage of 6 to 8 leaves and the overall weed pressure was estimated at less than 1 weed/m^2, which corresponds to a relatively low weed prevalence. Overall, the conditions correspond to what we consider as good spot spraying conditions. These are conditions where spot spraying can really demonstrate its utility, contrary to conditions with very high weed pressure, in which case spot spraying converges to a form of broadcast spraying.

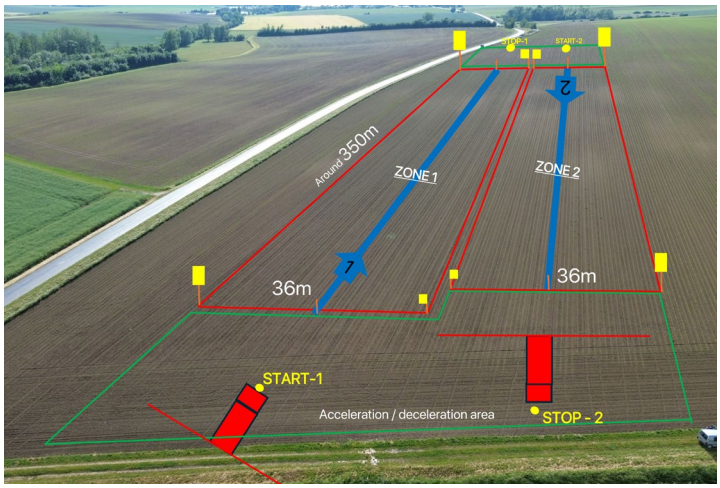


Figure 8 - Representation of the spot sprayer's deployment in the parcel. The zones considered in the study are Zone 1 and Zone 2. The acceleration and deceleration areas are not considered in the statistical analysis.

Each experiment, designed to study the influence of a specific factor on the system's detection performance, is therefore composed of a Zone 1 session and a Zone 2 session with each session having its own detection map (Figure 3).

The results of two different experiments will be shown in the following section: (1) First we study the *repeatability* of the system: do multiple sessions conducted under the *same* conditions lead to similar detection behavior? Indeed, a system that is not stable under the same conditions is not reliable and cannot be studied using the same statistical tools that suppose a stable system. For this reason, this factor is always the first to be analyzed before moving on to other factors. (2) The second factor studied is the sprayer's *speed* and how it influences the detection performance while keeping all other factors equal.

3/ RESULTS AND DISCUSSION

3.1 Episode I – Analysis of the Spatial Error

Figure 8 shows the results of Episode I trials on artificial targets. The 9 targets are represented on the x-axis, with the y-axis showing the signed distance between a detection point and its corresponding target. The distance is positive (>0) if the detection point is *after* the target in the direction of travel and negative (<0) if it is *before* the target. The large black dots represent the median signed distance between a target and its corresponding detection points. It is clear that the majority of the detection points are generated within ± 25 cm from their target, with around 90% of the median distances falling in this range. Therefore, we choose R = 25 cm as the radius of the buffer area as described in section '*"Definition of a "Detection".*'

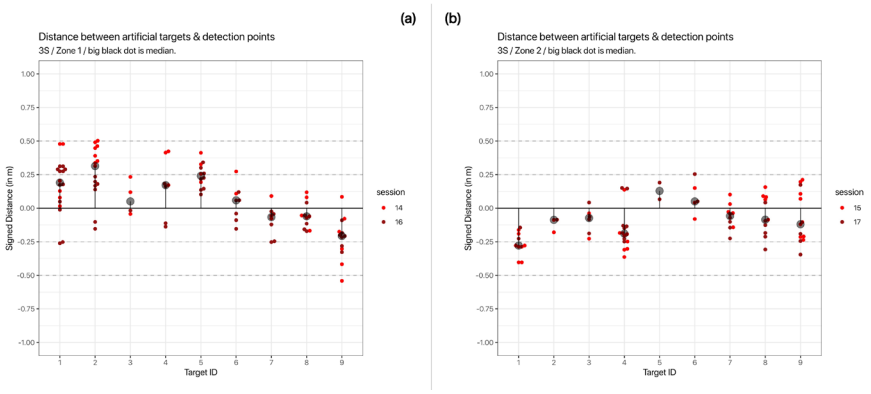


Figure 9 – Beeswarm plots of the signed distance between the detection points and their corresponding ground-truth artificial target (IDs on the x-axis). Each red point represents a detection point generated by the system. Black dots represent

3.2 Episode II – Performance Results Under Real-World Conditions

3.2.1 Repeatability

Four sessions, in each zone, have been conducted under exactly the same parameters and within short intervals of time in order to study the stability and repeatability of the spraying system under the same conditions.

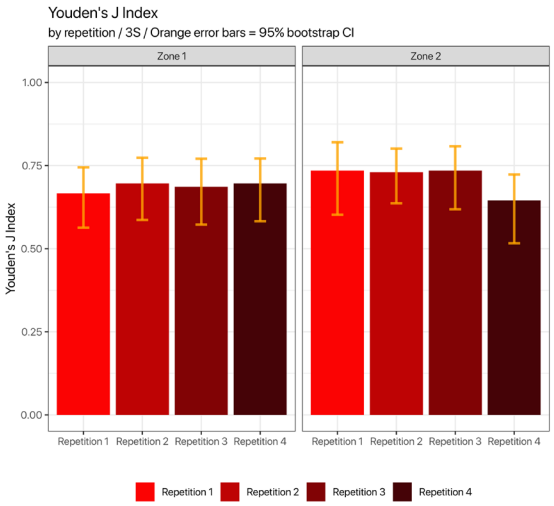


Figure 10 – Youden's J index for all 4 repetitions over the two zones with 95% confidence intervals in

Figure 9 shows Youden's *J* index for all 4 repetitions over the two zones. The figure summarizes the detection performance of the system under the same conditions. As we can see, the system exhibits, on average, a *J* index of around 0.6, indicating very good performance in detecting the weeds and missing the "control" points. The 95% confidence intervals (in orange) computed by bootstrap show us if the system exhibits high variability and if the slight differences seen between the repetitions are significant. As the intervals are highly overlapping, the small differences seen are not significant at the 5% confidence level. We can thus say that the system is stable under the same conditions and can be considered *repeatable*.

3.2.2 Speed

To study the influence of the sprayer's speed on the detection performance, we conducted two different sessions in each zone, one session at 10 km/h and the other at 14 km/h. The detection performance as measured by Youden's *J* is shown in Figure 10(a). We can observe conflicting results with respect to the zone, whereby in Zone 1 the system seems to be better performing at 14 km/h than at 10 km/h and vice versa in Zone 2. This may indicate that the relationship between speed and detection performance is not clear and that there may be another variable influencing the system's behavior.

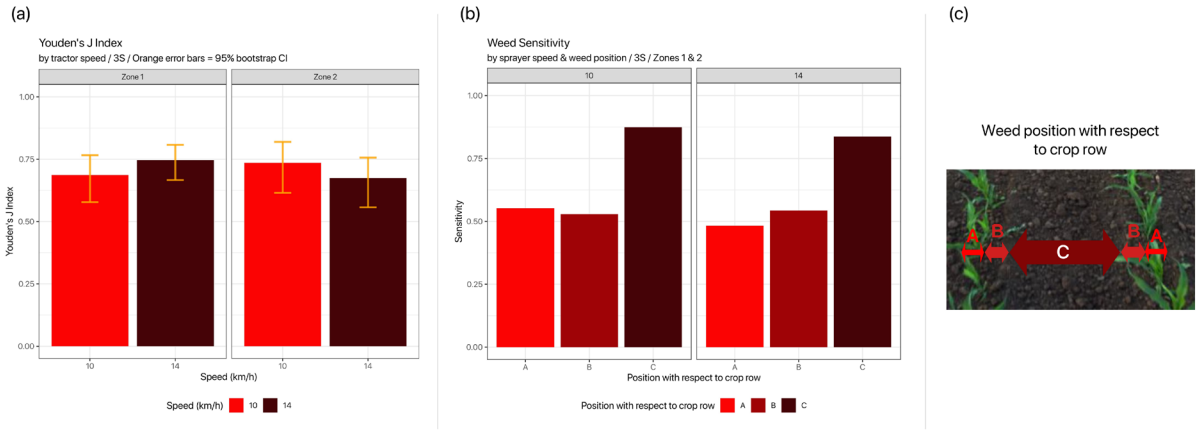


Figure 11 – Results of detection performance with respect to sprayer's speed. (a) Youden's *J* index in the two zones and for the two speed configurations. (b) The weed sensitivity for the two speed configurations (left panel for 10 km/h, right panel for 14 km/h) as a function of the weed's position in the crop row. (c) Representation of the three possible weed positions: [A] corresponds to weeds that are in the crop row (0 to 2 cm), [B] corresponds to weeds that are close to the crop row (2 to 10 cm), and [C] to weeds that are in inter-row position.

Further investigation reveals that one of the most important factors determining the model's performance is the weed's position in the crop row. Figure 10(b) shows the proportion of detected weeds (sensitivity) across the two speed configurations (in the two panels) and for the 3 weed position levels represented in Figure 10(c). We can see that increasing the sprayer's speed reduces the detection rate of weeds that are position in A from around 55% to 48%. On the other hand, the weeds that are in position B appear to be slightly better detected at higher speed. Finally, the sensitivity of weeds that are in position C is slightly reduced from around 82% to around 78%. This may indicate that if our priority is to detect inter-row weeds (in position C), then we can advance at higher speeds without heavily penalizing the sprayer's detection performance.

4/ CONCLUSIONS

In this article, we have proposed a methodology for evaluating the detection performance of a spot spraying system on real targets and under real-world conditions. This work constitutes a first proposal towards the development of reliable protocols for the evaluation of spot sprayers. Indeed, as this weeding approach gains in maturity and becomes more widely available, it becomes increasingly important to evaluate it objectively and faithfully.

The procedure is based on the comparison of spatial detection maps generated by the sprayer to ground-truth maps consisting of a sample of "weed" and "control" points that have been carefully mapped *a priori* in the experimental parcel (Episode II). The careful mapping of the weeds in the field constitutes a central step of the procedure because it grounds the evaluation into real "ground-truth" maps and allows us to study the performance of the system on these true points. In order to define what a "detection" really is, an empirical study of the spatial scatter of detection points around artificial targets has been conducted as a first episode (Episode I) in this protocol. Such an analysis is required since it is unrealistic to assume perfect spatial mapping and alignment between the detection and ground-truth maps.

Finally, we have deployed our proposed protocol to analyze the detection performance of the Spot Spray Sensor (3S) system under real-world conditions in a parcel in North-Eastern France. Carefully designed experiments shown in this article have demonstrated the system's repeatability when deployed under the same conditions and the mitigated impact of speed on the sprayer's performance.

Acknowledgements

The authors would like to thank Océane Bridenne, Lisa Charron, Vinciane Couvent, Ghislain Drohe, Lucie Dumont, Arthur Galaup and Louis Lelièvre for participating in the data collection procedure.

References

- Allmendinger, Alicia, Michael Spaeth, Marcus Saile, Gerassimos G. Peteinatos, and Roland Gerhards. 2022. "Precision Chemical Weed Management Strategies: A Review and a Design of a New CNN-Based Modular Spot Sprayer." Agronomy 12(7):1620. doi:10.3390/agronomy12071620.
- Foulle, Sébastien. 2025. "Mathematical Characterization of Better-than-Random Multiclass Models." Transactions on Machine Learning Research. https://openreview.net/forum?id=VdW9SkALSd.
- Holm, F. A., and E. N. Johnson. 2009. "The History of Herbicide Use For Weed Management on the Prairies." Prairie Soils and Crops 2:1–10.

- Hüllermeier, Eyke, and Willem Waegeman. 2021. “Aleatoric and Epistemic Uncertainty in Machine Learning: An Introduction to Concepts and Methods.” Machine Learning 110(3):457–506. doi:10.1007/s10994-021-05946-3.
- Melki, Paul. 2025. “Contributions to Conformal Prediction for Computer Vision-Based Decision-Making in Agriculture.” Theses, Université de Bordeaux.
- Regnier, Rémi, Guillaume Avrin, Virginie Barbosa, Daniel Boffety, Anne Kalouguine, and Sophie Lardy-Fontan. 2021. “Validation de méthodologies d’évaluation de solutions de désherbage autonomes, dans le cadre des projets Challenge ROSE et METRICS.” Revue Ouverte d’Intelligence Artificielle 2(1):11–32. doi:10.5802/roia.8.
- Van Bruggen, A. H. C., M. R. Finckh, M. He, C. J. Ritsema, P. Harkes, D. Knuth, and V. Geissen. 2021. “Indirect Effects of the Herbicide Glyphosate on Plant, Animal and Human Health Through Its Effects on Microbial Communities.” Frontiers in Environmental Science 9:763917. doi:10.3389/fenvs.2021.763917.
- Vijayakumar, Vinay, Yiannis Ampatzidis, John K. Schueller, and Tom Burks. 2023. “Smart Spraying Technologies for Precision Weed Management: A Review.” Smart Agricultural Technology 6:100337. doi:10.1016/j.atech.2023.100337.
- Youden, W. J. 1950. “Index for Rating Diagnostic Tests.” Cancer 3(1):32–35.
- Young, Stephen L., George E. Meyer, Wayne E. Woldt, and Francis J. Pierce. 2014. “Future Directions for Automated Weed Management in Precision Agriculture.” Pp. 249–59 in Automation: The Future of Weed Control in Cropping Systems, edited by S. L. Young and F. J. Pierce. Dordrecht: Springer Netherlands.
- Yu, Ping, and Stephen Christopher Marble. 2022. “Practice in Nursery Weed Control—Review and Meta-Analysis.” Frontiers in Plant Science 12. doi:10.3389/fpls.2021.807736.

MTAD: an Unsupervised Method to Identify Obstacles in Complex Agricultural Environments

Théo Biardeau[a,b,*], Anne-Sophie Capelle-Laizé[a], Salwan Alwan[b], David Helbert[a]

[a] Université de Poitiers, CNRS, XLIM, Poitiers, France
[b] Cyclair, Pressac, France
* Corresponding author. Email: theo.biardeau@univ-poitiers.fr

Abstract

In agricultural robotics, robot autonomy and safety rely in part on the detection of unexpected obstacles. However, spotting elements smaller than crops remains a major bottleneck, often beyond the reach of conventional sensors. Visual anomaly detection using deep learning offers a promising solution to this challenge. The principle consists in modeling the normal appearance of field in order to isolate any element that deviates from the learned distribution. Nevertheless, current architectures suffer from over-generalization. By reconstructing anomalies too faithfully, they end up masking their presence. To overcome this limitation, we present MTAD, a hybrid architecture combining a ViT encoder and a convolutional decoder, regulated by a memory module in the latent space. This memory constrains reconstruction solely to the normal patterns observed during training. Evaluated on the MVTec AD industrial reference benchmark as well as on two real agricultural datasets (Rosario and Cyclair), MTAD achieves high AUROC scores of 0.82 on MVTec, 0.95 on Rosario and 0.92 on Cyclair for anomaly detection.

KEYWORDS: Agricultural robotics, Unsupervised anomaly detection, Vision Transformers, Latent memory module, Artificial intelligence.

Complexity level: 5

1/ INTRODUCTION

Agriculture has undergone significant transformations in recent years, particularly with the automation of labour-intensive tasks such as seeding and mechanical weeding, facilitated by specialized rovers.
However, deploying rovers that weigh several tons requires stringent safety measures to prevent accidents which can temporarily incapacitate the robot or injure wildlife and humans to varying degrees. While safety sensors like LiDAR and RADAR are integral to this safety apparatus, they often fall short, especially in detecting obstacles smaller than the crops in dense fields. These sensors lack a discrimination system, making them ineffective for certain types of obstacles. A promising solution is integrating more sophisticated sensors, such as cameras used for navigation tasks. However, this requires advanced data processing and analysis to identify

obstacles. Therefore, it is essential to develop solutions capable of using cameras in addition to traditional safety sensors to ensure rover safety. Despite some progress in developing obstacle detection algorithms, research in this area remains limited.

In the scientific literature, Mujkic et al. (2023) proposed a comprehensive framework combining supervised algorithms like YOLOv5 (Jocher, 2020) with unsupervised approaches such as convolutional autoencoders (CAEs). Although supervised detectors provide reliable bounding box predictions, they are constrained by the closed-set assumption and demand extensive annotated datasets, an impractical requirement for capturing all potential hazards in agricultural environments. In contrast, unsupervised approaches operate under an open-set paradigm. Consequently, this unsupervised detection strategy is particularly well-suited for unstructured environments where hazards, such as wildlife in our application, are rare, unpredictable, or difficult to exhaustively annotate. Consequently, this paper focuses on unsupervised anomaly detection, aiming to enhance the safety and efficiency of agricultural rovers.

Anomaly Detection (AD) has recently attracted growing interest, mobilising significant research resources to find new methods. According to Ruff et al. (2021), "An anomaly is an observation that deviates significantly from some concept of normality. Also known as an outlier or novelty, such an observation may be described as unusual, irregular, atypical, inconsistent, unexpected, rare, erroneous, defective, fraudulent, malicious, unnatural or simply strange, depending on the situation". As mentioned by Ruff et al. (2021), anomaly detection methods can be broadly categorized into reconstruction-based, classification-based, probabilistic, and distance-based approaches. Among these, reconstruction-based encoder-decoder (ED) architectures remain the most prominent for visual inspection.

The use of transformers in visual AD was introduced by Mishra et al. (2021) using the VT-ADL method. The paper proposes a hybrid autoencoder (AE) composed of a ViT as an encoder and a convolutional decoder. The patches processed by the transformers are then fed to a Gaussian mixture density network, which finally feeds a decoder. AnoViT (Lee & Kang, 2022) demonstrates the superiority of transformers in AD. It comprises a ViT encoder and a convolutional decoder. This new architecture offers superior performance compared to convolutional AEs and opens new opportunities in the field of AD. The ADTR method (You et al., 2023) is similar in many ways to AnoViT. However, the network uses features calculated by the EfficientNet (Tan & Le, 2019) network instead of RGB images, yielding superior performance. HaloAE (Mathian et al., 2024) is a self-supervised method for AD consisting of a paste & cut augmentation strategy, feature extraction, a transformer-based ED, and a detection network. However, ViTs are computationally intensive, and it is impossible to apply them on a pixel-by-pixel basis. One solution is to reduce the image size by extracting features, or to divide the image into regions of a defined size (most often 16x16). Even this constraint tends to limit the detection of very small anomalies; however, the articles cited below demonstrate, through their results, that this constraint has a limited impact given the additional performance gains achieved. In addition, the aforementioned ED architectures still tend to overgeneralize. One solution is to incorporate a memory, which helps avoid the problem of shortcuts.

The memory-encoder-decoder-based AD method was introduced by Gong et al. (2019). In their paper, they propose several improvements for AD, including attention-based sparse addressing. This method enables better reconstruction of normal areas and poorer reconstruction of abnormal areas compared to the traditional convolutional ED-based approach. The memory incorporated in this approach prevents the model from over-interpreting abnormal input, resulting in a less accurate reconstruction of abnormal input. Gu et al. (2023) have developed memory-based AD methods using a student-teacher architecture, which follows the same principle. In addition to the memory-convolutional-based architecture, another architecture based on

memory transformer. Liu et al. (2024) introduced MemFormer, an architecture based on memory transformers that are capable of detecting abnormal videos and images in subways. Based on this new architecture, Lu et al. (2023) propose a multi-class unsupervised AD, using a hierarchical memory-based transformer. Nonetheless, all of these hybrid and memory-augmented approaches were tailored for and benchmarked against controlled industrial inspections (e.g., MVTec AD (Bergmann et al., 2021)). These settings feature fixed viewpoints, static illumination, and rigid objects. In contrast, outdoor agricultural robotics presents an unstructured environment characterized by environment variability including dynamic lighting, soil heterogeneity, moving foliage, and camera vibrations.

To address this gap and determine whether discrete memory constraints can withstand open-field conditions, we introduce Memory Transformers Anomaly Detection (MTAD). Our framework couples a ViT encoder with an explicit embedding discretization memory module and a convolutional decoder, balancing long-range field perception with constrained latent reconstruction. We implemented our method on three datasets. The first, MVTec AD dataset (Bergmann et al., 2021) is a benchmark for industrial anomaly detection. The Rosario dataset (Pire et al., 2019) as open agriculture data generated by robotic platform. The last is the Cyclair dataset, which is a private dataset generated from the acquisitions of a "Grillon" weeding rover that is in pre-production. The results show that our approach represents an improvement in anomaly detection in the industrial and agricultural sectors, with improvements in anomaly detection rates of 4% and 3%, respectively.

Consequently, we present the following contributions in this paper:

- A novel hybrid architecture (MTAD) combining a Vision Transformer encoder and a convolutional decoder, regulated by a discrete latent memory module to limit over-generalization.
- Extensive real-world validation across both industrial benchmarks (MVTec AD) and complex open-field environments, using the public Rosario dataset and an in-field dataset gathered from the Cyclair Grillon autonomous weeding rover.

The structure of this paper is as follows: Section 2 outlines the proposed method, and Section 3 presents both quantitative and qualitative experimental results. Finally, Section 4 provides a conclusion.

2/ MATERIALS AND METHODS

2.1 Dataset

In our approach to anomaly detection via reconstruction, the experimental protocol strictly distinguishes between three datasets. Training is performed exclusively on a training set consisting of normal images. At the same time, a validation set which also contains only unseen normal images, is used during the training phase to monitor loss. Finally, the final performance evaluation is conducted after training on a dedicated test dataset. This dataset consists of both normal and abnormal images, allowing us to quantify the model's detection and localization capabilities by calculating the AUROC.

2.2 MVTec

The MVTec AD dataset is designed for the comparative evaluation of anomaly detection methods in the field of industrial inspection. It comprises 15 categories (objects and textures) for a total of 5,354 images, divided into 3,629 normal images and 1,725 abnormal images. Pixel-level masks

delineating the anomaly region are provided, allowing for the measurement of performance in both anomaly localization and detection.

2.3 Rosario

The Rosario dataset provides sensor data (stereo, calibrated, odometry/inertial/GPS fusion) for autonomous mobile robotics in agricultural settings. The data were recorded in various environments (harvested fields, fields under cultivation, *etc*). Visual anomalies are present but not labeled at the pixel level. The training set comprises 4,565 normal images, the validation set contains 136 images, and the evaluation set contains 2,695 images, which may be either normal or abnormal.

2.4 Cyclair

The Cyclair database contains images acquired during scenario of weed-control operations in cornfields with *Grillon* rovers presented Figure 1. Training uses 777 normal images. Our validation set contains 100 normal images, and our evaluation set contains 253 images, 159 of which are abnormal but not labeled at the pixel level.



Figure 1 : Developed by Cyclair for field crops, the Grillon is a 1,500-kg autonomous tool-carrying robot (3 m working width, 8-hour electric autonomy) supervised on-site by a human operator. Its navigation relies on minimal georeferencing and a comprehensive suite of sensors: HDR cameras, 2D/3D LiDAR, ultrasonic sensors, bumpers, and GNSS RTK positioning with odometry on four-wheel drive and steering.

2.5 MTAD overview

Like many architectures, our anomaly detection method is based on the hybrid ViT-convolutional architecture, which is common in the literature (Lee & Kang, 2022). It consists of three key components, illustrated in Figure 2 : a pre-trained ViT (Dosovitskiy et al., 2020), which is frozen, a trained memory module and a convolutional decoder.

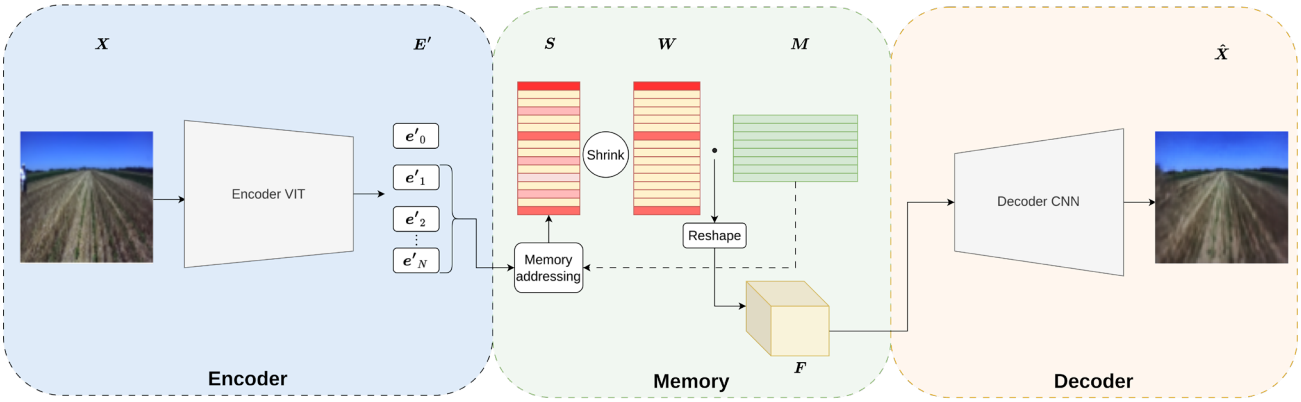


Figure 2 : MTAD architecture.

During inference, the input image is divided into patches and then processed through the ViT blocks. The features obtained at the ViT output are then mapped by the memory module to capture representations of normality, and subsequently upsampled by the convolutional decoder to reconstruct the image. The anomaly score map is calculated by measuring a reconstruction distance, pixel by pixel, between the original image and the reconstructed image. The following parts of this article are devoted to an in-depth explanation of this architecture. It is important to emphasize that MTAD operates with frozen weights during deployment and is strictly intended as a situational awareness and obstacle anticipation aid. It does not replace certified functional safety sensors (e.g., emergency stops or SIL-rated sensors) governed by the Machinery Regulation and the EU AI Act.

2.6 ViT Encoder

The goal of ViT is to perform image classification using a Transformer encoder and thereby take advantage of the benefits of attention. To process an image $\boldsymbol{X} \in \mathbb{R}^{H\times W\times C}$, it is first divided into N flat patches $\boldsymbol{X_{patch}} \in \mathbb{R}^{N\times(P^2C)}$, where $N = HW/P^2$ (P being the patch size). These patches are then projected into a D-dimensional space via a learnable linear layer, producing the sequence of embeddings $\boldsymbol{E} \in \mathbb{R}^{N\times D}$, where $\boldsymbol{e} \in \mathbb{R}^{N\times D}$ is an element of $\boldsymbol{E}$. A class token $\boldsymbol{e}_{cls} \in \mathbb{R}^{1\times D}$, is initialized randomly and concatenated with $\boldsymbol{E}$. This token serves to condense the overall information of the image for the classification task. Finally, the positional embeddings $\boldsymbol{E_{pos}} \in \mathbb{R}^{(N+1)\times D}$ initialized randomly are added to the patch embeddings (including the class token), thereby preserving spatial position information. The resulting sequence is processed l times by transformer encoder blocks, each consisting of a normalization layer, a multi-head attention block, a second normalization layer, and an MLP. This generates the output embedding sequence $\boldsymbol{E'} \in \mathbb{R}^{(N+1)\times D}$. The classification prediction is obtained by applying a final MLP only to the output class token $\boldsymbol{e'_{cls}}$ (the first row of $\boldsymbol{E'}$).
For AD, since the goal is to assign an anomaly score to each pixel, the output class token $\boldsymbol{e'_{cls}}$ is excluded. Selected embeddings are then sent to memory to be discretized and limit the over-generalisation.

2.7 Memory

Inspired by Gong et al. (2019), this module adapts parametric memory to the ViT architecture. It consists of a learnable matrix $\boldsymbol{M} \in \mathbb{R}^{K\times D}$ (K prototypes $\boldsymbol{m}_j \in \mathbb{R}^D$) and an attention-based addressing operator. By restricting the reconstruction to a small number of memorized normal elements, the representational capacity is bounded, abnormal embeddings are imperfectly reconstructed, which increases the final error.

To reconstruct the discretized matrix $\boldsymbol{E'_d} \in \mathbb{R}^{N\times D}$ from the embeddings $\boldsymbol{E'}$, we compute a sparse attention matrix $\boldsymbol{W} \in \mathbb{R}^{N\times K}$ such that:

$$\boldsymbol{E'_d} = \boldsymbol{W} \cdot \boldsymbol{M}.$$

The first step is to compute the pairwise cosine similarity between $\boldsymbol{E'}$ and $\boldsymbol{M}$ yields a distance matrix $\boldsymbol{D} \in \mathbb{R}^{N\times K}$:

$$\boldsymbol{D_{i,j}} = \frac{\boldsymbol{E'_i} \cdot \boldsymbol{m_j^T}}{\|\boldsymbol{E'_i}\|\|\boldsymbol{m_j}\|}.$$

Softmax normalization along the lines then produces the attention distributions $\boldsymbol{S} \in \mathbb{R}^{N\times K}$:

$$\boldsymbol{S_{i,j}} = \frac{e^{\boldsymbol{D_{i,j}}}}{\sum_{k=1}^{K} e^{\boldsymbol{D_{i,k}}}}.$$

To penalize the reconstruction of anomalies, a hard threshold λ filters out small addressing weights:

$$\widehat{\boldsymbol{w}}_{\boldsymbol{i,j}} = \frac{max(0, \boldsymbol{S} - \lambda)\boldsymbol{S}}{\boldsymbol{S} - \lambda + \epsilon}$$

with $\epsilon \cong 0$. Finally, the matrix $\widehat{W}$ is renormalized to ensure that the sum of each row is 1:

$$\boldsymbol{w_{i,j}} = \frac{\widehat{\boldsymbol{w}}_{\boldsymbol{i,j}}}{\sum_{k}^{K} \widehat{\boldsymbol{w}}_{\boldsymbol{i,k}}}.$$

The resulting representations $\boldsymbol{E'_d}$ are then passed to the convolutional decoder to be reconstructed at the initial image size.

2.8 Convolutional decoder

We chose to use a convolutional decoder because of its ability to reconstruct local patterns and oversample features from the latent space Z. The convolutional decoder-based approach aims to reconstruct $X^{(H\times W\times C)}$ at its original size from $\boldsymbol{E'_d}$. We must reshape $\boldsymbol{E'_d}$ into $F \in \mathbb{R}^{(\sqrt{N}\times\sqrt{N}\times D)}$ to feed our CNN decoder. The convolutional decoder consists of 5 transposed convolution blocks: $L_1(768 \to 256, 3\times 3, s = 1)$, $L_2(256 \to 128, 5\times 5, s = 1)$, $L_3(128 \to 64, 5\times 5, s = 2)$, $L_4(64 \to 32, 5\times 5, s = 2, p = 1)$, and $L_5\big(32 \to 3, 7\times 7, s = 3, p = 1, out_p = 1\big)$, each followed by batch normalization and GELU (only sigmoid for L_5).

2.9 Learning Objective

Since our model consists of several components (the encoder-decoder and the memory), the loss function comprises two distinct elements. First, we have the reconstruction loss $\mathcal{L}_c$. It evaluates the model's ability to correctly reconstruct $\widehat{\boldsymbol{X}}$ from $\boldsymbol{X}$. We choose the mean squared error (MSE) across channels, which allows the model to focus on the quality of the reconstruction, pixel by pixel:

$$\mathcal{L}_c = MSE\big(\boldsymbol{X}, \widehat{\boldsymbol{X}}\big).$$

The second loss function, $\mathcal{L}_m$, comes from (Gong et al., 2019):

$$\mathcal{L}_m = \sum \sum_{i=1}^{K} - \boldsymbol{w_i} \cdot log(\boldsymbol{w_i}).$$

Its goal is to train the memory to use a minimal number of elements $\boldsymbol{m_i}$ to represent $\boldsymbol{e_i}$ generated by the encoder. During the training phase, this parsimony constraint forces the memory to update itself using only its most relevant elements, thereby compelling it to store only the prototypical patterns of the normal distribution. Thus, the total training objective is described as:

$$\mathcal{L}_{Total} = \mathcal{L}_c + \alpha \mathcal{L}_m$$

where α is a ponderation. The memory and convolutional decoder are optimized using joint gradient descent. The training is considered finished after a large number of epochs, as performed in the literature (Lee & Kang, 2022; Mishra et al., 2021; You et al., 2023).

2.10 Anomaly score map generation

The anomaly score map is computed via pixel-wise Mean Squared Error across channels,

$$S(x, y) = MSE(\boldsymbol{X}, \widehat{\boldsymbol{X}}),$$

and smoothed with a Gaussian filter ($\sigma = 12$ for detection, $\sigma = 5$ for localization). We use the maximum of anomaly score map for detection and all anomaly score map for localization.

2.11 Experimental Protocol

All images are resized to a size of $3 \times 384 \times 384$ using bilinear interpolation. We use vertical flipping and color jitter as data augmentation. ViT-Base/16 pre-trained on ImageNet-1k is used as encoder.

2.12 Implementation Details

Due to the strictly unsupervised setup precluding anomaly-based validation metrics, the model was trained for 200 fixed epochs to ensure asymptotic loss convergence and stable memory prototype consolidation, in line with established literature practices. The batch size was set to 4, the image size to 384, the memory size to 8192 and the thresholding parameter λ = 0.96/8192 . $\alpha = 0.0015$. The Adam optimiser was employed with a learning rate of 1×10^{-4}. Images are normalized according to the ImageNet-1K recommendations. In line with standard protocols for the MVTec dataset, a separate model with dedicated weights was trained for each category, using only its normal samples. For the other datasets (Rosario and Cyclair), a single global model is trained using all available normal data.

3/ RESULTS AND DISCUSSION

To rigorously validate the performance of the MTAD model and gain a detailed understanding of the contributions of its various components, our experiments are structured around three complementary approaches. First, quantitative evaluation allows us to measure detection and localization capability at the image and pixel level using the AUROC metric. MTAD is compared with four state-of-the-art architectures: Conv-AE and AnoViT. (Lee & Kang, 2022), MemAE (Gong et al., 2019) and VQ-VAE (van den Oord et al., 2017). These algorithms were selected because they share an encoder-decoder structure. Some (MemAE, VQ-VAE) incorporate a memory component into their latent space. We excluded DAE (Vincent et al., 2010) which we deemed too similar to Conv-AE, and ADTR because it uses features extracted by an upstream network. Next, a

qualitative evaluation complements these results with a visual analysis of the anomaly score map. Finally, since memory is at the heart of MTAD, we conduct a comprehensive impact study on it. We first measure its direct contribution through an ablation study comparing the model with and without a memory block, thereby illustrating the phenomenon of overgeneralization. We then explore the internal dynamics of its addressing system by analyzing latent tokens. The object mean corresponds to the AUROC mean across the ten objects, the texture mean corresponds to the AUROC mean across the five textures, and the total mean corresponds to the AUROC mean across the fifteen classes.

3.1 Quantitative results and analysis

Table 1 shows that MTAD achieves the best detection performance on objects and textures. Its overall average AUROC (0.82) is 4 percentage points higher than that of AnoViT and MemAE (0.78). Conv-AE and VQ-VAE are outperformed. MTAD also exhibits the lowest variability (standard deviation of 0.11), indicating more stable performance across categories, followed by AnoViT (0.14) and VQ-VAE (0.15).

Table 1: Comparison of the performance of anomaly detection methods (AUROC at the image level) on MVTec AD. The best results are in **bold**; the second-best results are underlined.

Type	Conv-AE	AnoViT	VQ-VAE	MemAE	MTAD
Objects mean	0.70	0.81	0.75	0.72	**0.82**
Texture mean	0.78	0.74	0.73	0.75	**0.82**
Total Std	0.18	0.14	0.15	0.18	**0.11**
Total average	0.73	0.78	0.75	0.78	**0.82**

Table 2: Comparison of the performance of anomaly localization methods (pixel-level AUROC) on MVTec AD. The best results are in **bold**; the second-best results are underlined.

Type	Conv-AE	AnoViT	VQ-VAE	MemAE	MTAD
Objects mean	0.85	0.86	0.87	0.81	**0.93**
Texture mean	0.72	0.76	0.76	**0.84**	0.80
Total Std	**0.10**	0.14	0.13	0.14	**0.10**
Total average	0.81	0.83	0.82	0.82	**0.88**

Table 2 shows that MTAD perform in localization, achieving the best score on objects. Its overall average AUROC (0.88) is 5 percentage points higher than that of AnoViT (0.83), the second-best performer. MemAE (0.82) follows closely behind, with notable performance on textures. In terms of variability, MTAD and Conv-AE exhibit the greatest stability (standard deviation of 0.10).

Table 3: Comparison of anomaly detection performance on the Rosario dataset. The best result is shown in bold; the second-best result is shown in underlined.

Method	Conv-AE	AnoViT	VQ-VAE	MemAE	MTAD
AUROC	0.65	0.93	0.83	0.78	0.95

Since the labeling of the Rosario images is poor, only the detection performance can be quantified. Table 3 shows that MTAD achieves the best AUROC (0.95). AnoViT follows closely behind (0.93), outperforming VQ-VAE (0.83) and MemAE (0.78). Conv-AE performs the worst (0.65).

Table 4: Comparison of anomaly detection performance on the Cyclair dataset. The best result is in **bold**; the second-best results are underlined.

Method	Conv-AE	AnoViT	VQ-VAE	MemAE	MTAD
AUROC	0.78	0.89	0.87	0.89	0.92

Similar to Rosario, the Cyclair images are sparsely labeled, allowing only for the quantification of detection. Table 4 shows that MTAD achieves the best AUROC (0.92). MemAE and AnoViT are tied for second place (0.89), ahead of VQ-VAE (0.87) and Conv-AE (0.78).
MTAD demonstrates superior performance in both localization and detection, as illustrated by its results on objects from the MVTec AD dataset. This performance gain over purely CNN-based approaches is attributable to the hybrid ViT-CNN architecture, which leverages the global information from the ViT encoder and the local details from the CNN decoder. Furthermore, the integration of a memory module prevents reconstruction overgeneralization, thereby significantly improving MTAD's accuracy compared to AnoViT and memory-based CNN methods. This robustness is confirmed by the fact that, on agricultural data, MTAD achieves a 3% and 2% performance gain over AnoViT on the Cyclair and Rosario agricultural dataset. By contrast, CNN-based architectures lag behind MTAD by 5% in best case. This difference emphasises the importance of the ViT encoder's global attention capability, which is essential for understanding complex agricultural environments where CNNs struggle to capture large-scale relationships.

Nevertheless, we observe that CNN models, particularly MemAE, achieve better results in localizing texture anomalies. This difference can be explained, in part, by the continuous spatial processing inherent in CNNs, which avoids the patch-based characteristic of ViTs that can induce edge effects. On the other hand, texture anomalies are primarily characterized by a local break in coherence, a pattern that convolutional filters are naturally better equipped to isolate, unlike object-based anomalies, which require a global structural understanding. To corroborate these quantitative observations and analyze the behavior of our models in greater detail, we conduct a qualitative evaluation below.

As shown in Figure 3, transformer-based methods such as AnoViT and MTAD successfully detect small anomalies. However, for larger anomalies, both models suffer from reconstruction artifacts, making precise localization more challenging. Regarding score distributions, MTAD produces noticeably less background noise than AnoViT, especially in the presence of large anomalies. While the AE and MemAE methods tend to detect all anomalies, whether small or large, artifacts appear as the score increases in normal areas. Conversely, VQ-VAE struggles to preserve normal regions accurately, leading to degraded reconstruction quality across the background despite detecting some anomalies. In Figure 4, we observe that MTAD consistently detects anomalies of all sizes, ranging from about ten pixels to several thousand, with a stable score throughout the anomaly images. AnoViT also detects anomalies accurately, but with some variability in the scores. For example, in the score map representing a man, the shadow receives a much higher score than the man himself. The MemAE and VQ-VAE methods produce similar results, accurately detecting all anomalies except for the upper body of the man. In contrast, the AE fails to detect the man and exhibits considerable noise in the other images, indicating difficulty in identifying anomalies.

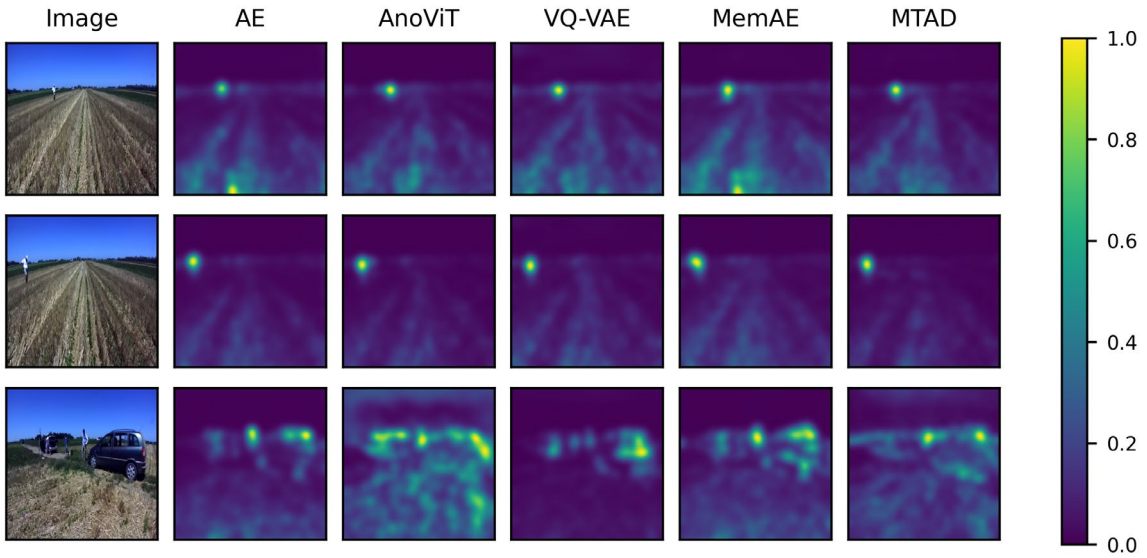


Figure 3: Qualitative results of anomaly detection on Rosario dataset. Anomaly is signaled by high score.

Overall, these qualitative results corroborate the findings from the quantitative evaluation. In challenging agricultural scenes characterized by non-uniform terrain and varying lighting conditions, MTAD establishes a superior trade-off between sensitivity to small anomalies and suppression of background artifacts. While traditional AEs and memory-based baselines exhibit noticeable degradation or excessive false-positive rates, MTAD reliably generalizes across diverse anomaly scales, confirming its effectiveness as a robust localization framework.

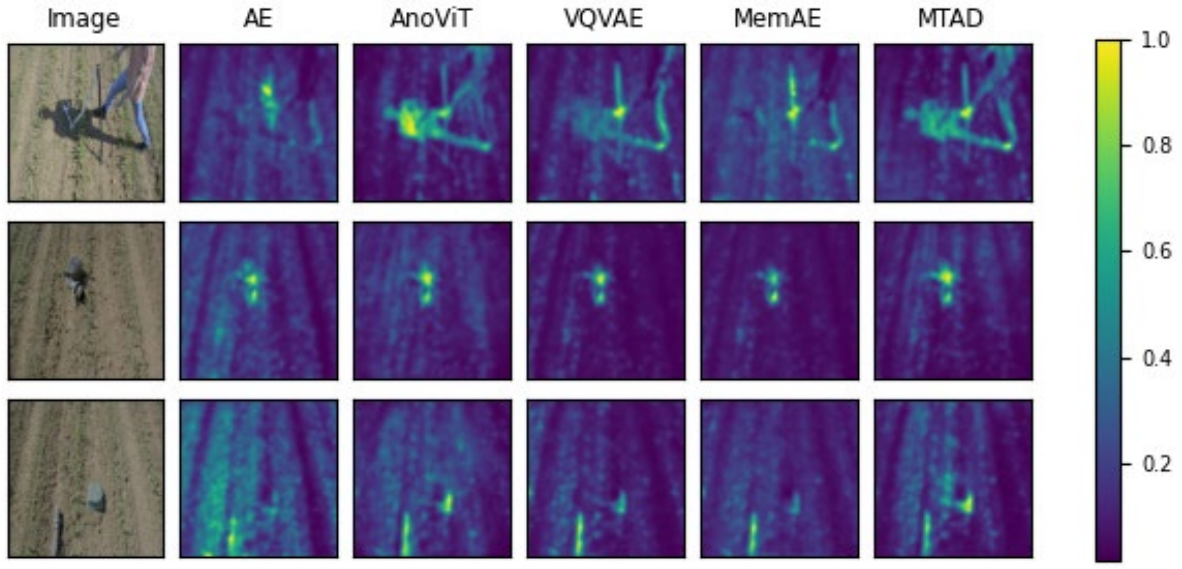


Figure 4: Qualitative results of anomaly detection on Cyclair dataset. Anomaly is signaled by high score.

3.2 Memory impact

It is important to evaluate the impact of memory within our architecture both quantitatively and qualitatively. To do so, we built a network identical to MTAD, but without latent-space memory. The same hyperparameters are used for both models. We evaluate the model on MVTEC because this dataset is the most comprehensive and includes anomaly labeling via masks.

Memory	Average detection	Std detection	average localization	Std localization
No	0.80	0.16	0.86	0.11
Yes	0.82	0.11	0.88	0.10

Table 5: Study of the impact of memory. The table shows the average AUROC for all objects in detection/localization, along with their respective standard deviations.

Table 5, which presents the results of the two architectures, shows that memory has a positive impact on anomaly detection and localization, yielding higher scores. It is important to note that the model is more stable and does not overperform on certain objects, as shown by the standard deviation metrics. This is not the case for the model without memory.

3.3 Inference Latency and Real-Time Feasibility

To assess the viability of MTAD for autonomous navigation on agricultural rovers, inference latency was benchmarked on an NVIDIA RTX 2000 Ada with an input resolution of 384×384 pixels. The end-to-end processing pipeline achieves an average inference time of 54 ms per frame (approximately 18.5 FPS). Given typical Grillon speeds (e.g., between 0 and 1.2 m.s-1), this latency indicates that MTAD has the potential to operate in real time for obstacle anticipation.

4/ CONCLUSIONS

This article presented the development of the MTAD anomaly detection method, which is based on an encoder-decoder architecture, a well-established approach in the literature. Our main contribution lies in the integration of a memory module within the latent space. The purpose of this memory is to limit the model's reconstruction capacity in order to reduce the phenomenon of overgeneralization, during which the network tends to reproduce the input, including anomalies.
Quantitative and qualitative evaluations validate the value of this approach. The results indicate that adding the memory improves detection and localization performance on both industrial and agricultural datasets, compared to baseline methods without memory. The ablation study highlights the positive impact of the memory, demonstrating performance gains.

At this stage, the presented approach remains limited to static, frame-by-frame processing. It does not exploit contextual and dynamic information from robotic platforms, which, due to their mobility, provide continuous video streams. Integrating this temporal dimension offers a potential avenue for increasing the robustness and reliability of detection.

References

- ADDIN ZOTERO_BIBL CSL_BIBLIOGRAPHY Bergmann, P., Batzner, K., Fauser, M., Sattlegger, D., & Steger, C. (2021). The MVTec Anomaly Detection Dataset: A Comprehensive Real-World Dataset for Unsupervised Anomaly Detection. International Journal of Computer Vision, 129(4), 1038–1059.
- Dosovitskiy, A., Beyer, L., Kolesnikov, A., Weissenborn, D., Zhai, X., Unterthiner, T., Dehghani, M., Minderer, M., Heigold, G., Gelly, S., Uszkoreit, J., & Houlsby, N. (2020, October 2). An Image is Worth 16x16 Words: Transformers for Image Recognition at Scale. International Conference on Learning Representations.
- Gong, D., Liu, L., Le, V., Saha, B., Mansour, M. R., Venkatesh, S., & Hengel, A. V. D. (2019). Memorizing normality to detect anomaly: Memory-augmented deep autoencoder for unsupervised anomaly detection. In Proceedings of the IEEE/CVF international conference on computer vision (pp. 1705-1714).

- Gu, Z., Liu, L., Chen, X., Yi, R., Zhang, J., Wang, Y., ... & Ma, L. (2023, October). Remembering normality: Memory-guided knowledge distillation for unsupervised anomaly detection. In 2023 IEEE/CVF International Conference on Computer Vision (ICCV) (pp. 16355-16363). IEEE.
- Jocher, G. (2020). YOLOv5 by Ultralytics (Version 3685) [Python].
- Lee, Y., & Kang, P. (2022). AnoViT: Unsupervised Anomaly Detection and Localization With Vision Transformer-Based Encoder-Decoder. IEEE Access, 10, 46717–46724.
- Liu, R., Liu, W., Duan, M., Xie, W., Dai, Y., & Liao, X. (2024). MemFormer: A memory based unified model for anomaly detection on metro railway tracks. Expert Systems with Applications, 237, 121509.
- Lu, R., Wu, Y., Tian, L., Wang, D., Chen, B., Liu, X., & Hu, R. (2023). Hierarchical Vector Quantized Transformer for Multi-class Unsupervised Anomaly Detection. Advances in Neural Information Processing Systems, 36, 8487–8500.
- Mathian, E., Liu, H., Fernandez-Cuesta, L., Samaras, D., Foll, M., & Chen, L. (2024). HaloAE: A Local Transformer Auto-Encoder for Anomaly Detection and Localization Based on HaloNet. 18th International Conference on Computer Vision Theory and Applications, 325–337.
- Mishra, P., Verk, R., Fornasier, D., Piciarelli, C., & Foresti, G. L. (2021). VT-ADL: A Vision Transformer Network for Image Anomaly Detection and Localization. 2021 IEEE 30th International Symposium on Industrial Electronics (ISIE), 01–06.
- Mujkic, E., Ravn, O., & Christiansen, M. P. (2023). Framework for environment perception: Ensemble method for vision-based scene understanding algorithms in agriculture. Frontiers in Robotics and AI, 9.
- Pire, T., Mujica, M., Civera, J., & Kofman, E. (2019). The Rosario dataset: Multisensor data for localization and mapping in agricultural environments. The International Journal of Robotics Research, 38(6), 633–641.
- Ruff, L., Kauffmann, J. R., Vandermeulen, R. A., Montavon, G., Samek, W., Kloft, M., Dietterich, T. G., & Müller, K.-R. (2021). A Unifying Review of Deep and Shallow Anomaly Detection. Proceedings of the IEEE, 109(5), 756–795.
- van den Oord, A., Vinyals, O., & kavukcuoglu, koray. (2017). Neural Discrete Representation Learning. Advances in Neural Information Processing Systems, 30.
- Vincent, P., Larochelle, H., Lajoie, I., Bengio, Y., & Manzagol, P.-A. (2010). Stacked Denoising Autoencoders : Learning Useful Representations in a Deep Network with a Local Denoising Criterion. The Journal of Machine Learning Research, 11, 3371-3408.
- You, Z., Yang, K., Luo, W., Cui, L., Zheng, Y., & Le, X. (2023, November). Adtr: Anomaly detection transformer with feature reconstruction. In International Conference on Neural Information Processing (pp. 298-310). Cham: Springer International Publishing.

Design and implementation of robotized agroecological cropping systems: challenges and limitations encountered in the Ninsar project

Manon Boulet[a,*], Marilys Pradel[a,*]

[a] National Research Institute for Agriculture, Food and Environment, INRAE, Montoldre, 03150, France

*Corresponding author. Email: manon.boulet@inrae.fr; marilys.pradel@inrae.fr

Abstract

Agricultural robotics is increasingly considered a key lever for supporting the agroecological transition, particularly in response to labor shortages, reduced physical strain, and growing constraints related to climate change. The Ninsar project (New ItiNerarieS for Agroecology using cooperative Robots) aims to assess the feasibility of implementing agroecological cropping systems based on the collaboration of multiple agricultural robots. This paper presents the experimental design, the robotic platforms mobilized, and the main challenges encountered when integrating these technologies under real field conditions.

Two experimental scenarios were developed over three cropping seasons (2024–2026): a row intercropping system combining cereals and legumes, and a pixel farming system enabling fine-scale spatial crop management with tri-specific plant associations. The experiments used a diverse set of robots from the Roboterrium infrastructure, varying in size, locomotion modes, and technical capabilities. The analysis focuses on the compatibility between robots, tools and field operations, as well as on the organizational and technical constraints associated with multi-robot coordination.

Object detection tests revealed a systematic decline in YOLO confidence as extinction increased. A critical extinction threshold was identified near 1.5m^(-1), corresponding to a meteorological visibility of about 2 m, beyond which reliable detection could no longer be achieved. The findings define a practical visibility limit for vision-based sensing in The results reveal several major limitations, including a mismatch between robot power and available tools, coordination between machines, and sensitivity to field conditions (soil moisture, crop development stage). These findings underline the need to rethink cropping systems, tools, and robotic platforms as a whole, rather than simply replacing human labor, while aligned with agronomic and technical realities.

Overall, this work highlights both the potential and the current limitations of integrating robotics into agroecological systems, and points toward the need to overcome technical and methodological barriers to enable operational deployment.

KEYWORDS: agroecology, pixel farming, intercropping, agricultural robotics

Complexity level: 2

1/ INTRODUCTION

Agricultural systems are currently undergoing profound transitions in response to several challenges: labor shortages, the need to reduce farmers' physical strain and exposure to chemical inputs, and the need to adapt production systems to climate change. The agroecological transition involves a redesign of cropping systems in order to increase biodiversity, strengthen ecosystem functions and reduce dependence on synthetic inputs (Altieri, 1995; Wezel et al., 2009). In this context, agricultural robotics is presented as a lever to support more sustainable and resilient systems, by enabling more precise and frequent interventions (Bechar and Vigneault, 2016; Duckett et al., 2018).

Developments in agricultural robotics have led to a strong diversification of platforms and applications: from autonomous tractors and implement carriers to more compact robots dedicated to repetitive tasks such as weeding, monitoring or certain small-scale crop operations (Slaughter et al., 2008; Fountas et al., 2020). Within the Ninsar project (New ItiNerarieS for Agroecology using cooperative Robots), these robots are brought together and tested within the Roboterrium, a "vivarium" of robots that is diverse in terms of dimensions, traction capacity, locomotion modes and levels of autonomy. This technological diversity is put forward as a response to the limitations of conventional mechanization, particularly in terms of intervention windows, soil compaction and the capacity to manage complex and heterogeneous systems (Roboterrium, 2026). However, most existing robotic applications are designed for conventional systems, based on the assumption that crop operations are carried out by a single robot, whereas agroecological systems involve greater spatial and temporal diversity, as well as more complex organization of operations (Ditzler and Driessen, 2022).

Intercropping, and especially cereal–legume associations, is an example of agroecological practices. Legumes, thanks to their root nodules, can fix atmospheric nitrogen. Once their own needs are met, the surplus nitrogen they have fixed is released into the soil and therefore made available to nearby cereals. This combination of species improves resource use efficiency and reduces reliance on synthetic nitrogen fertilization. The presence of several species also increases soil cover and therefore strengthens competition against weeds (Hauggaard-Nielsen et al., 2001; Bedoussac et al., 2015). Their implementation induces a more complex system, both spatially (alternation or distribution of several species within the same field) and temporally (sometimes different intervention schedules).

The concept of pixel farming goes further, by structuring the cultivated area into small, differently managed units. This concept, explored in particular by Wageningen University & Research in several experimental setups (Van Apeldoorn et al., 2020; Ditzler and Driessen, 2022), relies on frequent, localized interventions that are difficult to carry out with conventional farm equipment. Therefore, agricultural robotics appears to be a well-suited technology to carry out a pixel farming experiment, and offers an opportunity to assess the capacity of robotic systems to implement complex agroecological technical itineraries. In this context, it was decided that three species would be planted within the same pixel, in order to test the differentiated management capabilities of agricultural robots. The choice of species was guided by the principle of allelopathy, defined as "any process involving secondary metabolites produced by plants, algae, bacteria and fungi that influences the growth and development of agricultural and biological systems" (International Allelopathy Society, 1996). Species choices took into account beneficial interactions between plants and detrimental effects on pests.

The Ninsar project, funded by the Priority Research Program and Equipment (PEPR) "Agroecology and Digital Technologies" and coordinated by Inria (Inria, 2022), aims to define agroecological

itineraries that can be implemented by a fleet of several cooperating elementary robots, operating at the plant scale. This paper presents the experimental design and lessons learned from the 2024–2026 cropping seasons, based on two experimental scenarios using the agroecological systems presented above: a row intercropping scenario (Scenario 1, S1) and a pixel farming scenario (Scenario 2, S2).

2/ MATERIALS AND METHODS

2.1 Localization of the experiments

The experiments were conducted at the INRAE experimental site of Montoldre (Allier, France). The field dedicated to the experiments is characterized by a sandy–clay soil. The cropping seasons presented here cover the years 2024, 2025 and 2026, within the framework of the Ninsar project, and build on previous work initiated in 2018 as part of the TIARA and METRICS-ACRE projects.
The Montoldre site is an integral part of the Roboterrium, an infrastructure site enabling the testing of cooperation between robots, interaction between robots and natural environments, and interaction between humans and robots under real field conditions.

2.2 Robotic platforms

To date, the Roboterrium infrastructure comprises ten robotic platforms (Figure 1). This vivarium is shared between several research organizations: INRAE, CEA, CNRS, Georgia Tech Europe (Metz), Institut Pascal (Clermont-Ferrand), XLIM (Limoges) and LAAS (Toulouse). It brings together agricultural and off-road robotic platforms, as well as a variety of onboard sensors for perception, state estimation (i.e. the robot's ability to estimate its own state, including its position and mobility) and control.

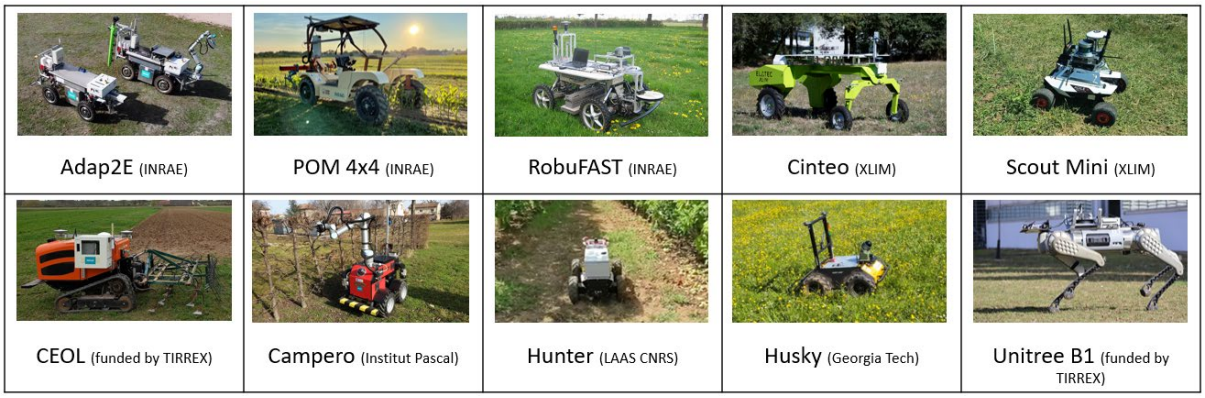


Figure 12. The Roboterrium robotic fleet (as of August 2026).

Another robotic platform, the Trektor, was used for experimental purposes (Figure 2). As the heaviest and largest robot, it has been a valuable asset due to its compatibility with conventional implements available. Despite being equipped with a hybrid engine, it was used exclusively in electric mode.
Detailed characteristics of each platform are provided in Table 1. The onboard sensors can vary depending on the user's needs, but the ones listed in the table are the default for each platform.



Figure 13. The Trektor robotic platform on the Ninsar experimental plot (photo: 04/11/2025).

Table 2. Detailed characteristics of the Roboterrium fleet as well as the Trektor robotic platform. The ones mobilized for the Ninsar agricultural interventions (soil preparation, sowing, hoeing) are highlighted in green.

Robot name	Manufacturer	Energy	Locomotion mode	Max speed (m/s)	Autonomy (h)	On-board sensors	Scenario used in	Types of operations
Adap2E	INRAE	Electric	Wheels	5	4	GPS, IMU, LiDAR	None	
Campero	Robotnik	Electric	Wheels	2	2	GPS, IMU, 4 LiDARs	None	
Ceol	Agreen-culture	Electric	Tracks	2	4	GPS, IMU, LiDAR	S1	Soil preparation
Cinteo	INRAE	Electric	Wheels	1	4	GPS, LiDAR	S1	Crop/weed discrimination
Hunter	Agilex	Electric	Wheels	2	4	4 Realsense, LiDAR	None	
Husky	Clearpath Robotics	Electric	Wheels	1	8	GPS, IMU, LiDAR, camera	S1	Trajectory only
POM 4x4	Sabi Agri	Electric	Wheels	2,5	4	GPS, IMU, LiDAR	S1, S2	Soil preparation - Sowing - Hoeing
Robufast	INRAE	Electric	Wheels	10	4	GPS, IMU, LiDAR	None	
Scout mini	Agilex	Electric	Wheels	3	3	GPS, IMU, LiDAR	S2	Trajectory only
Unitree B1	Unitree	Electric	Legs	3	4	GPS, IMU, 3 Realsense	S2	Trajectory only
Trektor	SITIA	Hybrid	Wheels	2,5	4	GPS, IMU, LiDAR, camera	S1, S2	Soil preparation - Sowing - Hoeing

For the experiments presented in this article, three of these robots were mobilized (highlighted in green in Table 1), selected on the basis of their compatibility with available tools, their sufficient traction capacity for the intended operations, and their level of technological maturity. This paper focuses on the results related to crop operations (e.g. sowing, weeding). Monitoring operations, although possible with several platforms, are outside the scope of the present article.

2.3 Cropping systems

S1 is a cropping system composed of three different and asynchronous intercropping associations, established on three fields of approximately 0.25 ha each, measuring 15 m in width and 150 m in length, with part of the third being used for S2 experiments (Figure 3). This temporal staggering allows Ninsar project partners to access fields cultivated with different species and at different growth stages. It also implies that the robots used within the project are exposed to varying pedoclimatic conditions.

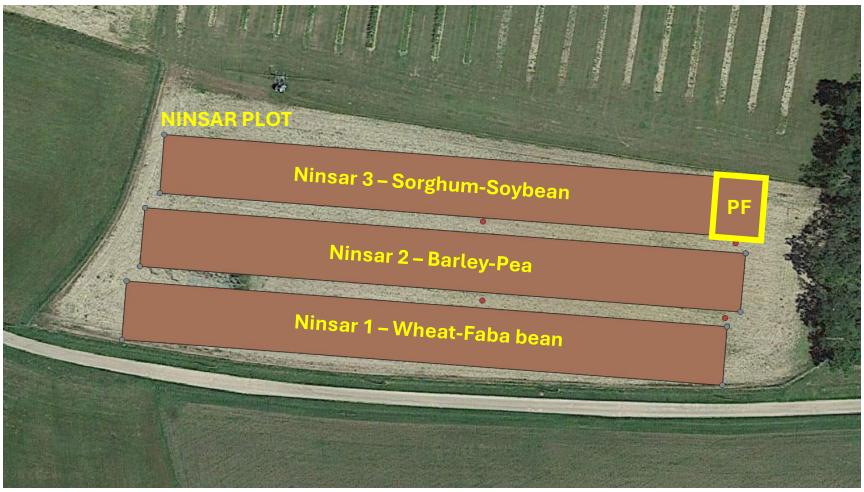


Figure 14. Satellite view of the Ninsar experimental plot (Extracted from QGIS, 2026). PF = Pixel Farming.

A winter wheat–faba bean association is established in autumn, in October or November. As a legume, faba bean supplies nitrogen to wheat in the soil. In March, barley is sown together with spring pea. Like faba bean, pea is a legume and is therefore able to release nitrogen in the soil for barley. However, barley also benefits pea, as it can serve as a trellis by wrapping its tendrils around the stem, enabling more vertical growth and thus easier harvesting (in pure stands, pods that are too close to the ground are not collected, or are collected with too many impurities).

Finally, the third and last association is sown at the end of spring, after mid-May. Sorghum benefits from soybean being a legume, using the nitrogen it releases into the soil. Moreover, as sorghum is much less water-demanding than for example maize, soybean, which is also water-demanding, can use the majority of the soil's available water reserve. The implementation of intercropping systems tests the ability of agricultural robots to manage several different species simultaneously: discrimination between crops and weeds, differentiated interventions, etc.

S2 is a pixel farming experiment; this scenario is also composed of three tri-specific associations. The first is more compatible with conventional farm equipment, consisting of an association of spring wheat, spring pea and flax. As in S1, wheat and pea are mutually beneficial from both a nutritional and structural point of view. Flax can also serve as a trellis for pea and is also classified as a melliferous plant, flowering at the same time as pea, which improves pollination chances. The second association consists of cabbage, mint and carrot. Cabbage and carrot were chosen because they occupy the aerial and underground space of the pixel, respectively. Mint was added due to its negative allelopathic effect on pests. Finally, the last association is that of tomato, basil and marigold. Basil and tomato are mutually beneficial and stimulate each other's development through a beneficial allelopathic relationship. Marigold is a plant known for its repellent action against pests such as nematodes. This pixel farming setup requires very fine-scale spatial management, with localized interventions at the pixel scale (around one square meter) and strong within-field heterogeneity. Therefore, it constitutes a demanding use case for robots, which must be able to position themselves precisely, distinguish between different species within the same pixel, and adapt their trajectories and tools according to the spatial configuration of the plants.

2.4 Deployment of robots in the two scenarios

Robots were mobilized differently according to the scenarios, depending on the targeted crop operations, the tools available on the farm and the technical capabilities of the platforms (Table 1). This section describes the operations carried out or planned, the associated robots and tools, as well as the levels of autonomy and field conditions encountered.

The operations carried out or planned within the two scenarios include soil preparation, sowing and/or transplanting, mechanical weeding and harvesting. As mentioned previously, monitoring interventions (growth monitoring, stress detection, disease and pest detection) will not be the focus of this paper, as the robots capable of carrying out these tasks are still at the testing stage. To date, each platform has only completed a few passes, primarily to evaluate and refine their trajectory algorithms before regular, agronomically relevant operations can be implemented over a full cropping season. Since the aim of the project is to follow agroecological principles, by reducing synthetic inputs, no inorganic fertilization or chemical weeding was performed.

For each type of operation, robots were selected based on their compatibility with the tools available on the experimental farm and their ability to operate under the field conditions encountered (soil moisture, crop growth stage).

In S1, robots were mobilized for all crop operations except monitoring and harvesting. These operations require the ability to follow crop rows, adapt the working width according to the inter-

row spacing, and discriminate between crop plants and weeds, particularly in cereal–legume associations where the canopy structure is more heterogeneous than in monoculture.
In S2, robots were used to sow the first combination (wheat–pea–flax). One of the teams involved in the Ninsar project is currently designing and developing a robotic platform that would be perfectly suited to perform the entirety of the crop cycle for S2, from sowing or transplanting, to harvesting fruits on the plants. As it will be available in January 2027, most of the tasks were performed by humans during the 2026 campaign: transplanting, weeding (inter- and intra-pixel), and harvesting. Monitoring the pixels by acquiring images, estimating soil coverage and detecting stresses (drought, nutrient deficiency) is planned for 2027 and 2028 campaigns. Irrigation was automatic thanks to sprinklers connected to the INRAE domain's lake.

The level of autonomy of the operations varies according to the robots and tasks: some operations were carried out in teleoperated mode, others in semi-autonomous mode (automatic guidance with human supervision) and some, more limited, in autonomous mode.

2.5 Evaluation indicators

Several indicators were collected to assess the feasibility and performance of robotized technical itineraries in the two scenarios. These indicators can be grouped into four categories: technical, energy-related, agronomic and environmental. This categorization makes it possible to appreciate both the maturity of the robotic platforms, the effect of the itineraries on crops and the environment, and the organizational feasibility of integrating robotics at a larger scale into agroecological systems.

Technical indicators mainly concern the performance of robots and tools: operation success rate (e.g. percentage of rows or pixels correctly treated), effective working time per operation, time of human interventions required (teleoperation, manual rework), and frequency of breakdowns or malfunctions. These indicators make it possible to assess the robustness of the platforms and their suitability for the intended operations. They also provide information on the ability of robots to maintain an acceptable level of performance under varying field conditions, which is a central issue for their deployment in real production systems.

Energy-related indicators focus on the amount of electrical energy required to perform on-field tasks. The calculation takes into account energy production and distribution, enabling comparisons between robots. This calculation allows an estimation of the environmental impact of the use of these robotic platforms. While a LCA (Life Cycle Assessment) analysis takes into account the entirety of a robot's life cycle, from manufacturing to recycling, the analysis performed for the Ninsar project involves only the manufacturing and usage periods of a robot's life cycle. Indeed, these technologies are still fairly new and their lifetime remain unclear, as their end-of-life. The amount of energy needed to function can be translated into GHG (greenhouse gases) emissions. These estimations allow for a comparison between robots, and also between a robot and conventional machinery such as a tractor.

Agronomic indicators aim to characterize the effect of technical itineraries on crops and the environment: soil compaction, biomass produced, weed pressure (density, coverage), crop health status (disease symptoms, presence of pests), the damages from robotic interventions sustained by the crops and, when available, yield by species and by field. These indicators provide elements to assess the potential agroecological benefits of robotized itineraries, in terms of reduced weed pressure, crop diversification and input limitation.

3/ RESULTS AND DISCUSSION

This section presents the main lessons learned from the field experiments conducted within the Ninsar project over the 2024–2026 cropping seasons. The analysis is also based on the evaluation indicators introduced in the Materials and Methods section, focusing on technical, energy-related, agronomic and environmental aspects of the robotized itineraries. Results highlight the main constraints encountered in terms of robot–tool compatibility, operational performance and field work organization.

The experiments carried out within the Ninsar project revealed several limitations related to the integration of agricultural robots into agroecological technical itineraries. A first difficulty concerns the lack of dimensional standards between the different robotic platforms. The robots of the Roboterrium infrastructure indeed exhibit highly heterogeneous dimensions (width, wheelbase, ground clearance), which makes the design of fields with fixed inter-row spacing complex. In several cases, it was impossible to define a row spacing compatible with the entire fleet without at least one of the robots risking driving over the plants, thus limiting intervention possibilities and imposing compromises in the design of experimental setups. This is why, for S2, it was decided to implement two pixel size modalities (Figure 3).

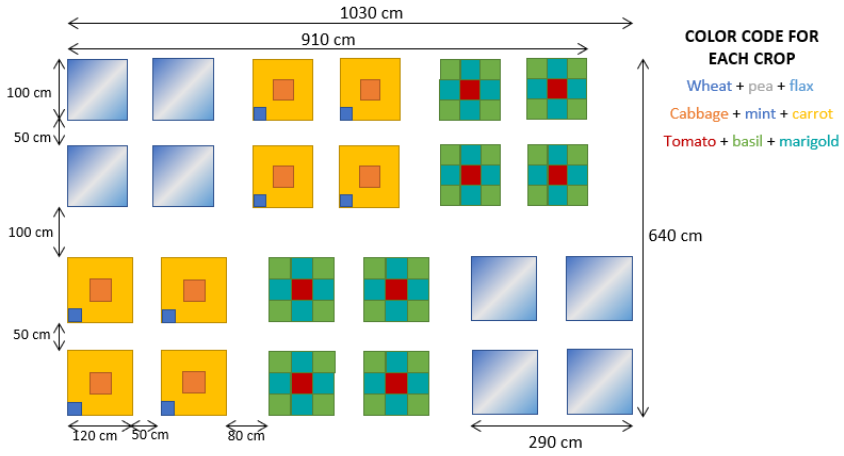


Figure 15. The pixel farming experimentation (INRAE, 2026).

The spacing between plants and the overall pixel dimensions were specifically designed to allow small scouting robots to pass between pixels, while enabling larger robots to move over the pixels without causing damage to the crops. This dual configuration was necessary to ensure that all types of platforms could operate within the same experimental setup, while respecting the agronomic constraints of the pixel farming system.

A second major limitation concerns the absence of power take-off on the mobilized robots. This constraint strongly restricts the choice of hitchable implements, particularly for sowing operations. To date, only a gravity-fed seed drill is compatible with the robots, which means that seeds are not deposited at regular intervals along the row, unlike what conventional pneumatic seed drills would allow. This limitation affects sowing precision and, consequently, the uniformity of emergence and competitiveness against weeds. This highlights the need to either develop new implements specifically adapted to robotic platforms, or to use robots only for the operations they were originally designed for, rather than attempting to retrofit them with conventional farm equipment.

Furthermore, the implements hitched behind the farm's tractors often exceed one ton, making them incompatible with the traction capacity and payload of the Roboterrium robots. It was

therefore necessary to use smaller and lighter implements, often with reduced working width. Even among these smaller implements, however, the power demand varies considerably depending on the tool and the operation (Figure 5): for instance, the cultivator requires up to 12 kW, while the hoe requires less than 2 kW. The reduction in working width implies a higher number of passes to cover the entire field, resulting in a loss of time and productivity, as well as increased soil compaction risk despite the lower weight of the robots compared to conventional tractors.

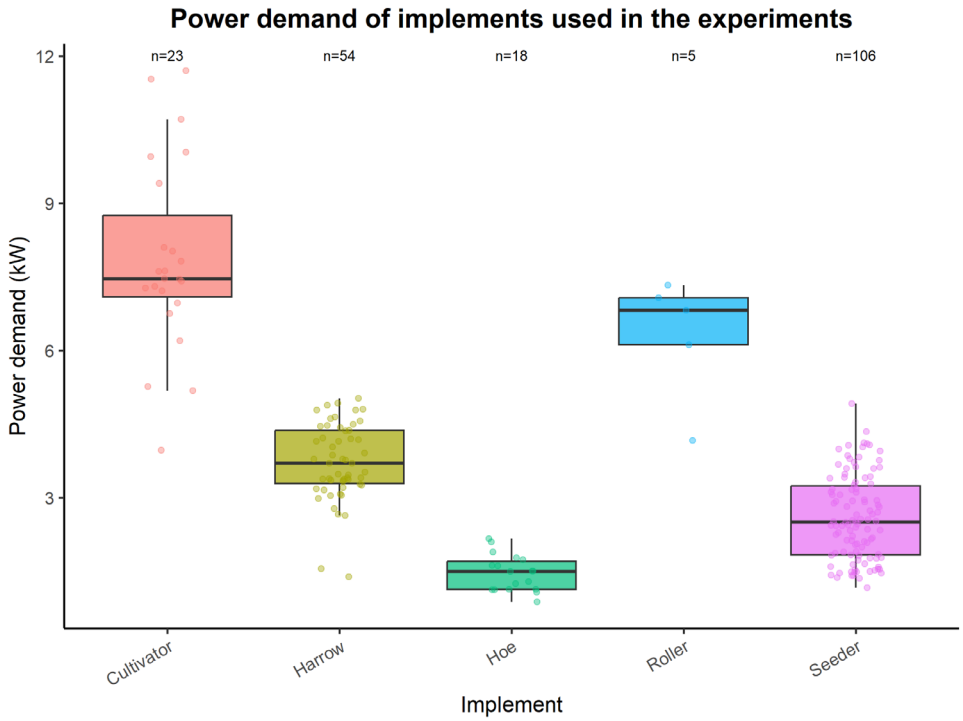


Figure 16. Power demand of the different implements used with one of the Roboterrium robots: the Sabi Agri POM4x4

Therefore, compaction tests were carried out in a sand bin to assess the impact of the robotic platforms on soil structure, in comparison with a conventional tractor (John Deere 6R 110) (Figure 6). The results show that, in the upper soil horizon (10 cm), the stress levels induced by the robots are comparable to — or even higher than — those of the conventional tractor, particularly for the Trektor and POM4x4, due to their higher tire inflation pressure. However, at deeper soil horizons (30–35 cm), the stress induced by the robots decreases rapidly, while the conventional tractor maintains significant pressure at these depths. These results suggest that the lower weight of the robots allows for reduced compaction in deeper soil horizons, which are the slowest to recover. The CEOL platform, equipped with tracks, produces the lowest stress at all depths thanks to a better load distribution. However, as shown in Figure 6, only one test was performed for the Trektor and CEOL platforms, thus these results must be interpreted with caution.

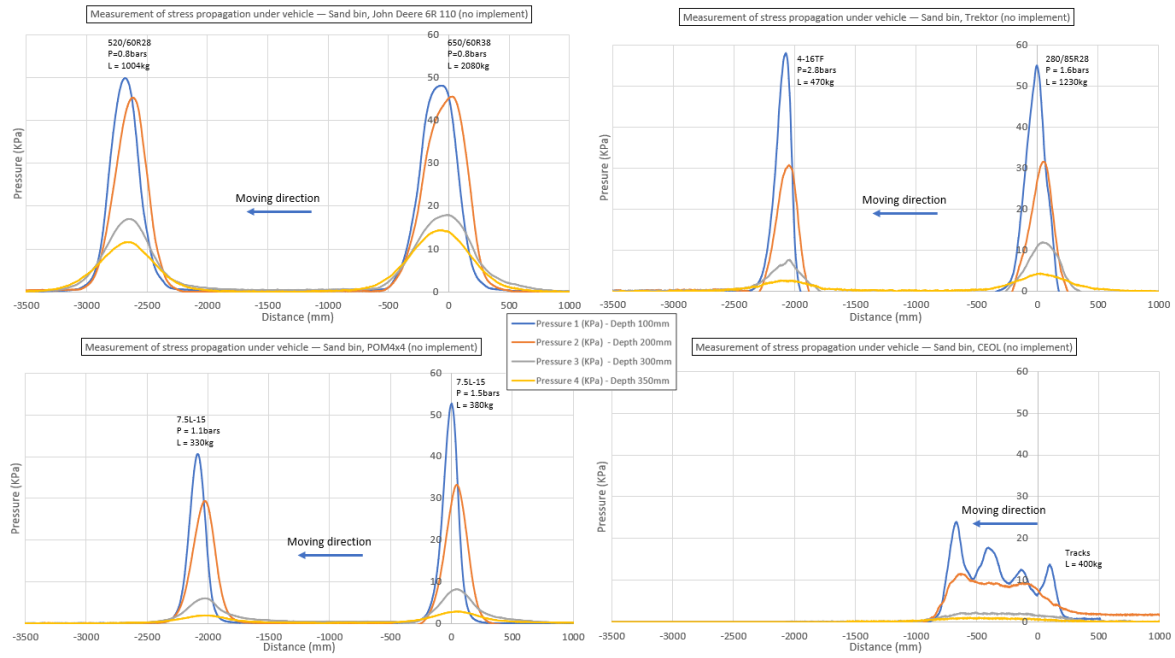


Figure 17. Stress propagation under vehicle in a sand bin (no implement): conventional tractor vs robotic platforms at four soil depths. P = tire pressure; L = load, equals to the weight on one wheel (or tracks) from the right side of the vehicle; N = number of tests performed.

Beyond technical compatibility issues, current regulatory and safety requirements also constrain the operational deployment of agricultural robots in France (Entraid, 2026). Under the EU Machinery Regulation and the EU AI Act, autonomous or semi-autonomous agricultural machines are generally classified as high-risk systems and must be operated under effective human supervision, with an operator able to monitor the machine and intervene at any time (via an emergency-stop procedure) (AiAgriculture, 2026). In addition, the robotic platforms used in this study are not type-approved for circulation on public roads, as they fall under the EU type-approval regime for mobile machinery (IGARR, 2025). Consequently, they must be transported by trailer between the experimental site and the fields, even when the distance to be covered is only a few hundred meters. These transport, set-up and supervision requirements increase the non-productive time associated with robot deployment and must therefore be considered when assessing the operational feasibility of robotized agroecological itineraries.

Several indicators were selected to assess the performance and feasibility of the robotized technical itineraries. Working speed and field productivity (expressed as effective work time and area covered per unit time) were used to characterize the operational efficiency of the robots. In addition, GHG emissions associated with the energy consumption of the robotic platforms were estimated to provide an initial comparison with conventional tractor-based operations (Bras et al., 2024). Preliminary results show that the field work rate of the robots remains below 1 ha/h for all implements used in the experiments, whereas typical field work rates for conventional tractors in arable farming are generally in the range of 2–5 ha/h depending on the operation and working width. In contrast, GHG emissions associated with robot operations are overall low, thanks to the use of decarbonated electrical energy (as French power mix is mainly nuclear) rather than fossil fuels. Moreover, because the robots are deployed within agroecological systems, the pesticide treatment frequency index (TFI) is null, and no synthetic fertilizers were applied. This is particularly relevant given that the production and use of mineral nitrogen fertilizers are responsible for significant GHG emissions, primarily through nitrous oxide (N_2O) release and energy-intensive manufacturing processes. Avoiding synthetic inputs therefore contributes to reducing the

environmental footprint of the cropping systems, even if current robotic platforms still exhibit lower operational performance than conventional machinery.

Therefore, despite promising features, current robotic platforms remain far from matching the performance of conventional tractor-based systems. In addition, battery autonomy is a critical constraint: energy consumption during field operations results in substantial autonomy loss, requiring frequent recharging stops. These recharging periods, combined with lower working speeds and reduced field efficiency, further decrease overall productivity compared to conventional machinery. As a result, the operational performance of agricultural robots like those used in this study is still limited, and their deployment at farm scale would require significant improvements in speed, autonomy and energy management.

These results should however be interpreted with caution, as the dataset remains limited at this stage, and only concerns the robots used for the experiments. The experiments presented here constitute a first set of field trials, and additional data are needed to draw robust conclusions on the long-term performance and feasibility of robotized agroecological itineraries. Ongoing and upcoming projects will significantly expand this evidence base. The STAIRS project (Solutions Technologiques partagées: Analyse d'impact, Interopérabilité et Ressources pour la durabilité de Systèmes robotiques), launched in 2025 and led by INRAE and RobAgri, aims to develop standards, tools and methodologies for efficient, interoperable and environmentally responsible agricultural robots. In parallel, the AGROBOSCOPE project (AGriculture and Robotics: Structuring a Collaborative and Organized Network of Test Platforms to Evaluate Performance), launched in 2026 and led by CTIFL and RobAgri, is setting up a national network of test platforms to generate reliable, comparable references on the technical, economic and agro-environmental performance of robotic solutions across multiple sectors. Together, these initiatives will help to consolidate the present findings and to better assess the potential of agricultural robotics for supporting the agroecological transition at farm scale.

Overall, these results underline that the transition towards robotic systems cannot be reduced to a simple replacement of tractors by robots, but requires a co-design of tools, robots and cropping systems.

4/ CONCLUSIONS

The experiments conducted within the Ninsar project demonstrate both the potential and the current limitations of integrating agricultural robots into agroecological technical itineraries. Row intercropping and pixel farming scenarios confirmed that robotic platforms can, in principle, carry out key crop operations while respecting agroecological principles (no synthetic fertilization or chemical weeding). However, the results also highlight major constraints related to dimensional heterogeneity among robots, lack of power take-off, limited compatibility with conventional implements, reduced working speeds, and significant autonomy and recharging constraints. Regulatory requirements for human supervision and the absence of road approval further increase non-productive time and logistical complexity.

At this stage, these limitations restrict the range of feasible operations and the scalability of robotized agroecological systems. Robotics can contribute to reducing the physical strain of agricultural work and improving farm organization, but only if their deployment does not generate excessive new constraints for farmers. The present findings suggest that this will require a co-design approach, jointly adapting robots, implements and cropping systems, rather than attempting to retrofit conventional equipment onto existing platforms.

Ongoing initiatives such as the STAIRS and AGROBOSCOPE projects will provide additional experimental data, standardized evaluation methods and a broader diversity of robotic platforms and cropping systems. These efforts combined with the Ninsar project results should help to identify realistic niches where current robots already offer agronomic and organizational benefits, and to define the technical and organizational conditions under which agricultural robotics can meaningfully support the agroecological transition at farm scale.

References

- AiAgriculture. (2026). Intelligence artificial intelligence in agriculture 2025: Legal and regulatory trends. https://aiagriculture.fr/blog/intelligence-artificielle-agriculture-2025-tendances-juridiques-et-reglementaires
- Altieri, M.A. (1995). Agroecology: The Science of Sustainable Agriculture (2nd ed.). Westview Press, Boulder, CO, USA.
- Bedoussac, L., Journet, E.-P., Hauggaard-Nielsen, H., Naudin, C., Corre-Hellou, G., Jensen, E.S., Prieur, L., Justes, E. (2015). Ecological principles underlying the increase of productivity achieved by cereal–grain legume intercrops in organic farming: A review. Agronomy for Sustainable Development, 35(3), 911–935. https://doi.org/10.1007/s13593-014-0277-7
- Bechar, A., Vigneault, C. (2016). Agricultural robots for field operations: Concepts and components. Biosystems Engineering, 149, 94–111. https://doi.org/10.1016/j.biosystemseng.2016.06.014
- Bras, A., Montanaro, A., Pierre, C;, Pradel, M., Laconte, J. (2024). Toward a Better Understanding of Robot Energy Consumption in Agroecological Applications. https://arxiv.org/abs/2410.07697
- Ditzler, L., Driessen, C. (2022). Automating agroecology: How to design a farming robot without a monocultural mindset? Journal of Agricultural and Environmental Ethics, 35(1):2. https://doi.org/10.1007/s10806-021-09876-x
- Duckett, T., Pearson, S., Blackmore, S., Grieve, B., et al. (2018). Agricultural robotics: The future of robotic agriculture. UK-RAS White Paper. https://arxiv.org/abs/1806.06762
- Entraid. (2026). Regulations for agricultural robots: What are they? https://www.entraid.com/articles/reglementations-des-robots-agricoles
- Fountas, S., Mylonas, N., Malounas, I., Rodias, E., Hellmann Santos, C., Pekkeriet, E., et al. (2020). Agricultural robotics for field operations. Applied Sciences, 10(9), 2672. https://doi.org/10.3390/app10092672
- Hauggaard-Nielsen, H., Ambus, P., Jensen, E.S. (2001). Temporal and spatial distribution of roots and competition for nitrogen in pea–barley intercrops – a field study employing ^{32}P technique. Plant and Soil, 236(1), 63–74. https://doi.org/10.1023/A:1012793822722
- IGARR. (2025). EU: New EU type approval regime for mobile machinery. https://igarr.com/2025/11/17/eu-new-eu-type-approval-regime-for-mobile-machinery/
- NINSAR Project Consortium (2022). New ItiNerarieS for Agroecology using cooperative Robots (NINSAR). https://project.inria.fr/ninsar/ (accessed on July 24th, 2026).
- Slaughter, D.C., Giles, D.K., Downey, D. (2008). Autonomous robotic weed control systems: A review. Computers and Electronics in Agriculture, 61(1), 63–78. https://doi.org/10.1016/j.compag.2007.05.008
- TIRREX Project Consortium (2023). Roboterrium – Vivarium of mobile manipulator robots for research in off-road and agricultural robotics. https://tirrex.fr/plateforme/roboterrium/ (accessed on August 25th, 2026).
- Van Apeldoorn, D., Ditzler, L., Bos, E., et al. (2020). Optimal Pixel Cropping Layouts. Wageningen University & Research, Wageningen, The Netherlands. https://www.uu.nl/sites/default/files/pixel_cropping_report.pdf

- Wezel, A., Bellon, S., Doré, T., Francis, C., Vallod, D., David, C. (2009). Agroecology as a science, a movement and a practice: A review. Agronomy for Sustainable Development, 29(4), 503–515. https://doi.org/10.1051/agro/2009004

Research and Testing Bench for Alternative Weed Control Solutions

Daniel Boffety [a,*], Lama Al Bassit[b], Laurick Genestas[a],

[a] Université Clermont Auvergne, INRAE, UR TSCF, AgroTechnoPôle, 03150 Montoldre, France
[b] Université Clermont Auvergne, INRAE, UR TSCF, 63178 Aubière, France
* Corresponding author. Email: daniel.boffety@inrae.fr

Abstract

The transition towards more sustainable agricultural practices is driving the development of autonomous technologies for intra-row weed control in row crops. Targeted weeding systems aim to reduce or eliminate the use of plant protection products, particularly chemical herbicides, while maintaining effective weed management. The development and validation of such systems require extensive experimental campaigns under field conditions, which are time-consuming, costly, and difficult to reproduce. To address these limitations, INRAE, within the framework of the AgroTechnoPôle initiative, has developed dedicated research and testing bench for the characterization and preliminary qualification of alternative weeding technologies. The bench provides controlled, reproducible and repeatable experimental conditions, enabling system performance to be assessed prior to field validation. It is designed to support the development process and reduce the number of field trials required.

The bench is organized into three functional modules. The first reproduces relevant experimental artificial conditions, including soil, crops, and weeds. The second provides an adaptable interface to accommodate the technical specifications and operating principles of the perception, detection, and weeding technologies under evaluation. The third integrates metrological instrumentation for data acquisition and the measurement of relevant performance indicators, together with data processing and analysis tools. The proposed test bench can be used to evaluate both plant perception and detection systems and complete weeding solutions combining perception, decision-making, and targeted weeding operations. By providing controlled, reproducible and repeatable testing conditions, the test platform constitutes a first validation step between laboratory development and field-scale validation of intra-row weeding technologies.

KEYWORDS: Test and qualification bench, Weed control technologies, Evaluation of weeding action accuracy, Artificial representation of a test environment

Complexity level: 2

1/ INTRODUCTION

In an agro-environmental context where the agroecological transition is increasingly regarded as a promising pathway towards improving the sustainability and resilience of agricultural systems,

reducing the reliance on chemical products for crop weed management has become a key objective promoted by various national and European initiatives. Since 2018, the “Technologies and Information Systems for Agroecosystems” (TSCF) research unit at the INRAE Clermont-Ferrand research center, in partnership with the French National Laboratory of Metrology and Testing (LNE), has organized a series of challenges addressing this objective. These initiatives have primarily taken the form of field evaluation campaigns aimed at assessing autonomous intra-row weeding solutions under real-world conditions, on experimental plots previously established with crops–weeds associations (Avrin et al., 2020).

The establishment of experimental plots with the highest possible degree of uniformity and comparability across participants, as well as the organization and implementation of the evaluation trials, involved substantial technical and organizational challenges. These constraints were further exacerbated by the low Technology Readiness Levels (TRLs) of the participating solutions, which limited their ability to fully exploit the experimental evaluation framework and demonstrate their potential under field conditions. Given the significant technical and environmental challenges involved, the investigations conducted led to the development of an initial testing stage based on repeatable experiments under controlled and reproducible conditions, prior to conducting field trials under real-world conditions. Accordingly, within the framework of the development of the AgroTechnoPôle collaborative platform at the INRAE Montoldre site, the development of a dedicated test bench for alternative weed management solutions was initiated.

The research and testing bench for alternative weeding solutions presented in this paper was designed and developed by INRAE, primarily based on the knowledge and experience acquired through previous experimental campaigns and challenges and with the technical expertise of the SPIE/LOGIROAD consortium selected for its manufacturing. This test bench reproduces experimental conditions in a controlled environment by integrating artificially soil, crop plants and weeds with dedicated technological and metrological solutions for each of its technical part. This setup provides an initial level of performance assessment under fully controlled, reproducible, and repeatable conditions. The bench is intended to support the qualification of both perception and decision-making systems based on the detection and identification of weeds and/or crop plants as well as complete weed management systems integrating the final weeds removal. By providing a controlled testing environment prior to field trials, this facility enables the evaluations independently of the technical, meteorological, and organizational challenges associated with the preparation and establishment of experimental plots and the organization of field evaluation campaigns.

2/ MATERIALS AND METHODS

2.1 General overview of the INRAE test bench

The INRAE test bench is designed to artificially reproduce soil environments with crops plants and weeds providing an initial level of performance qualification for plant perception and detection systems as well as for complete weed management systems combining perception, detection and final weeding action. The platform is designed to accommodate a wide range of weed management technologies and operating principles, including mechanical, electrical, laser-based, and spraying systems. All evaluations can be performed under fully controlled, reproducible, and repeatable conditions. System performance is assessed by characterizing the accuracy of the tested systems along the three spatial axes (x, y and z) as well as over time (t). This approach enables the spatial and temporal accuracy of the perception, detection, decision-making, and/or weeding action to be quantitatively characterized. The test bench provides

multiple experimental configurations with precisely controlled spatial distributions of crop plants and weeds. These configurations are used to assess the accuracy of the tested weed management systems at the Perception, Decision, and/or Action levels. By modifying the spatial arrangement and characteristics of the plants, the platform can reproduce a range of artificial working conditions representative of situations that may be encountered in the field. These conditions include variations in plant spatial distribution, plant morphology and color, ambient conditions, illumination and dust levels. The research and testing platform is primarily composed of three dedicated technical subsystems. Their design and development were driven by the functional requirements identified in the system specifications.

2.2 Description of the test bench components

2.2.1 Artificial representation of soil, crop plants, and weeds: Base Module

One of the main objectives of the test bench is to provide a reference artificial representation of soil containing crop plants and weeds, with predefined spatial arrangements in terms of inter-rows and inter-plants distances. This configuration constitutes the Base Module. To obtain maximum flexibility in arranging crop plants and weeds, a modular design was adopted. Individual base modules represent soil sections measuring 1.5 m in length and either 0.25 m or 0.5 m in width. These individual modules are constructed from 10 mm thick honeycomb aluminum panels and can be assembled to form the final reference test area, including the soil, crop plants, and weeds. Through the combination of individual base modules, the dimensions of the reference test area can be adjusted according to the experimental requirements with a configurable width ranging from 0.25 to 2 m and a length ranging from 1.5 to 15 m (Figure 1).

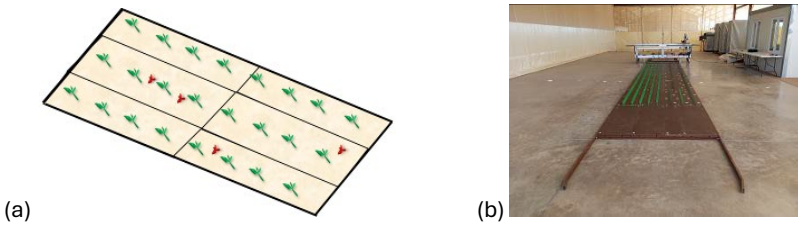


Figure 18. (a) Schematic representation of Base Module with the spatial distribution of crop plants (green) and weeds (red); (b) Base Module forming the test area with the Algeco shelter on the right housing the fixed user workstation

Each individual base module is designed to reproduce one of the experimental conditions considered including bare soil or soil containing artificial crop plants and/or weeds. These artificial plants are generated from predefined three-dimensional models. Each individual module is also equipped with four digital “STAG” markers which are used to determine plant positions and to perform the self-calibration of the HD cameras employed for measurement purposes. Three crops’ types at early growth stages were selected for artificial representation on the test bench. Bean and maize plants at the four-leaf stage were selected to represent, respectively, an open-field vegetable crop and a crop characterized by wide inter-rows spacing. Wheat at the two-leaf stage was selected to represent a cereal crop. The artificial crops plants have a height of 8 cm. Two weeds’ species were selected to represent different weeds morphologies: mustard as a broadleaf weed and matricaria as a narrow leaf weed, both represented at the four-leaf developmental stage and with an artificial plant height of 2 cm (Figure 2). On each individual base module, the position of every crop plant and weed is predefined with millimeter-level accuracy. This configuration provides precise knowledge of the three-dimensional position of each crop plant and weed along the x, y, and z axes. These positions are systematically verified before each experiment to ensure that the initial test conditions conform to the predefined configurations and experimental models.

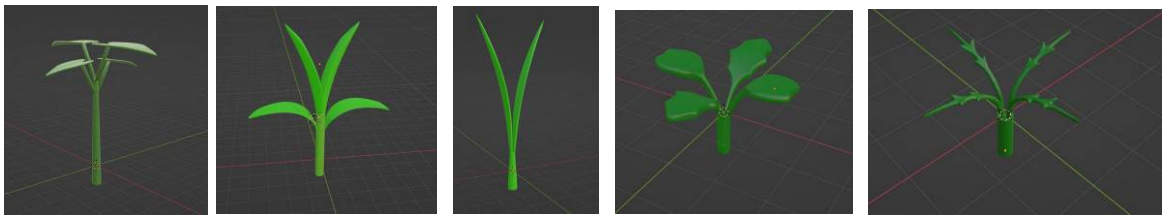


Figure 19. Three-dimensional models of crop plants (bean, maize, and wheat) and weeds (mustard and matricaria)

Depending on the predefined combinations of soil, crops plants, and/or weeds, the spatial distribution of plants varies from one individual base module to another. In its current configuration, the test bench provides three reference configurations combining soil with artificial crop plants and weeds. Each configuration is obtained by assembling individual base modules, each assigned a specific position to cover the defined test area. Changing the position or orientation of individual base modules makes it possible to generate additional experimental configurations. The different Base Module configurations are assembled within a metal supporting structure consisting primarily of two longitudinal metal rails connected by transverse spacers. This structure can be installed outdoors on a stabilized soil surface or indoors on a concrete floor. For indoor experiments, artificial lighting can be combined with the existing lighting conditions to adjust the illumination level within the test area according to the experimental requirements and to reproduce different natural lighting conditions encountered in the field. Under indoor conditions, tests can be performed at travel speeds of up to 10 km/h, higher operating speeds are intended to be evaluated outdoor.

2.2.2 Accounting for the technical specificities and operating conditions of the technologies under Test: Support Module

The test bench is designed to accommodate and evaluate both perception–decision (P/D) systems and complete perception–decision–action (P/D/A) systems, regardless of the weed management principle employed, including chemical, mechanical, electrical, thermal, laser-based, and other approaches. The systems under evaluation may be integrated into agricultural machinery, such as tractor-mounted or self-propelled implements or into mobile robotic platforms. They may either move autonomously along the test bench or consist of fully independent systems without a mobile carrier. Accordingly, the support module of the test bench can be provided either by the actual machinery incorporating the technology under evaluation or by the test bench's mobile carriage. The latter can be manually moved along the two rails enclosing the Base Module and is designed to carry the technical solution under evaluation (Figure 3). The mobile carriage enables the system under test to be transported along the test area while providing the mechanical and technical means required to conduct the experiments.



Figure 20. Test bench support module consisting of the mobile carriage

Systems under evaluation that are already integrated into mobile carriers are generally complete systems provided by the manufacturers. The operation of these systems may require the use of GNSS-based positioning information through suitable onboard receivers. For indoor testing of mobile platforms equipped with GPS receivers, the test bench provides a positioning emulation solution based on known reference coordinates. This solution uses the positioning data provided

by a Leica AT930 laser tracker measurement system, enabling GNSS/GPS-based positioning information to be emulated without modifying the integrity or architecture of the system under evaluation.

2.2.3 Metrology for the qualification of tested systems: Metrology Module

The test bench is equipped with a set of metrology instruments and associated functionalities designed to acquire information provided by the system under test and to record the data generated during the experiments. The Metrology Module consists of an embedded computing unit connected via wired interfaces to the various measurement devices installed on the test bench, including a 4K scanning camera, HD cameras, and laser pointers. This embedded computing unit maintains a permanent wireless (Wi-Fi) connection with the fixed control computer located inside an Algeco shelter. The measurement devices and associated digital solutions can be installed either directly on the machine under test or on the test bench support carriage. This configuration enables the qualification of systems operating in P/D or P/D/A configurations by determining for each test performed:

- The precise spatial mapping of crop and weed plants within the reference configuration of the Base Module, established and verified before each test (Figure 4a).
- The positioning parameters associated with the motion of the mobile platform carrying the P/D or P/D/A system under evaluation, including travel speed and position. These parameters are obtained from the selected reference configuration and/or from measurements performed using the Leica AT930 laser tracker (Figure 4b).
- The operating state of the weeding actuator under evaluation, including its activation state (On/Off) and dynamic trajectory during the test. These parameters are determined from RGB image acquisitions (Figure 5) and AI-based image-processing algorithms. The resulting data are compared with the reference data to quantify the spatial errors associated with the weeding actions and derive a set of accuracy metrics for the weed management technologies under evaluation.
- The environmental conditions during testing, including temperature, relative humidity and the characteristics of the test environment.

(a)  (b) 

Figure 21. (a) Test bench support carriage equipped with a 4K RGB scanning camera mounted on its central mast (b) Leica AT930 laser tracker measuring system targeting its reference target mounted on the support carriage

(a)  (b) 

Figure 22. (a) HD RGB camera capturing the green cross projected by the laser pointer which indicates the area of effect of the weeding operation and its operating status (On/Off); (b) embedded computer mounted on the support carriage, which can be transferred to the platform of the system under test, together with the required sensors and measurement devices, such as HD cameras and laser pointers

2.2.3.1 Detection of the spatial distribution of plants in the reference test Base Module

The Base Module, obtained by combining the different individual base modules representing the soil and plants, is installed on the ground within the test area. The exact positions of the planting points of each individual plant are determined with an accuracy of ±1 mm in the global coordinate system of the test area, thereby providing the reference data required for the final qualification of the tested systems. A very high-definition RGB camera (4K), mounted on the test bench support carriage, enables the test area to be accurately scanned before each test series. Using STAGs (Stable Fiducial Marker System) (Benligiray et al., 2019) attached to each individual base module, a Leica AT930 laser tracker measurement system targeting the mobile carrier and artificial intelligence algorithms, the precise positions of the plants and the areas they occupy within the global coordinate system assigned to the test area are determined and recorded. The spatial referencing provided by the STAGs, combined with the use of the high-precision laser tracker measurement system, also enables the positions of the support module and the weeding operations performed during the tests to be accurately determined and recorded.

2.2.3.2 Determination of the motion parameters of the mobile platform supporting the tested equipment

The motion parameters of the machine tested, the mobile carrier or the support carriage of the test bench, carrying the P/D or P/D/A system under qualification, including its instantaneous position and travel speed, can be determined using two different approaches:

- Using the Leica AT930 laser tracker measurement system, positioned near the test area. This system enables the real-time detection and tracking of a dedicated target, such as a mirror, mounted on the machine under test, the mobile carrier, or the support carriage of the test bench. This makes it possible to determine its position with very high accuracy (1/100 mm) and its travel speed within the local coordinate system of the laser tracker measurement system. Once the measurements have been performed, a coordinate transformation is applied to obtain and record all displacement, instantaneous position, and speed data in the global coordinate system of the test area.
- By acquiring motion data including travel speed, instantaneous positions and other motion-related parameters provided by the manufacturer of the machine under test and available via a standardized communication bus, such as a CAN bus or ISOBUS.

2.2.3.3 Determination of the operating status of the weeding end-effector

While the qualification of the P/D component can be performed directly from the acquisition and processing of the geospatial data of the crop plants provided by the system evaluated on the test bench, the complete qualification of a P/D/A weeding system requires the determination of the operating status of the weeding end-effector and the measurement of its position relative to the crop plants present within the test area.
The operating status and actuation duration of the weeding end-effector can be determined by detecting the start and stop of the end-effector performing the weeding operation without the weeding action itself actually being carried out. This qualification procedure primarily depends on the type of weeding end-effector implemented by the system under test.
Weeding systems can be classified according to the number of degrees of freedom of their end-effector relative to its support structure on the mobile carrier. Three main categories can be identified:
i) systems with fixed weeding end-effectors rigidly attached to the frame of the mobile platform**,** mainly comprising nozzle-based spraying systems;
ii) systems with mobile weeding end-effectors having a single degree of freedom relative to the frame of the mobile platform, predominantly representing mechanical weeding systems;

iii) systems with mobile weeding end-effectors having two or more degrees of freedom relative to the frame of the mobile platform, which may encompass the most advanced weeding technologies and technical solutions.
During testing, the main step in the qualification of weeding systems consists of detecting or determining the instantaneous position of the weeding end-effector and/or determining the projection of the area covered by its weeding action onto the horizontal plane of the Base Module representing the soil and the crop plants. This information can be obtained using the test bench's metrological instrumentation, which consists of:

- A Leica AT930 laser tracker measurement system, together with its measurement target, which can be mounted either on the mobile platform or directly on the fixed end-effector;
- Four STAG-type fiducial markers mounted on each individual base module forming the overall Base Module;
- Four laser pointers, which can be mounted on an end-effector to identify its action areas on the Base Module or used to simulate the action of an end-effector;
- Mini-STAG fiducial markers, which can be mounted on a weeding end-effector to track its motion;
- Four high-definition (HD) RGB cameras, which can be mounted either on the test bench support carriage or on the Mobile platform carrying the weeding system under test. The cameras can be used individually or in combination to track the action of the weeding end-effector, as represented by the trace of a laser pointer or a mini-STAG marker attached to the moving end-effector, while simultaneously capturing the STAG markers mounted on the individual base modules representing the soil.

These devices and sensors provide different measurement modes for determining the instantaneous positions of the end-effector within the global coordinate system of the test area. The measurement mode is selected according to the category of the weeding system under test and is predefined in the test bench monitoring HMI.

These measurements of the instantaneous end-effector positions, synchronized with measurements of its operating status (On/Off), enable the positions of the weeding actions to be determined with millimeter-level accuracy.

All cameras, laser pointers, and end-effector operating-status detection sensors are connected via wired connections to the computer embedded on the mobile platform of the system under test or on the test bench support carriage.

2.2.3.4 Test configuration, monitoring, and measurement data processing

The test bench is equipped with a fixed computer workstation installed in a protected area inside an Algeco-type modular building located near the test area. This fixed workstation maintains a permanent Wi-Fi connection with the onboard computing unit installed either on the test bench support carriage or on the mobile platform of the equipment under test. The user performs the tests by following the steps displayed by the test bench's interactive interface (Figure 6). The user interface software, specifically developed for the test bench, enables test configuration and monitoring. It also provides additional functionalities, including the creation and modification of test configurations, visualization of recordings from all cameras, three-dimensional visualization of the scanning camera trajectory, and graphical visualization of the end-effector action areas. The data acquired by the onboard computer during the calibration phase or following a test are automatically transferred to the fixed workstation for subsequent processing.

Various procedures associated with the test bench's metrological and computing tools enable the configuration data required for test execution, as well as data acquisition and processing, to

be defined. These procedures subsequently allow the tested systems to be qualified according to predefined and precise metrics and the results obtained to be formally documented.

(a) 

(b) 

Figure 23. User interface screen showing: (a) the different stages of a test; (b) images recorded by the 4K or HD cameras.

As mentioned in 2.1 section, the test configurations are created by combining preconfigured individual base modules incorporating soil and crop and weed plants. The test bench software includes a graphical library containing all the individual base modules of the three basic configurations and allows additional modules to be created and added as required. It enables the test configuration to be prepared, parameterized, and displayed through a graphical interface representing the actual test area, whose length and width can also be adjusted according to the testing requirements.

The software also enables the user to enter technical information related to the systems under test, such as their categories, whether their end-effectors are fixed or mobile, the shape of the action area of their end-effectors and other relevant characteristics. It also allows the user to specify the type of instrumentation used, including cameras, laser pointers and all other sensors required for data acquisition and evaluation.

The software guides the user through the preparation and execution of the tests which begin with a scanning phase of the Base Module constituting the test area. When the Leica AT930 laser tracker measurement system is used, an additional calibration phase is required to accurately determine the position of each individual base module forming the overall Base Module representing the soil within the test area. This calibration then enables the positions of the cameras mounted on the mobile platform to be accurately determined.

The qualification of the final weeding action performed on the test bench is achieved by synchronizing and processing all the collected information. For the qualification of a mechanical weeding action, the approach is based on prior knowledge of the kinematics of the weeding end-effector. The collected information regarding the end-effector motion is then synchronized and combined with other data, such as the position and travel speed of the weeding system support, to determine whether the trajectory of the active part of the end-effector, consisting of blades, shares, or grippers, intersects the position of a weed or crop plant within the reference spatial configuration.

At the end of each test, quantitative results are obtained and presented to the user to assess the accuracy performance of the weeding system. Based on the intersections between the instantaneous positions of the weeding action areas and the reference positions of crop plants and weeds, scores indicating the success or failure of the weeding actions performed are assigned at each time step of the test and for each plant.

At the end of the test, these scores are used to calculate a set of metrics, including the number of weeds that were not detected due to missed detections or false negatives, the number of crop plants that were inadvertently subjected to a weeding action, the exposure intensity of weeds to

the weeding action and the average success rate of the actions which reflects the accuracy of weed detection and targeting.

3/ RESULTS AND DISCUSSION

The research and testing bench for alternative weeding solutions was designed and developed by INRAE with technical expertise provided by the SPIE/LOGIROAD consortium which was selected for its manufacturing. Installed in early 2025 in a dedicated building at the INRAE AgroTechnoPôle site in Montoldre (Figures 1b et 4a), the test bench was initially used to perform the tests required to debug specific functionalities and to fully validate its operation prior to its commissioning.

3.1 Implementation of the test bench for intra-row weeding action tests and results

Several series of validation tests were conducted using an electromechanical simulation device designed to reproduce mechanical weeding actions within the inter-row area of a row crop. Developed by INRAE, this device was installed on the test bench support carriage with a mini-STAG fiducial marker attached to the tip of its active component to enable its motion to be tracked using one of the test bench's HD cameras. Additional tests were then conducted on the test bench using a mechanical weeding device from a machinery manufacturer, designed to perform weeding operations between plants in a row crop (Figure 8). This tool performs weeding operations using an electrically actuated mechanical weeding end-effector whose operation is synchronized with the motion of the autonomous mobile platform carrying the system based on crop-plant detection data provided by its onboard vision system. For the tests conducted on the test bench the active component of the mechanical weeding end-effector was replaced with a similar metal component to which a mini-STAG fiducial marker was also attached, allowing its motion to be tracked using an HD camera from the test bench.

The objective of these tests was to track and record the successive positions of the mechanical weeding end-effector relative to the artificial crop plants on the Base Module of the test bench in order to assess its operational accuracy and subsequently support further investigation and the identification of potential areas for improvement.

For each test, the mobile platform carrying the weeding device was driven once across the Base Module of the test bench installed on the ground. Prior to each test and depending on the planned test conditions, the travel speed and the platform control mode were adjusted accordingly. The platform could either be remotely operated using a teleoperation mode or operated in fully autonomous mode using all of its onboard equipment and functions for autonomous guidance.

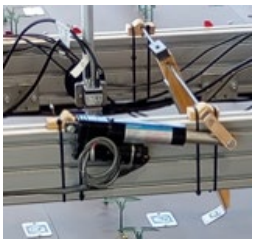
(a)  (b) 

Figure 24. Mechanicals intra-row weeding devices for row crops tested on the bench using a mini-STAG fiducial marker: (a) INRAE electromechanical weeding simulation device; (b) Technical solution on autonomous mobile platform.

Before starting each test:

- The mobile platform was switched to manual mode and positioned at the starting point located at the beginning of the Base Module test area.
- The initial position and orientation of the mobile platform at the beginning of the Base Module were manually adjusted as accurately as possible taking into account the crop rows and the footprint of the weeding equipment under test.
- Once the mobile platform had been positioned on the test bench Base Module and the test configuration had been set through the bench HMI, the test was initiated from the test bench software. As soon as data acquisition was enabled, the mobile platform was started to perform the desired test trajectory across the Base Module with its weeding equipment activated.

The measurement data are recorded continuously throughout the trajectory performed within the test area. At the end of the trajectory, the mobile platform is stopped and data acquisition on the onboard computer is terminated. The data recorded on the onboard PC are then transferred to the fixed workstation via the permanent Wi-Fi connection after which the analysis of the acquired data is initiated to generate the results of the test.

All measurement data and calculated accuracy metrics are compiled in an Excel file in .xlsx format. The results are presented graphically including a map showing the areas covered by the weeding actions on the Base Module with two histograms summarizing the results of the weeding actions performed on weeds and the potential impacts on the crop plants present (Figure 9 and 10).

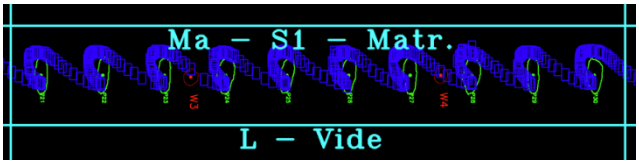


Figure 25. Mapping showing the intra-row weeding action of a mechanical weeding tool tested on the bench.

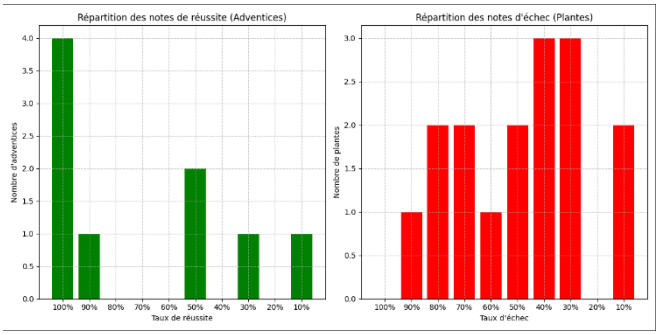


Figure 26. Histograms illustrating the test results obtained for a weeding tool on the bench.

The previous mapping (Figure 9) excerpt illustrates an example of a test result obtained for the mechanical weeding tool after processing the information acquired through the test bench interface. The maize crop plants on the Base Module used for the tests are shown in green while the weeds are shown in red. The trajectory of the weeding tool recorded during the test is represented by a sequence of small blue rectangles whose dimensions are determined from the configuration parameters specified prior to the test through the test bench user interface.

In this example, the mechanical weeding tool passes very close to the crop plants with occasional damaging interactions with some plants, notably plants P24, P25, and P28.

To simulate a targeted weeding action, validation tests were conducted using a laser pointer with its associated HD camera, both mounted on the test bench support carriage. When powered, the laser pointer projects a green cross to simulate a targeted weeding action such as localized spraying or the action of an electrical or laser-based weeding device on a weed.

In the test result mapping (Figure 11), the weeding actions performed are represented by small blue circles whose diameter is defined by the configuration parameters specified prior to the test through the bench user interface. The following mapping excerpt illustrates an example of result obtained for a targeted weeding tool after processing the data acquired through the bench software interface.

The simulated targeted weeding action, fixed laterally relative to the direction of travel, appears to pass very close to some crop plants without contacting them. The diameter of the blue circle representing the impact area of the targeted action should be adjusted according to the type of action being performed.

Overall, the results of these initial tests conducted on the test bench indicate an evaluation accuracy on the order of several millimeters. Further improvements, supported by additional testing, are expected to improve this level of accuracy.

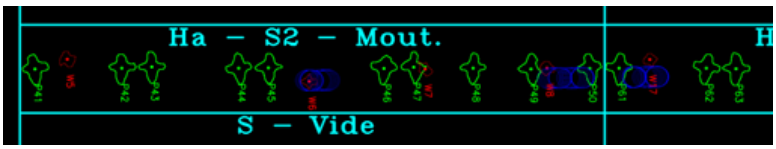


Figure 27. Mapping of examples of targeted weeding actions obtained on the test bench.

3.2 Test bench implementation for crop plant perception and detection and results obtained

Perception and detection tests were conducted on the bench using an autonomous mobile platform from a machinery manufacturer with its weeding device deactivated. The objective was to refine and validate the procedure for the perception and detection (P/D) test mode, based on the detection of crop plants performed by the manufacturer's proprietary software embedded in the system under test.

For each test, the autonomous mobile platform carrying the crop-plants perception and detection system was driven once across the Base Module of the test bench. Prior to each test, and depending on the predefined test protocols, the travel speed and platform control mode were adjusted accordingly. As for the P/D/A tests, the mobile platform was able to be remotely operated using a teleoperation mode or operated in fully autonomous mode using its onboard equipment and functions to navigate across the surface of the Base Module.

The plants positions data for the artificial crop plants and/or weeds on the bench Base Module, recorded by the software of the system in evaluation, were stored as data files. These files were subsequently exported to the bench fixed workstation and processed using a dedicated software application specifically developed for this purpose, enabling comparison with the reference position data.

The following mapping excerpt illustrates an example of a perception and detection test result obtained after processing the acquired data files. The maize crop plants on the Base Module used for the tests are represented in yellow, orange, or red according to their detection status by the

system under test, corresponding respectively to correctly detected, incorrectly detected, and undetected plants.

A focused graphical representation of the detections and positioning associated with an individual plant can also be generated to provide an indication of the positional accuracy of the detections performed (Figures 12 and 13).

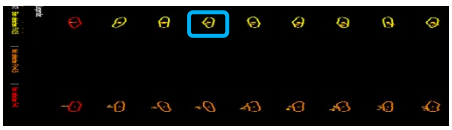


Figure 28. Mapping showing the results of a detection test with a system using two cameras to detect only crops

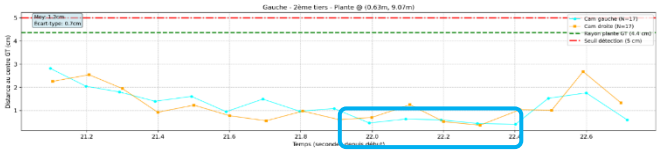


Figure 29. Detailed view of the detection and positioning of a crop plant over time

4/ CONCLUSIONS

The research and testing bench for alternative weeding systems presented in this paper is an innovative infrastructure currently in the final stage of development. Functional validation activities have been underway since late 2025, using tests involving weeding systems representative of the main machine categories identified in the specifications.

The initial results obtained with the test bench currently indicate an evaluation accuracy in the range of 2–3 mm. Continued testing and ongoing improvements are expected to bring the system closer to the initial target of millimeter level accuracy. Once this validation phase completed, the test bench would have to become fully operational by the end of 2026. It will enable artificial configurations of soil, crop plants and weeds to be reproduced, thereby providing an initial level of performance qualification for plant perception and detection systems as well as perception and detection systems combined with a final weeding action, under fully controlled, reproducible and repeatable conditions. The current configurations of crop plants and weeds available on the Base Module can be progressively expanded as testing requirements evolve, thereby increasing the range of applications and test scenarios supported by the test bench.

A final and important experimental phase will consist of comparing the results obtained from tests of weeding solutions on the test bench with the results obtained from tests of the same weeding solutions under real field conditions using the same crop types. This comparison will make it possible to determine the degree of correspondence between bench-based and field-based performance.

This test bench will provide valuable support to developers, machinery manufacturers, equipment suppliers and researchers by enabling them to validate their developments prior to final validation stages under field conditions.

Acknowledgements

The authors would like to thank all the staff members of SPIE and Logiroad for their valuable technical contributions and for the work carried out throughout the development of this research and testing bench for alternative weeding solutions.

The authors dedicate this Agritech Days 2026 contribution to the memory of their colleague Jacky Mazoyer, metrologist at the Technologies and Information Systems for Agrosystems Research Unit (UR TSCF) at the INRAE Montoldre site. He contributed to the measurement accuracy goal of this project through his expertise and knowledge in metrology. He suddenly passed away in this summer of 2026.

References

- Avrin, G.; Boffety, D.; Lardy-Fontan, S.; Regnier, R.; Rescoussie, R.; Barbosa, V. (2020) Design and validation of testing facilities for weeding robots as part of ROSE Challenge. *In Proceedings of the IA (EPAI)*, Saint-Jacques-de-Compostelle (Virtual Conference), Spain. (https://hal.science/hal-03010299v1).
- Benligiray, B., Topal, C., Akinlar, C.,(2019). STag: A stable fiducial marker system, *Image and Vision Computing*, Volume 89, Pages 158-169, https://doi.org/10.1016/j.imavis.2019.06.007 .

What are the mechanical alternatives to glyphosate for arable crops?

Damien Brun[a,*], Nassim Hamiti[b], Elena Kazakou[c], Jerome Labreuche[b], Geoffroy Oudoire[b], Fanny Vuillemin[d]

[a] ARVALIS Institut du Végétal, Station expérimentale, 91720 BOIGNEVILLE, France
[b] FNCUMA, 43 rue Sedaine, 75011 PARIS, France
[c] INSTITUT Agro Montpellier, 2 place Vialla, 34060 MONTPELLIER, France
[d] TERRES INOVIA, 110 chemin de la Cote Vieille, 31450 BAZIEGE, France
* Corresponding author. Email: d.brun@arvalis.fr

Abstract

The AGILE project investigated mechanical alternatives to glyphosate for arable crops. The most viable alternative remains tillage using implements designed to work the entire soil surface. Whilst using the proper implement is effective, it is not sufficient on its own, as the timing of the operation is crucial to its success: the soil must be crumbly to allow the tillage to uproot the plants, and conditions must be dry following the operation. By making use of a decision-making tool (J Distas), it is therefore possible to identify periods that are highly favourable, unfavourable and uncertain for mechanical weed control operations between crops.

In systems that use glyphosate without tillage (as is the case with Conservation Agriculture), no mechanical alternative that does not involve soil disturbance has been identified as effective in all situations. The various knife rollers and electrical weeding methods tested all share a lack of effectiveness against grasses (cereal volunteers or weeds) that may be present in the cover crop. This fundamental point raises the issue of grass management, which was previously well controlled with glyphosate but is now the weak point of alternative techniques

KEYWORDS: Glyphosate, tillage, mechanical destruction, alternative techniques, weeds

Complexity level: 3

1/ INTRODUCTION

In a political environment where synthetic chemical use is discouraged, the Casdar AGILE project focused on exploring alternatives to glyphosate for arable crops. Three main actions formed the core of this project: firstly: implementation of technical management trials in situations where glyphosate is still permitted (Conservation Agriculture or CA, hydromorphic clay soils and superficial stony soils). Secondly, multi-criteria evaluations of these situations on the basis of a typical farm (using the Systerre® software). Finally, analytical trials of agricultural equipment represent the third and final action of this project with implementation in autumn (cover crop destruction) or in spring (destruction of cereal volunteers or weeds before maize planting). These correspond to the typical periods of glyphosate use in current farming practices, with a total of five trials over the total duration of the project.

2/ MATERIALS AND METHODS

Firstly, a range of weeding products offered by manufacturers were identified, in order to classify them into different groups on the basis of their mode of action (tillage, no tillage) and then on the basis on the working parts used (in the case of tillage tools) or on the technology used: use of electrical energy, use of laser...).

Technology/ farm machinery	Manufacturers
Knife roller	Numerous
Knife roller with sliding effect	Actisol, Roll'N'Sem
Electrical weeding	AgXTend, Crop Zone, Rootwave
Thermal weeding	Carré, 2EBalm
Laser weeding	Nothing sold yet
Scalper/ Spring tine cultivator	Numerous
Field cultivator with pick up	EcoMulch, KvickFinn
Rotary tiller	Numerous
Disc chain harrow	Kelly Tillage, Fliegl

Table1. Provisional list of tools to be tested (project proposal, 2021)

This initial approach made it possible to group the equipment into families of tools with the range of tools varying in size depending on the family. In the second stage, they were implemented in order to establish their efficiency in weed control under different situations

Farm machinery	Soil disturbance	Manufacturers	Cover crop destruction	Weed/ volunteer intercrop destruction
Scalper	Yes	Numerous	✓	✓
Spring tine cultivator	Yes	Numerous	✓	✓
Field cultivator with pick up	Yes	Kvick Finn	✓	✓
Rotary tiller	Yes	Numerous	✓	✓
Disc chain harrow	Yes	Fliegl, Kelly tillage	✓	✓
Knife roller	No	Numerous	✓	NS
Knife roller with a sliding effect	No	Actisol, Roll'N'Sem, Dickson Kerner	✓	NS
Electrical weeding	No	Nucrop, Rootwave	✓	✓
Thermal weeding	No	Carré, 2EBalm, EcoMulch		
Laser weeding	No	depending on changes in supply		
New tools launched on farm shows	?			

Techniques with soil disturbance

Techniques without soil disturbance

Table 2. Final list of equipment x situations tested

✓ Referenced ✓: Referenced and tested
NS: not suitable

As shown in Table 2, not all equipment could be tested in the field for various reasons:

- A mismatch between the operations performed and the requirements for glyphosate substitution. This was the case for laser weeding, which selectively targets weeds at the seedling stage, and thermal weeding, which is generally carried out after sowing or planting, at the cotyledon stage. Furthermore, neither of these techniques currently offers equipment that is truly suitable for large-scale arable farming.
- Equipment unavailability during the trial period, as was the case for the disc chain harrow in autumn 2025.

- Limited availability of distributors or manufacturers to participate in the trials. For example, the manufacturer of the Grindstar machine, an innovative tool that received an award at the Agritechnica 2023 exhibition, was unwilling to travel to the trial site.

For each trial, a detailed characterisation of the initial conditions was carried out including soil moisture, weed density and species composition, weed growth stage and cover crop biomass. To enable statistical analysis, a standard three-block design was implemented. The performance of each implement was assessed through measurements of tillage depth, fuel consumption, and the resulting soil profile after the pass. Weed control efficacy was evaluated at regular intervals during the month following treatment and analysed in relation to the prevailing meteorological conditions.
For autumn operations, efficacy was expressed as the percentage reduction in weed biomass relative to an untreated control plot. For spring operations, efficacy was expressed as the percentage of weed destruction, based on the number of weeds recorded before and after the implement pass.

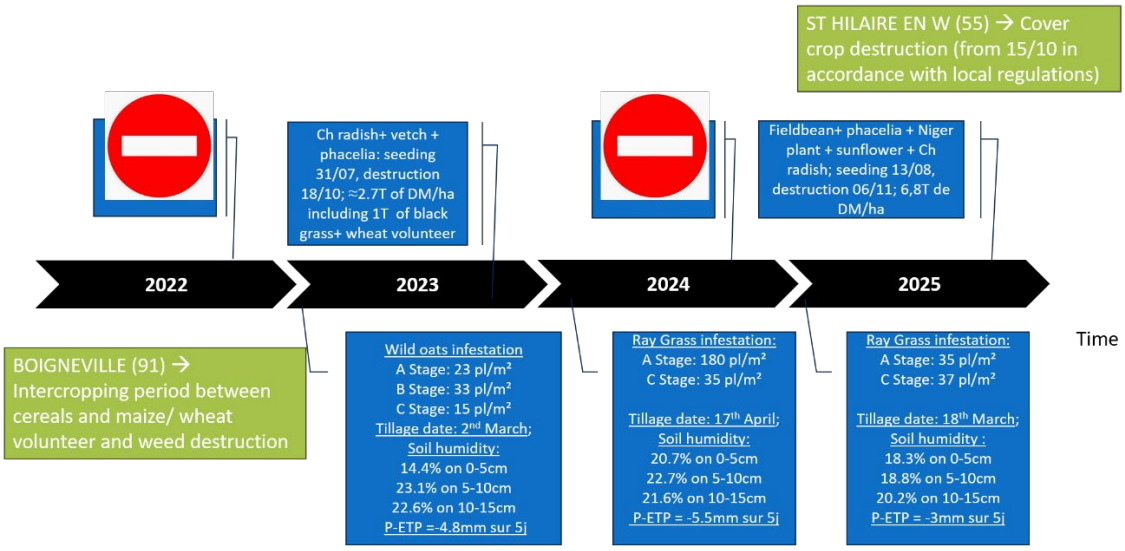


Figure 1. Summary of the field trials conducted during the project period

3/ RESULTS

3.1 Immediate actions

Some data were measured or recorded during the execution of field operations, such as working speed and fuel consumption, while other parameters, including average working depth and soil profile, were assessed in the days following the operations. The variables collected and their measurement method are presented in Table 3.

Site	Farm machinery	Average working depth (in cm)	Working speed (in km/h)	Fuel consumption (in l/ha)
Boigneville 2023	Rotary tiller	6.6	5	12.8
	Spring tine cultivator	7.6	10	5.3
	Power harrow*	5.7	5	14
St Hilaire en Woëvre 2023	Knife roller	-	11	2
	Knife roller with sliding effect	-	13	3
	Electrical weeding	-	3.5	15
	Rotary tiller	6.4	7	14.3
	Field cultivator with pick up	4.7	8	12
Boigneville 2024	Electrical weeding	-	2.5	18
	Rotary tiller	5.3	6.5	13
	Spring tine cultivator	4.2	11	6
	Scalper	6.2	10	6
Boigneville 2025	Rotary tiller		6	-
	Spring tine cultivator		10.5	-
	Scalper		10.5	-
St Hilaire en Woëvre 2025	Knife roller	-	10	2.5
	Knife roller with sliding effect	-	10	3
	Horizontal axis shredder	-	6	12.5

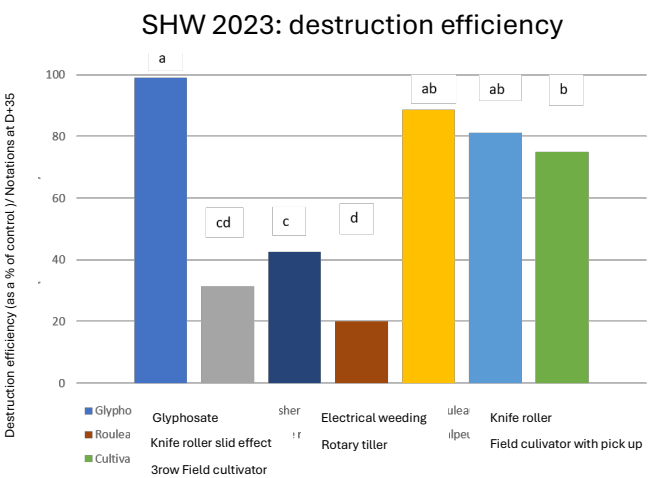
Table 3. Data collected during the trials

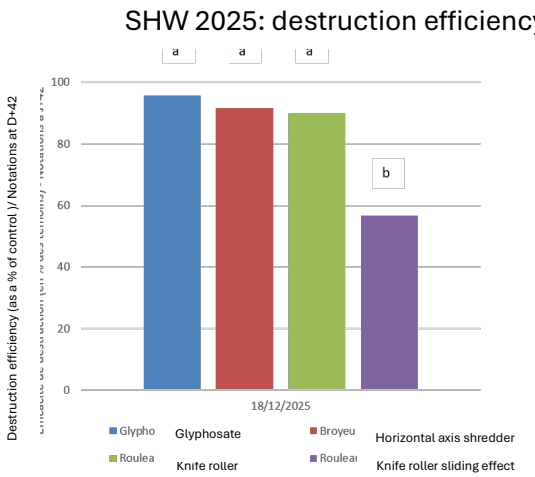
*: Tool not listed but added in connection with the trials of action 2

3.2 Mid term action: destruction efficiency of alternative techniques

Let us first consider on the cover crop destruction trials conducted on the Meuse site.
The first trial, conducted in autumn 2023, compared a range of techniques, including both soil-disturbing and non-soil-disturbing methods. Assessments were carried out at regular intervals, and the charts below presents the final evaluation performed 35 days after treatment.
In contrast, the autumn 2025 trial focused exclusively on non-soil-disturbing techniques. The final assessment was conducted 42 days after treatment.

Charts 1 and 2. Efficacy ratings from the 2023 and 2025 Saint Hilaire en Woëvre (SHW) trials.





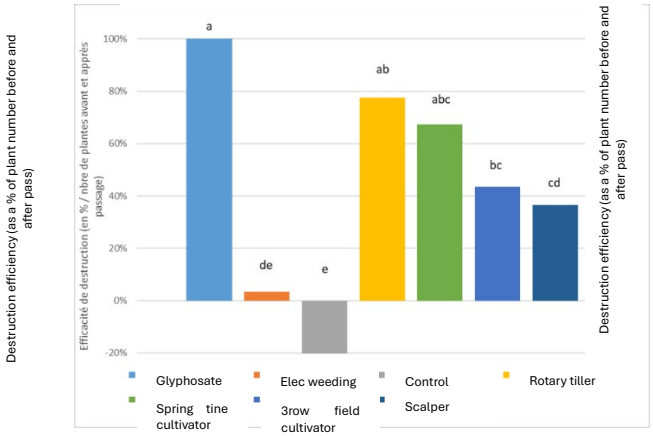
The results of these two trials highlight several important findings. First, a marked difference was observed between the two scenarios for the alternative non-tillage techniques. Their efficacy was poor in 2023 but ranged from good to very good in 2025, whereas the glyphosate treatment delivered consistently high levels of control in both trials.

In contrast, the tillage-based alternative techniques evaluated in 2023 achieved satisfactory levels of efficacy, although they did not match the performance of the non-selective herbicide. Finally, a consistent ranking was observed between the two knife roller designs. In both 2023 and 2025, the "with sliding" version was less effective than the standard design.

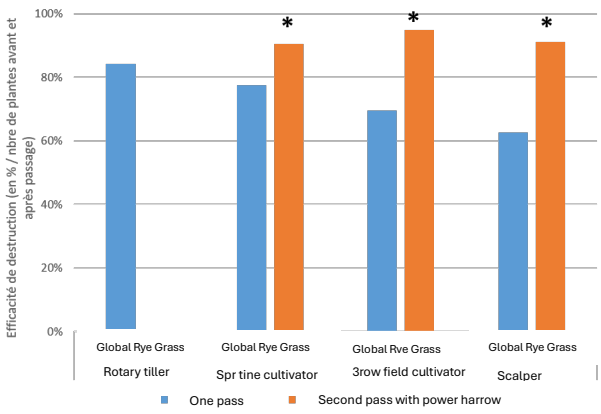
Let us now consider the destruction of cereal volunteers and weeds in intercrops prior to maize establishment. Conducted over three consecutive years at the Essonne research station, these trials focused primarily on grass weeds, particularly ryegrass.
Of the three trials conducted, only two are presented below because they provide the most relevant insights. The 2024 trial enabled the comparison of a wide range of treatments, including several tillage-based approaches and an electric weeding treatment applied in a single pass.
A similar experimental approach was adopted in 2025. However, the protocol was adjusted to better reflect practical farming conditions by incorporating a second mechanical pass to improve the control of tillered grass weeds.

Charts 3 and 4. Efficacy ratings from the 2024 and 2025 Boigneville (BG) trials

BG 2024: Destruction Efficiency



BG 2025: Destruction Efficiency



* Statistical difference between the modality and the scalper, Contrast method at the 10% threshold

3.3 Discussion

Comparing these two trials is particularly informative because they shared a similar starting point, namely the presence of tillered grass weeds, while being conducted under different weather conditions.

Conducted relatively late in the season (17 April), the 2024 trial highlighted the limitations of the non-tillage approach represented by electrical weeding. It also demonstrated the variable performance of the tillage-based alternatives, with substantial differences observed between the most effective and least effective treatments (rotary tiller and scalper, respectively).

The 2025 trial was carried out under conditions that were broadly comparable to those of 2024. The results showed a similar ranking of the tillage-based alternatives, although the differences were not statistically significant because of greater field heterogeneity. When only a single pass was performed, treatment efficacy remained variable. However, the addition of a second pass with the implement, in this case a power harrow, improved the performance of the initially less effective treatments and ultimately eliminated the observed differences between techniques.

One of the key challenges associated with alternative weed control techniques is the ability to operate machinery under suitable field conditions. Soil moisture must be compatible with trafficability, soil consistency, and the risk of compaction, while post-treatment conditions must favour the desiccation of uprooted vegetation. This fundamental issue is addressed later through simulations of the number of available days for mechanical operations.

The trials conducted at the Meuse site provide a clear illustration of this constraint. Over the four years of the project, mechanical interventions were possible in only two years, highlighting the highly weather-dependent nature of these operations.

Another important finding relates to the level of grass weed infestation within the cover crops. In 2023, weed pressure was high, with approximately 1 t DM ha^{-1} of cereal volunteers and blackgrass. In contrast, grass weed presence was almost negligible in 2025. These grass species are particularly problematic for alternative destruction techniques, especially those that operate without soil disturbance.

Whether based on electrical weeding, knife rollers, or knife rollers with a sliding effect, non-soil-disturbing techniques proved largely ineffective against dense grass weed populations (Cordeau, 2023). Consequently, the success of cover crop destruction using these approaches is highly dependent on establishing cover crops with minimal grass weed infestation.

Although the performance of conventional knife rollers appeared superior to that of knife rollers with a sliding effect, this difference should be interpreted with caution. The comparison may be partly confounded by differences in implement design, as the sliding-effect roller was equipped with a single drum, whereas the conventional knife rollers used in the trials were fitted with two or three drums depending on the experiment.

If we now focus on the intercrop management trials conducted prior to maize establishment, one of the main challenges concerns the availability of weather-permitted windows for field operations. To achieve effective weed control, mechanical tools must work the entire soil surface with adequate overlap, and the working depth must be adapted to the target flora. Inadequate depth was, for example, one of the factors explaining the poor performance of the scalper in the 2024 trial.

For well-developed grass weeds at the Barralis C growth stage, the electrical weeding tool tested (Nucrop) proved largely ineffective, confirming previous findings (Brun, 2020). Its performance differed little from that of the untreated control.

The tillage-based alternative techniques could be ranked according to their level of aggressiveness (Brun, 2024). Powered implements, such as the rotary tiller, achieved higher efficacy than non-powered implements, including the scalper and spring-tine cultivator.
In challenging situations, a two-pass strategy may represent a practical solution. Combining a non-powered implement with a subsequent pass using a power harrow can provide high levels of efficacy while relying on machinery that is commonly available on farms. This approach may therefore offer a more accessible alternative to the rotary tiller, which is less frequently available on arable farms (Arvalis, 2022).

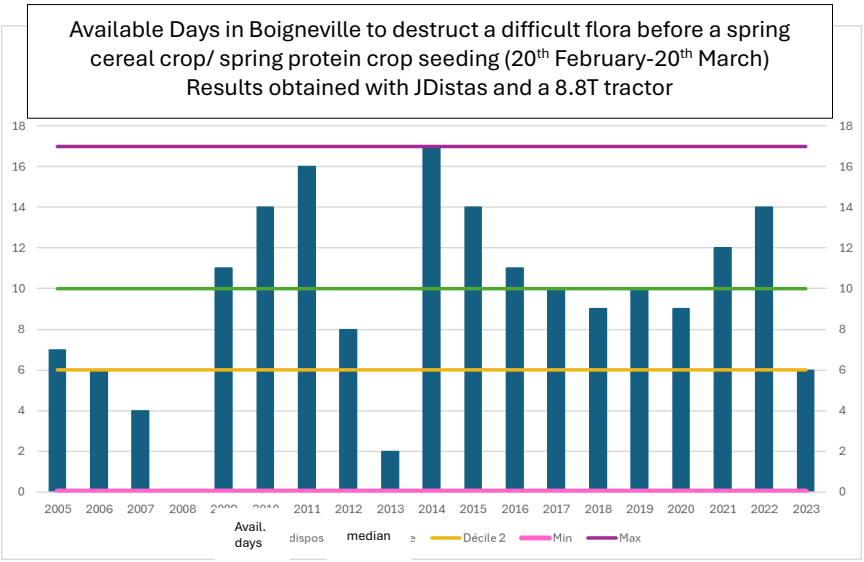
3.4 Available days for mechanical destruction

The influence of pedoclimatic conditions on the feasibility of mechanical alternatives has already been highlighted. To better quantify this aspect, Arvalis and its partners developed the J-Distas decision making tool (Métais et al., 2025). This model combines input data relating to soil

characteristics, climatic conditions, cropping practices, and machinery. These data are used to drive the CHN soil water balance model (Bessard Duparc et al., 2017), while indicators of workability, drying conditions, and compaction risk are calculated using the Terranimo model (Stettler, 2014). The resulting intermediate indicators are then aggregated through a set of decision rules to determine whether a given day is suitable for field operations. Simulations are performed using daily weather data. To account for climatic variability, analyses are generally based on weather records from the previous twenty years for a given location.

Among the different operations available in J-Distas, mechanical weed destruction in intercrops can be assessed according to two levels of weed control difficulty: easy or difficult. This distinction, developed within the Agate project (Labreuche et al., 2022), reflects the nature and development stage of the target weeds. Difficult situations correspond primarily to grass weeds at the tillering stage, whereas easy situations include broadleaf weeds or young grass weeds that are generally easier to control mechanically.

The results can be expressed as the number of available days for field operations over a given period of the year, such as the cereal sowing period or the establishment of spring protein crops. Because of the high level of interannual variability, summary statistics such as the median and the 2nd decile over a 20-year period are commonly used to characterise field accessibility and to estimate the likelihood of operational success or failure. These indicators provide a more robust assessment of operational feasibility than annual values alone, as they account for the considerable variability in weather conditions from one year to the next. The results can then represent the number of available days over a given period of the year (e.g. the period with sowing of cereals or spring protein crops). Faced with a large interannual variability, the notions of median or decile 2 over 20 years are often used to describe the number of available days in relation to a level of success/failure.

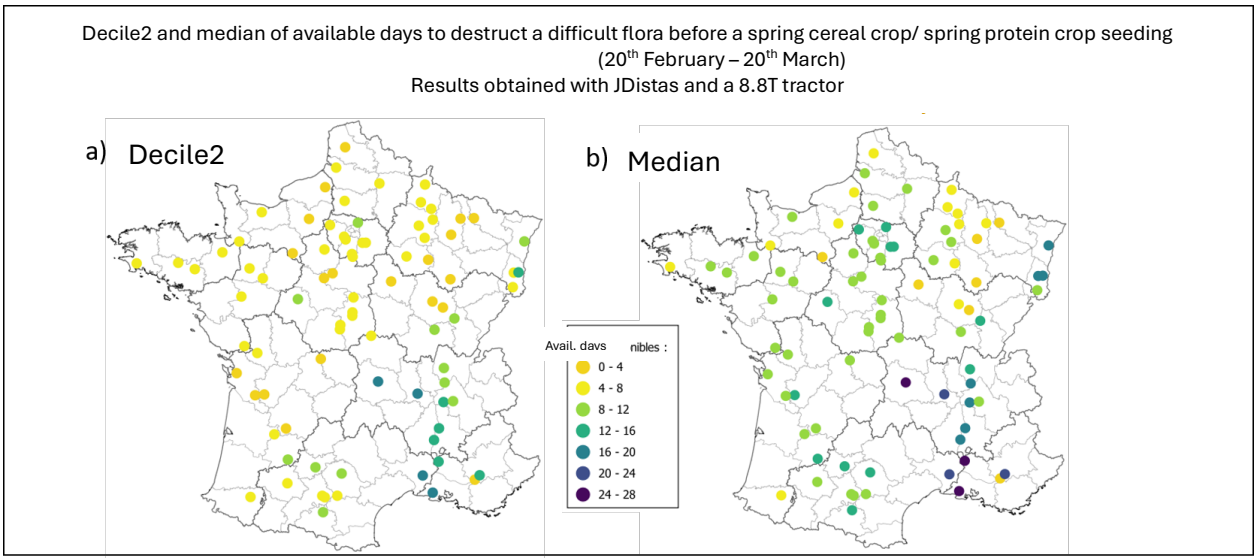


The criterion often used is the decile2 (success in 80% of cases/ failure in 20% of cases) which is equal to 6 days.

The median is much higher (10 days) but it carries a much greater risk of failure (50% of cases) making this notion often only illustrative!!

Chart 5. Available days in Boigneville during the period from 20 February to 20 March with difficult flora

After the example on a typical case (weather station * given soil type); the exercise was carried out throughout France with 85 standard cases.



Charts 6 and 7. Available days across France during the period from 20 February to 20 March with difficult flora

Considerable variability was observed among the standard scenarios over a given period. Based on the 2nd decile, the number of available days ranged from 0 to 8 days in most cases, indicating a relatively limited operational window.
With a few exceptions, the scenarios offering the greatest number of available days were located in southern France and along the Rhône Valley, where climatic conditions are generally more favourable for field operations.
Additional periods were also analysed (21 March to 20 April and 1 October to 30 October). The main results for these periods are summarised in Table 4

Period/ Available days	Medium	0-4 available days	4-8 available days	8-12 available days	12-16 available days	16-20 available days	20-24 available days	24-28 available days
01 October -30 October	6.15j	37.2%	27.7%	25.5%	9.6%	-	-	-
February 20 - March 20	6.21d	26.6%	48.9%	12.8%	7.4%	4.3%		
March 21 – April 20	12.07d	10.6%	4.3%	35.1%	28.7%	14.9%	6.4%	

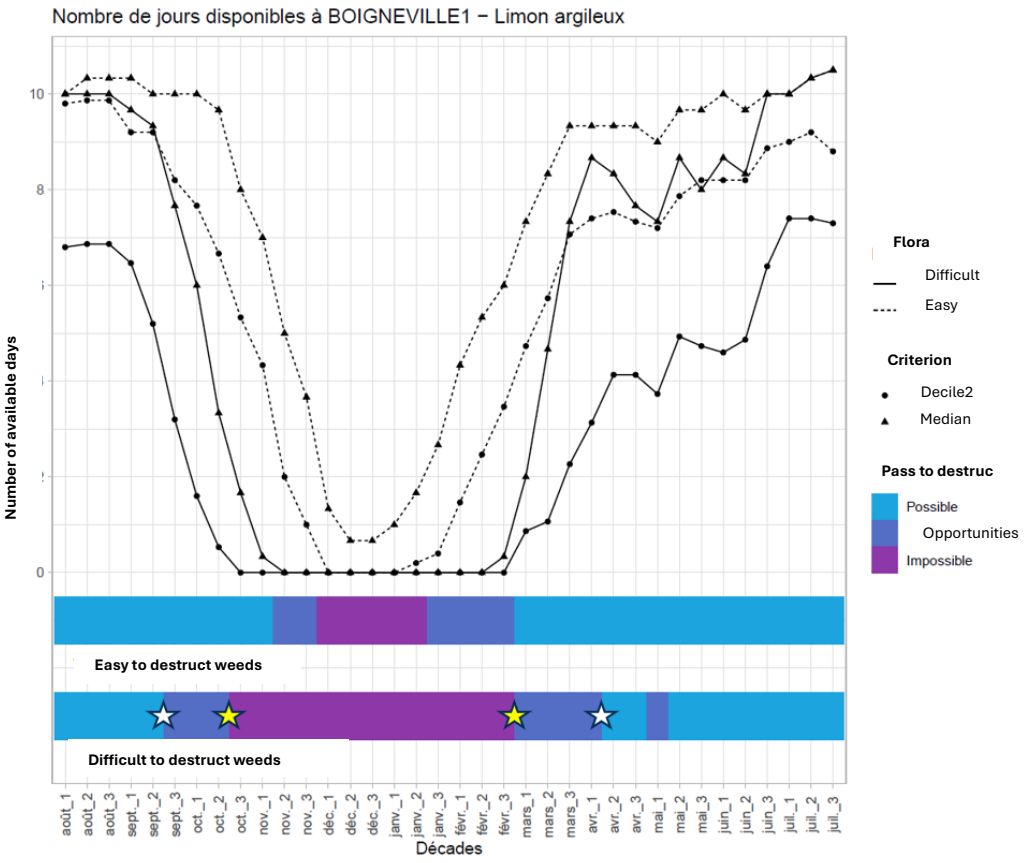
Table 4. Proportion of standard cases by class of available days for the whole of France/ Decile2 - Difficult flora with an 8.8t tractor

Finally, a complementary approach was developed based on the categorisation of ten-day periods (decades). Building on the previous analysis, this method uses a ten-day time step and classifies each decade according to a set of predefined decision rules.
The objective is to identify critical decades, that is, periods during which weather and soil conditions strongly influence the feasibility of field operations. Depending on the conditions encountered during these key periods, the likelihood of carrying out mechanical interventions can shift significantly from favourable to unfavourable, or vice versa.
This approach provides a more detailed understanding of seasonal field accessibility by highlighting the periods that have the greatest influence on the success or failure of mechanical operations under the defined decision rules.

Pass	Easy/ Difficult weeds	
	Decile2	Median
Possible	≥ 4 d/dec	≥ 2 d/dec
Opportunity	< 4 d/dec	≥ 2 d/dec
Impossible	< 4 d/dec	< 2 d/dec

Decision rule / number of days per decade to define the different periods offering more or less work opportunities.

Chart 8. Available days in Boigneville throughout the year for easy (dotted) and difficult (solid line) flora with the decision rules



	Possible	Opportunities	Impossible	Opportunities	Possible
Pivot Decade (1)		Sept_3	Nov_1	Mars_1	Juin_1	
% cumulative case studies/ total		80%	67%	80%	97.7%	

(1) Decade with the largest number of test cases: they correspond to the stars in the figure above

Table 5: Pivotal decade and percentage of cumulative standard cases in the period / Decile2 – difficult flora

This study highlights several important findings:

- The limited number of days available for mechanical weed destruction in autumn and early spring, which may constrain the timely establishment of subsequent crops.

- The particularly restrictive nature of the winter period (from early November to early March), during which suitable conditions for field operations are rarely encountered.
- The existence of weather-dependent windows of opportunity in both autumn and spring, although their duration varies considerably. In this study, these periods corresponded to approximately five decades in autumn and nine decades in spring.

Together, these results underline the highly variable and weather-dependent nature of mechanical weed destruction. Successful implementation therefore requires a high level of operational flexibility and responsiveness in order to take advantage of often short-lived windows of opportunity. Cropping and machinery strategies must consequently be adapted to these constraints. This may involve selecting equipment with greater working widths to increase field capacity, or favouring implement designs that remain operational under a wider range of soil moisture conditions, for example by limiting components that are sensitive to wet soils.

4/ CONCLUSION

This study focused on alternatives to glyphosate within no-till systems, whereas conventional ploughing generally facilitates glyphosate-free weed management. The mechanical alternatives evaluated rely primarily on tillage operations performed with appropriately selected implements capable of working the entire soil surface. In addition, their success depends heavily on favourable weather conditions following the intervention, particularly conditions that promote the desiccation of uprooted vegetation. This latter aspect is directly linked to the availability of suitable working days, which represents a key determinant of the success of mechanical interventions. While opportunities for mechanical operations are generally abundant during summer, they become much more uncertain in autumn and spring, despite these periods being critical for the establishment of winter and summer crops. Consequently, cropping systems requiring field operations between early November and mid-February face particularly severe constraints in terms of field accessibility and operability. The trials also demonstrated that non-soil-disturbing techniques are not consistently effective, particularly in situations where grass weeds are abundant within intercrops. This finding raises important questions regarding the long-term viability of Conservation Agriculture systems, which may ultimately need to reintroduce some degree of tillage if glyphosate use is restricted or if herbicide-resistant weed populations become more widespread.

A third key point concerns the technical and economic implications of these alternative strategies. As expected, mechanical interventions are generally slower and more expensive than chemical control using a non-selective herbicide. Depending on the initial situation, including the level of weed infestation and the current dependence on glyphosate, the additional labour requirement can vary considerably, ranging from a few extra working days per year to more than a month of additional fieldwork.

Acknowledgements

The authors would like to thank Dubrulle Downs for their support throughout this project. We are also grateful to CERI SN and the LAMCUBE laboratory for providing the research environment, technical resources, and collaborative framework that made this study possible.

References

- Arvalis, 2022. Le Projet Praigly - Destruction des prairies sans glyphosate ni labour. Brochure Arvalis Institut du végétal, sept 2022, 16p

- Bessard Duparc, P., Laberdesque, M., Soenen, B., Métais, P., Trochard, R., Le Bris, X., 2017. CHN: practical case of valorization of a dynamic crop model to estimate the number of available days for cultivation works, in: EFITA WCCA 2017 Conférence. Presented at the EFITA WCCA 2017 Conférence, Montpellier Supagro, Montpellier, p. paper number 38.
- Brun, D. (2020). Le désherbage électrique : une efficacité dépendant de nombreux facteurs. Perspectives Agricoles 476, 58-61
- Brun, D. (2024). Grandes cultures : quels outils pour remplacer le glyphosate ? Perspectives Agricoles 525, 62-64
- Cordeau, S., Busset, H., Colombet, C., Laurent, E., Matejicek, A., Mosa, B., Vieren, E., Spor, A., Martin-Laurent, F. 2023. Evaluation des effets intentionnels et non intentionnels de méthodes de destruction de la végétation en interculture sans pesticide de synthèse, in: 25ème Conférence du Columa Journées internationales de lutte contre les mauvaises herbes- 5,6 et 7 décembre 2023. Orleans, pp. 48.
- Labreuche, J., Vuillemin, F., Métais, P., Dubois, S., Gautellier, L., Piraux, F., 2022. Alternatives au glyphosate : des leviers aux efficacités variables, in: 3èmes biennales de l'innovation céréalière. Presented at the Phloème, Paris, pp. 93–102.
- Metais, P., Nicolas Rogier, Marine Lacoste, Pierre Dul, Thomas Leborgne, et al.. J-DISTAS : construction d'un outil de calcul des jours disponibles pour les grandes cultures. Innovations Agronomiques, 2025, 107, p. 421-440. 10.17180/ciag-2025-vol107-art30. hal-05383320
- Labreuche, J., Vuillemin, F., Duval, R., Duroueix, F., Bonin, L., Dessienne, C., 2021b. L'interculture sans glyphosate en pratique : des solutions proposées au cas par cas. Perspectives agricoles 484, 56-61.
- Labreuche, J., Vuillemin, F., Rodriguez, A., Perriot, B., Duval, R., Gautellier, L., Piraux, F., 2023. Etude d'itinéraires alternatifs à l'usage du glyphosate en grandes cultures, in: 25ème Conférence du Columa Journées internationales de lutte contre les mauvaises herbes- 5,6 et 7 décembre 2023. Orleans, pp. 93–102.
- Stettler, M., Keller, T., Weisskopf, P., Lamandé, M., Lassen, P., Schjonning, P., 2014. Terranimo ® - a web-based tool for evaluating soil compaction. Landtechnik 69(3): 132-138.

Evaluation of energy consumption of field operations in a dairy farm

Antti Lajunen*
Department of Agricultural Sciences, University of Helsinki, Helsinki, Finland
* Corresponding author. Email: antti.lajunen@helsinki.fi

Abstract

This research investigates the energy consumption of field operations on a dairy farm context by simulation-based analysis. The case study farm has 100 dairy cows and 150 hectares of cultivated fields, representing a large-scale production system in Finland. The operational requirements of the farm machinery were quantified using the ASAE D497.7 standard to determine implement-specific draft forces and PTO power demands under representative operating conditions. These power requirements were integrated with energy consumption maps derived from detailed tractor powertrain simulations, allowing the estimation of energy use across all major fieldwork, transport, and livestock-support operations. The results revealed the distribution of energy consumption among different fieldwork operations. The analysis identified the most energy-intensive operations and demonstrated the potential of alternative powertrains to reduce overall energy consumption and dependence on fossil fuels in dairy farm operations.

KEYWORDS: Energy consumption, dairy farm operations, field machinery, tractor simulation, operating efficiency

Complexity level: 3

1/ INTRODUCTION

Agriculture plays a fundamental role in global food production and rural livelihoods, with family farms and smallholder farms accounting for a substantial share of agricultural activity worldwide [1]. At the same time, the sector faces increasing pressure to improve its environmental sustainability, reduce greenhouse gas (GHG) emissions, and decrease dependence on fossil fuels. Livestock production, including dairy farming, is recognized as a significant contributor to global agricultural emissions, making the identification of mitigation opportunities an important research priority [2], [3]. In dairy farming systems, field operations such as soil cultivation, manure spreading, planting, fertilization, forage harvesting, and feed production require extensive use of agricultural machinery, resulting in considerable energy consumption and fuel use. Therefore, understanding the energy demands of field operations is essential for improving farm efficiency and reducing environmental impacts.

Agricultural tractors are the primary energy consumers in most field operations. Traditionally, tractor fleets rely almost exclusively on diesel engines, which contribute not only to fuel consumption but also to exhaust emissions and associated environmental burdens [4]. As climate change mitigation and energy transition policies become increasingly important, there is growing interest in evaluating the energy use of agricultural machinery and identifying opportunities for efficiency improvements. Quantifying energy consumption at the operation level provides valuable information for farm management, machinery selection, and the development of sustainable production practices.

Accurate measurement and modelling of tractor-based field operations are critical tools for achieving these objectives [5]. Field measurements enable the collection of real-world operational data, including fuel consumption, traction requirements, engine load, and work productivity [6]. Such data can reveal inefficiencies and provide benchmarks for comparing different machinery configurations and operating strategies. However, experimental measurements alone can be time-consuming and costly, particularly when evaluating multiple machinery concepts or varying operating conditions [7]. Consequently, simulation and modelling approaches have emerged as valuable complements to field testing. Modelling allows researchers to estimate energy consumption under a wide range of operating scenarios and supports the evaluation of technologies that may not yet be commercially available. Recent simulation-based studies have demonstrated the effectiveness of modelling tools for assessing the energy consumption and performance of alternative tractor powertrains under representative agricultural workloads [8].

The ongoing electrification of agricultural machinery further highlights the importance of detailed energy consumption analysis. Significant research efforts have focused on battery-electric, hybrid-electric, and hydrogen fuel cell-powered agricultural vehicles as potential alternatives to conventional diesel tractors [9], [10], [11]. These emerging technologies offer the potential to reduce fossil fuel consumption, lower operating emissions, and support agricultural decarbonization strategies [12]. However, their feasibility depends strongly on the specific energy requirements of field operations. Reliable assessments of energy consumption are therefore necessary to determine battery sizing requirements, evaluate charging and refuelling strategies, and compare the environmental and economic performance of different powertrain concepts. Studies investigating hybrid, electric, and fuel cell tractors have indicated promising opportunities for reducing energy use and carbon footprints, while also identifying challenges related to energy storage, costs, and operational flexibility [13], [14], [15].

Therefore, evaluating the energy consumption of field operations in dairy farming is an important step toward improving operational efficiency and supporting the transition to more sustainable agricultural systems. By combining measurements and modelling techniques, it becomes possible to characterize energy demands accurately, identify opportunities for efficiency improvements, and assess the suitability of alternative fuels and powertrain technologies for future dairy farm operations. Such knowledge is essential for reducing environmental impacts, supporting evidence-based machinery development, and advancing the decarbonization of agricultural production.

2/ MATERIALS AND METHODS

A representative Finnish dairy farm with 150 ha of cultivated land was used as the reference production system. The farm included 100 ha of grass silage and 50 ha of cereal production. Grass silage was harvested twice annually, with a four-year rotation resulting in approximately 25 ha of annual grassland renewal. Cereal production was divided equally between conventional mouldboard ploughing and reduced tillage based on chisel ploughing followed by disc harrowing.

The main general values related to dairy farm tractor-machinery operations are presented in Table 1. Long-term average crop yields were obtained from Finnish national agricultural statistics [16] and used to estimate annual quantities of silage, grain, and straw requiring harvesting, transport, and storage. Representative transport distances between fields and the farm centre were also included. Manure production was estimated using standardized ASAE values supplemented by published dairy-farm data [17], [18]. Cereal straw was assumed to provide sufficient bedding material for the livestock system. The resulting production system was used to quantify annual requirements for tillage, sowing, fertilization, crop protection, harvesting, transport, manure application, forage handling, feeding, and bedding operations.

Machinery power requirements were estimated according to the ASAE D497.7 standard [17]. For drawbar-powered implements, draft force was calculated from implement characteristics, working width, operating speed, tillage depth, and soil texture. PTO power requirements were calculated using standard machine-specific relationships incorporating no-load power, working width, and material throughput. Where suitable ASAE coefficients were unavailable, draft requirements were estimated from machine mass and rolling resistance, while PTO requirements were obtained from published specifications and engineering estimates. The draft force requirement of farm implements was calculated with the Equation 1 [17]

$$D = F_i(A + B(S) + C(S)^2)WT \quad (1)$$

where D is the implement draft (N), F_i is a dimensionless soil texture adjustment parameter (i = 1 for fine, 2 for medium and 3 for coarse textured soils). A, B and C are machine-specific parameters. The chosen operational parameters are S (field speed, km/h), W (machine width in meters or number of rows or tools) and T (tillage depth: (cm) for major tools, 1 (dimensionless) for minor tillage tools and seeding implements). The light transport with trailer corresponds to activities with an empty trailer and the heavy transport corresponds to necessary heavy transport activities such as grain transport form the field to the farm. Table 2 describes the selected farm machinery for grain production in the reference dairy farm. Combine harvester operation was excluded from the analysis.

Description	Value	Units
Harvesting area, silage	100	ha
Yield, silage	17500	kg/ha
Harvesting area, grain	50	ha
Yield, grain	3500	kg/ha
Average distance to field blocks	4	km
Average loading distance	50	m
Manure production	3394500	kg
Slurry volume	3429	m^3
Straw yield	2000	kg/ha
Grain trailer capacity	8000	kg
Bale trailer capacity	12000	kg
Slurry trailer capacity	22	m^3
Fertilizer spreader capacity	2000	kg
Feed mixer capacity	24	m^3
Average weight of a silage bale	850	kg
Average weight of a straw bale	350	kg

Table 1. General parameters for a dairy farm in Finland.

Machine	T: depth (cm)	W: width	S: speed (km/h)	F_i: soil parameter	A	B	C
Moldboard plow	30	2.03 m	7	1	652	0	5.1
Chisel plow	20	9 tools/row	10	1	91	5.4	0
Disk harrow	10	5 m	10	1	254	13.2	0
Spring tooth harrow	5	5 m	8	1	2000	0	0
Grain drill	4	32 coulters/ row (4m)	8	1	300	0	0
Sprayer		20 m	10				
Trailer, light transport			25				
Trailer, heavy transport			15				

Table 2. Farm machinery parameters for grain production.

Table 3 presents the chosen farm machinery for silage production and silage, feed, and manure processing. The machine parameters a, b and c were retrieved from the ASAE standard [17] for the machinery that requires rotary power from tractor's PTO. The corresponding PTO power requirement can be calculated with the Equation 2

$$P_{PTO} = \mathrm{a} + b \cdot \mathrm{w} + c \cdot \mathrm{p} \qquad (2)$$

where a, b and c parameters represent the no-load power requirement, the power requirement per unit of machine operating width and the power per unit of material feed rate. Operational parameters are the operating width w and processing performance p with units t/h. Trailer operations refer to the transport of bales from the fields to the farm. Slurry spreader corresponds to a slurry tanker with a manure injector. The fertilizer spreader is a conventional twin disc centrifugal spreader. Front-end loading work includes loading and unloading the silage and straw bales. The feed-mixer is used daily for producing feed for dairy cows and followers. The sawdust spreader is also used daily basis for spreading bedding material for the animals

Machine	s: speed (km/h)	w: width	p: performance (t/h)	a (kW)	b (kW/m)	c (kWh/t)
Mower-conditioner	10	3 m		0	8	0
Tedder	10	6 m		0	1.5	0
Round baler	7	2.05 m	22.0	4	0	1.1
Trailer (light transport)	25					
Trailer (heavy transport)	15		10.0			
Slurry spreader	8	10 m				
Slurry transport, light	25					
Slurry transport, heavy	15					
Fertilizer spreader	12	20 m				
Front-end loading	5		10.0			
Feed mixer	3		9.0	0	0	2.3
Sawdust spreader	2		0.3			

Table 3. Farm machinery parameters for silage production and silage, feed, and manure processing.

The operational performance of various tractor models, equipped with both conventional and alternative powertrains, has been established in our earlier research [8], [19]. The energy consumption results from those research results served as reference values for evaluating energy use in field operations and road transport. The reference tractor model was a large conventional tractor powered by a 225-kW diesel engine. Simulations were performed under tillage, PTO

operation, and road cycle conditions, incorporating different workloads. The outcomes from these simulations were utilized in this study to determine the energy consumption of alternative tractors during various field operations. Figure 1 illustrates the power required at the wheel for the reference tractor as a function of workload and driving speed, along with the corresponding energy consumption for the diesel-powered tractor.

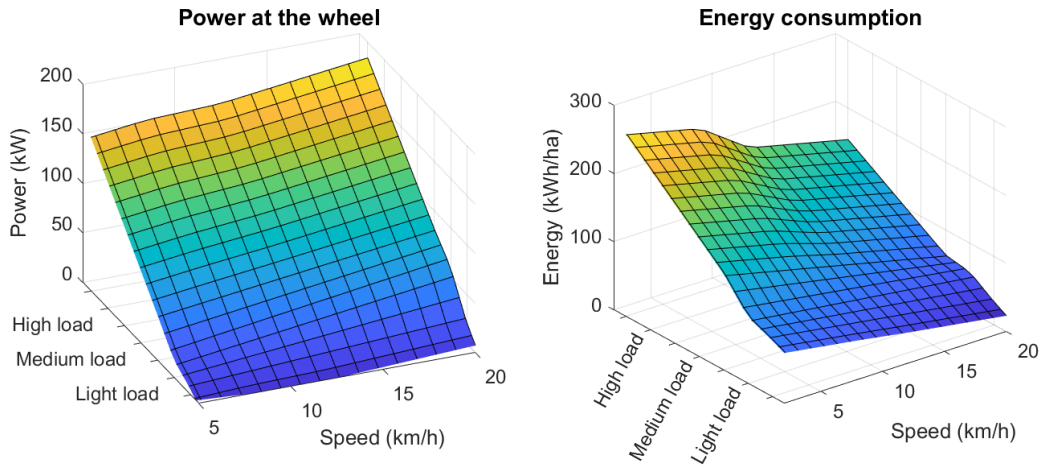


Figure 1. Calculated power requirement and energy consumption at the wheel in function of driving speed and external load for the conventional diesel tractor [20].

The calculated drawbar and PTO power requirements were subsequently applied to the tractor simulation model. This provided annual estimates of fuel or energy consumption for the complete range of field, transport, forage, manure, and livestock-related operations and enabled comparison under representative Finnish dairy farming conditions.

3/ RESULTS AND DISCUSSION

The energy consumption in each machine operation was calculated by using the tractor specific energy consumption maps and the calculated power requirement. The latter was defined based on the draft force and PTO power demand. The hydraulic and electrical power requirements of field machinery were generally neglected assuming those were not significant in relation to total energy consumption. Only in the case of front-end loading, the hydraulic power requirement was estimated.

The grain production operations for the dairy farm are practically similar in the case of a grain farm except for the renewal of grass production fields from crop rotation (25 ha). Tables 4 and 5 show the operational performance data for the grain, silage and dairy production. The descriptions of the data presented in Tables 4 and 5 are as follows:

- Area (ha): Field area that is operated yearly.
- Time (h): Theoretical operation time of the machine which depends on the working width, speed, and area.
- Efficiency (%): Field or transport operating efficiency.
- Total time (h): Total time used in the operation with efficiency included.
- Productivity (ha/h): Field area divided by the total time.
- Draft force (kN): Required draft force of the machine, calculated by using equation 1. Estimated for trailer operations from the simulation results.
- Power (kW): Required average power at the wheels of the tractor. For the sprayer, also the PTO power (12 kW) was included.

Machine	Area (ha)	Time (h)	Efficiency (%)	Total time (h)	Productivity (ha/h)	Draft force (kN)	Power (kW)
Moldboard plow	50	35.2	85%	41.4	1.21	55.0	106.9
Chisel plow	25	8.3	85%	9.8	2.55	26.1	72.5
Disk harrow	25	5.0	90%	5.6	4.50	19.3	53.6
Spring tooth harrow	75	18.8	85%	22.1	3.40	50.0	111.1
Grain drill	75	23.4	70%	33.5	1.68	38.4	85.3
Sprayer	100	5.0	65%	7.7	13.00	2.0	17.6
Trailer 1		4.5	85%	5.3		3.0	20.8
Trailer 2		7.5	85%	8.8		9.0	37.5

Table 4. Calculated performance and requirements for farm machinery operations in grain production and soil cultivation for dairy farm.

The calculations of the power requirements for silage production and silage, feed, and manure processing were similar than in the grain production. Table 5 presents the operational data and power requirements for each farm machinery or operation. The draft force was estimated for the trailer operations, slurry transport, feed mixer and sawdust spreader.
The estimated annual energy consumption of machinery operations on the reference dairy farm revealed substantial differences between individual field and livestock-related activities. The results indicate that the highest energy demands were associated with manure management, feed preparation, forage harvesting, and material handling, while conventional grain production operations accounted for a smaller proportion of the total annual energy use.

Machine	Area (ha)	Time (h)	Efficiency (%)	Total time (h)	Productivity (ha/h)	Draft force (kN)	Power (kW)
Mower-conditioner	150	50.0	80%	62.5	2.40	2.0	29.6
Tedder	150	25.0	80%	31.3	4.80	1.0	11.8
Round baler	200	123,9	65%	190.6	0.93	4.0	36.0
Trailer (light transport)		36.5	95%	42.9		2.0	13.9
Trailer (heavy transport)		60.8	95%	71.5		8.0	33.3
Slurry spreader	150	18.8	80%	23.4	6.40	32.8	112.9
Slurry transport, light		27.5	85%	32.4		4.0	27.8
Slurry transport, heavy		45.9	85%	54.0		10.0	41.7
Fertilizer spreader	150	11.3	70%	16.1	16.80		4.0
Front-end loading		112.0	90%	124.1			10.0
Feed mixer		365.0	90%	405.6		1.5	22.0
Sawdust spreader		146.0	90%	162.2		0.5	5.3

Table 5. Calculated performance and requirements for farm machinery operations in silage production and silage, feed, and manure processing.

Figure 2 presents the yearly energy consumption for grain production and soil preparation. The relatively high energy consumption of the spring tooth harrow and grain drill can be explained by

the large, cultivated area and the annual repetition of these operations across all grain fields. Although moldboard plowing is highly power-intensive on a per-hectare basis, its total annual energy consumption remained lower because only part of the cultivated area was plowed each year. The comparison between moldboard plowing (9.1 MWh) and reduced-tillage operations consisting of chisel plowing (3 MWh) and disc harrowing (2.5 MWh) demonstrates the substantial energy-saving potential of conservation tillage practices. The combined energy consumption of chisel plowing and disc harrowing was approximately 40% lower than that of moldboard plowing, highlighting one opportunity for reducing farm-level energy use.

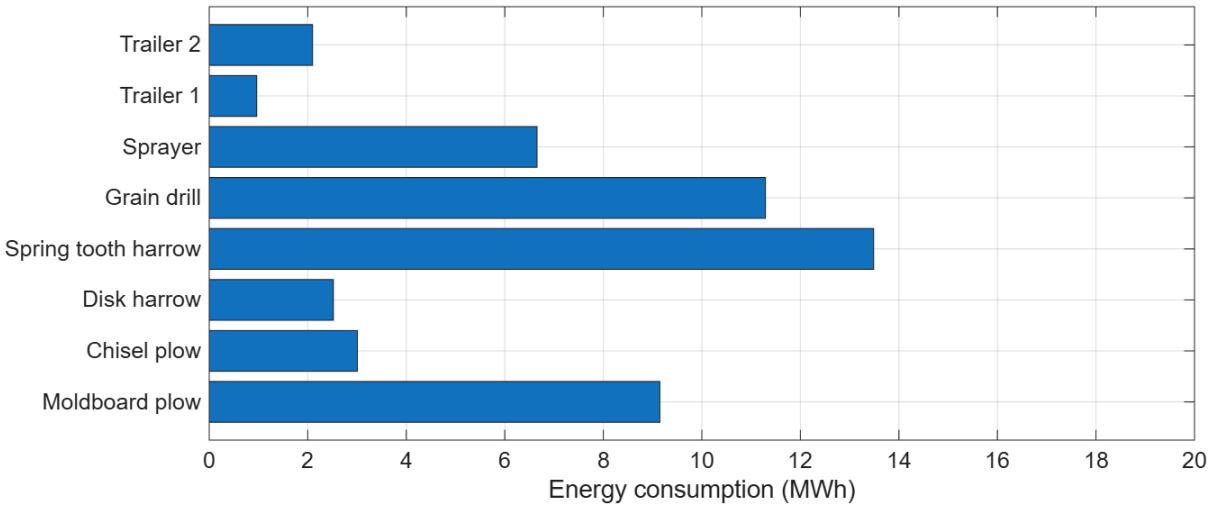


Figure 2. Yearly energy consumption in grain production and soil cultivation.

The yearly energy consumptions in dairy production related work operations are shown in Figure 3. The exceptionally high energy requirement of feed mixing (70 MWh) is primarily explained by its daily use throughout the year. Unlike seasonal field operations, feed preparation represents a continuous process that accumulates a significant annual operating time. Similarly, manure handling operations accounted for a substantial proportion of the total farm energy consumption. When slurry spreading, light slurry transport, and heavy slurry transport are combined, manure management requires approximately 48 MWh annually, making it one of the most significant energy-consuming activities on the farm.

The results further demonstrate that transport and material handling form a major component of forage production energy use. Bale handling operations together with trailer transport consumed over 48 MWh annually. These findings indicate that logistics-related operations, often overlooked in crop production analyses, can account for a considerable share of the total machinery energy demand in dairy farming systems.

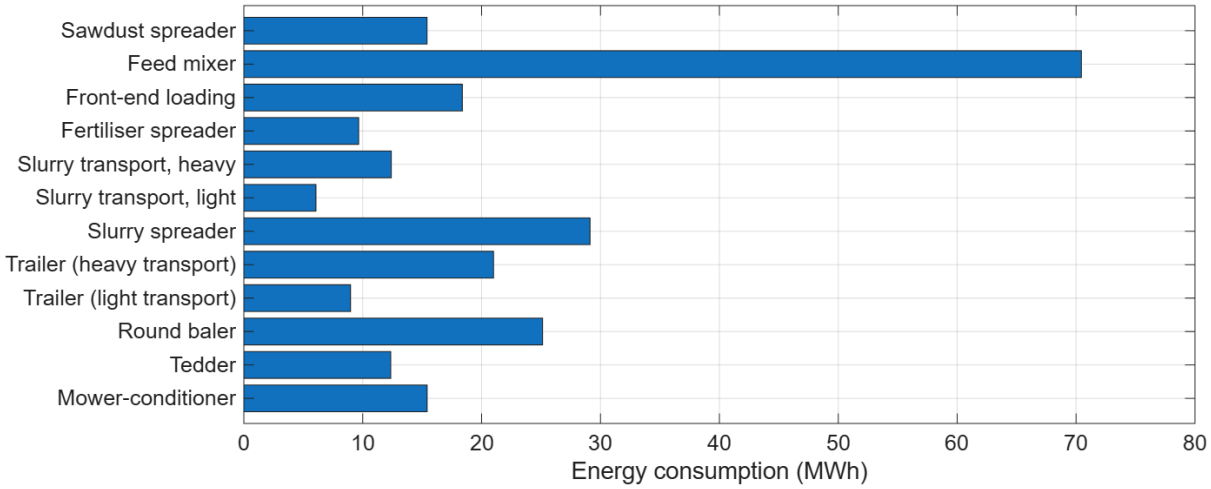


Figure 3. Yearly energy consumption in silage production and silage, feed, and manure processing.

The combined annual energy consumption of all analysed machinery operations was approximately 294 MWh. Of this total, grain production and associated transport operations accounted for approximately 49 MWh, while silage production, manure management, feeding, and animal-care operations accounted for approximately 245 MWh. This result reflects the fundamental difference between dairy and arable farming systems. In addition to crop cultivation, dairy farms require continuous feed production, feed processing, manure management, and bedding operations, all of which increase machinery use throughout the year. Therefore, evaluating only field cultivation activities would significantly underestimate the total energy requirements of dairy farming.

4/ CONCLUSION

This study evaluated the annual energy consumption of tractor-based field operations and livestock-support activities on a representative Finnish dairy farm. A simulation-based methodology was developed by combining machinery performance calculations derived from the ASAE D497.7 standard with energy consumption maps generated from detailed tractor powertrain simulations. The approach enabled the estimation of energy requirements across the complete dairy farm production system, including crop cultivation, silage production, transport, manure management, feeding, and bedding operations.

The results demonstrated that machinery energy consumption on dairy farms is strongly influenced by livestock-related activities. While grain production and soil cultivation accounted for a relatively modest share of the total annual energy demand, forage production, feed preparation, manure handling, and material transport dominated overall energy consumption. Feed mixing was identified as the single largest energy-consuming operation, followed by slurry spreading, forage harvesting, transport, and loading activities. These findings highlight the importance of considering year-round livestock-support operations when assessing agricultural energy use, as analyses focusing solely on field cultivation may significantly underestimate total farm energy demand.

The comparison of tillage practices further demonstrated the influence of management choices on farm energy consumption. Reduced tillage operations required substantially less energy than conventional moldboard plowing, indicating that cultivation strategy represents an effective means of improving energy efficiency without major investments in new machinery technologies.

Similarly, transport and material-handling operations were shown to contribute significantly to annual energy use, emphasizing the importance of farm logistics in overall energy management.

The developed methodology also provides a useful framework for evaluating alternative tractor powertrains and fuels. By linking operational power requirements with powertrain-specific energy consumption models, the suitability of diesel, hybrid-electric, battery-electric, and fuel-cell tractors can be assessed under realistic farm operating conditions. The results suggest that electrification potential varies between different operation types. High-power seasonal tasks such as tillage, slurry spreading, and forage harvesting present challenges due to their substantial energy requirements, whereas repetitive farmyard operations such as feed mixing, front-end loading, and bedding distribution appear particularly well suited for battery-electric technologies. Consequently, partial electrification targeting the most frequently used daily operations may provide an effective pathway toward reducing fossil fuel use and greenhouse gas emissions on dairy farms.

Overall, the study demonstrates that a comprehensive understanding of machinery energy consumption is essential for improving the sustainability and energy efficiency of dairy farming systems. The presented methodology enables detailed quantification of farm energy demand and supports the assessment of future low-carbon machinery technologies. Future research should extend the analysis to include economic assessments, seasonal energy storage requirements, renewable energy integration, and life-cycle environmental impacts of alternative agricultural powertrain technologies. Such analyses would provide valuable information for farmers, machinery manufacturers, and policymakers seeking to support the transition toward more sustainable agricultural production systems.

Acknowledgements

The author would like to acknowledge the Henry Ford Foundation Finland for the research funding.

References

[1] S. Lowder, J. Skoet, T. Raney, The number, size, and distribution of farms, smallholder farms, and family farms worldwide, World Development 87 (2016) 16–29.
[2] P. Gerber, H. Steinfeld, B. Henderson, A. Mottet, C. Opio, J. Dijkman, A. Falcucci, G. Tempio, Tackling climate change through livestock: a global assessment of emissions and mitigation opportunities, Food and Agriculture Organization of the United Nations (FAO), 2013.
[3] Murawska, E. Goryńska-Goldmann, Greenhouse gas emissions in the agricultural and industrial sectors—change trends, economic conditions, and country classification: Evidence from the European Union, Agriculture 13 (2023).
[4] D. Lovarelli, J. Bacenetti, Exhaust gases emissions from agricultural tractors: State of the art and future perspectives for machinery operators, Biosystems Engineering 186 (2019) 204–213.
[5] S.K. Pitla, N. Lin, S.A. Shearer, J.D. Luck, Use Of Controller Area Network (Can) Data To Determine Field Efficiencies Of Agricultural Machinery, Applied engineering in agriculture 30 (2014) 829-839.
[6] G. Steinberger, M. Rothmund, H. Auernhammer, Mobile farm equipment as a data source in an agricultural service architecture, Computers and Electronics in Agriculture 65 (2009), 238-246.
[7] A.Lajunen, H. Hovio, Development of a low-cost telematics system for smart farming operations, ASABE Annual International Meeting, 28-30 July 2024, Anaheim, CA, USA, pp: 1-7.
[8] A.Lajunen, K. Kivekäs, V. Freyermuth, R. Vijayagopal, N. Kim, Simulation-based assessment of energy consumption of alternative powertrains in agricultural tractors, World Electric Vehicle Journal 15 (2024).

[9] E. Scolaro, M. Beligoj, M. Perez Estevez, L. Alberti, M. Renzi, M. Mattetti, Electrification of agricultural machinery: A review, IEEE Access 9 (2021) 164520–164541.
[10] F. Mocera, A. Somà, Analysis of a parallel hybrid electric tractor for agricultural applications, Energies 13 (2020).
[11] V. Martini, F. Mocera, A. Somà, Numerical investigation of a fuel cell powered agricultural tractor, Energies 15 (2022).
[12] V. Olkkonen, L. A., E. Rosenberg, L. Kvalbein, Electrification of the agricultural sector in Norway in an effort to phase out fossil fuel consumption, Energy 276 (2023).
[13] O. Lagnelöv, G. Larsson, A. Larsolle, P.-A. Hansson, Life cycle assessment of autonomous electric field tractors in 144wedish agriculture, Sustainability 13 (2021).
[14] M. Beligoj, E. Scolaro, L. Alberti, M. Renzi, M. Mattetti, Feasibility evaluation of hybrid electric agricultural tractors based on life cycle cost analysis, IEEE Access 10 (2022) 28853–28867.
[15] V. Martini, F. Mocera, A. Somà, Carbon footprint enhancement of an agricultural telehandler through the application of a fuel cell powertrain, World Electric Vehicle Journal 15 (2024).
[16] Natural Resources Institute Finland (Luke), Statistics, https://www.luke.fi/en/statistics (accessed 7 September 2026), 2026.
[17] American Society of Agricultural and Biological Engineers (ASABE), ASAE D497.7 March 2011 (R2020) Agricultural Machinery Management Data, 2011.
[18] Natural Resources Institute Finland (Luke), Natural resources and bioeconomy studies 68/2023, Excretion calculations of cattle in Finland – Amount and composition of faeces and urine, 2023.
[19] A.Lajunen, K. Kivekäs, V. Freyermut, R. Vijayagopal & N. Kim, Simulation of Alternative Powertrains in Agricultural Tractors. International Electric Vehicle Symposium and Exhibition (EVS36), 11-14 June 2023, Sacramento, CA, USA, pp: 1-11.
[20] A.Lajunen, Evaluating energy consumption of different powertrain technologies in agricultural field operations, ASABE Annual International Meeting, 28-30 July 2024, Anaheim, CA, USA, pp: 1-7.

Towards an Optimal Model of Energy and Agronomic Performance for Barley Sowing Operations

Diego Urbina Salazar [a,b,*], Andrii Yatskul[b,c], Hamza Mohieddinne[d], Julien Guidet[b], Carolina Ugarte[a,b], Arnaud Dujany[c]

[a] AGHYLE, UniLaLalle, SFR Condorcet FR CNRS 3417, 19, rue Pierre Waguet, 60000 Beauvais, France

[b] Chair in Agricultural Machinery and New Technologies
AMNT, Polytechnical Institute UniLaSalle, 19, rue Pierre Waguet, 60000, Beauvais, France

[c] Institut Polytechnique UniLaSalle, GeNumEr, 14 Quai de la Somme, 80082 Amiens, France

[d]UMR CNRS 7058, Écologie et Dynamique des Systèmes Anthropisés (EDYSAN), Université de Picardie Jules Verne, Amiens Cedex 1, France

* Corresponding author. Email: diego.urbinasalazar@unilasalle.fr

Abstract

Optimizing the energy and agronomic performance of tractor–tire–tool systems remains challenging, as no transferable model currently identifies combinations of tractor speed, soil working depth, axle load distribution, and tire inflation pressure that jointly could minimize fuel consumption and maximize barley emergence. Three barley sowing experiments (Winter 2020, Spring 2021, and Winter 2021) were conducted to evaluate whether bootstrapping could improve the validation performance of interpretable polynomial models, assess their usefulness for multi-objective optimization of fuel consumption and barley emergence, and identify the factors limiting their transferability across seasons. To address these objectives, second- and third-order polynomial models were fitted to raw data and compared with models fitted to bootstrap-augmented datasets using a consistent calibration–validation framework.

Bootstrapping consistently improved validation performance, converting two models with negative validation R^2 into reliable models and yielding R2 values of 0.21–0.70, with RPIQ > 2 in most cases. The resulting equations provided direct interpretation of parameter effects and supported multi-objective optimization of fuel consumption and barley emergence under five weighting scenarios. However, optimal parameter combinations and the direction of key effects, including tractor speed, varied across seasons, and the Winter 2021 emergence model was not reliable enough for optimization. These results demonstrate the potential of bootstrapping to improve interpretable models fitted to small datasets, while highlighting the importance of accounting for pedoclimatic and soil variability to improve model transferability across seasons.

KEYWORDS: Fuel consumption; Barley emergence; Bootstrapping; Multi-objective optimization; Tractor–tire–tool systems, Soil conservation.

Complexity level: 4

1/ INTRODUCTION

Energy and agronomic performance in agricultural systems have been studied extensively over the past decades, yet they remain persistent challenges for farmers, who continue to rely on experience-based adjustments rather than formal optimization (Gupta et al., 2023). Within a tractor–tire–tool system, four parameters are readily adjustable by the operator: tractor speed (Ts), soil working depth (Swd), axle load distribution (Ald), and tire inflation pressure (Tp) and are well established as critical determinants of soil physical quality and fuel consumption (Adewoyin & Ajav, 2013; Damanauskas et., 2015; Mohieddinne et al., 2023). Since the right setting depends on soil, pedoclimatic, and topographical conditions, no reliable, transferable Global Model currently tells a farmer which combination of these four parameters jointly secures energy efficiency (fuel consumption) and good agronomic performance (Crop emergence) across different field conditions.

The Agronomic and Energy Optimization project (AgrEnOp), led by the Chair in Agricultural Machinery and New Technologies (AMNT) at UniLaSalle Beauvais, France, addresses this gap for winter and spring barley sowing. Three field experiments: Winter 2020, Spring 2021, and Winter 2021; were conducted to build season-specific optimization models identifying the best combination of Ts, Swd, Ald, and Tp for each season.

Modelling that combination formally raises a further question: which model class to use. Random forests are well suited to complex and nonlinear data as they combine many trees to improve prediction stability (Breiman, 1996, 2001; Chlingaryan et al., 2018). However, their complexity makes it difficult to clearly understand how each input affects the prediction, which can limit their practical use when decisions must be made directly in the field (Rudin, 2019; Rudin et al., 2022). Polynomial regression offers the opposite advantage, as its coefficients and response surfaces can be directly interpreted. However, its estimates may become unstable when fitted to the small datasets commonly obtained from designed field experiments. In this context, the objective of this study is threefold: (i) to assess the effect of bootstrapping on the validation performance of interpretable polynomial models fitted to the AgrEnOp field experiments, relative to models fitted to the raw data; (ii) to use the resulting equations to support multi-objective optimization of fuel consumption and barley emergence under five weighting scenarios; and (iii) to identify the factors currently limiting model transferability across seasons to develop a more general and transferable modelling framework.

2/ MATERIALS AND METHODS

2.1 Study site and experimental design

Two field experiments were conducted at the UniLaSalle experimental farm in Beauvais, northern France, and a third experiment was conducted at a site located approximately 5 km from the UniLaSalle campus (Figure 1a). The experimental design consisted of 36 treatment strips (T01–T36), each approximately 60 m in length and 3 m in width (Mohieddinne et al., 2023). Each treatment represented a specific combination of the four adjustable parameters investigated during the sowing process (Table 1), allowing the effects of their different combinations on the tractor–soil–implement system to be evaluated under field conditions. All experiments were performed on silty loam soils across three sowing seasons: Winter 2020 (36 treatments), Spring 2021 and Winter 2021 (36 treatments × 2 replicates; 72 observations per season). In Winter 2020, a 190 hp four-wheel-drive tractor (Massey-Ferguson 7719 DYNA VT) equipped with 540/65 R28 front tires and 650/65 R38 rear tires was used; in Spring and Winter 2021, a 150 hp four-wheel-

drive tractor (Massey-Ferguson 6714 S) equipped with 480/70 R28 front tires and 580/70 R38 rear tires was used instead. In both cases the tractor pulled an air seeder (Kuhn Espro 3000) combining tillage, consolidation, and sowing in a single pass (Figure 1b). Specific fuel consumption (L/ha) data were collected with flowmeters RS- 511-3965 installed on inlet and outlet of motor. Data was recorded by a data logger (SIRIUSi 8xSTG+, DEWESoft) at the same time scale. Computing processing and conversions were made through the post-processing software (Devesoft X) provided by DEWESoft. Barley emergence was assessed at the one- to two-leaf stage by counting the emerged plants over a 1m length in two consecutive sowing rows.

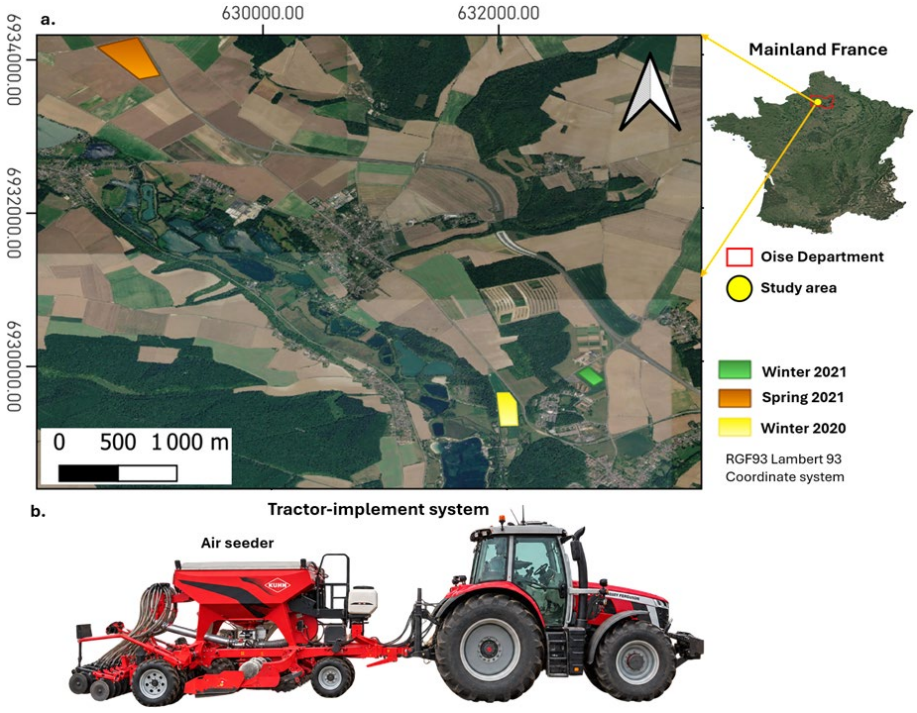


Figure 1. Study area location and Tractor-implement system

Factor	Factor meaning	Levels	Unit
X1	Soil working depth (Swd)	5,10	cm
X2	Tractor speed (Ts)	10, 12, 14	km/h
X3	Axle load distribution (rear/front) (Ald)	60/40 and 50/50	–
X4	Tire inflation pressure (Tip)	0.8, 1.0, 1.4	bar

Table 1. Operator-adjustable experimental factors and tested levels.

2.2 Modelling and Optimization Framework

Machine-learning approaches, such as random forest models, were not considered in the present study, as they had previously been evaluated within the same experimental framework by Mohieddinne et al. (2024). Instead, this study focused on interpretable polynomial models to assess the benefits of bootstrap data augmentation, support multi-objective optimization of fuel consumption and barley emergence, and investigate the factors limiting model transferability across growing seasons.

For each response variable (Fuel consumption "Y1" and Barley emergence "Y2") and season (Winter 2020, 2021 and spring 2021), polynomial regression models were developed using the four operator-adjustable factors (X1, X2, X3, and X4), incorporating their main effects together with interaction terms, quadratic and cubic terms. Second- and third-order models of this form were first fitted directly on the raw experimental data (n = 36–72 observations per season), using a 70% calibration / 30% validation approach to assess how well the model generalized beyond the treatments it was calibrated on. This raw-data model served as the baseline against which the benefit of resampling was subsequently evaluated.
To test whether resampling could improve on this baseline, the raw observations for each season and response variable were then augmented through bootstrapping, into pseudo-samples of 500, 1000, or 1500 observations. The same 70/30 calibration/validation approach used for the raw-data models, including the same split ratio and the same term-selection procedure, was then applied to each bootstrapped dataset. For each season and response variable, the augmentation size (500, 1000, or 1500) that produced the highest validation R^2 was retained, with RMSE used as a tie-breaker.

In both the raw-data and the bootstrap-augmented approach, the complete set of candidate terms, up to 10 terms at order 2 and up to 16 additional cubic terms at order 3, was reduced to a final model using the same three criteria, applied consistently across both approaches and all three seasons: (i) backward ANOVA elimination, removing the least significant term until every remaining term satisfied $p < 0.05$; (ii) hierarchical priority, favouring base terms over interactions, and interactions over cubic terms, whenever both were statistically viable; and (iii) a marginal-gain requirement, retaining a higher-order term only if it improved calibration R^2 by at least 3 percentage points

The models were evaluated by the coefficient of determination (R^2) (Eq. (1)), root mean square error (RMSE) (Eq. (2)), and ratio of performance to inter-quartile distance (RPIQ) (Bellon-Maurel et al., 2010) (Eq. (3)):

$$R^2 = \sum_{i=1}^{n}(\ddot{y}i - \bar{y})^2 / \sum_{i=1}^{n}(Yi - \bar{y})^2, \quad (1)$$

$$RMSE = \sqrt{\frac{1}{n}\sum_{i=1}^{n}(\ddot{y}i - Yi)^2}, \quad (2)$$

$$RPIQ = IQ/RMSE, \quad (3)$$

Where "ÿ" is the predicted value; "Y" is the observed value; "$\bar{y}$" is the mean of the observed values; "n" is the number of samples (varying from i to n); and "IQ" is the difference between the quartile below 75% of the samples and the quartile below 25% of the samples.

Multi-objective optimization was developed from the best performing polynomial equations predicting fuel consumption Y1 (L/ha) and plant emergence Y2 (plants/0.15 m^2). For each season, these equations were evaluated across the full factorial design space, and each predicted value was then converted into an individual desirability score (Derringer and Suich, 1980). A composite desirability score was then calculated and evaluated under five scenarios reflecting different farmer objectives and decision-making priorities, from prioritizing reducing fuel consumption to prioritizing crop emergence:

Scenario 1: Y1 = 50%, Y2 = 50%
Scenario 2: Y1 = 75%, Y2 = 25%
Scenario 3: Y1 = 90%, Y2 = 10%
Scenario 4: Y1 = 25%, Y2 = 75%
Scenario 5: Y1 = 10%, Y2 = 90%

3/ RESULTS

3.1 Polynomial versus Hybrid Polynomial–Bootstrap Modelling Performance

Table 2 compares the models fitted to the raw data (no bootstrap) with those obtained after bootstrapping for each season and response variable. Without bootstrapping, calibration R2 values ranged from 0.50 to 0.88, whereas validation R2 reached values as low as −0.74, indicating that some models fitted the calibration data well but had limited predictive performance on the validation data. Bootstrapping improved or maintained validation performance in all cases. In particular, the two models that showed negative validation R2 when fitted to the raw data reached validation R2 values of 0.21–0.70 after bootstrapping, with RPIQ values mostly above 2. These results show that bootstrapping was particularly beneficial for models that performed poorly when fitted directly to the original data.

Season	Response	Method	R^2cal	R^2val	RMSE	RPIQ	Performance
Winter 2020 (n=36)	Y1	No bootstrap	0.501	-0.737	1.1	0.54	Poor
	Y1*	Bootstrap (n=500)	0.575	0.598	0.49	2.15	Good
	Y2	No bootstrap	0.884	0.361	7.78	1.31	Moderate
	Y2*	Bootstrap (n=1500)	0.692	0.702	3.44	2.25	Good
Spring 2021 (n=72)	Y1	No bootstrap	0.715	0.425	0.71	0.91	Moderate
	Y1*	Bootstrap (n=1000)	0.692	0.688	0.57	2.57	Good
	Y2	No bootstrap	0.606	0.421	6.24	1.92	Moderate
	Y2*	Bootstrap (n=500)	0.549	0.569	4.17	2.76	Good
Winter 2021 (n=72)	Y1	No bootstrap	0.722	0.429	1.21	1.79	Moderate
	Y1	Bootstrap (n=1500)	0.609	0.631	0.83	2.06	Good
	Y2	No bootstrap	0.409	-0.704	6.47	1.08	Poor
	Y2	Bootstrap (n=500)	0.210	0.211	4.08	1.42	Poor

Table 2. Model performance for Y1 and Y2 before and after bootstrapping across three seasons

* Best-performing models used for multi-objective optimization

3.2 Model equations and parameter effects

The equations corresponding to the best-performing bootstrap-augmented models for Y1 and Y2 in each season are presented below. The model coefficients indicate the direction and magnitude of the effects associated with the four adjustable parameters and their interactions, providing a direct representation of how changes in the input variables affect the predicted responses.

3.2.1 Fuel consomption (Y1)

$$Y1\ (\text{Winter 2020}) = 6.709 + 0.260 \cdot X4 + 0.083 \cdot X1 - 0.367 \cdot (X3 \cdot X4) + 0.333 \cdot (X42) - 0.380 \cdot (X1 \cdot X2 \cdot X4) + 0.214 \cdot (X1 \cdot X2 \cdot X3) + 0.337 \cdot (X22 \cdot X1)$$

$$Y1\ (\text{Spring 2021}) = 7.803 + 0.446 \cdot X1 + 0.393 \cdot X3 - 0.493 \cdot X2 - 0.419 \cdot (X42) + 0.295 \cdot (X1 \cdot X3 \cdot X4) + 0.263 \cdot (X2 \cdot X3 \cdot X4)$$

$$Y1\ (\text{Winter 2021}) = 7.169 + 0.592 \cdot X1 + 0.539 \cdot X3 + 0.297 \cdot X2 - 0.415 \cdot (X1 \cdot X4) - 0.712 \cdot (X22) - 0.290 \cdot (X1 \cdot X3) + 0.555 \cdot (X22 \cdot X3) - 0.541 \cdot (X42 \cdot X3)$$

In the Winter 2021 equation, X1, soil working depth (+0.592), X3, axle load distribution (+0.539), and X2, and tractor speed (+0.297), all three are positive. Since Y1 is to be minimized, a positive

coefficient indicates that moving the corresponding factor toward its high level increase predicted fuel consumption: increasing working depth from 5 cm to 10 cm is therefore associated with higher fuel consumption, consistent with the additional draft force required to till deeper into the soil profile. The Spring 2021 equation illustrates a different, less immediately intuitive reading. Here the coefficient on X2, tractor speed, is negative (−0.493), the largest main-effect coefficient in that equation. Increasing speed from 10 km/h toward 14 km/h is therefore associated with a reduction in predicted fuel consumption per hectare, an outcome consistent with less time spent in the field to cover the same area, and a finding an operator can read directly from the equation without needing to infer it from a black-box prediction. The equations also retain quadratic and interaction terms. In the Winter 2020 equation, the quadratic term X42 (+0.333) shows that, considered alone, extreme tire pressures (0.8 and 1.4 bar) are less favourable than the intermediate setting (1.0 bar), raising predicted fuel consumption rather than lowering it. However, X4 also appears in three other terms of the same equation, so its overall effect on Y1 depends on their combined contribution and warrants further investigation.

3.2.2 Barley emergence (Y2)

Y2 (Winter 2020) = 42.918 + 5.816·X3 + 3.676·X4 − 1.979·(X42) + 1.351·(X1·X2) − 3.258·(X42·X3) + 2.495·(X22·X3)

Y2 (Spring 2021) = 47.503 − 4.549·X3 − 1.683·(X1·X3·X4)

In Winter 2021, the Y2 model showed poor predictive performance (Table 2) for reliable interpretation and was therefore excluded from the multi-objective optimization analysis.
In the Winter 2020 equation, the coefficient on X3, axle load distribution, is +5.816, the largest coefficient in the equation, the positive sign indicates that shifting axle load toward the more uneven 60/40 configuration is associated with the largest predicted gain in emergence among all retained terms. The Spring 2021 equation offers a direct contrast. Here X3 again dominates, but with the opposite sign (−4.549): increasing X3 toward 60/40 is now associated with a decrease in predicted emergence, so that the 50/50 setting becomes the more favourable configuration for this season. The two equations show that the direction of the optimal axle-load setting for barley emergence is not fixed across seasons.

3.3 Multi-objective optimization: best-performing combination by season

For each season, the validated equations were evaluated under the five weighting scenarios described in Section 2.2, and the combination that best reconciled the objective of minimizing fuel consumption with the maximizing barley emergence was identified.

For Winter 2020, results showed an optimal combination (Swd = 5 cm, Ts = 14 km/h, Ald = 60/40, Tp = 1.0 bar) under scenario 1 (balanced, 50/50), achieving a composite score of 89.5%. This solution effectively minimizes fuel consumption (Y1 = 6.076 L/ha) while maximizing plant emergence (Y2 = 49.87 plants·0.15 m^{-2}), making it the best option among all configurations for this scenario. The same combination remains optimal under scenarios 2 and 3, with the composite score rising to 90.4% and 91.0% respectively as priority shifts further toward fuel consumption. Once priority shifts substantially toward crop emergence, under scenarios 4 and 5, the recommended combination changes to (Swd = 5 cm, Ts = 10 km/h, Ald = 60/40, Tp = 1.0 bar), achieving composite scores of 94.1% and 97.6% respectively. This alternative trades a higher fuel consumption (Y1 = 6.504 L/ha) for near-maximal crop emergence (Y2 = 52.58 plants·0.15 m^{-2}), showing that tractor speed is the only parameter that needs to change between the two priority regimes for this season.

For Spring 2021, results showed a near-optimal combination (Swd = 5 cm, Ts = 12 km/h, Ald = 50/50, Tp = 0.8 bar) under scenario 1, achieving a composite score of 96.3%. This solution maximize crop emergence (Y2 = 53.735 plants·0.15 m^{-2}) and brings fuel consumption close to (Y1 = 6.250 L/ha), and its composite score remains above 93% under every one of the five weighting scenarios. Once fuel consumption is prioritized strongly, under scenario 3, this combination is displaced by an alternative (Ts = 14 km/h, Tp = 1.4 bar), which further lowers fuel consumption (Y1 = 6.08 L/ha) at the cost of reduced emergence (Y2 = 50.36 plants·0.15 m^{-2}, score 95.5%), showing that the recommended combination does shift once fuel consumption is weighted heavily enough in this particular season.

4/ DISCUSSION

4.1 Improving predictive performance while preserving model interpretability

Across all the seasons, bootstrapping consistently improved model performance compared with the corresponding raw-data models. The largest improvements were observed for Y1 in Winter 2020, where validation R^2 increased from −0.737 to 0.598, and for RPIQ, which increased from below 1 to above 2 in all seasons. This pattern is consistent with the increased risk of overfitting when multi-term regression models are calibrated on small datasets. Bootstrap resampling reduced this risk by decreasing the dependence of the model estimates on the original sample (Efron & Tibshirani, 1994). Importantly, the benefit of bootstrapping extended beyond low-performing models. Even for models with moderate performance in Spring 2021, bootstrapping produced a further improvement in validation performance.

A key property preserved throughout this study is that every retained model remains a closed-form polynomial equation, in which each coefficient quantifies the direction and magnitude of a specific parameter's effect on the response variable. As shown in Section 3.2, the sign and magnitude of each coefficient, together with the interaction and quadratic terms retained in the model, directly indicate which of the four adjustable parameters exerts the greatest influence on a given season's outcome, and how this effect is modulated by the remaining parameters.

A direct empirical comparison is available for this same dataset. In a previous analysis of the same three experiments, Random Forest models reached R^2 = 0.55 for fuel consumption and R^2 = 0.90 for barley emergence, across all seasons (Mohieddinne et al., 2024). For fuel consumption, the bootstrapped polynomial equations obtained in this study achieved validation R^2 values of 0.60–0.69 (Table 2), which were comparable to or higher than the Random Forest benchmark. This indicates that, for this response variable, the interpretability of a closed-form equation can be retained without necessarily compromising predictive performance. For barley emergence, the Random Forest achieved a higher validation R^2 of 0.90 than the best polynomial model obtained in this study (R^2val = 0.70). This difference is noteworthy because the polynomial models also accounted for non-linear effects through interaction, quadratic, and cubic terms. The stronger Random Forest performance may therefore indicate that barley emergence involves more complex relationships among the four adjustable parameters, or interactions with factors not included in our models, that were only partially captured by the polynomial approach. This asymmetry between the two response variables highlights the need for further investigation into the factors and relationships governing fuel consumption and barley emergence.

4.2 Seasonal variability as a challenge for model transferability

The optimization results in Section 3.3 show that the relationship between fuel consumption and barley emergence varies across seasons. In Winter 2020, the two objectives (Reduce fuel consumption and increase crop emergence) were in tension: the optimal combination changed when greater weight was placed on emergence, since tractor speed (Ts) had opposite effects in the two equations. This represents a conventional trade-off between competing response surfaces within desirability-based multi-objective optimization (Derringer & Suich, 1980), consistent with previous evidence that agronomical and energetical performance involve a trade-off within the same tractor-tire-tool system (Mohieddinne et al., 2023). In Spring 2021, by contrast, the two objectives were decoupled because the emergence equation did not include Ts, allowing this parameter to be optimized for fuel consumption without affecting predicted crop emergence. Winter 2021 could not be evaluated using the same criteria, since no well-performing crop emergence equation was obtained. Thus, both the magnitude of the trade-off and the ability to characterize it varied between seasons, suggesting that factors beyond the four adjustable parameters may influence barley emergence and fuel consumption.

This seasonal variability also highlights the main challenge in moving from season-specific equations towards a more general model. Barley emergence depends not only on machinery and operational settings but also on soil and seedbed conditions, including variables such as soil temperature, rainfall, moisture, and aggregate size distribution, which are recognized as important emergence drivers in crop-emergence modelling (Durr et al., 2001). More broadly, attainable agronomic performance is strongly influenced by local soil, environmental, and management conditions (Van Ittersum et al., 2013). These factors were not used directly in the present experiments and were therefore implicitly represented by the season. Their omission may help explain both the differences in the emergence equations between seasons and the inability to obtain a reliable equation in Winter 2021.

Future experiments should therefore incorporate these pedoclimatic and seedbed variables directly into the experimental design and modelling framework. A larger dataset covering multiple seasons and environmental conditions would help distinguish the consistent effects of the four adjustable parameters from variation caused by seasonal conditions. This would require repeated measurements of soil and crop conditions across seasons and at the spatial and temporal scales relevant to the experiments. Emerging Soil remote-sensing technologies, such as drone-based imaging, could provide a practical means of collecting this information repeatedly and consistently, thereby improving the characterization of seasonal variability (Urbina Salazar et al., 2026). Taken together, the results indicate that the four adjustable parameters provided reliable prediction of fuel consumption across all three seasons, whereas barley emergence was reliably modeled over only two growing seasons and showed greater sensitivity to seasonal conditions. These findings provide a basis for moving from season-specific equations towards a more general and transferable polynomial model, while highlighting the need for a broader experimental dataset that captures both the effects of the four adjustable parameters and the environmental variability observed across seasons.

5/ CONCLUSIONS

Overall, the polynomial models showed promising predictive performance, with validation R2 ranging from 0.60 to 0.69 for fuel consumption across all three seasons and from 0.57 to 0.70 for barley emergence in two of the three seasons. Bootstrapping contributed substantially to this improvement, consistently increasing validation performance compared with models fitted to the raw data and improving two initially unreliable models from negative validation R2 to values as

high as 0.70. The polynomial equations also provide direct insight into how the four adjustable parameters affect each response through their estimated coefficients, making the models practically useful rather than black-box predictors.

These equations enabled multi-objective optimization of fuel consumption and barley emergence under five weighting scenarios. However, the optimization results also revealed substantial seasonal variability. The optimal combination of the four adjustable parameters differed between seasons, and even the direction of some effects, such as tractor speed, was not consistent. In addition, the barley emergence model for Winter 2021 did not achieve sufficient validation performance to support its use in the optimization. Together, these results indicate that the effects of the four adjustable parameters cannot yet be assumed to be stable across growing seasons. This seasonal variability likely reflects the influence of environmental, soil and seedbed conditions that were not directly accounted for in the models, including soil moisture, temperature, and aggregate size. Developing a more stable and transferable model will therefore require a largest dataset covering multiple seasons and sites, together with direct consideration of these sources of environmental variability. Such an approach would help separate the effects of the four adjustable parameters from season-specific variation and provide a stronger basis for moving from season-specific equations towards a more general and transferable polynomial modelling framework.

Acknowledgements

This work was supported by the Chair in Agricultural Machinery and New Technologies at the Polytechnic Institute UniLaSalle, with financial contributions from the Michelin Corporate Foundation, AGCO Massey Ferguson, and KUHN. The authors gratefully acknowledge T. Beeuwsaert (UniLaSalle) for support in field operations and sowing.

References

[1] Adewoyin, A.O., Ajav, E.A., 2013. Fuel consumption of some tractor models for ploughing operations in the sandy-loam soil of Nigeria at various speeds and ploughing depths. Agric. Eng. Int. CIGR J. 15, 67–74

[2] Bellon-Maurel, V., Fernandez-Ahumada, E., Palagos, B., Roger, J. M., & McBratney, A. (2010). Critical review of chemometric indicators commonly used for assessing the quality of the prediction of soil attributes by NIR spectroscopy. TrAC Trends in Analytical Chemistry, 29(9), 1073–1081. https://doi.org/10.1016/j.trac.2010.05.006

[3] Breiman, L. (1996). Bagging predictors. Machine Learning, 24(2), 123–140. https://doi.org/10.1007/BF00058655

[4] Breiman, L. (2001). Random forests. Machine Learning, 45(1), 5–32. https://doi.org/10.1023/A:1010933404324

[5] Chlingaryan, A., Sukkarieh, S., & Whelan, B. (2018). Machine learning approaches for crop yield prediction and nitrogen status estimation in precision agriculture: A review. Computers and Electronics in Agriculture, 151, 61–69. https://doi.org/10.1016/j.compag.2018.05.012

[6] Damanauskas, V., Janulevicius, A., Pupinis, G., 2015. Influence of extra weight and tire pressure on fuel consumption at normal tractor slippage. J. Agric. Sci. 7, p55.

[7] Derringer, G., & Suich, R. (1980). Simultaneous optimization of several response variables. Journal of Quality Technology, 12(4), 214–219. https://doi.org/10.1080/00224065.1980.11980968

[8] Durr, C., Aubertot, J.-N., Richard, G., Dubrulle, P., Duval, Y., & Boiffin, J. (2001). SIMPLE: A model for SIMulation of PLant Emergence predicting the effects of soil tillage and sowing operations. Soil Science Society of America Journal, 65(2), 414–423. https://doi.org/10.2136/sssaj2001.652414x

[9] Efron, B., & Tibshirani, R. J. (1994). An Introduction to the Bootstrap. Chapman & Hall/CRC.

[10] Gupta, S., Rikhtehgar Berenji, H., Shukla, M., & Murthy, N. N. (2023). Opportunities in farming research from an operations management perspective. Production and Operations Management, 32(6), 1577–1596
[11] Mohieddinne, H., Yatskul, A., Ugarte, C., Thibaut, J., Guidet, J., Ritz, S., 2023. Trade-off between agronomical and energetical performances during barley sowing varying adjustable parameters in a tractor-tire-tool system. Soil and Tillage Research 226, 105582. https://doi.org/10.1016/j.still.2022.105582
[12] Mohieddinne, H., Araujo, H., Yatskul, A., & Ugarte, C. (2024). Model to simulate fuel consumption and sowing performance based on adjustable settings on tractor-tire-tool system for barley on loamy soil. 2024 International Soil Tillage Research Organisation Conference. Abstract Proceedings ISTRO 2024 https://www.arec.vaes.vt.edu/content/dam/arec_vaes_vt_edu/eastern-shore/istro-2024/abstract-book/AbstractBook_ISTRO2024_17October2024.pdf
[13] Rudin, C. (2019). Stop explaining black box machine learning models for high stakes decisions and use interpretable models instead. Nature Machine Intelligence, 1(5), 206–215. https://doi.org/10.1038/s42256-019-0048-x
[14] Rudin, C., Chen, C., Chen, Z., Huang, H., Semenova, L., & Zhong, C. (2022). Interpretable machine learning: Fundamental principles and 10 grand challenges. Statistics Surveys, 16, 1–85. https://doi.org/10.1214/21-SS133
[15] Urbina Salazar, D., Yatskul, A., Pinet, F., Dujany, A., & Ugarte, C. (2026). Integrating tractor-tire-tool adjustable parameters and UAV-derived Spectral indices to predict fuel consumption and crop emergence in spring barley sowing. Proceedings of the International Conference on Precision Agriculture (ICPA). https://www.ispag.org/icpa/proceedings/?&action=home
[16] Van Ittersum, M. K., Cassman, K. G., Grassini, P., Wolf, J., Tittonell, P., & Hochman, Z. (2013). Yield gap analysis with local to global relevance—A review. Field Crops Research, 143, 4–17. https://doi.org/10.1016/j.fcr.2012.09.009

From Diesel to BioCNG and Hydrogen: Transforming Agricultural Mobile Machinery with Internal Combustion Engine

Olivier Marchand[a,*], Thierry Bernard[a], Quentin Depoorter[a]
[a]CRMT, 3 chemin de la brocardière, 69570 Dardilly, France
* Corresponding author. Email: omarchand@crmt.fr

Abstract

Agricultural decarbonization requires alternative fuels capable of maintaining the performance levels expected from modern tractors and self-propelled machines. This study evaluates the feasibility of operating an agricultural engine, AGCO 4.9, converted for gaseous fuels, namely bio-compressed natural gas (bioCNG) and hydrogen, while maintaining compliance with Stage V emission regulations.

The engine was converted from diesel operation in a retrofit manner and tested over 200 hours and a wide operating range to assess its combustion behavior, efficiency, emissions, and maximum achievable power output. Power of 115 kW and 110 kW were achieved with bioCNG and hydrogen, respectively.

Bion operation was strongly constrained by thermal loading and cooled exhaust gas recirculation (EGR) would be essential for controlling combustion temperatures while maintaining stoichiometric combustion, similarly to on-road natural gas engines. This would enable the continued use of a 3-way catalyst required to comply with Stage V limits defined by Regulation (EU) 2016/1628 and potentially future more stringent emission standards. Hydrogen operation offered additional power potential, and the results suggest that further improvements in performance could be achieved through improvements to hydrogen injection and ignition systems and a dedicated air system for ultra-lean operation.

The study concludes that both fuels are technically suitable to convert agricultural tractor engines, but certification procedures would need to be adapted, potentially using RDE measurements, to remain compatible with small production series.

These findings could help identify the power classes and applications where gaseous-fuel tractors could provide a viable decarbonization pathway for agriculture.

KEYWORDS: Alternative fuels, Gaseous fuels, Retrofit, Powertrain, Vehicles

Complexity level: 3

1/ INTRODUCTION

Mobile agricultural machinery has historically been optimized for Diesel compression-ignition powertrains due to the high energy density of liquid fossil fuels at ambient temperature and pressure. This energy density enables long autonomies, high continuous load and severe torque requirements associated with demanding heavy-duty agricultural duty cycles. Over the past two decades, in Europe, pollutant emissions from diesel engines, including those used in agricultural machinery, have been significantly reduced and regulation 2016/1628 (Stage V) applies. However, despite these advancements, Diesel remains a fossil fuel whose combustion leads to significant greenhouse gas (GHG) emissions.

In that context, the agricultural sector is facing strong pressure to decarbonize its machinery while preserving peak on-field productivity, reliability, and operational flexibility. In this context, low-carbon gaseous fuels, such as bio-compressed natural gas (bioCNG) and hydrogen (H2), are emerging as highly credible alternatives to Diesel for modern turbocharged HD combustion engines [1]. Many conversion projects aim to achieve diesel-like power output.

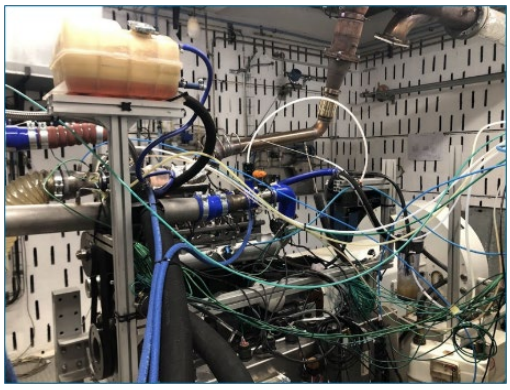


Fig 1: AGCO 4.9 in CRMT's test laboratory in bioCNG or H2 configuration.

This study evaluates the feasibility of operating a Diesel agricultural engine, AGCO 4.9, converted for bioCNG and H2, while maintaining compliance with Stage V emission regulation (mainly NOx < 0.46g/kWh - NRTS cycle). The engine was converted by CRMT in a retrofit-like manner and tested in its engine laboratory over a wide operating range to assess its combustion behavior, efficiency, emissions, and maximum achievable power output (Fig. 1 and [2]). The engine transformations are first explained. It uses CRMT's kits for CNG and H2. The H2 kit was further developed during this work. And as the agricultural sector encompasses a wide variety of engine platforms, one objective of the present project was therefore to develop a simple and adaptable conversion kit that can be implemented with minimal hardware modifications while retaining as many common components as possible between the versions and the original engine and tractor. Here the targets for the H2 option were a engine max power 116 Kw @ 1900rpm and a max torque of 726 Nm @ 1500rpm while complying with Stage V emission level with no aftertreatment system which could be possible when the air-to-hydrogen equivalence ratio, λ, is sufficiently high (> 2.2) (Fig. 2).

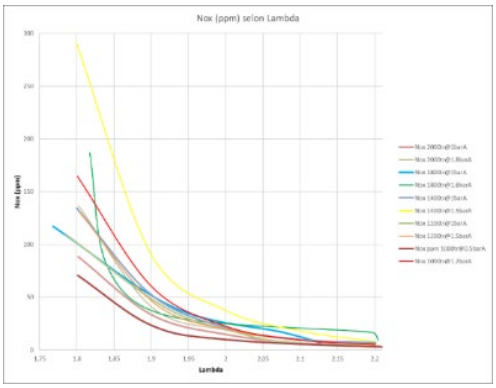


Fig 2: NOx engine out vs lambda in H2 combustion (AGCO 4.9 in H2)

Finally, the study concludes that both gaseous fuels are technically suitable for agricultural tractor engines conversion but require different optimization strategies despite sharing common parts. For bioCNG operation, cooled exhaust gas recirculation (EGR) would be essential for controlling combustion temperatures while maintaining stoichiometric combustion to continue the use of a 3-way catalyst required to comply with Stage V defined by Regulation (EU) 2016/1628 and more stringent emission standards. For hydrogen, the results suggest an additional power potential which could be achieved through the implementation of more capable hydrogen injection and ignition systems and a dedicated air system for ultra-lean operation. These findings

could help identify the power classes and applications where gaseous-fuel tractors could provide a viable decarbonization pathway for agriculture. Such tractors should then be developed in future including the modifications required for gaseous-fuel storage.

Remarks:
The characteristics of H2 and bioCNG (CNG or methane or biomethane, all being the same in this paper) vary over a large range. Their mass, energy densities, ignition and combustion characteristics change much more than other hydrocarbon fuels. Amongst the most important of these properties can be found in the table below extracted from [3].
Hydrogen or natural gas was injected into the intake manifold upstream of the engine combustion chamber, and combustion was initiated by an electrical spark. The engine operated in spark-ignition mode with a premixed combustion process. No exhaust gas recirculation (EGR) was implemented. Reference [3] also discusses dual-fuel combustion, a concept often considered for retrofit applications. However, this approach was not investigated in the present study, as it would require more complex exhaust after-treatment systems to control pollutant emissions.

		Gasoline	Diesel	H2 (700b)	CNG (200b)	NH3 (10b)
Density	kg/m3	737	830	40	435	603
LHV	kJ/g	43	43	120	50	19
Relative Vol. Energy Density	-	1.0000	1.1166	0.1502	0.6805	0.3547
Stiochiometric Air-Fuel Ratio	m/m	14.6	14.7	34.1	13.7	6.1
Cetane Number	-	11	>46	-	-	-
Octane Number	-	92	-	115	120-130	110
Adiabetic Flame Temperature	K	2274	2104	2254	1963	1800
Ignition Energy at Stoichiometric & NTP	µJ	~250	-	18	280	14000
Laminar Flame Speed	m/s	0.34	-	1.4	0.35	0.05
Flammability Range	% (vol/vol)	1.3/7.6	-	4/75	5/15	15/28

Figure 4: Fuel Physical Properties – NOTE: Indicative values taken for component mass fractions to illustrate a typical variation in concentration and properties

Fig 3. Fuel characteristics. Physical properties of H_2 and bioCNG compared with diesel, adapted from [3].

2/ MATERIALS AND METHODS

2.1 AGCO4.9 base engine modifications for bioCNG and H2 operation

The experimental evaluation was conducted on an AGCO Power 4.9-liter, 4-cylinder diesel engine, adapted for the MF6S tractor. The engine was transformed from conventional compression-ignition Diesel engine into a spark-ignition gaseous powertrain for bioCNG in 2023 and for H2 in 2025 and 2026 using a retrofit approach, i.e. as direct as possible and keeping the original single turbocharger (Table 1). The transformation intentionally omitting an EGR loop to preserve the standard packaging layout. Both modifications were engineered by CRMT from a 3D model of the engine provided by AGCO SAS and were tested in CRMT's engine laboratory. Many parts and systems were adapted and added. The main transformation is described here.

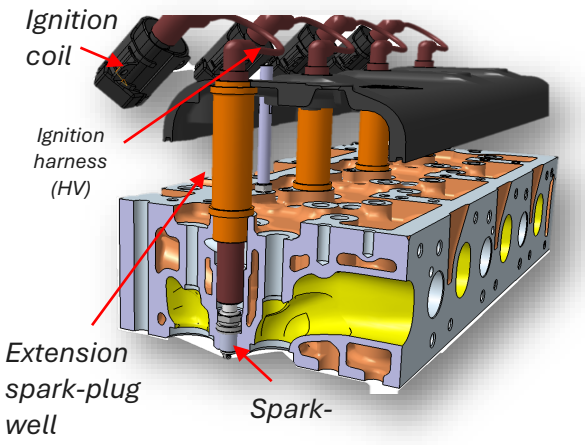


Fig. 4: 3D model of the cylinder head conversion

For the fuel system, in bioCNG, it was managed via a Single-Point Injection (SPI) arrangement utilizing four specific gas injectors from Keihin integrated into a rail assembly. For H2, an intake manifold was developed to support a Port Fuel Injection (PFI) layout for two Bosch NGI2 injectors per cylinder positioned directly in front of each cylinder's intake port (8 injectors in total) (Fig. 5). This made it possible to meet the fuel flow rate with adequate mixture preparation and to isolate each cylinder individually, preventing hydrogen migration between cylinders and reducing the risk of backfire or intake manifold explosions. This PFI configuration simplifies the engine conversion compare with direct injection (DI) while preserving most of the original engine architecture. It fits within the available envelop in the MF6S tractor. Provision was also made for a water injection system intended to moderate and mitigate abnormal H2 combustion. It was not tested. The H2 design can also handle bioCNG, but it was not available at the time bioCNG was tested. The low-pressure bioCNG line features a HD pressure regulator configured to an output pressure of 4.0 bar. Both bioCNG and hydrogen injection were controlled sequentially. For hydrogen, a maximum injection duration of 240°CA was selected. Consequently, a sufficient hydrogen injection phasing window was required, with injection occurring during the intake valve open period to minimize backfire and backflow phenomena.

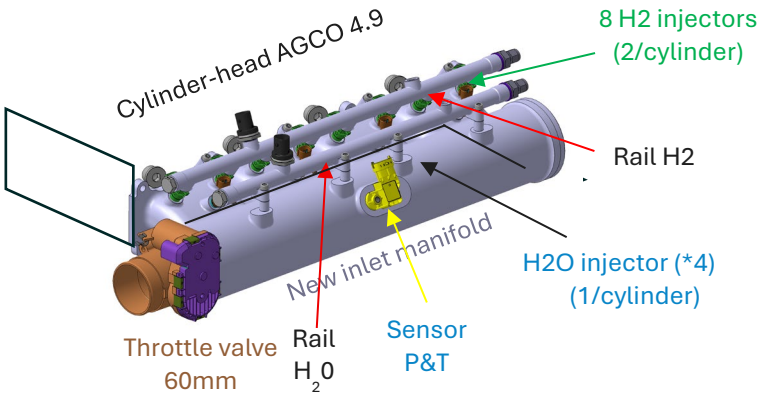


Fig. 5: Sketch of the new inlet manifold with H2 and H2O components

Cylinder Head and Ignition Rail: The high-pressure diesel fuel injectors were removed, and the injector wells were machined for M14 spark plugs. A high-voltage ignition harness and four ignition coils, 1 per cylinder, were selected. The design remained the same for both fuels enabling synergies (Fig. 4).

Piston adaptation (machining): The It was too high for either bioCNG or H_2 combustion. As the diesel piston had enough material to lower the CR directly, the pistons were re-machined to achieve a compression ratio of approximately 12:1, a typical value for bioCNG operation to mitigate knock propensity while ensuring efficiency capacity. In H2, 2 piston shapes with different CR, 12:1 and 13:1, were tested as they play an important role in the mixing of air and fuels and combustion efficiency (Fig. 6). The piston rings were not changed for both gaseous fuels.



Fig. 6: Piston modifications

Ignition: A dwell time sweep was executed across different engine speeds to map out spark demand. At low engine speeds and partial loads, the dwell time was set at 5.5 milliseconds. Under peak load and maximum boost conditions, the dwell time was extended to 6 milliseconds to supply sufficient ionization energy across the spark gap. Spark-plugs high wear was noted over the testing.

Air Management Loop: In bioCNG, the metered methane was discharged upstream of an electronically 60 mm Bosch throttle valve. The intake loop is complemented by a dump valve (blow-off valve) to manage transient turbocharger boost pressure. Combined pressure and temperature sensors are deployed both upstream and downstream of the throttle body to map volumetric efficiency. The same configuration was used for H2 but with injectors located after the throttle.

ECU and the control system: CRMT provided the ECU and a full control system. Parameters including spark timing calibration, injection duration, and boost pressure wastegate strategy were investigated during the testing. Torque structure was developed in the project to control the engine auxiliaries (engine torque indicated by CAN).
Engine oil: special oils were used both for bioCNG and H2 with a low ash content and compatible with the higher water-vapor content of hydrogen-engine exhaust and blow-by gases.
Remark: Hydrogen-compatible components had limited commercial availability during the project.

Engine version	AGCO 4.9 bioCNG	AGCO 4.9 H2
Lambda	1 (stoichiometric)	2 (average - lean burn)
Ignition order	1-2-4-3, with cyl.1 located on the valve-gear side, as on the diesel engine	
Compression ratio	12:1 (diesel adapted)	13:1 (diesel adapted)
Turbocharger (TC) + waste-gate (WG)	TC: Original Diesel + WG: open	TC: Original Diesel + WG: Close
Injectors	Keihin KN8	Bosch NGI2
Injection configuration	SPI: Single point	PFI (MPI): Port-Injection (or Multi)
Ignition coil	Delphi	
Spark-plug	NGK	Bricks
Engine oil	CNG (Total Rubia)	H2 (special R&D formulation)
ECU + SW	C5 CRMT + CNG SW	C5 CRMT + H2 SW
Combustion pressure	Cylinder 3	
Lambda sensor	Broadband (NGK)	

Table 1: Main characteristics of the AGCO 4.9 engine converted to bioCNG and H2

2.2 Test Bench Setup

The prototype engines, bioCNG and H2, were coupled to a brake at CRMT to apply load. The H2 test cell fully renovated for H2 with associated safety was used. For bioCNG, exhaust gas emissions (NOx) were measured using an NOx automotive sensor checked in-front of the test. In operation H2, a HORIBA MEXA analyzer was used to measure the exhaust gases emissions.
The composition of bioCNG was typically 94% of CH4, the rest being ethane, propane and azote. The H2 quality was 4.5.

Combustion analysis: to enable high-resolution thermodynamic analysis, Cylinder n°3 was equipped with an in-cylinder piezo-electric pressure sensor from Kistler. A sleeve was machined and integrated into the cylinder-head, positioning the sensor element flush with the combustion chamber ceiling to eliminate any acoustic signaling delays or thermal shocking bias.

2.3 Experimental Methodology

First the converted engine was tested for bioCNG. The lambda was kept to 1 and a comprehensive spark timing sweep was performed to find the Maximal Best Torque (MBT) at different engine load. A turbine inlet temperature limit of 700°C was selected first before an investigation at a higher temperature to protect standard components. The engine was subsequently converted to hydrogen operation.

The hydrogen testing was taken in 2 phases: phase 1, an initial evaluation for validation with the CNG combustion chamber (piston) to define a baseline and check component integrity, phase 2,

a dedicated combustion and components investigation. The wastegate control strategy was also optimized in phase 2 as excess air is required in H2 combustion targeting an ultra-lean hydrogen-air mixture with a lambda value close to 2 and with an intake manifold temperature regulated at 40°C.

Cold-start behaviour was not investigated because of project time constraints. Although previous experience with gaseous fuels did not indicate any specific difficulty, cold-start performance should be assessed in future work because of its relevance to agricultural operation.

3/ RESULTS AND DISCUSSION

The converted engine achieved maximum brake power outputs of 115 kW with bioCNG and approximately 110 kW with hydrogen. These results demonstrate that both gaseous-fuel configurations can retain a substantial proportion of the original diesel-engine power.

In bioCNG operation, a torque of 520 Nm at 1500 rpm and a brake power of 93 kW were initially obtained while limiting the turbine inlet temperature to 700 °C to protect the original diesel turbocharger. A maximum power of 115 kW was subsequently reached when the allowable turbine inlet temperature was increased to approximately 800 °C. However, this temperature level would not be considered suitable for continuous operation without further adaptation and durability validation. The hydrogen configuration reached approximately 110 kW under lean-burn operation. The results nevertheless indicated additional power potential, provided that the air-supply capacity, hydrogen-injection system and combustion calibration are further developed.

The maximum brake efficiency reached approximately 36% with bioCNG and 39% with hydrogen. For both fuels, the highest efficiencies were observed close to the maximum calibrated torque region. The lower efficiency obtained with bioCNG can be partly attributed to the ignition calibration margin required to prevent knocking. Further efficiency improvements would therefore require different development strategies for the two fuels: cooled EGR and combustion optimization for higher efficiency for bioCNG, and further air-management, injection and combustion development for hydrogen for combustion control.

3.1 BioCNG operation

Thermal constraints and emission at the exhaust (NOx)
The operation was primarily constrained by the high thermal load associated with stoichiometric combustion. Stoichiometric operation was selected to allow the use of a three-way catalyst, which provides a compact and effective solution for controlling NOx, CO and unburned hydrocarbons. Engine-out NOx concentrations between approximately 2,000 and 3,000 ppm were measured upstream of the aftertreatment system (> 10g/kWh). These values confirm that an appropriate catalytic aftertreatment system is necessary to meet Stage V pollutant-emission limits (similar to Euro VI).

The experimental results also show that simply increasing boost pressure and fuel flow is not sufficient to reach the target power continuously, because turbine inlet temperature becomes the principal limitation. The 115 kW operating point was obtained at an exhaust temperature close to 800 °C, whereas limiting turbine inlet temperature to 700 °C reduced the maximum brake power to 93 kW.
Cooled EGR therefore appears to be the most relevant development route for the bioCNG configuration. It would reduce in-cylinder combustion and turbine inlet temperatures while maintaining an exhaust composition compatible with three-way-catalyst operation, as for on-road application (previous work [4] indicated that an EGR rate of approximately 20% could reduce

turbine inlet temperature by about 150 °C). Its implementation would nevertheless require specific development and validation to control EGR flow.
This result highlights a fundamental characteristic of the bioCNG conversion. The principal limitation is not the ability to supply sufficient fuel or to achieve stable combustion, but rather the control of combustion and exhaust temperatures under stoichiometric, high-load operation.

3.2 Hydrogen operation

NOx emissions and air-system requirements
Hydrogen operation followed a fundamentally different strategy. The engine was operated with a large excess of air to limit combustion temperature and engine-out NOx emissions. Under sufficiently lean stationary operating conditions, NOx concentrations below approximately 25 ppm were measured over part of the mid-load operating range.

The tests also showed a strong sensitivity of NOx formation to the air-fuel ratio. When the mixture became richer, particularly below a lambda value of approximately 1.95, NOx emissions increased rapidly, reaching values of up to approximately 120 ppm at high load. Consequently, low-NOx hydrogen operation requires accurate control of both the global lambda value and the cylinder-to-cylinder mixture distribution, requiring very high air mass flow rates. The air-supply capability of the retained diesel turbocharger therefore became one of the main limitations of the hydrogen configuration.

These results indicate that ultra-lean combustion can provide very low engine-out NOx emissions under stabilized conditions, but they do not by themselves demonstrate Stage V compliance over a complete regulatory cycle. Transient operation, lambda excursions, must also be considered. Depending on the final engine calibration and the applicable emission requirements, a reduced-size SCR system may remain necessary for NOx reduction.

3.3 Additional results and discussion in hydrogen operation

3.3.1 Hydrogen combustion stability

The hydrogen engine exhibited specific combustion-instability phenomena near its high-load operating limit. These included misfire, pre-ignition and backfire, which constrained the achievable boost pressure and power density (Fig. 7a, Fig. 7b).

Cylinder-pressure measurements showed large cycle-to-cycle variations under unstable operating conditions. During the most severe events, the measured pressure reached the 150 bar acquisition limit and was accompanied by high-amplitude pressure oscillations. These results demonstrate that the high-load limit of the converted hydrogen engine was determined by abnormal combustion.

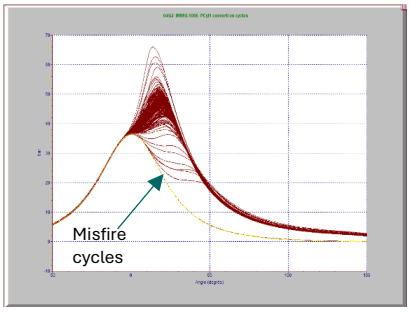


Fig. 7a: Cylinder-pressure cycles during misfiring

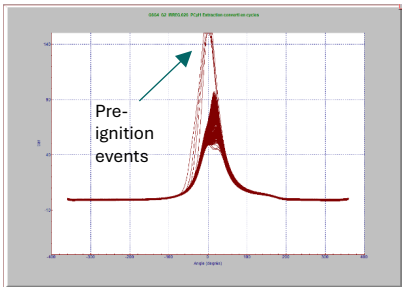


Fig. 7b: Cylinder-pressure cycles during pre-ignition events

3.3.2 Injection phasing and backfire

Hydrogen backfire occurred more frequently at high boost pressure when the end of injection was delayed to approximately 470°CA. Advancing the injection event and selecting a start-of-injection window between approximately 390 and 400°CA reduced the occurrence of these events during the investigated operating conditions. The improved behavior is attributed to better synchronization between hydrogen injection and intake-valve opening, which reduces hydrogen accumulation and backflow within the intake manifold. The use of two port-fuel injectors per cylinder provided the required hydrogen flow capacity and improved cylinder-specific fuel distribution. Nevertheless, the results show the intake-manifold geometry, mixture homogeneity, valve timing and injection phasing must be considered together when increasing hydrogen-engine power density in Port Fuel Injection (PFI) (Fig. 8).

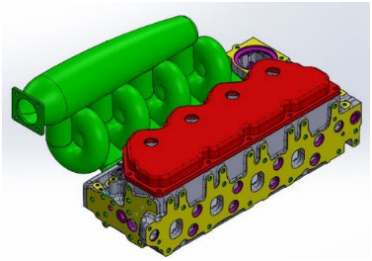


Fig. 8: Potential inlet-manifold with longer runners

3.3.3 Ignition-system sensitivity

The ultra-lean hydrogen-air mixture proved sensitive to spark energy, spark-plug gap and in-cylinder flow conditions. Stabilizing the center of combustion, CA50, at approximately 10 to 11°CA after top dead center required systematic optimization of the ignition parameters. These observations, together with the spark-plug wear identified during the campaign, confirm that ignition-system durability and performance are critical development areas for high-load, ultra-lean hydrogen operation.

3.3.4 Lambda measurement

A further experimental difficulty concerned lambda measurement. A dedicated high-accuracy hydrogen lambda sensor was not available during the test campaign. Consequently, the sensor response required an ECU correction strategy. This limitation must be considered when interpreting the absolute lambda values. Future development should include hydrogen-specific calibration of the lambda measurement system and, where possible, independent verification based on measured air and hydrogen mass flows.

3.3.5 Influence of intake-air temperature

Increasing the regulated intake manifold temperature to approximately 40 to 45 °C substantially reduced the stable operating range of the hydrogen engine. At these temperatures, the occurrence of pre-ignition and backfire increased near the high-boost boundary. At 1,500 rpm, maintaining stable combustion required approximately 1°CA of additional ignition retard, while the maximum stable torque was reduced to approximately 450 Nm. The engine therefore showed a significant sensitivity to intake temperature under high-load operation.

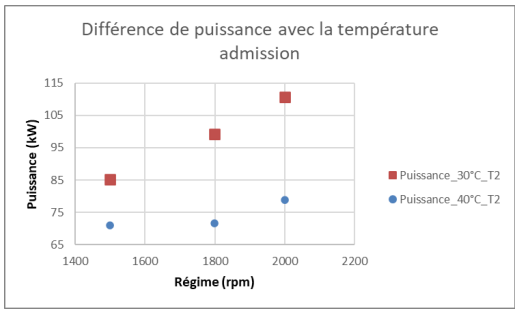


Fig. 9: Engine power versus inlet-manifold temperature

These results are particularly relevant for agricultural applications, where the engine may operate continuously at high load under elevated ambient temperatures and with restricted cooling conditions. A production engine would therefore require a calibrated thermal-protection strategy in which the torque target is adjusted as a function of intake-air and coolant temperatures.

3.4 Comparative interpretation and further development (Table 2)

Although the bioCNG and hydrogen conversions shared several hardware elements, including the modified cylinder head, ignition architecture and parts of the control system, their principal development constraints were fundamentally different.

For bioCNG, the main limitation was exhaust thermal loading under stoichiometric combustion. Development should therefore focus on cooled EGR, combustion-temperature control and integration of an efficient three-way catalyst.

For hydrogen, the exhaust thermal load remained comparable with lean-burn diesel-engine operation, but the required excess-air ratio placed much greater demands on the air system. Maximum power was constrained by turbocharger flow capacity, injection phasing and abnormal combustion phenomena, particularly pre-ignition and backfire.

The hydrogen results are consistent with published observations on dedicated off-road hydrogen engines, for which control of valve timing, injection timing, mixture distribution and abnormal combustion remains central to increasing power density. The present work further demonstrates the influence of intake-air temperature and retained diesel-engine hardware in a retrofit-oriented configuration.

Further development of the hydrogen engine should therefore focus on (not exhaustive):

- optimization of intake-manifold geometry and mixture distribution;
- increased hydrogen-injector flow capacity;
- improved ignition energy and spark-plug durability;
- hydrogen-specific lambda measurement;
- validated thermal-protection and torque-derating strategies.

Several of these topics will be investigated further within the GH-SAFE project.

3.4.1 Next step:

Finally, the limitations observed on the converted AGCO 4.9 hydrogen engine are consistent with those reported by Kubota for a dedicated 3.8 L off-road hydrogen engine [6]. In both studies, abnormal combustion phenomena, particularly backfire and pre-ignition, were identified as barriers to increasing power density. Kubota demonstrated that careful control of valve timing, injection timing and mixture homogeneity is required to suppress these phenomena, while the present results highlight similar sensitivities related to injection phasing, air management and intake-manifold design. Comparable limitations have also been reported by INNIO Jenbacher based on more than 5,000 cumulative hours of operation with large stationary engines fuelled with 100% hydrogen [7]. Overall, these findings indicate that the remaining challenges are primarily related to controlling abnormal combustion under high-load conditions rather than to sustaining hydrogen combustion itself.

4/ CONCLUSIONS

This study demonstrated the technical feasibility of converting an existing agricultural diesel engine to spark-ignition operation with either bioCNG or hydrogen, using intake-manifold gas injection without replacing the original cylinder-head casting. A significant proportion of the original engine architecture was retained. The bioCNG and hydrogen versions shared several major components, including the modified cylinder head, ignition system, and parts of the air-management and control systems. BioCNG may therefore provide an initial transition pathway

towards hydrogen, particularly given the limited production volumes expected during the early stages of market deployment.

Maximum power outputs of 115 kW with bioCNG and approximately 110 kW with hydrogen were achieved. Peak brake efficiencies reached 36% and approximately 39%, respectively. These encouraging results confirm that both fuels can deliver performance levels compatible with agricultural applications, although further optimization is required, using fundamentally different strategies for each fuel.

For bioCNG, the main limitation was the high exhaust thermal load resulting from stoichiometric operation, with turbine inlet temperatures exceeding 700 °C. Cooled exhaust gas recirculation should therefore be introduced to control combustion and turbine inlet temperatures while maintaining compatibility with an efficient three-way catalyst. For hydrogen, ultra-lean operation resulted in very low engine-out NOx emissions and could potentially enable compliance with Stage V limits with limited or no NOx aftertreatment under specific operating conditions. However, maximum power density remained constrained by abnormal combustion phenomena, particularly pre-ignition and backfire. Further development should therefore focus on air-supply capability, injection phasing, ignition performance, combustion-chamber design, and thermal derating strategies.

The remaining challenges extend beyond the engine itself. On-board gaseous-fuel storage affects vehicle packaging, mass, range, and operating autonomy. Safe handling procedures, appropriate maintenance practices, and operator training will also be essential. Consequently, the technical viability of gaseous-fuel agricultural machinery must ultimately be assessed at the vehicle level, considering reliability, operational constraints, safety, and an acceptable total cost of ownership for farmers.

Finally, conventional engine-based certification procedures may be disproportionately costly for retrofit applications and small production series. Adapted certification approaches based on real-driving emissions measurements using portable emissions measurement systems should therefore be considered. Further work within the GH-SAFE project will investigate hydrogen-specific developments and address several of the technical limitations identified in this study.

Item	Diesel	bioCNG	Hydrogen
Main issue	-	Exhaust temperature	Combustion control: pre-ignition/backfire
Torque / Power	Baseline	Close to Diesel but cooled EGR is required	Close to Diesel but combustion optimization is required (ignition, injection, CR optimisation, air management, etc.)
Engine efficiency	Baseline	Close to Diesel	Close to Diesel
Lambda (λ) target	Baseline (~1.6)	1	> 2
Exhaust aftertreatment system	SCR (deNOx) + DOC + DPF + NH3	Three-Way-Catalyst	None to light SCR (deNOx)
CO_2 abatement	Fossil CO2 emissions	-80% (WTW)	-100% (TTW)
NOx (raw from engine outlet)	High	High	Very low
NOx	Stage V compliant	Stage V compliant	Stage V or more stringent limits (to be demonstrated

			on certification cycles)
Particles	Low with DPF	Low	Very low
Range (fuel autonomy)	100 %	Limited, depending on possible storage 50-80 %	Limited, depending on possible storage 20-50 %
Tank volume	1x	3-5x	5-10x
Integration complexity	Baseline	Moderate to high	High
Fuel storage cost	Low	High	High (very)

Table 2 summarizes the main differences between diesel, bioCNG, and hydrogen in terms of engine performance, emissions, fuel storage, and vehicle-integration constraints.

Acknowledgements

CRMT thanks AGCO SAS as part of the ARHYSTOTE project for the authorization to use real data.

GH-SAFE project has received funding from ANR, FCT, MESRI, MUR, DSTI-NRF, ARI, ProjekträgerJülich PTJ, LGI under the European Union's Horizon Europe research and innovation programme and the African Union through the LEAP-SE programme (GA: 101172838)" GH-SAFE is a dedicated project co-funded by the European Union under the LEAP-RE initiative.



References

[1] Etude ACV de véhicules roulant au GNV et bioGNV - **Life Cycle Assessment of Natural Gas and Biomethane Vehicles**, A. Bouter et al. , 2019, IFP Energies Nouvelles https://www.ifpenergiesnouvelles.fr

[2] www.crmt.fr

[3] **Future Gaseous Fuel, latest developments in injection, ignition and combustion**, G. Dober, L. Doradoux, M. DaGraca, S. Coster, J. Ängeby, PHINIA, Luxembourg/France/UK/Sweden – 47th Internal Vienna Motor Symposium 2026 – 2026-33 – DOI : https://doi.org/10.62626/uesj-ztx6

[4] NGV / bioNGV Trucks Engines (Euro VI) - Modes de combustion et Dépollution - **Combustion Modes and Emission Control Technologies**, O. Marchand, 2025, CRMT

[5] **H2ICE the future of ICE for coming regulation**, Jean-Marc Neveu, VOLVO GTT Powertrain, March 2023, SIA

[6] **Fueled Internal Combustion Engine for Off-Road Applications**, KUBOTA, SAE Technical Paper 2025-32-0066, 2025, DOI :10.4271/2025-32-0066.

[7] **Operational Experiences with Hydrogen & Natural Gas Dual Fuel Engines for Combined Heat and Power Generation**, 14th Dessau Gas Engine Conference WTZ 2026**,** Dr.-Ing. Christoph Kraus, Alexander Zuschnig, Simona Zecca, Zita Baumann ·INNIO Jenbacher GmbH & Co. OG; Dr. Peter Christiner, Dominik Gruber · Robert Bosch GmbH

Centrifugal spreading ability of granular products

Sylvain Villette[a,b,*], Emmanuel Piron[b*], Denis Miclet[b], Tien-Thinh Le[b]

[a] Institut Agro, 26 bd Docteur Petitjean, F-21000 Dijon, France

[b] Université Clermont Auvergne, INRAE, UR TSCF, AgroTechnoPôle, Domaine des Palaquins, 40 route de Chazeuil, F-03150 Montoldre, France

[*] Corresponding authors. Email: sylvain.villette@institut-agro.fr; emmanuel.piron@inrae.fr

Abstract

This study aims to characterize the influence of the physical properties of fertilizers, and more generally of granular products, on their spreading ability. This ability is defined as the product aptitude to be uniformly broadcast over large working widths using centrifugal spreaders. Given the limitations of physical experimentation in isolating variables, Monte Carlo numerical simulations were conducted on 3800 virtual products (combining selected particle size distributions, densities, and drag coefficients) injected into a ballistic model.

Polynomial regressions identified the drag coefficient, specific density, and modal diameter as the fundamental parameters dictating the mean spread radius (or mean throw distance) and the maximum working width. The study also highlights the direct correlation between mean spread radius and maximum working width. This correlation was also observed across 2000 experimental measurements carried out using the CEMIB test bench at the AgroTechnoPôle (Montoldre, France). These models provide designers with predictive tools to accelerate the development of future granular products and spreading systems.

KEYWORDS: particle size distribution, drag coefficient, density, throw distance, working width, spread pattern

Complexity level: 2

1/ INTRODUCTION

In centrifugal spreading, pursuing wide working widths must not compromise the quality of product distribution. While the ejection characteristics of particles leaving the spinning disks depend on the spreader characteristics and the particle-spreader interaction, the ballistic flight phase is only influenced by the particle characteristics and their interaction with the air. Consequently, due to differences in their physical characteristics, not all granular products (particularly fertilizers), have the same ability to be spread over large widths while maintaining the target spreading quality.

Historically, the study of fertilizer physical properties has primarily focused on preventing ballistic segregation during the application of blended fertilizers. Numerous experimental studies have documented these segregation issues, largely attributing them to size variability among the different components of a blend (**Gimenez and Giosa, 2026; Hoffmeister et al., 1964; Thaper et al., 2021; Virk et al., 2013; Yule, 2011**). However, these studies failed to establish definitive

mathematical relationships between the physical properties of a fertilizer and its actual spreading performance**. Miserque et al. (2008)** were the first to mathematically connect fertilizer physical properties to ground distribution characteristics. They focused on the "spreading width" (defined as the total distance between the extreme left and right landing points of the fertilizer) and developed a regression model to predict this width based on the median particle diameter of the blend and the density of its heaviest component. While this successfully demonstrated how particle characteristics dictate projection distance, the scope remained limited to assessing segregation risks for fertilizer mixtures.

Evaluating the impact of physical properties experimentally presents two major difficulties: the inability to isolate the on-disk phase from the off-disk phase, and the difficulty of isolating the impact of individual properties. Consequently, researchers have turned to theoretical ballistic flight models. **Pitt et al. (1982)** utilized approximating equations for ballistic trajectories to evaluate how particle size variability affects throw distance under fixed initial velocities and heights. They concluded that size variation has only a mild effect on lateral distribution. However, the effect of particle size distribution on the transverse spread pattern were not studied and adjacent overlaps were not considered. Other researchers have proposed alternative metrics and design frameworks. **Parkin et al. (2005)** analyzed the transverse spread patterns of granulated urea, prilled urea, and ammonium nitrate, suggesting that a theoretical "stop distance" could serve as a comparative parameter for the capacity of the fertilizer to achieve a given spreading width. Nevertheless, this approach has not been explored in subsequent studies. Later, **Antille et al. (2013)** suggested that the particle size range of new fertilizers could be intentionally designed to match a target working width, using ballistic flight computations to assess the suitability of particle diameters. However, their model only predicted individual particle throw distances without simulating the overall spread pattern or addressing the working width. Similarly, **Grafton et al. (2015)** used a ballistic model to investigate the influence of fertilizer characteristics on working width. They compared experimentally deduced working widths with computed throw distances for mean particle sizes, but established no mathematical relationship.

Ultimately, existing literature lacks a general relationship between maximum achievable working width and other spreading characteristics such as the mean radius of the spread pattern. Furthermore, no mathematical model exists to connect fertilizer physical properties directly to maximum working width. Consequently, existing models fail to evaluate and compare fertilizers based on their ability to achieve a uniform distribution at a target working width. Additionally, no model makes it possible to evaluate the respective contribution of the different physical properties. This leaves fertilizer producers without clear guidance on which product properties to modify to improve fertilizer spreading ability.

To address these gaps, this study aims to demonstrate that maximum achievable working width is linearly related to the mean radius of the spread pattern, and to express these two spreading characteristics as functions of the fertilizer physical properties. Because working width is highly complex (influenced by ballistic behavior, spreader adjustments, and pass overlap) experimental study is unrealistic, and classical mechanical approaches are insufficient. The originality of this research lies in using numerical simulations to compute spread patterns, transverse coefficients of variation (CV) after overlapping, and the corresponding optimal working widths for a large database of virtual fertilizers. This database is then used in a regression analysis to establish the missing mathematical relationships between maximum working width and fertilizer physical characteristics. Overall trends are also confirmed by a large number of experimental observations.

2/ MATERIALS AND METHODS

The fertilizer spreading ability was studied using numerical simulations by computing two spreading performance indicators: the maximum working width WWCV10 ensuring a satisfying uniformity (CV≤10%) and the mean radius Rm of the spread pattern. To isolate the impact of the physical properties of fertilizers on these two indicators, independently of spreader characteristics, the study assumed the same initial conditions of ballistic flight for all fertilizers.

2.1 Initial conditions of ballistic flight

The initial conditions for the ballistic flight of the particles (when they leave the disk) were computed using the kinematic relationships established by **Villette et al. (2008, 2017)**. Specifically, the horizontal and vertical components of the outlet velocity are defined as follows:

$$v_H = \frac{r\omega}{\cos\theta_{out} + \sin\theta_{out}\tan\alpha} \quad (1)$$

$$v_V = v_H \times \tan\Omega_{out} \quad (2)$$

where r is the radius of the vane, ω is the revolution speed of the disk, θ_{out} is the horizontal outlet angle, Ω_{out} is the vertical outlet angle and α is the pitch angle of the vane.

To provide simulations with realistic initial conditions, the values of the virtual disk parameters were taken from the S8 disk, commonly used with AXIS 50.1 spreaders supplied by RAUCH Company (Germany), and considering a disk rotation speed of 900 rpm. The horizontal and vertical outlet angle values were derived from experimental measurements carried out using urea and two custom-made disks equipped with short or long vanes. The horizontal outlet angle was measured using a free rotating wind vane forced in direction by the particle flow movement. The vertical outlet angle distribution was measured using a collecting elbow pipe simultaneously recording the vertical location of the device and the weight of particles collected in a load cell container. The angular mass flow distributions (for short and long vanes) around the disk was derived from static spread patterns measured with the rotating test bench **(EN 13739-2, 2011)** developed by **Piron and Miclet (2005)** and called CEMIB. The mass flow proportions feeding the short and long vanes were derived from the disk geometry.

2.2 Ballistic flight Model

The ballistic flight model considered the gravity force and the drag force due to the motion of the particle through the air. The resulting particle motion is governed by the following equations:

$$\begin{cases} \frac{d^2x}{dt^2} = -\frac{1}{2m} C_D A_p \rho_{air} vx \sqrt{vx^2 + vy^2 + vz^2} \\ \frac{d^2y}{dt^2} = -\frac{1}{2m} C_D A_p \rho_{air} vy \sqrt{vx^2 + vy^2 + vz^2} \\ \frac{d^2z}{dt^2} = -g - \frac{1}{2m} C_D A_p \rho_{air} vz \sqrt{vx^2 + vy^2 + vz^2} \end{cases} \quad (3)$$

where *x, y, z* are the coordinates of the particle, m is the particle mass, CD is the drag coefficient, A_p is the projected surface area of the particle, ρ_{air} is the air density (set at 1.21 kg m-3), *vx, vy, vz* are the velocity components of the particle, g is the acceleration due to gravity.
The particle mass was related to the particle density □ and diameter d as follows:

$$m = \rho \frac{4}{3} \pi \left(\frac{d}{2} \right)^2 \tag{4}$$

2.3 Virtual fertilizers

A set of virtual fertilizers (combining different characteristics) was defined to study the influence of fertilizer physical properties.
The probability density function $f(d)$ of particle diameters was modelled by a combination of two Gaussian membership functions as follows:

$$f(d) = \begin{cases} \frac{1}{(s_1 + s_2)} \sqrt{\frac{2}{\pi}} \exp\left(-\frac{1}{2} \left(\frac{d - D_m}{s_1} \right)^2 \right) & \text{for } d \le D_m \\ \frac{1}{(s_1 + s_2)} \sqrt{\frac{2}{\pi}} \exp\left(-\frac{1}{2} \left(\frac{d - D_m}{s_2} \right)^2 \right) & \text{for } d > D_m \end{cases} \tag{5}$$

where D_m is the modal value of the distribution (diameter value at which the probability density function reaches its maximum value), s_1 and s_2 are the standard deviations of the left and right Gaussian membership functions respectively.
The shape of the probability density function $f(d)$ is illustrated in **Fig. 1**.

The range of values investigated for Dm, s_1 and s_2 was derived from particle size distributions analyzed for 82 commercially available fertilizers using a laboratory-developed videogranulometer **(Le et al., 2018)**. A total of 152 particle size distributions defined by triplets of values (Dm, s_1, s_2) were considered in this study. These were generated by selecting D_m from 1 to 5 mm (in steps of 0.5 mm) and choosing values for s_1 and s_2 within the triangular area presented in **Fig. 2**.
The study investigated C_D values ranging from 0.4 to 0.6 (in steps of 0.05) and values from 1200 to 2000 kg m^{-3} (in steps of 200 kg m^{-3}), resulting in 25 distinct (C_D, ρ) parameter pairs.
Combining the selected particle size distributions, C_D and ρ values provided 3800 virtual fertilizers with different physical characteristics, each defined by a 5-tuple of values (C_D, ρ, D_m, s_1, s_2).

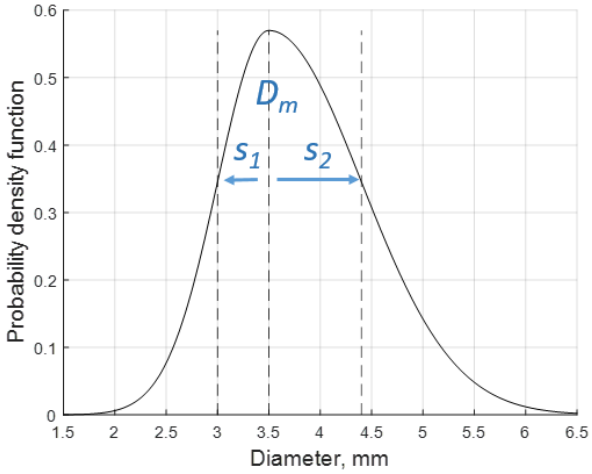


Fig. 1 - Particle diameter distribution: example when D_m=3.5, s_1=0.5 and s_2=0.9.

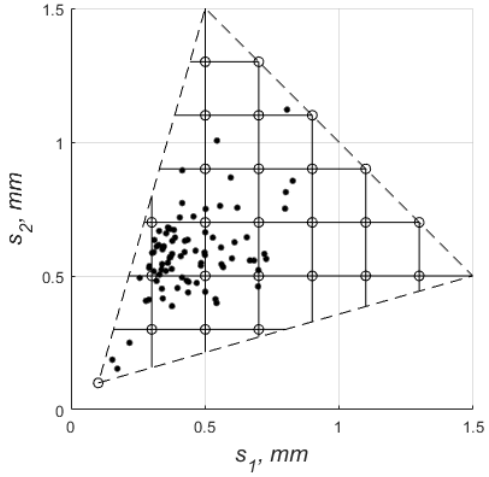


Fig. 2 - Particle size distribution parameters (s_1 and s_2) measured for 82 commercially available fertilizers (black points) and discretized pairs of values chosen to simulate a set of virtual fertilizers (circles).

2.4 Actual fertilizers

The physical characteristics (C_D, ρ, D_m, s_1, s_2) of 47 commercially available fertilizers were experimentally determined, allowing their corresponding spread patterns to be computed using the same method as that used for the virtual fertilizers.

2.5 Spread pattern simulation and maximum working width calculation

For each virtual fertilizer, a Monte Carlo process was used to compute the motion of approximately 175 000 particles, whose characteristics were randomly drawn from pre-established statistical distributions. For each virtual fertilizer defined by the 5-tuple (C_D, ρ, D_m, s_1, s_2), the spread pattern was first computed for the right spinning disk. The spread pattern resulting from the left disk was then deduced from the right spread pattern by symmetry with respect to the travel direction.

The setting of the virtual spreader consisted of rotating the right and left spread patterns by the same angle, α_{set} counterclockwise for the right disk and clockwise for the left disk. This simulates modifying the angular location of the feeding point on each disk. The twin-disk spread pattern was then deduced by combining the left and right spread patterns after translating the particle coordinates by half the disk spacing (1.4 m) in the respective left or right direction.

For each spreader setting α_{set} and working width W_W, the resulting distributions were shifted right and left by multiples of W_W to represent virtual adjacent passes and reproduce spread overlap. From this, the overall transverse distribution was deduced, and the transverse coefficient of variation (CV) was calculated (EN 13739-2, 2011). For each virtual fertilizer, the CV map (Fig. 3) was established as a 2D function of the setting angle and the working width. To assess the ability of the fertilizer to be spread across a wide working width with good uniformity, the maximum working width maintaining a CV≤10% (denoted as W_{WCV10}) was computed from the CV map for each virtual fertilizer.

For each virtual fertilizer, the mean spread radius R_m was also computed.

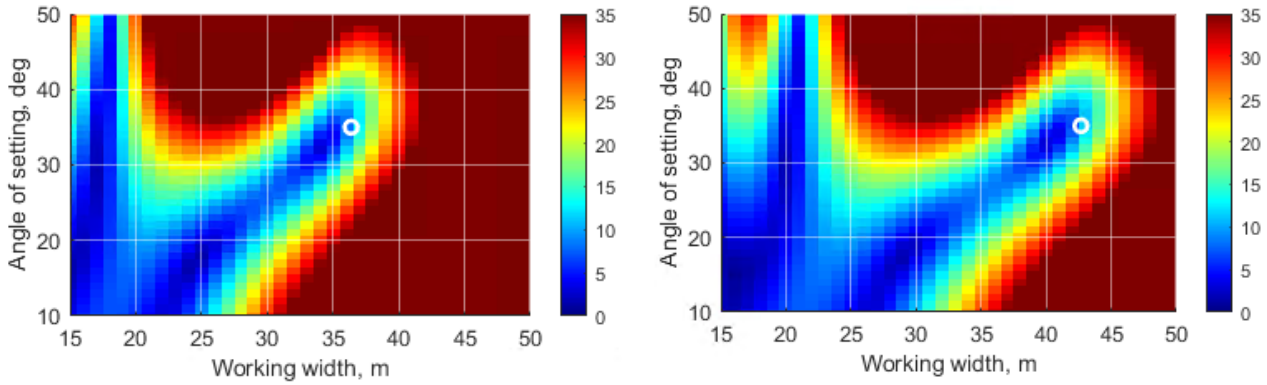


Fig. 3 - Example of CV map computed with C_D=0.5, ρ=1600 kg m^{-3}, s_1=0.5 mm, s_2=0.5 mm, D_m=2.5 mm (left) and D_m=3.5 mm (right). The color scale corresponds to the CV value (%). The maximum working width respecting a CV ≤10% is plotted (as a white circle).

2.6 Experimental spread patterns

A database of experimental spread patterns, measured using the CEMIB test bench (Piron and Miclet, 2005; EN 13739-2, 2011), was used to analyze the relationship between the mean radius and the maximum working width across a large number of actual spreading situations. The data

considered in this study included more than 2,000 experimental spread patterns, combining two commercial spreader brands, six spinning disks, 287 fertilizers, as well as a variety of flow rates and disk rotation speeds.

3/ RESULTS AND DISCUSSION

3.1 Regression model based on simulation results

Regression models were used to relate the mean spread radius R_m and the maximum working width W_{WCV10}, to the physical characteristics of the particles (C_D, ρ, D_m, s_1 and s_2), for all virtual fertilizers. The same model structure was applied to both R_m and W_{WCV10} as described in Eqs (6) to (9).

First, 25 values were obtained for each of the seven coefficients C_{Ri} and C_{Wi} using Eqs (6) and (7) based on the the 25 pairs of (C_D, ρ) selected for the virtual fertilizers. Second, each coefficient C_{Ri} and C_{Wi} was modeled as a function of C_D and ρ using Eqs (8) and (9).

$$R_m = \begin{pmatrix} C_{R1}(\rho,C_D) \\ C_{R2}(\rho,C_D) \\ C_{R3}(\rho,C_D) \\ C_{R4}(\rho,C_D) \\ C_{R5}(\rho,C_D) \\ C_{R6}(\rho,C_D) \\ C_{R7}(\rho,C_D) \end{pmatrix}^T \times \begin{pmatrix} D_m^{\,2} \\ D_m \\ D_m s_1 \\ D_m s_2 \\ s_1 \\ s_2 \\ 1 \end{pmatrix} \quad (6)$$

$$W_{WCV10} = \begin{pmatrix} C_{W1}(\rho,C_D) \\ C_{W2}(\rho,C_D) \\ C_{W3}(\rho,C_D) \\ C_{W4}(\rho,C_D) \\ C_{W5}(\rho,C_D) \\ C_{W6}(\rho,C_D) \\ C_{W7}(\rho,C_D) \end{pmatrix}^T \times \begin{pmatrix} D_m^{\,2} \\ D_m \\ D_m s_1 \\ D_m s_2 \\ s_1 \\ s_2 \\ 1 \end{pmatrix} \quad (7)$$

$$C_{Ri}(\rho,C_D) = c_{Ri1}\rho + c_{Ri2}C_D + c_{Ri3} \quad (8)$$

$$C_{Wi}(\rho,C_D) = c_{Wi1}\rho + c_{Wi2}C_D + c_{Wi3} \quad (9)$$

The values for coefficients C_{Ri1}, C_{Ri2}, C_{Ri3}, C_{Wi1}, C_{Wi2}, C_{Wi3} and the corresponding determination coefficients (R^2) are provided in Tables 2 and 3.

Table 2.

i	C_{Ri1}	C_{Ri2}	C_{Ri3}	R^2
1	-1,02E-04	3,20E-01	-1,84E-01	0,991
2	1,46E-03	-4,47E+00	4,31E+00	0,995
3	3,17E-05	-1,21E-01	5,76E-03	0,898
4	-2,93E-04	8,69E-01	-8,33E-01	0,994
5	-4,27E-04	1,40E+00	-9,80E-01	0,988
6	1,63E-03	-4,91E+00	5,93E+00	0,992
7	2,28E-03	-7,15E+00	4,11E+00	0,988

Table 3.

i	C_{Wi1}	C_{Wi2}	C_{Wi3}	R^2
1	-1,78E-04	5,72E-01	-3,37E-01	0,985
2	3,17E-03	-9,95E+00	9,50E+00	0,995
3	-1,43E-04	4,78E-01	-4,65E-01	0,984
4	-6,62E-04	2,04E+00	-1,90E+00	0,989
5	0	0	0	
6	3,91E-03	-1,19E+01	1,42E+01	0,992
7	5,21E-03	-1,59E+01	9,99E+00	0,988

Fig. 4 illustrates the satisfactory quality of the models, which synthesize the results of 3800 simulation results to relate R_m and W_W to the physical characteristics of the particles for a given spreading situation. The results from the experimental data obtained for 47 actual fertilizers show greater dispersion. These discrepancies are notably due to ballistic initial conditions that differ from the values kept intentionally constant in the simulations.

For the given initial flight conditions, the predicted values calculated using the coefficient matrices (provided in Tables 2 and 3) allow for a comparison of fertilizer spreading ability and an evaluation of the contributions of the different physical properties. However, they are not intended to predict the absolute working width achievable with different spreaders.

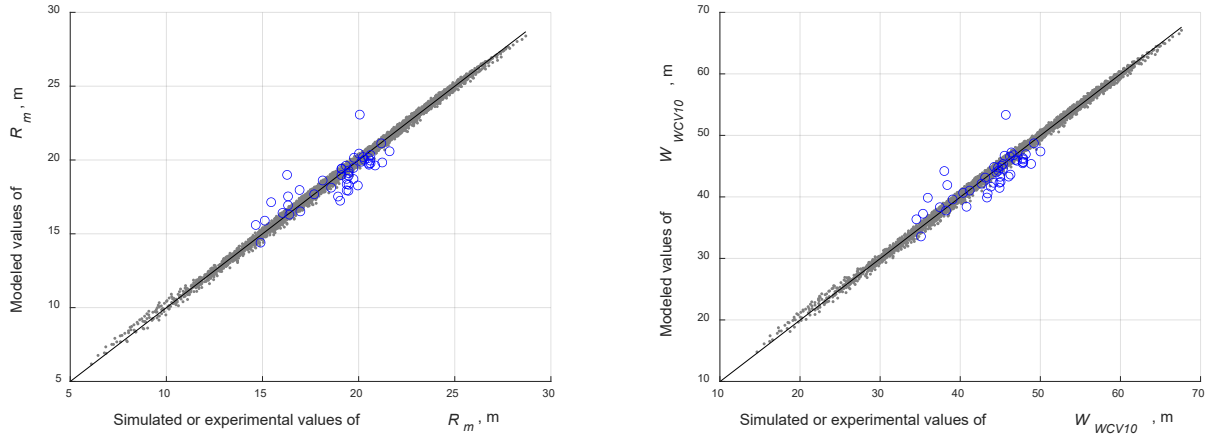


Fig. 4 - Modeled values of Rm (left) and WWCV10 (right) with respect to values computed through numerical simulations (grey points) or experimental values (blue circles). The continuous line is the identity line.

3.2 Sensitivity of R_m and W_{WCV10} to the different physical properties of the particles

The sensitivity analysis was performed by calculating the partial derivatives of R_m and W_{WCV10} with respect to the independent variables as follows:

$$dR_m = \frac{\partial R_m}{\partial D_m} dD_m + \frac{\partial R_m}{\partial s_1} ds_1 + \frac{\partial R_m}{\partial s_2} ds_2 + \frac{\partial R_m}{\partial \rho} d\rho + \frac{\partial R_m}{\partial C_D} dC_D \quad (10)$$

$$dW_{WCV10} = \frac{\partial W_{WCV10}}{\partial D_m} dD_m + \frac{\partial W_{WCV10}}{\partial s_1} ds_1 + \frac{\partial W_{WCV10}}{\partial s_2} ds_2 + \frac{\partial W_{WCV10}}{\partial \rho} d\rho + \frac{\partial W_{WCV10}}{\partial C_D} dC_D \quad (11)$$

The analytical descriptions of the partial derivatives of R_m are provided in Eqs. (12) to (16), as follows:

$$\frac{\partial R_m}{\partial D_m} = 2C_{R1(\rho,C_D)} D_m + C_{R2(\rho,C_D)} + C_{R3(\rho,C_D)} s_1 + C_{R4(\rho,C_D)} s_2 \quad (12)$$

$$\frac{\partial R_m}{\partial s_1} = C_{R3(\rho,C_D)} D_m + C_{R5(\rho,C_D)} \quad (13)$$

$$\frac{\partial R_m}{\partial s_2} = C_{R4(\rho,C_D)} D_m + C_{R6(\rho,C_D)} \quad (14)$$

$$\frac{\partial R_m}{\partial \rho} = C_{R11} D_m^{\,2} + C_{R21} D_m + C_{R31} D_m s_1 + C_{R41} D_m s_2 + C_{R51} s_1 + C_{R61} s_2 + C_{R71} \quad (15)$$

$$\frac{\partial R_m}{\partial C_D} = C_{R12} D_m^{\,2} + C_{R22} D_m + C_{R32} D_m s_1 + C_{R42} D_m s_2 + C_{R52} s_1 + C_{R62} s_2 + C_{R72} \quad (16)$$

Similarly, partial derivatives of W_{WCV10} are obtained by substituting R_m with W_{WCV10} and C_{Ri} with C_{Wi} in Eqs. (12) to (16).

To illustrate the use of these equations, Fig. 5 shows how a 10% increase in each parameter (C_D, ρ, D_m, s_1 and s_2) affects the mean spread radius R_m and the maximum working width W_{WCV10}. Thus, a 10% increase in the drag coefficient C_D reduces the working width W_{WCV10} by approximately 2 m. This reduction can be counterbalanced by a 10% increase in either density ρ or particle modal diameter D_m, which increases W_{WCV10} by approximately 2 m. Regarding the particle size distribution parameters, the figure shows that D_m is the most influential parameter for increasing R_m and W_{WCV10}. The positive effect of s_2 is less pronounced, while the negative effect of s_1 is negligible.

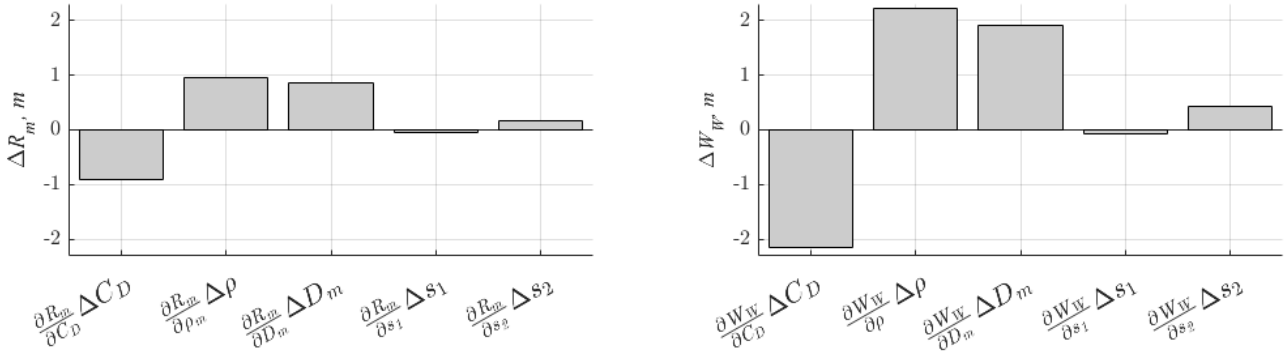


Fig. 5 - Variations of Rm (left) and WWCV10 (right) related to 10% of increase for each parameter when the initial values are Dm=3 mm, s1=0.5 mm, s2=0.5 mm, ρ=1600 kg/m3, and CD=0.5.

More details concerning the sensitivity of R_m and W_{WCV10} to C_D, ρ, D_m, s_1 and s_2 can be found in Le et al. (2025).

3.3 Relationship between R_m and W_{WCV10}

Using simulation results, Fig. 6 demonstrates W_{WCV10} is directly correlated to R_m.

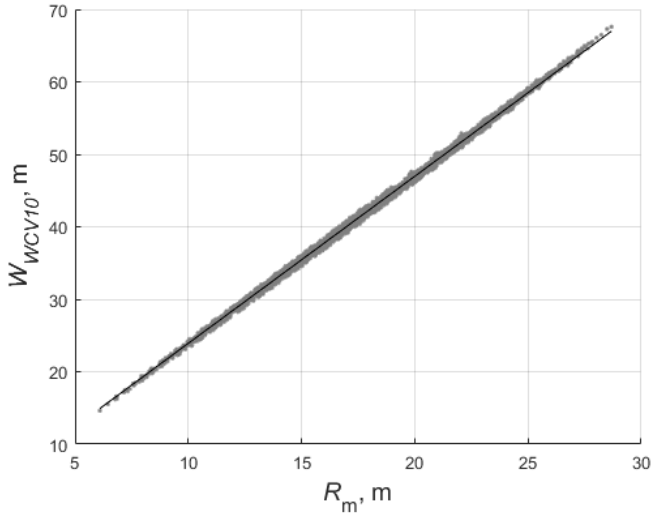


Fig. 6 - Simulated values of W_{WCV10} with respect to R_m

The linear regression is as follows:

$$W_{WCV10} = 2.305R_m + 0.87 \quad (R^2>0.998) \tag{17}$$

These findings demonstrate the necessity of a large mean spread radius to achieve a wide working width while maintaining uniform spreading.

3.4 Consistency with experimental data

Based on experimental measurements obtained with the Cemib test bench, Fig. 7 plots the maximum working widths $W_{WCV10\%}$ with respect to *Rm*. This dataset represents 2000 spreading situations involving 2 anonymized commercial spreaders (A and B), each equipped with 3 commercial disks (numbered 1 to 3). Extracted from various studies and different industrial partnerships, these situations encompass 287 different fertilizers, as well as a variety of flow rates and disk rotation speeds.

Despite the wide variety of experimental conditions, Fig. 7 demonstrates a clear general trend in the relationship between $W_{WCV10\%}$ and *Rm*. Excluding 165 outliers, the overall linear regression fitted to 1835 data points (combining all spreaders and disks) is as follows:

$$W_{WCV10} = 2.097 R_m + 4.29 \quad (R^2 = 0.96) \tag{18}$$

The linear regressions, established independently for each spreader and disk, are provided in Fig 7.

Outliers may result from specific spread pattern shapes, threshold effects (such as a sharp shift in working width between a CV of 10% and a slightly higher value) or experiments involving specific situations (such as machines under development). Although some causes for the outliers have been identified, a detailed investigation remains to be conducted.

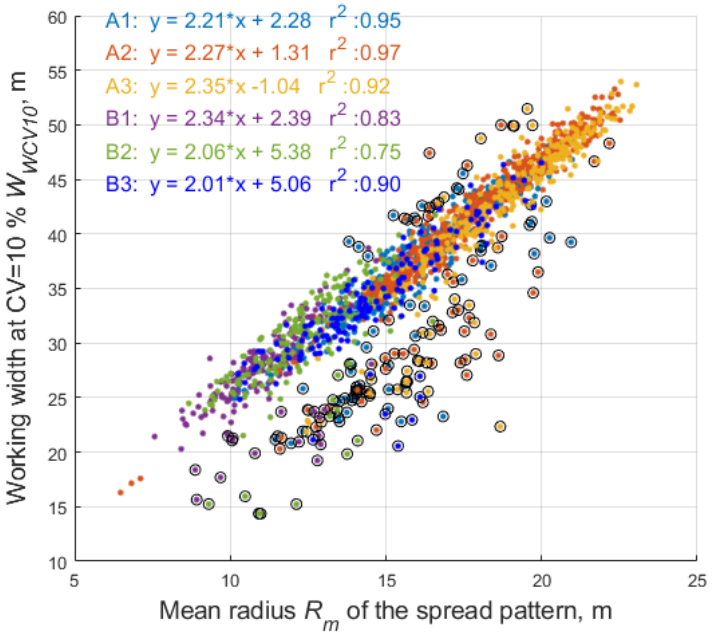


Fig. 7 - Experimental maximum working width with respect to the mean spread radius of the spread patterns obtained with 6 anonymized commercial disks: A1, A2, A3 mounted on spreader A, and B1, B2, B3 mounted on spreader B. Outliers excluded from the linear regressions are indicated by circles.

The performance of the overall model Eq. (18) in predicting W_{WCV10} from R_m is evaluated in Fig. 8, which shows the residual differences between experimental and predicted values. Fig. 9 shows the histograms of these residuals, analysed separately for each spreader and disk. This illustrates the capability of the general relationship to describe how W_{WCV10} is related to R_m across a variety of machines configurations, despite some data dispersion.

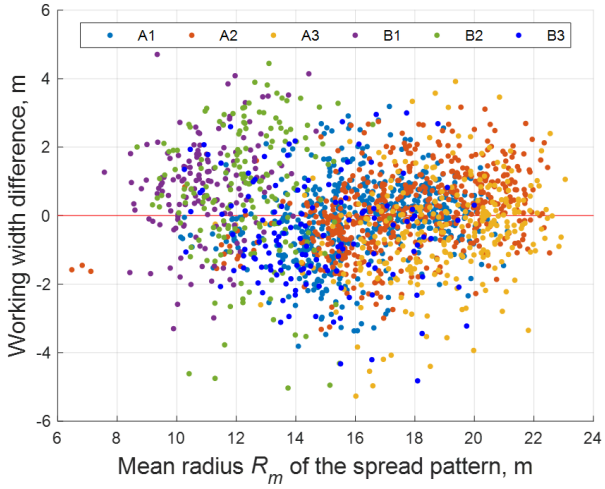


Fig. 8 – Differences between experimental and predicted W_{WCV10} values from the overall model (outliers removed).

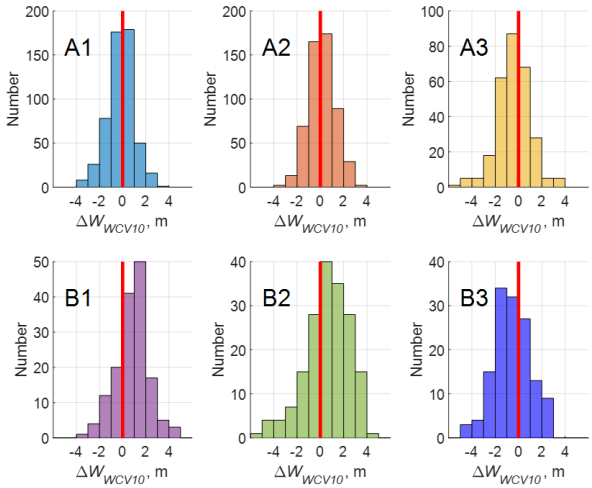


Fig. 9 – Histograms of the differences between experimental and predicted W_{WCV10} values from the overall model (outliers removed).

For a given disk (A2) and rotation speed, Fig. 10 illustrates the dependence of the experimental mean radius R_m and working width W_{WCV10} on particle diameter and density. Similar trends were observed for all disks and rotation speeds. This figure demonstrates the consistency between experimental results and simulation outcomes. It also highlights the difficulty of experimentally studying the individual impact of particle physical parameters, given their interactions within the overall ballistic behavior and their differing initial flight conditions. It thus highlights the value of simulation-based studies in defining how each physical parameter contributes to increasing the mean spread radius and working width.

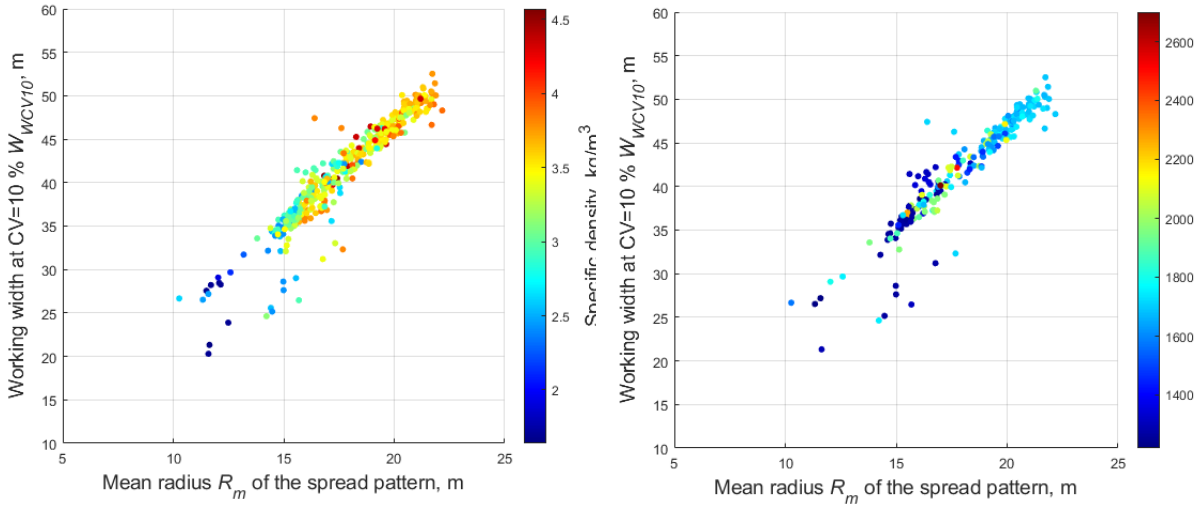


Fig. 10 – Illustration of the impact of mean particle diameter (left) and specific density (right) on the mean spread radius and maximum working width for disk A2 at a specific rotation speed.

4/ CONCLUSIONS

The study demonstrates that computer simulations are a powerful tool for assessing the ability of granular products to be spread over large working widths. By analyzing 3,800 virtual fertilizers, this approach generated a vast dataset that successfully isolated fertilizer physical properties from spreader performances. For the first time, models were developed to link maximum working width and mean spread radius to five physical properties: drag coefficient, specific density, and three size distribution parameters. An analytical model using partial derivatives quantified the contribution of each variable, identifying the drag coefficient C_D, specific density ρ, and modal diameter D_m as the key drivers. As representative case study showed, the reduction in maximum working width caused by a 10% increase in the drag coefficient can be counterbalanced by a 10% increase in either density ρ or particle modal diameter D_m. By contrast, a 10% increase of the right standard deviation s_2 of the particle size distribution shows a slight positive effect on working width, while the same relative variation of the left standard deviation s_1 has a negligible negative effect.

The simulations also confirmed a strong correlation between the maximum working width and the mean spread radius. This correlation was also found within the experimental data provided by a selected set of 2000 spread patterns extracted from the CEMIB database.
By quantifying the spreading ability of granular products, the established models aim to accelerate the development of new products and spreading systems. They provide manufacturers and designers with efficient tools to guide their decisions in a context of evolving practices and user expectations. Consequently, a numerical simulator is regularly used by the research unit to answer inquiries on this issue.

More generally, this study illustrates the research approach developed at the AgroTechnoPôle. Regardless of the technological topic addressed, it relies on a methodological framework combining:

- Acquiring metrics using high-performance measurement benches;
- Modeling, notably by hybridizing mechanistic and experimental approaches;
- Using results via numerical simulators (or even digital twins) to explore the relationships between the characteristic variables of complex processes.

References

- Antille, D.L., Gallar-Redondo, L., Godwin, R.J., 2013. Determining the particle size range of organomineral fertilisers based on the spreading characteristics of the material, ASABE Annual International Meeting, Kansas City, Missouri, July 21-July 24, 2013. American Society of Agricultural and Biological Engineers, p. 18.
- EN 13739-2, 2011. Agricultural machinery - Solid fertilizer broadcasters and full width distributors - Environmental protection - Part 2: Test methods, European Committee for Standardization, Bruxelles.
- Grafton, M., Yule, I., Robertson, B., Chok, S., Manning, M., 2015. Ballistic Modeling and Pattern Testing to Prevent Separation of New Zealand Fertilizer Products. Applied Engineering in Agriculture 31.
- Gimenez, L., Giosa, L., 2026. Interactive effects of fertilizer particle-size distribution and spreader settings on application uniformity and particle segregation. Engenharia Agrícola 46.
- Hoffmeister, G., Watkins, S., Silverberg, J., 1964. Fertilizer Consistency, Bulk Blending of Fertilizer Material: Effect of Size, Shape, and Density on Segregation. Journal of Agricultural and Food Chemistry 12, 64-69.
- Le, T.-T., Miclet, D., Heritier, P., Piron, E., Chateauneuf, A., Berducat, M., 2018. Morphology characterization of irregular particles using image analysis. Application to solid inorganic fertilizers.
- Le, T.-T., Piron, E., Miclet, D., Villette, S., 2025. Simulation-based study of the influence of particle physical properties on fertilizer spreading ability. Computers and Electronics in Agriculture 229, 109753.
- Miserque, O., Pirard, E., Schenkel, Y., Mostade, O., Huyghebaert, B., 2008. Spreading segregation of blended fertilizers: influence of the particles properties. Applied engineering in agriculture.
- Parkin, C., Basford, B., Miller, P., 2005. Spreading accuracy of solid urea fertilisers. DEFRA report NT2610. Dept. Environment, Food, Rural Affairs., London, UK.
- Piron, E., Miclet, D., 2005. Centrifugal fertiliser spreaders: a new method for their evaluation and testing, Conference of the International Fertiliser Society, York, United Kingdom. The International Fertiliser Society, p. 22p.
- Pitt, R., Farmer, G., Walker, L., 1982. Approximating equations for rotary distributor spread patterns. Transactions of the ASAE 25, 1544-1552.
- Thaper, R.K., Fulton, J.P., McDonald, T.P., Fasina, O.O., 2021. Potential of fertilizer segregation during application using spinner disc spreader. Precision Agriculture.
- Villette, S., Piron, E., Cointault, F., Chopinet, B., 2008. Centrifugal spreading of fertiliser: Deducing three-dimensional velocities from horizontal outlet angles using computer vision. Biosystems Engineering 99, 496-507.
- Villette, S., Piron, E., Miclet, D., 2017. Hybrid centrifugal spreading model to study the fertiliser spatial distribution and its assessment using the transverse coefficient of variation. Computers and Electronics in Agriculture 137, 115-129.
- Virk, S.S., Mullenix, D.K., Sharda, A., Hall, J.B., Wood, C.W., Fasina, O.O., McDonald, T.P., Pate, G.L., Fulton, J.P., 2013. Case Study: Distribution uniformity of a blended fertilizer

applied using a variable-rate spinner disc spreader. Applied Engineering in Agriculture 29, 627-636.

- Yule, I., 2011. The effect of fertilizer particle size on spread distribution. NZ Centre for Precision Agriculture, Massey University, Palmerston North, New Zealand, 1-9.

Morphogeometric characterization of fertilizer particles under field conditions: Comparison of an approach based on controlled sampling and expert algorithm with a machine learning approach under bulk conditions

Emeric Leclair[a,*]

[a] Sky Agriculture, Burel Group, 35220 Châteaubourg, France

* Corresponding author. Email: eleclair@burel-group.com

Abstract

In centrifugal fertilizer spreading, predicting ballistic dispersion and ground application uniformity strictly requires high-fidelity particle size and morphology distributions, rather than aggregated scalar averages. Within precision agriculture, rapid in-field characterization of these comprehensive distributions remains a key operational challenge. This study evaluates the distributional fidelity, precision, and trueness of two in-field image-based methods—an expert rule-based algorithm on controlled monolayers and a deep learning instance segmentation pipeline on bulk heaps—benchmarked against a laboratory dynamic particle analyzer across 235 mineral fertilizers.

The monolayer approach using an expert rule-based algorithm achieved superior distributional fidelity, yielding a 2-Wasserstein distance (W_2) of 0.28 mm for diameter and 0.024 for angularity, alongside a precision of 1.6% and 0.7%, and a trueness (MAPE) of 8.0% and 2.1%, for diameter and angularity respectively. Conversely, the multi-head U-Net pipeline operating on bulk heaps yielded a 2-Wasserstein distance of 0.53 mm and 0.031, a precision of 0.5% and 0.4%, and a trueness of 17.1% and 1.7%, for diameter and angularity respectively.

These findings demonstrate that monolayer individualization remains essential to capture accurate population distributions required for predictive ballistic simulations, whereas bulk deep learning provides superior repeatability under field constraints.

KEYWORDS: Computer vision, Machine learning, Particle segmentation, 2D particle morphology, Mineral fertilizer, Granulometry, Precision agriculture, Centrifugal spreading.

Complexity level: 4

1/ INTRODUCTION

In modern agriculture, centrifugal spreaders are widely employed for the broadcast distribution of granular mineral fertilizers. Application uniformity depends critically on controlling particle dynamics through the metering and spinning disc systems, which govern individual ballistic

trajectories and transverse distribution patterns on the ground. Recent physical and ballistic modeling frameworks increasingly rely on stochastic Monte Carlo simulations, where accurate prediction of ground deposition patterns requires high-fidelity probability distributions of particle size and morphology (such as angularity) rather than simple averages (Le, Piron, Miclet, & Villette, 2025). In practice, machine adjustments—such as application rate, disc rotational speed, disc tilt, feeding drop point, and boundary spreading deflectors—depend directly on these distributional parameters. Within the precision agriculture paradigm, rapid and reliable in-field determination of these comprehensive distributions represents a vital operational challenge.

While conventional methods depend on manufacturer databases references (Burel Group, 2007) (Bogballe A/S, 2013) (Kverneland Group France S.A.S., 2018) (Amazonen-Werke, 2019) (Le, et al., 2018) or collection trays (Amazonen Werke, 2015) (Amazonen Werke, 2025) (Rauch Landmaschinenfabrik Gmbh, 2025), computer vision now enables mobile characterization. However, extracting physical attributes hinges on faithfully segmenting individual particle boundaries. Two contrasting paradigms exist:

Mechanically controlled individualization: Granules are spread into a monolayer using physical sampling devices and segmented via deterministic, rule-based algorithms (France Patent No. EP4749263, 2021) (Germany Patent No. EP3275302, 2016).

In-bulk visual separation: Piled, overlapping granules are captured without physical dispersion and delineated using deep-learning instance segmentation models (Netherlands Patent No. EP3889907, 2020) (Zeng, et al., 2022) (Inarix, 2024) (Amazonen Werke, 2025).



Figure 30: FertiEye optical characterization device (Sky Agriculture) (Burel Group, 2025)

The metrological accuracy and repeatability of these field-deployable solutions relative to laboratory-grade instruments remain poorly documented. Accordingly, this study evaluates and compares the trueness, precision, and operational robustness of both in-field vision approaches for granulometric and morphological characterization, benchmarked against ground-truth measurements from a laboratory dynamic particle analyzer (Retsch Technology GmbH, 2014).

2/ MATERIALS AND METHODS

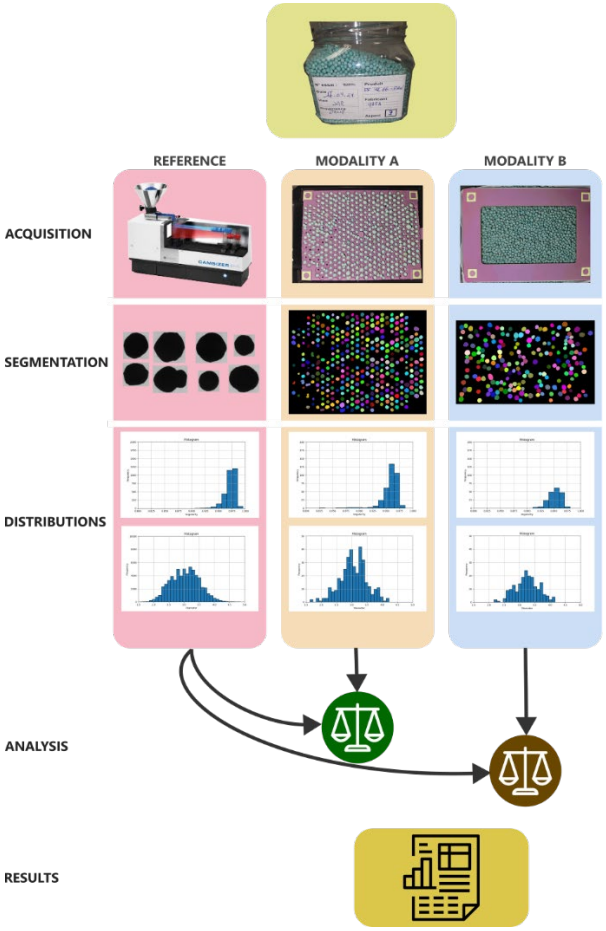


Figure 31: Schematic overview of the experimental acquisition and metrological validation framework

2.1 Granular Material Repository and Benchmark Dataset

The experimental investigation was conducted on an initial repository of 235 mineral fertilizer products stored in 1 L sealed containers at the Burel Group research laboratory (Châteaubourg, France). From this repository, a balanced benchmark subset of $N = 60$ distinct fertilizer products was constructed for comparative evaluation. Stratified random sampling was implemented across the repository's cumulative distributions of size and shape: 7 products were randomly drawn from the 1st quartile, 8 from the 2nd quartile, 8 from the 3rd quartile, and 7 from the 4th quartile of median particle diameter, with an equivalent stratification applied to particle angularity. The remaining products ($n = 175$) were allocated to train and cross-validate the deep-learning instance segmentation architecture.

2.2 Reference Laboratory Measurements

Laboratory ground-truth measurements were established using a dynamic digital image processing particle analyzer Camsizer P4 (Retsch Technology GmbH, 2014). Each 1 L fertilizer sample was passed through the instrument, recording dynamic projections for 3,000 to 10,000 particles per product. For each individual particle, the system directly extracted the minimum Feret diameter (x_d), defined as the minimum caliper distance over all projection angles (Toussaint, 1983). Because the Camsizer P4 does not natively output particle angularity, the raw particle projection silhouettes captured during the analysis were exported. Angularity (x_{ang}) was

subsequently determined via an equivalent-ellipse perimeter matching algorithm standardized by INRAE spreading mechanics specialists (Le, et al., 2018).

2.3 Monolayer Sampling Device (FertiEye)

The first in-field approach deployed the patented FertiEye mechanical sampler and calibration tray (Burel Group, 2025) (France Patent No. EP4749263, 2021). The device mechanically isolates a representative sub-sample into a non-overlapping planar monolayer on a flat background. The sampler was fabricated via 3d printing using Polyamide 12 (PA12). The sample tray incorporates four peripheral fiducial markers positioned at its corners.

2.4 Bulk Sampling Device

The second approach addresses granules deposited in bulk. A custom sampler was fabricated via 3d printing in Polylactic Acid (PLA). The device consists of a receptacle capable of accommodating a granular bed, upon which a registration frame is seated. The internal dimensions and the spatial arrangement of the four corner fiducial markers match the FertiEye calibration tray, ensuring identical perspective registration and spatial scaling across both modalities.

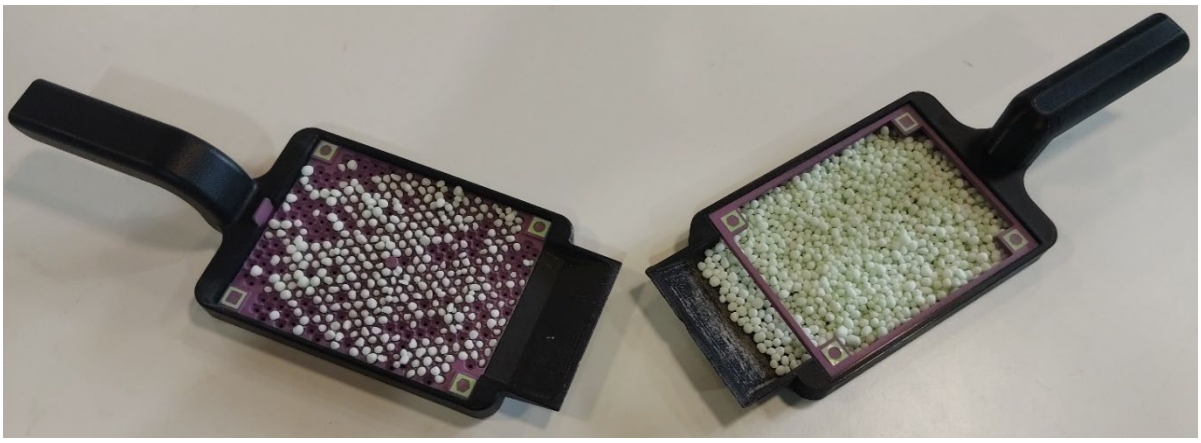


Figure 32: The monolayer FertiEye sampler (left) and the custom bulk sampler (right)

2.5 Test Bench and Controlled Acquisition Protocol

To decouple ambient environmental fluctuations from optical performance, a dedicated rigid darkroom enclosure was engineered. Within this bench, an environmental illumination variable was introduced—contrasting complete darkness with intense grazing light—to simulate challenging on-field lighting regimes, such as unassisted night acquisitions, direct grazing angles typical of sunrise or sunset, and directional single-source illumination frequently encountered in agricultural sheds. The enclosure accommodated two parallel mounting fixtures aligned symmetrically:A mid-range Android smartphone (Samsung Galaxy A34).

1. A high-end iOS smartphone (Apple iPhone 15).

Both fixtures maintained fixed optical distances and perpendicular angles such that the four corner markers occupied positions within 10% of the image diagonal relative to each corner.
A directional 48 W LED spotlight (Pixetool, AC 165–265 V, color temperature: 6,000 K, luminous flux: 4,800 lm) was placed at coordinates $(X = 60\ \text{mm}, Y = 60\ \text{mm}, Z = 20\ \text{mm})$ with Euler tilt angles $\left(R_x = 0°, R_y = -40°, R_z = 0°\right)$ relative to the sampler geometric center, providing controlled grazing illumination.

To prevent human-induced mechanical vibration during triggering inside the closed enclosure, shutter triggers were executed via wireless/remote control:

- Samsung A34: USB tethering in developer mode controlled via SCRCPY v4.0 (Genymobile, 2025) on Windows 11.
- iPhone 15: Wi-Fi remote triggering via the Teleshot application v13.2 (Yu Lihsuan, 2026) running on a paired remote host.

For each of the 60 benchmark products, three consecutive image replicates were acquired across eight experimental combinations:

Modality Tag	Smartphone	Sampler	Grazing Illumination
S_F_N	Samsung Galaxy A34	FertiEye	Off
S_F_L			On
S_V_N		Bulk tray	Off
S_V_L			On
I_F_N	Apple iPhone 15	FertiEye	Off
I_F_L			On
I_V_N		Bulk tray	Off
I_V_L			On

Table 3: Experimental combinations

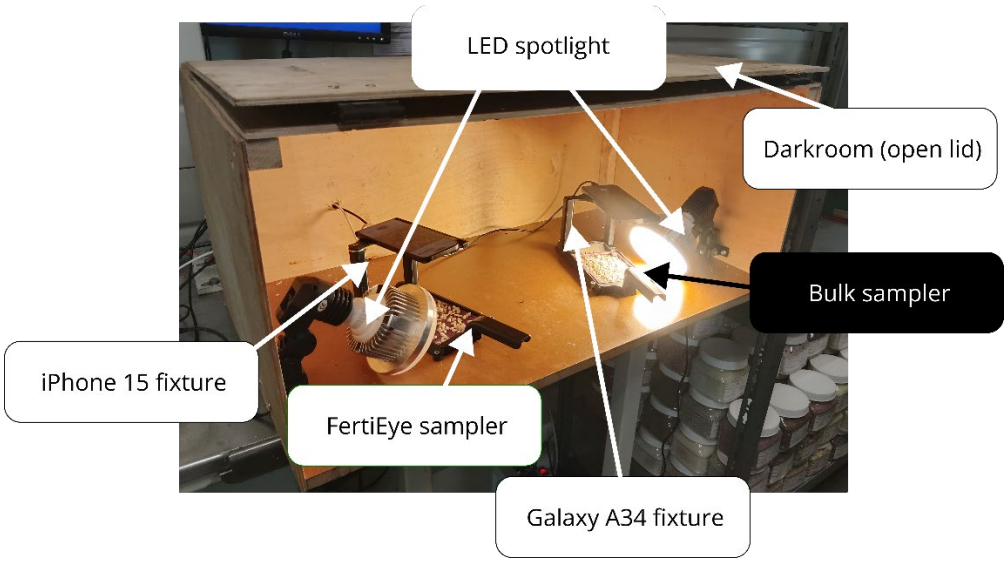


Figure 33 : Experimental acquisition bench inside the darkroom enclosure (shown with open top lid): parallel smartphone mounting fixtures, directional grazing LED spotlights, and comparative sampling trays (monolayer FertiEye on the left, bulk bed on the right)

2.6 Monolayer Rule-Based Expert Algorithm (FertiEye)

The FertiEye processing pipeline was implemented in C++17 utilizing the OpenCV library (OpenCV, 2000) within Visual Studio 2022 on Windows 11. The deterministic sequence consists of:

1. Fiducial Corner Localization: Detecting peripheral registration markers to compute a planar homography matrix.
2. Perspective Rectification & Rescaling: Warping the image to a standardized metric coordinate space ($mm \cdot px^{-1}$).
3. Color Balance Normalization: Applying a RGB calibration against the interior ground-truth chromatic signature of the markers.

4. Adaptive Binarization: Segmenting high-contrast foreground regions from the tray background.
5. Candidate Extraction & Watershed Disambiguation: Discarding multi-particle clusters and delineating contiguous boundaries.
6. Feature Extraction: Measuring the minimum Feret diameter (Toussaint, 1983) and angularity (Le, et al., 2018) for all isolated boundaries, exporting coordinates and particle attributes into structured JSON files.

2.7 Instance Segmentation: Ground-Truth Annotation Workflow

A semi-automated ground-truth pipeline was established to generate pixel-accurate polygon annotations of unoccluded foreground particles on bulk piles (Python 3.12):

1. Zero-Shot Pre-Segmentation: perspective rectified images (same step 1 and 2 than FertiEye algorithm) were processed using the Segment Anything Model (SAM, ViT-H architecture; (Kirillov, Mintun, Ravi, Mao, & Rolland, 2023)) in automatic mask generation mode, generating class-agnostic instance masks.
2. Geometric Curation Filters:
   - Area filtering: Candidate masks were area-filtered (1.5 to 8.0 mm).
   - Separation check: Euclidean distance maps were thresholded (50% peak prominence) to isolate single unmerged particles.
   - Border exclusion: Any contour touching a margin ($d_{min}/2$) was pruned to remove field-of-view truncations.
   - Occlusion filtering via Solidity: Overlapping particles were pruned using solidity S (Gallagher, Nikam , Kerr , & McFadden , 2025); an operator interactively set a quantile threshold q (default $q = 0.30$) to filter concavities satisfying $S < Q_q(S)$.
3. Human-in-the-Loop Validation: An interactive graphical interface enabled human annotators to verify, correct, or toggle the validity status of detected instances. The curated contours were serialized into separate valid and invalid into structured JSON files.

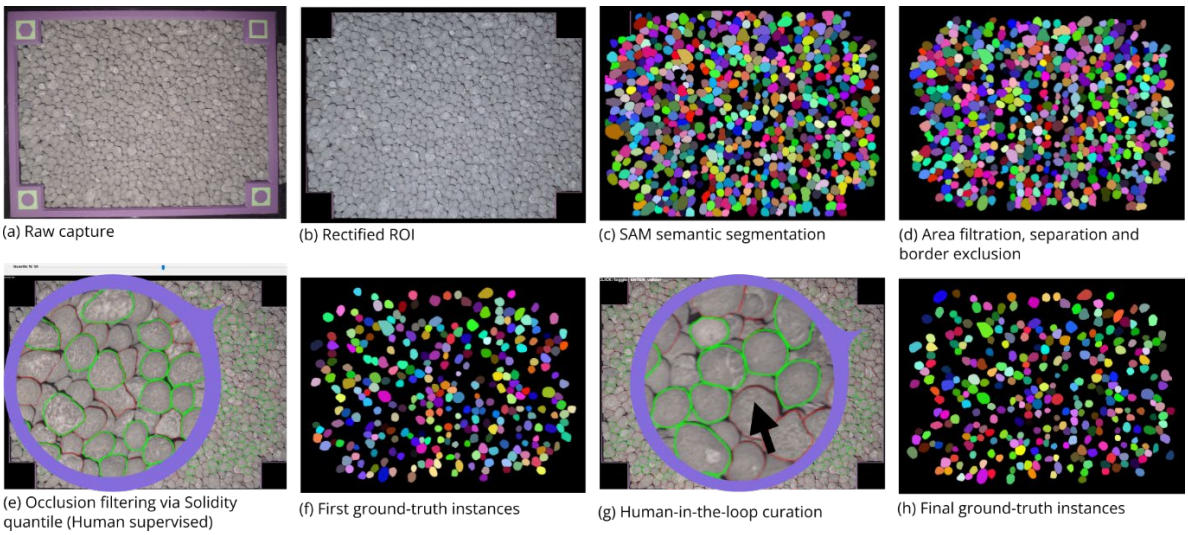


Figure 34 : Semi-automated ground-truth annotation workflow: (a) raw smartphone capture with fiducial frame; (b) perspective-rectified region of interest; (c) pre-segmentation using SAM; (d) geometric filtering; (e) solidity thresholding; (f) interactive human validation and correction; (g) curated ground-truth masks of unoccluded foreground particles.

2.8 Instance Segmentation : Multi-Head U-Net Architecture

Instance segmentation was formulated as a multi-task dense regression-classification problem. A multi-head U-Net architecture (Ronneberger, et al., 2015) was deployed using a ResNet-34 backbone (He, Zhang, Ren, & Sun, 2016) pre-trained on ImageNet:

- Encoder: ResNet-34 feature extractor.
- Decoder: Symmetric 5-stage convolutional decoder with skip connections.
- Prediction Heads: Three independent 1×1 convolutions with sigmoid activations operating on the final 16-channel feature map at native resolution:
  1. $\mathrm{P}_{fg} \in [0,1]^{H \times W}$: Foreground probability map of any granular matter.
  2. $\mathrm{M}_{dist} \in [0,1]^{H \times W}$: Instance-normalized Euclidean distance transform, peaking at 1.0 at particle geometric centroids to serve as watershed elevation topologies.
  3. $\mathrm{P}_{valid} \in [0,1]^{H \times W}$: Validity probability indicating an unoccluded foreground granule suitable for metrology.

The loss function was optimized end-to-end with unit weights:

$$\mathcal{L}_{total} = \mathcal{L}_{fg} + \mathcal{L}_{dist} + \mathcal{L}_{valid}$$
$$\mathcal{L}_{fg} = \mathcal{L}_{BCE}\left(\mathrm{P}_{fg}, \mathrm{Y}_{fg}\right) + \mathcal{L}_{Dice}\left(\mathrm{P}_{fg}, \mathrm{Y}_{fg}\right)$$
$$\mathcal{L}_{dist} = \mathrm{MSE}\left(\mathrm{M}_{dist} \odot \mathrm{Y}_{fg}, \mathrm{Y}_{dist} \odot \mathrm{Y}_{fg}\right)$$
$$\mathcal{L}_{valid} = \mathcal{L}_{BCE}(\mathrm{P}_{valid} \odot \mathrm{M}_{mask}, \mathrm{Y}_{valid} \odot \mathrm{M}_{mask})$$

where M_{mask} explicitly masks out valid particles that are artificially truncated by the patch boundary, ensuring edge-truncated granules do not penalize the validity head.

The model was implemented in Python 3.12 (PyTorch, Albumentations, OpenCV, NumPy) within PyCharm Community Edition 2024.2.2 on Windows 11. Training utilized 512×512 pixel patches sampled with foreground-bias, augmented via affine transforms, color jittering, Gaussian noise, and elastic deformations. Dataset splitting was performed at the image level (70% training, $n = 123$; 30% validation, $n = 52$) to preclude spatial data leakage. Optimization used AdamW (initial learning rate: 10^{-4}, halved upon validation plateaus).

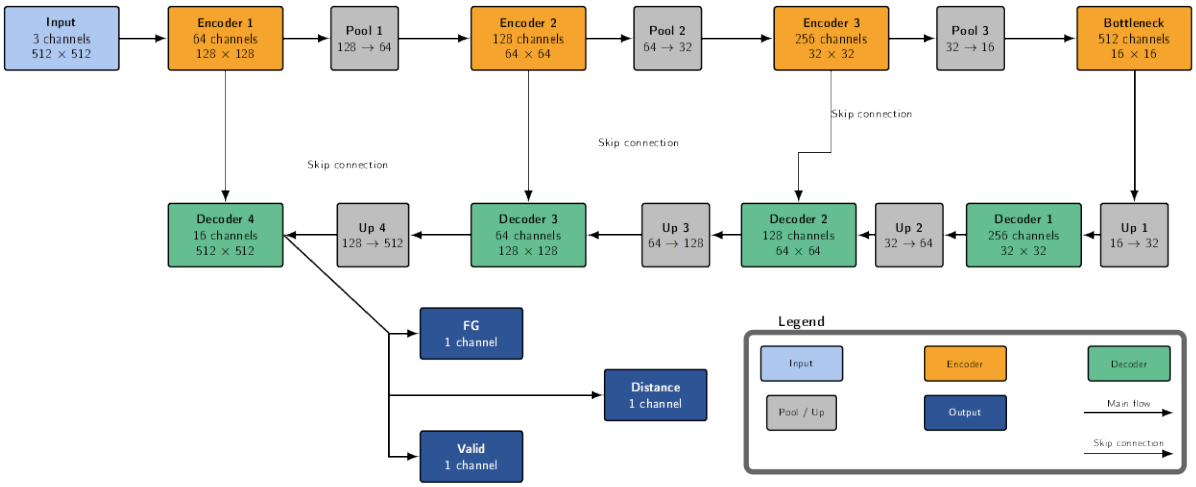


Figure 35: Multi-Head U-Net Architecture

2.9 Instance Segmentation : Tiled Inference and Particle Extraction

Full-resolution inference avoided boundary artifacts through overlapping sliding tiles (512×512 pixels, stride: 384 pixels, 128-pixel overlap) blended via a 2D separable Bartlett (triangular) window function:

$$\mathrm{W}(\mathrm{x},\mathrm{y}) = \left(1 - \frac{|2\mathrm{x} - \mathrm{K}|}{\mathrm{K}}\right)\left(1 - \frac{|2\mathrm{y} - \mathrm{K}|}{\mathrm{K}}\right), \quad \mathrm{K} = 512$$

Individual instances were segmented by marker-controlled watershed:

1. P_{fg} was binarized at a threshold of 0.5.
2. M_{dist} was smoothed via a Gaussian kernel ($\sigma = 1.5$), and regional maxima satisfying minimum peak prominence and minimum spatial separation distance were extracted as seeds.
3. The topological watershed was executed on $-\mathrm{M}_{dist}$ constrained by the foreground binary mask.
4. Each segmented instance was scored by averaging P_{valid} over its constituent pixels: regions with $\bar{P}_{valid} \geq 0.5$ were retained as unoccluded particles. Minimum Feret diameter and angularity were calculated on their vector boundaries and coordinates, particle attributes were exported into structured JSON files.

2.10 Metrological Performance Metrics and Statistical Analysis

Particle measurements were bounded to $x_d \in [1.5,8.0]$ mm and $x_{ang} \in [0.4,1.0]$ to filter segmentation debris. For each product ($N = 60$), the mean of three technical replicates was benchmarked against the Camsizer P4 reference. Metrological trueness was assessed using the Mean Absolute Percentage Error (MAPE) (de Myttenaere, Golden, Le Grand, & Rossi, 2016). Precision across replicates was characterized by the repeatability standard deviation (σ_r) using Shewhart's range method with factor $d_2 = 1.693$ (ISO 5725-2, 2025) (ISO 7870-2, 2023) and normalized as the repeatability coefficient of variation (CV_r). Finally, distributional fidelity between fitted 1D Gaussian representations of the modalities and reference was evaluated via the closed-form 2-Wasserstein distance W_2 (Givens & Shortt, 1984).

3/ RESULTS AND DISCUSSION

Figure 5 illustrates the comparative Gaussian probability density functions for a representative mineral fertilizer (Product 2213, NPK) across all eight imaging modalities against the Camsizer P4 reference distribution (dashed black curve).

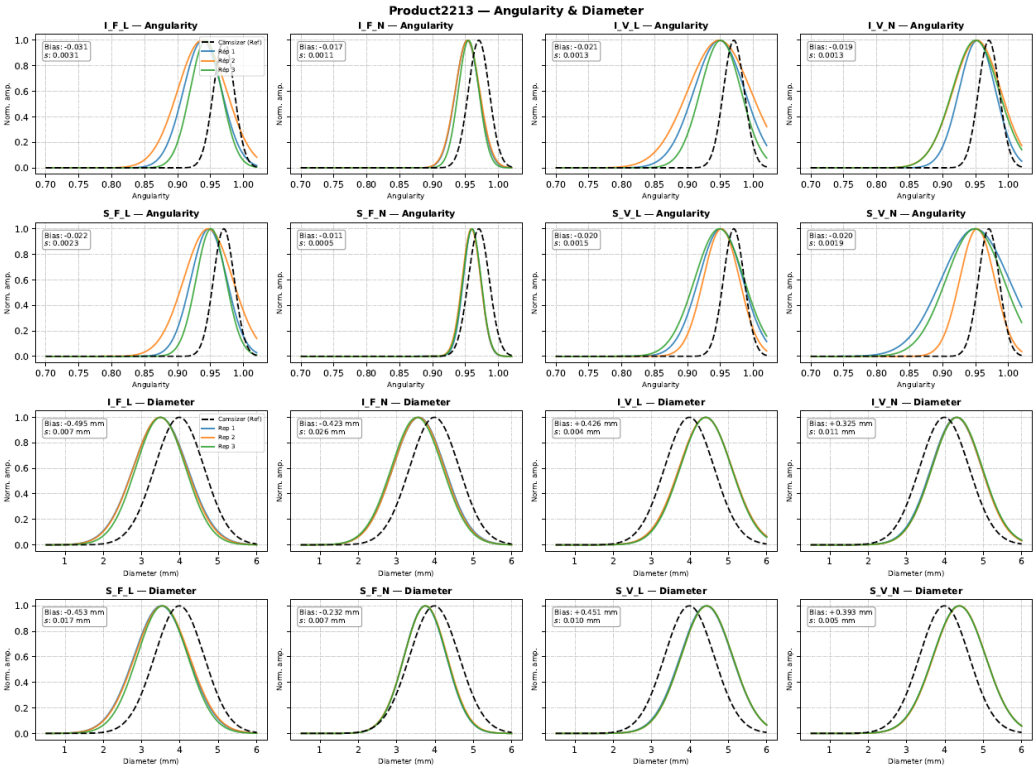


Figure 36 : Example of modalities distribution curves for one product (NPK from LAT Nitrogen)

The granular breakdown of metrological indices across the eight factorial combinations of imaging devices (Samsung Galaxy A34 vs. Apple iPhone 15) and illumination regimes (grazing light On vs. Off) is presented in Table 1.

Measured value	Method	Smartphone	Grazing Illumination	Unit	MAPE (%)	CV_rep (%)	W2
Angularity	FertiEye	Galaxy A34	Off	-	2.04	1.37	0.0222
			On		1.93	0.17	0.0226
		iPhone 15	Off		1.91	1.19	0.0204
			On		2.58	0.24	0.0294
	Bulk	Galaxy A34	Off		1.58	0.28	0.0289
			On		1.29	0.45	0.0273
		iPhone 15	Off		2.00	0.33	0.0345
			On		1.86	0.44	0.0327
Feret min diameter	FertiEye	Galaxy A34	Off	mm	7.07	2.70	0.245
			On		6.88	0.66	0.243
		iPhone 15	Off		7.18	1.91	0.256
			On		10.98	1.22	0.392
	Bulk	Galaxy A34	Off		15.52	0.48	0.485
			On		21.85	0.54	0.678
		iPhone 15	Off		14.05	0.39	0.439
			On		16.93	0.52	0.529

Table 4: Results for each modalities and experimental variations

For the FertiEye system, activating grazing illumination sharply improved repeatability: angularity CV_{rep} dropped from 1.37% to 0.17% on the Galaxy A34, and from 1.19% to 0.24% on the iPhone 15, with diameter repeatability improving from 2.70% to 0.66% on the Galaxy A34. However, assessing cross-condition reproducibility reveals distinct operational sensitivities between both

methodologies. Across smartphone hardware variations, FertiEye demonstrated high reproducibility under baseline lighting (diameter MAPE shifting only from 7.07% on the Galaxy A34 to 7.18% on the iPhone 15), but exhibited vulnerability to directional lighting perturbations on the iOS sensor, where grazing illumination degraded sizing trueness to 10.98% and expanded distributional error (W_2 increased from 0.256 to 0.392 mm). Conversely, the bulk pipeline displayed poor sizing reproducibility under grazing light: direct illumination induced heavy shadowing and cast contours across heaps, systematically inflating diameter MAPE by +6.33% on the Galaxy A34 (15.52% to 21.85%) and +2.88% on the iPhone 15 (14.05% to 16.93%), with severe distribution degradation (W_2 peaking at 0.678 mm). In contrast, morphological reproducibility remained remarkably consistent for both methods, with angularity metrics exhibiting negligible deviations across devices and lighting regimes. The synthetic metrological performance across all 60 benchmark mineral fertilizers is summarized in Table 2. Both computer vision methodologies demonstrated distinct operational trade-offs between measurement trueness (MAPE), technical precision (CV_{rep}), and environmental reproducibility.

Measured value	Method	Unit	MAPE (%)	CV_rep (%)	W2
Angularity	FertiEye	-	2.11	0.74	0.0237
	Bulk		1.68	0.37	0.0308
Feret min diameter	FertiEye	mm	8.02	1.62	0.284
	Bulk		17.09	0.48	0.532

Table 5: Synthetic results for studied modalities

For particle angularity, both approaches exhibited outstanding agreement with the laboratory Camsizer standard, maintaining a relative error below 2.2%. The in-bulk deep learning approach achieved marginally superior trueness (MAPE $= 1.68\%$) and enhanced repeatability ($CV_{rep} = 0.37\%$) compared to the FertiEye monolayer method (MAPE $= 2.11\%$, $CV_{rep} = 0.74\%$). However, FertiEye yielded slightly better overall distribution concordance, characterized by a lower mean 2-Wasserstein distance ($W_2 = 0.0237$ vs. 0.0308).
Conversely, for the minimum Feret diameter, the rule-based monolayer method demonstrated substantial superiority in trueness. FertiEye achieved an average MAPE of 8.02% and a W_2 distance of 0.284 mm, outperforming the in-bulk deep learning pipeline (MAPE $= 17.09\%$, $W_2 = 0.532$ mm). Nonetheless, the deep learning bulk pipeline exhibited higher repeatability across consecutive captures, yielding a CV_{rep} of 0.48%, compared to 1.62% for FertiEye.

4/ CONCLUSIONS

This study benchmarked an expert rule-based monolayer method (FertiEye) against a multi-head U-Net bulk instance segmentation pipeline for in-field characterization of 235 mineral fertilizers, evaluated against a laboratory Camsizer P4 reference. The results demonstrate that distribution fidelity (W_2) serves as the primary discriminator between sampling modalities. The monolayer approach achieved superior distribution concordance, yielding a 2-Wasserstein distance of 0.284 mm and 0.0237, alongside a precision of 1.62% and 0.74%, and a trueness of 8.02% and 2.11%, for diameter and angularity respectively. Conversely, the bulk deep learning pipeline yielded a 2-Wasserstein distance of 0.532 mm and 0.0308, a precision of 0.48% and 0.37%, and a trueness of 17.09% and 1.68%, respectively.

In the context of stochastic centrifugal spreading models (Le, Piron, Miclet, & Villette, 2025), capturing high-fidelity particle size and morphology distributions is critical: relying on distorted input distributions or suffering a 17% sizing bias severely misestimates aerodynamic drag and flight trajectories in Monte Carlo dispersion simulations. Granular size segregation during bulk

heap preparation accounts for this dimensional discrepancy, whereas monolayer individualization preserves population distribution fidelity.

However, these benchmark findings remain bound to a semi-controlled darkroom enclosure designed to isolate optical variables. Under actual farmyard and field conditions, unconstrained environmental factors—such as direct sunlight and erratic hand-held angles can substantially diverge operational performance from laboratory benchmarks. In this practical context, the physical FertiEye tray secures the acquisition pipeline: its mechanical grid forces spatial separation, while rigid peripheral fiducial markers guarantee sub-millimeter homography, metric scaling, and color normalization directly at the machine side. In contrast, unconstrained bulk heap acquisitions offer no physical reference in the field; uncontrolled heap geometry and natural granular percolation leave deep learning inferences vulnerable to out-of-distribution shifts. Future work should therefore validate both modalities under unassisted field conditions, with particular focus on deploying deep learning segmentation directly onto physically individualized monolayer samples to combine metrological distribution fidelity with optical robustness.

References

- Amazonen Werke. (2015). EasyCheck. (Amazone) Retrieved from https://amazone.net/en/service-support/for-farmers-contractors-and-councils/fertiliser-service/easycheck-47354
- Amazonen Werke. (2025). AMAZONE ZA-TS 01 AutoSpread. (Amazone) Retrieved from https://amazone.net/en/agritechnica/agritechnica-2025-innovations/innovation-details/amazone-za-ts-01-autospread-2064660
- Amazonen Werke. (2025). EasyMatch. (Amazone) Retrieved from https://amazone.net/en/agritechnica/agritechnica-2025-innovations/innovation-details/amazone-easymatch-2064380
- Amazonen-Werke. (2019). MySpreader. (Amazone) Retrieved from https://amazone.net/en/products-digital-solutions/digital-solutions/software/agapps/myspreader-app-59098
- Bogballe A/S. (2013). Table d'épandage. (Bogballe) Retrieved from https://charts.bogballe.com
- Burel Group. (2007). Fertitest. (Sky Agriculture) Retrieved from Fertitest: https://fertitest.sky-agriculture.com
- Burel Group. (2025). SKY Agriculture récompensé d'une médaille d'argent aux « AGRITECHNICA Innovation Award » pour son FERTIEYE. (Sky Agriculture) Retrieved from https://sky-agriculture.com/actualites/sky-agriculture-recompense-d-une-medaille-d-argent-aux-agritechnica-innovation-award-pour-son-fertieye/
- De Boer, B. (2020, 04 03). Netherlands Patent No. EP3889907.
- de Myttenaere, A., Golden, B., Le Grand, B., & Rossi, F. (2016). Mean Absolute Percentage Error for time series forecasting. Neurocomputing 192, pp. 38-48.
- Fröschle, H., & Ströbel-Fröschle, M. (2016, 07 25). Germany Patent No. EP3275302.
- Gallagher, C., Nikam , S., Kerr , E., & McFadden , S. (2025). Shape characterisation for mounted additive manufacturing powders. Results in Engineering 27, 106605. doi:10.1016/j.rineng.2025.106605
- Genymobile. (2025). SCRCPY: Android Screen Mirroring Tool . Retrieved from https://scrcpy.org/
- Givens, C. R., & Shortt, R. M. (1984). A class of Wasserstein metrics for probability distributions. The Michigan Mathematical Journal 31(2), 231-240.
- He, K., Zhang, X., Ren, S., & Sun, J. (2016). Deep Residual Learning for Image Recognition. Computer Vision and Pattern Recognition. doi:10.48550/arXiv.1512.03385
- Inarix. (2024). PocketLab. (Inarix) Retrieved from https://inarix.com/fr/platforms/pocketlab
- ISO 5725-2. (2025). Accuracy (trueness and precision) of measurement methods and results, Basic method for the determination of repeatability and reproducibility of a standard measurement method. International Organization for Standardization.
- ISO 7870-2. (2023). Control charts, Shewhart control charts. International Organization for Standardization.
- Kirillov, A., Mintun, E., Ravi, N., Mao, H., & Rolland, C. (2023). Segment Anything. ICCV(10.1109/ICCV51070.2023.00371), 3992-4003.
- Kverneland Group France S.A.S. (2018). Tableau d'épandage. (Kverneland) Retrieved from https://www.kvernelandspreadingcharts.com
- Le, T.-T., Miclet, D., Heritier, P., Piron, E., Chateauneuf, A., & Berducat, M. (2018). Morphology characterization of irregular particles using image analysis. Computers and Electronics in Agriculture, 147(10.1016/j.compag.2018.02.022), 146–157.
- Le, T.-T., Piron, E., Miclet, D., & Villette, S. (2025). Simulation-based study of the influence of particle physical properties on fertilizer spreading ability. Computers and Electronics in Agriculture 229, 109753.

- Leclair, E., Léveillé, L., Gripon, N., & Juhel, T. (2021, 09 30). France Patent No. EP4749263.
- OpenCV. (2000). OpenCV team. Retrieved from https://opencv.org/
- Rauch Landmaschinenfabrik Gmbh. (2025). XCheck. (Rauch) Retrieved from https://rauch.de/en/smart-farming/xcheck.html
- Retsch Technology GmbH. (2014). Particle Analyzer CAMSIZER® P4. 42781 Haan, Allemagne: Retsch Technology.
- Ronneberger, O., Fischer, P., Brox, T., Navab, N., Hornegger, J., Wells, W. M., & Frangi, A. F. (2015). U-Net: Convolutional Networks for Biomedical Image Segmentation. Springer International Publishing, MICCAI 2015, Part III, LNCS 9351(10.1007/978-3-319-24574-4_28), 234-241.
- Toussaint, G. T. (1983). Solving geometric problems with the rotating calipers. Proceedings of IEEE MELECON'83, A10.02/1--4.
- Yu Lihsuan. (2026). App Store. Retrieved from https://apps.apple.com/us/app/teleshot/id1447386405
- Zeng, L., Li, T., Wang, X., Chen, L., Zeng, P., & Herrin, J. S. (2022). UNetGE: A U-Net-Based Software at Automatic Grain Extraction for Image Analysis of the Grain Size and Shape Characteristics. MDPI Sensors, 22, 5565(10.3390/s22155565).

RTK autosteering in agriculture: uses, perceptions and implications for the agroecological transition

Rémi Druesne[a], Eve Faivre[a], Lydiane Marrec[a], Alexis Morel[a], Gawain Jones[b], Damien Calais[c,*], Caroline Desbourdes[d], Régis Hélias[d], Stéphane Volant[e]

[a] Engineering students, Agricultural Equipment Science and Technology (STEA), Institut Agro Dijon, France
[b] Teacher–Researcher, Institut Agro Dijon, France
[c] Lecturer, Institut Agro Dijon, France
[d] Engineers, ARVALIS, France
[e] Project Officer, FR CUMA de l'Ouest, Pacé, France
*Corresponding author. Email: damien.calais@institut-agro.fr

Abstract

RTK autosteering systems can contribute to precision farming and support the agroecological transition. Agricultural engineering students at Institut Agro Dijon conducted a survey among users of agricultural vehicles to assess their perceptions of accuracy at ground level and their satisfaction with their equipment. 890 complete questionnaires were collected, including 506 from users of RTK-autosteered vehicles. The results show that users' perceptions of potential or actual discrepancies between specified and achieved levels of accuracy vary according to their experience and the requirements of their farming practices. Interviews with professionals in the agricultural equipment sector confirm that they are aware of the issues encountered by users. However, they tend to attribute these issues to improper use or environmental factors beyond their control.

In contrast, experience at ARVALIS suggests that manufacturing tolerances in vehicle components may contribute substantially to the discrepancies reported by users. Proper assessment and calibration of RTK autosteering systems appear to be essential for achieving the expected performance. However, no universal and straightforward method is currently available for this purpose. ARVALIS engineers therefore propose the development of a test bench or certification scheme. The survey indicates that such an initiative would be welcomed by most users, although concerns remain about the additional cost it could entail. Professionals in the agricultural equipment sector expressed mixed views on the proposal. Nevertheless, the survey highlights the potential value of such an initiative for the sector, as it could address an unmet need and contribute to renewed growth in the agricultural equipment market.

KEYWORDS: Accuracy, Certification, Configuration, Parameters, Precision farming, Test bench

Complexity level: 2

1/ INTRODUCTION

1.1 Context

The present study was commissioned by two engineers at ARVALIS, Caroline Desbourdes and Régis Hélias, and by Stéphane Volant, a project officer at the French Western Federation of Farm Machinery Cooperatives (FR CUMA de l'Ouest). It was conducted between October 2025 and March 2026 by four agricultural engineering students specialising in agricultural equipment science and technology (STEA) at Institut Agro Dijon: Rémi Druesne, Eve Faivre, Lydiane Marrec and Alexis Morel. The project was supervised by the sponsors and by two members of the agricultural equipment teaching team at Institut Agro Dijon, Gawain Jones and Damien Calais.
This article was written by Gawain Jones, Damien Calais, Caroline Desbourdes and Régis Hélias, based on the dissertation presented by the four students. Damien Calais consolidated the contributions from all authors and prepared the final English version.

1.2 Background

Autosteering systems are increasingly used on agricultural vehicles for field-crop production. They can improve driving performance by reducing operator fatigue and fuel and input consumption. They can also support variable-rate fertilisation and other operations for which basic correction services provide sufficient accuracy, ensure reliable crop establishment in seed maize, and enable crop management sequences requiring RTK centimetre-level repeatibility, such as spring sowing after autumn or winter strip-tillage or hoeing narrow-row crops without cameras or feelers.

Engineers at ARVALIS, a French applied research institute supporting innovation and technical development in field-crop production, have observed discrepancies between the positioning accuracy reported by RTK systems and the pass-to-pass accuracy achieved at ground level. Although RTK positioning at the antenna is typically accurate to within ±2 cm for 95% of measurements, pass-to-pass accuracy at ground level can be substantially lower unless the autosteering system is properly calibrated. Engineers at ARVALIS experienced that the optimum settings vary from one machine to another, even between two machines of the same model manufactured at the same factory. In most cases, an RTK-level pass-to-pass accuracy can be achieved with hydraulic steering systems, but not with electric steering systems (see Figure 1). However, even with a hydraulic steering system, the expected ±2 cm pass-to-pass accuracy may not always be achieved. These differences may be attributed to dimensional tolerances in the machine's components and to discrepancies between the nominal and actual flow rates of the hydraulic steering valves. Other factors may also affect performance under field conditions, such as soil preparation and tyre pressure imbalance.

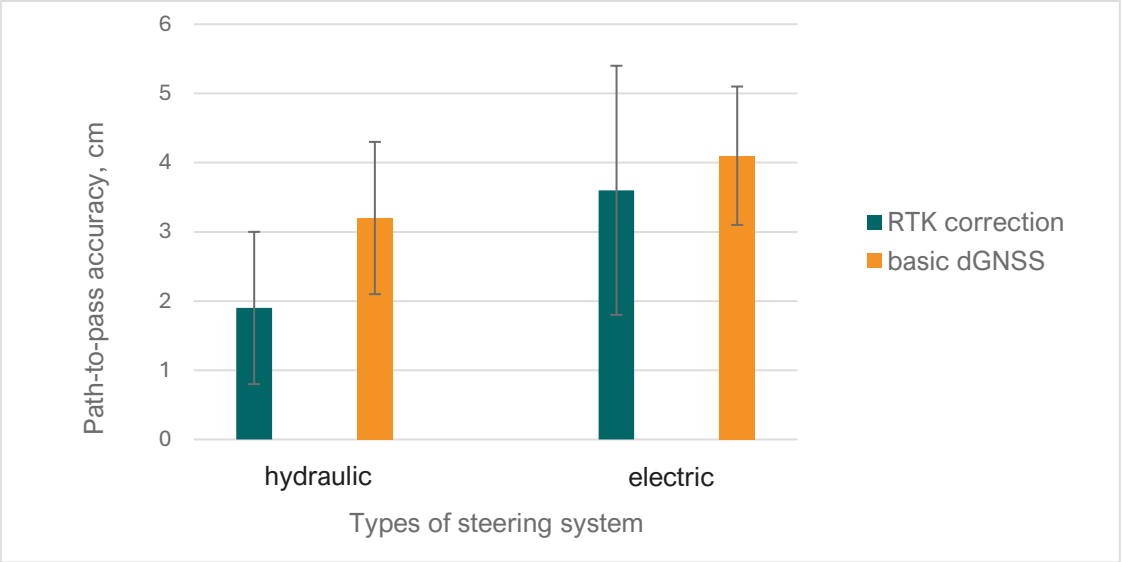


Figure 1: Tractor path-to-pass accuracy measured on-farm across 5,000 hectares of sowing (Piel, 2026, based on a study by Caroline Desbourdes, 2008-2013)

1.3 Assessing RTK autosteering performance: a key step for the continued development of precision farming

At present, assessing the performance of an autosteering system is not straightforward. Methods based on physical reference points — for example, measuring the distance between one or more stakes and the tractor during a return pass — are not entirely satisfactory. Several sources of bias can affect the assessment of accuracy, including the 'guide rail' effect of wheel tracks carried over from the previous pass and the use of too few measurement points. To address these limitations, ARVALIS has developed a method based on recording the RTK position of the tractor's antenna 10 times per second over several passes of identical width (see Figure 2). The resulting dataset can then be statistically analysed, thereby providing more reliable accuracy measurements.

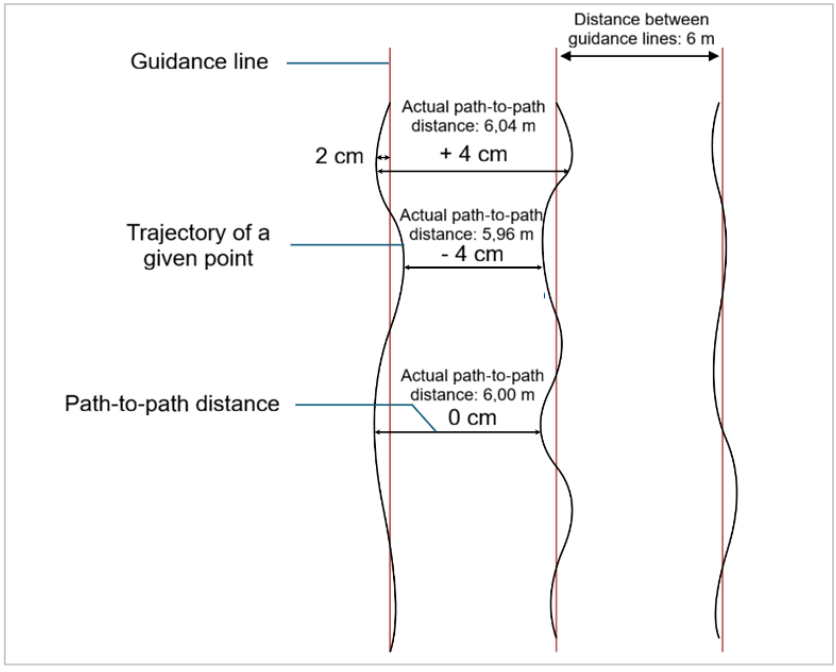


Figure 2: ARVALIS method to assess RTK autosteering performance (Piel, 2026)

Drawing on its expertise, ARVALIS regularly highlights discrepancies between the accuracy figures reported by manufacturers and those actually measured in the field. While manufacturers typically report average accuracy relative to the guidance line, ARVALIS considers that pass-to-pass accuracy achieved 95% of the time is a more relevant and useful measure of performance for farmers. This is particularly important when a high degree of accuracy is required for crop management operations such as sowing followed by hoeing relying on RTK autosteering (Desbourdes, 2014).

It is virtually impossible for a farmer to assess the accuracy of an autosteering system. However, the method currently used by ARVALIS is time-consuming. The idea of developing a system for rapid accuracy assessment or a test bench is not new to ARVALIS. Neither has yet been developed, but such an approach could offer several advantages, including:

- speed of use
- repeatability under standardised conditions, independent of site-related variability
- transfer of skills to other users
- troubleshooting and maintenance checks for the autosteer and its control systems
- reconfiguration of settings in the tractor's in-cab terminal to improve accuracy, using a protocol specific to each manufacturer or autosteering system supplier
- advanced tests that could be carried out, depending on the characteristics of the test bench: assessing the effect of differential wheel slip, slope, off-centre implements, implements that pull the tractor to one side, tyre type and inflation pressure, etc.

Such an assessment system could be highly valuable to manufacturers, dealers, farm machinery cooperatives, and contractors. The test bench would make it possible to suggest settings even before the tractor is delivered to the end user.

1.4 Objectives

A survey was conducted to address the following questions: Are users of RTK autosteering systems and professionals in the agricultural machinery sector aware of the recurring discrepancies between positioning accuracy at the antenna and pass-to-pass accuracy at ground level? Do they consider this discrepancy to be an issue that could hinder the development of innovative agricultural practices fostering the agroecological transition? Eventually, to what extent are users and industry professionals willing to support the development of a test bench or the introduction of a certification scheme to ensure compliance with the expected RTK pass-to-pass accuracy?

2/ MATERIALS AND METHODS

2.1 Hypotheses and general approach

Consistent with previous work conducted by ARVALIS, the approach is based on the general hypothesis that the accuracy achieved under field conditions depends not only on the quality of GNSS reception and RTK corrections, but also on the overall autosteering system, including tractor settings and calibration, equipment specifications, and environmental conditions.

Three working hypotheses guided the design of the study. First, discrepancies between the antenna positions estimated by the RTK system and the actual trajectory of the tractor may affect high-precision operations such as sowing, hoeing or certain harvesting activities. Second, the perception of these discrepancies is likely to vary depending on users' experience and accuracy requirements, with RTK users and non-users potentially having different perceptions. Finally, the introduction of a standardised system for assessing or certifying accuracy is likely to be welcomed

by most professionals and organisations involved in agriculture and agri-equipment, although its acceptance will depend on the cost and time required for implementation as well as organisational considerations.

To test these hypotheses from complementary perspectives, a two-part approach was adopted. The first part consisted of a quantitative approach based on a questionnaire targeting users of guidance and autosteering systems, while the second relied on a qualitative approach based on semi-structured interviews with professionals involved in the design, marketing, installation, or technical and after-sales support for RTK systems. This combined approach makes it possible to compare the responses of a large number of users with the more detailed accounts provided by professionals from the agricultural equipment sector.

2.2 Survey population and data collection

Two groups of participants were surveyed based on their relationship with RTK autosteering. The first group consisted of end users, including farmers and farm workers, agricultural contractors, and members of farm machinery cooperatives. For this group, an online questionnaire was used to facilitate participation among individuals with demanding work schedules and to allow respondents to complete the survey at a time that suited them.

The second group comprised professionals in the agricultural equipment sector involved in RTK autosteering, including manufacturers, dealers, and other stakeholders likely to provide insights into its use, configuration, or development. Semi-structured interviews were conducted with these participants to elicit detailed accounts of their experiences and perspectives. This approach also allowed the questions to be adapted to each interviewee's professional background and enabled specific issues arising during the interviews to be explored in greater detail.

The questionnaire and interview guides were developed jointly to ensure that a set of common themes was addressed across the different categories of stakeholders. The questions focused on the use of RTK autosteering, associated farming practices, accuracy observed under field conditions, discrepancies between displayed and actual accuracy, challenges encountered in practice, and interest in a potential assessment or certification scheme. Some questions were asked after participants had been presented with the findings of previous ARVALIS work examining discrepancies between specified, displayed and actual levels of accuracy.

All the data were collected in mainland France. The initial respondents were recruited through the Institut Agro Dijon student network. Additional respondents were subsequently contacted through chambers of agriculture, farm machinery cooperatives (CUMA), agricultural contractors, and equipment dealerships. Finally, ARVALIS distributed the questionnaire by mass email to approximately 45,000 farmers.

Once the responses had been screened, 890 complete questionnaires were retained for analysis. These comprised 850 farmers or agricultural workers, 35 employees of agricultural contracting businesses, and 5 employees of farm machinery cooperatives (CUMA). Among these respondents, 506 had access to free and/or paid RTK correction services. The interviews included representatives from a range of organisations involved in agricultural technology, including dealers, manufacturers, and equipment suppliers. Given the limited number of interviews conducted within each category, these interviews were treated as a source of qualitative information, intended to identify trends rather than to provide a statistically generalisable representation of each professional group.

2.3 Variables studied and data processing

The questionnaire was used to collect both descriptive information about the respondents and data on their use and perceptions of RTK. The variables considered included the type of agricultural activity, the total agricultural area of the farm, whether or not RTK was used, the practices performed using RTK, the estimated accuracy in the field, compliance with the accuracy specified by the manufacturer, the occurrence of discrepancies between the displayed and actual accuracy, and the potential impact of these discrepancies on current and future practices.

Incomplete questionnaires were excluded from the analysis to ensure that comparisons across variables were based on the same set of respondents. Responses to open-ended questions were processed manually to standardise the data. This involved correcting typographical errors and grouping items under a common designation when they referred to the same device but were identified using different names.

Descriptive analyses were conducted primarily using Excel, including cross-tabulations of responses to examine relationships between user profiles, equipment, farming practices, and perceptions of accuracy. The geographical distribution of respondents was mapped using RStudio (v4.4.2).

The interviews were analysed using a comparative qualitative approach. Comparing the different categories of stakeholders highlighted areas of convergence and divergence in their perceptions. These findings were then considered alongside those obtained from the user survey.
The combination of quantitative and qualitative analyses therefore allows for an examination of perceived RTK accuracy, its potential implications for farming practices, and the conditions required for the implementation of an accuracy control or certification scheme.

3/ RESULTS AND DISCUSSION

3.1 Geographical distribution and profile of respondents

The map of the geographical distribution of users (Figure 3) indicates that the vast majority of respondents are located in the Paris Basin and in northern and north-eastern France. These regions are predominantly characterized by field-crop production, with cereal crops such as wheat and barley, as well as processing crops, such as sugar beet.

Among the farms retained for analysis, there is a predominance of specialisation in cereal crops (which account for 67% of the sample). Mixed crop-livestock systems represent the second largest group (29%). The remaining farm types, including viticulture, vegetable production (either field-scale or market gardening), and other mixed farming activities (e.g. cereal production combined with viticulture), account for only a marginal share of the sample. For all farm types, mean utilized agricultural area (UAA) per farm is larger in the sample than the corresponding national mean (Table 1).

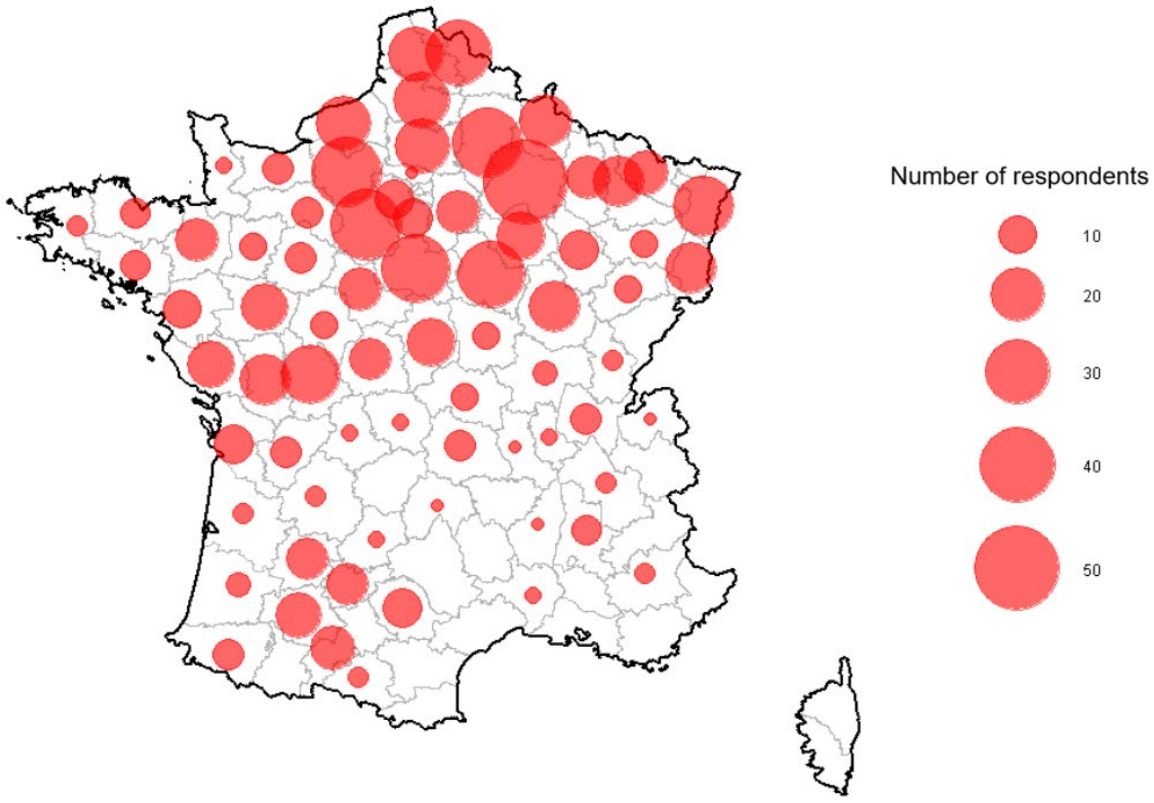


Figure 3: Geographical distribution of respondents across French departments

Farm types	Sample size	Mean UAA (hectares), sample	Standard deviation (hectares), sample	Mean UAA (hectares), mainland France (Agreste, 2025)
Cereal crops	570	219	163	134
Mixed crop-livestock	244	189	117	118
Viticulture	9	117	78	25
Vegetable production	9	124	63	51
Other mixed activities	18	295	318	-
Total	*850*	*210*	*156*	*76*

Table 1: Distribution and mean UAA of farms

3.2 The uses of autosteering and RTK correction

506 of the 890 respondents who completed the questionnaire use RTK autosteering. Of these, 68% pay for access to an RTK correction service, whereas 35% use the free Centipede RTK signal (3% use both a paid service and Centipede).
Among 306 users of agricultural vehicles without RTK autosteering, 53% stated that the cost of equipping their vehicles with RTK autosteering was a barrier. 40% did not consider it necessary for their operations.

RTK autosteering is used for sowing (98% of users), tillage (89%) and spraying (66%). RTK autosteering is also used, to a lesser extent, for hoeing (37%), harvesting (8%) and the application

of mineral or organic fertilisers (7%). The main harvesting operations mentioned are silaging, grain harvesting and potato harvesting.

The use of RTK autosteering for both tillage and sowing is not sufficient to determine whether the two practices are related, for example, whether the seedbed has been prepared using strip tillage. Using RTK autosteering for tillage does not necessarily imply that the positioning data will be reused for sowing. It can therefore be understood only as a means of saving time and fuel and reducing driver fatigue. The same applies to the sowing and spraying pair: band spraying in the crop rows is not distinguished from other types of spraying. The only meaningful combination that can be identified with a high degree of confidence is between sowing and hoeing. 183 respondents reported using RTK autosteering for both practices — that is, whenever RTK autosteering is used for hoeing — with one exception that may be due to an omission by the respondent.
Hoeing with an autosteered tractor may rely on RTK alone (62% of cases) or combine RTK with one or more cameras mounted on the hoe frame (35%). Less commonly, autosteering of the tractor for hoeing combines RTK with track markers (3 respondents) or relies on cameras alone (2 respondents).

All respondents who use RTK autosteering agreed on its benefits, which were also acknowledged in interviews conducted with staff at dealerships and equipment suppliers. Users cited driver comfort and time and cost savings achieved by reducing overlap between passes and by mapping plot boundaries, crop rows and tramlines. One of the staff members interviewed at an equipment supplier added that RTK autosteering facilitates controlled traffic farming (CTF) and allows the same vehicle to be driven by different operators.

Users also mentioned negative experiences, such as connection issues and stolen antennas. Some respondents spoke of their dependence on the technology once they had adopted it for sowing and hoeing, particularly in seed maize cultivation. One of the staff members interviewed at a dealership described this dependence as a cause of stress in digital and precision farming departments: ‘Consider that when autosteer is not working, the tractor is out of action’.

3.3 Overall satisfaction, but recurring issues with pass-to-pass inaccuracy

Users of RTK autosteering rated their satisfaction with the performance of their equipment on a scale of 1 to 10, depending on the operation. The highest mean scores are for haymaking (9.0) and tillage (8.7), and the lowest for hoeing (7.6). This lower rating is likely due to the need for a high level of accuracy when hoeing according to seed location mapping. Although accuracy can be lower than expected or subject to discrepancies between the displayed and actual figures, the ratings are mostly good to very good. Depending on their practices, users do not always need 2 cm accuracy or can mitigate inaccuracies, for example by setting an implement width slightly narrower than the actual width in the tractor’s in-cab terminal. This technique is used in soil preparation and has virtually no negative effect, except in strip-tillage where it cannot be applied. Of the respondents who use RTK autosteering, 31% estimate that their systems provide 2 cm pass-to-pass accuracy. Among respondents who do not use RTK autosteering, 41% believe they would achieve 2 cm accuracy if they were to use this technology. These figures suggest that non-users are overly optimistic. However, 7% of non-users estimate the achievable pass-to-pass accuracy to be only 5 to 10 cm. Similarly, 7% of RTK autosteering users estimate that their systems do not offer better than 5 to 10 cm accuracy.

57% of RTK autosteering users reported discrepancies between the displayed and actual accuracy of the autosteering system. In interviews with staff at dealerships, these discrepancies were acknowledged as a problem for users. However, they were not spontaneously attributed to inappropriate configuration of autosteering parameters. The interviewees instead cited signal

drops or antenna inaccuracies caused by solar storms, proximity to forest, cellular dead zones, or network failures. Interference caused by wind turbines or high-voltage power lines was also mentioned.

Another issue frequently reported by RTK autosteering users is path-tracking instability. When not caused by signal loss or antenna inaccuracies, path-tracking instability was attributed by staff at dealerships to improper calibration of the terrain compensator or to operator errors. Staff at equipment suppliers highlighted the complexity of configuring and using RTK autosteering systems. They placed responsibility for path-tracking instability not only on users but also on dealership technicians, or even, in one interviewee's view, on the tractor's assembly.

Staff at dealerships pointed out the difficulty of providing users with sufficient training to make the most of their autosteering system. In two of the three dealerships where interviews were conducted, users are given hands-on training in the farmyard but not in the field. A half-day course is sometimes provided for groups of four or five, and a summary booklet is handed out. This training appears insufficient given the comments made by two interviewees at dealerships: they estimated that getting familiar with an RTK autosteering system takes a few days for users who are more comfortable with new technologies and several months for novices. The third dealership where interviews were conducted offers user onboarding over several days and on-field training if requested.

When asked whether pass-to-pass inaccuracy limits possible applications, 38% of RTK autosteering users replied 'yes' in relation to their current practices, compared with 67% for potential future practices. Those who replied 'yes, absolutely' account for 7% for current practices, and 20% for future practices. Pass-to-pass inaccuracy of RTK autosteering can therefore be a stumbling block to the development of innovative agricultural practices.

3.4 Views on a potential system for assessing pass-to-pass accuracy

Most users of agricultural vehicles (whether or not they use RTK) are in favour of introducing a system to assess pass-to-pass accuracy: 80% support a test bench and 77% support certification by vehicle manufacturers. The same respondents generally favour both a test bench and certification. Those who oppose an assessment system underline the cost it would incur; they fear that this cost will be passed on to users.

Users' positive or negative opinions are not linked to the estimated level of pass-to-pass accuracy but to practices that are considered impossible without optimal accuracy. Those who plan to use RTK autosteering for sowing and hoeing are the most in favour of a test bench or certification. Those who are more interested in precision spreading or precision spraying are the least in favour of such systems.

Of those in favour of a test bench, 54% believe that the vehicle manufacturer should be responsible for it. 31% think that an independent body should take charge of it. 15% would entrust this task to their dealership.

Within digital and precision farming departments at dealerships, the interviewees expressed concerns about the potential cost and time involved in implementing a test bench or certification scheme. Some interviewees believed that it should not be up to the dealerships to bear the cost of such systems: they argued that the degree of inaccuracy is the same across all brands and that the problems are more often linked to a lack of user skills than to the technical specifications of the machinery and autosteering systems. However, at another dealership, an interview was conducted with the manager of the digital and precision farming department. According to this

manager, the main source of the problem is that the estimation of accuracy is left to the judgement of the technician who sets up the autosteering system. This technician may be more or less skilled and meticulous. Moreover, calibration procedures differ depending on the brand of the autosteering system as well as the brand of the vehicle. The manager was therefore in favour of introducing a certification scheme managed by the vehicle manufacturer, and equipping the dealership with a test bench.

As for the staff interviewed at equipment suppliers, they questioned the feasibility of such projects and the willingness of manufacturers to cooperate. In addition to the time and money they would require, some equipment suppliers have already developed their own assessment systems and would be reluctant to collaborate on developing a shared tool. Nevertheless, they considered certification to be desirable, with the exception of one interviewee at a supplier of RTK autosteering systems. The support adviser interviewed at this supplier believed that certifying pass-to-pass accuracy is impossible due to the sheer number of factors that would have to be taken into account: weight and load distribution between the axles, tyre pressure, antenna position, weather and soil conditions, user behaviour, and usage patterns.

4/ CONCLUSIONS

RTK autosteering systems can contribute to precision farming and support the agroecological transition. Agricultural engineering students at Institut Agro Dijon conducted a survey among users of agricultural vehicles to assess their perceptions of accuracy at ground level and their satisfaction with their equipment. 890 complete questionnaires were collected, including 506 from users of RTK-autosteered vehicles. Semi-structured interviews with professionals in the agricultural equipment sector were also conducted to explore specific issues.
Among the key findings of the survey carried out is a contrast between users whose vehicles are fitted with RTK autosteering, even though there is no real technical need for this level of accuracy in their current practices, and, conversely, users who combine RTK with cameras to autosteer their tractor-implement combination, even though RTK should, in theory, be sufficient on flat ground if the specified accuracy were actually achieved in the field.
In this regard, 69% of RTK autosteering users estimate that the accuracy they achieve between two passes is greater than the 2 cm frequently specified, while 7% estimate that the accuracy they achieve is only 5 to 10 cm. 38% of RTK users already consider the lack of accuracy to be a limit on their current practices. 67% regard it as an obstacle to the implementation of innovative practices.
These results confirm the interest of an accuracy assessment system for RTK autosteering users. Indeed, 80% of them say they are in favour of a test bench and 77% in favour of certification. Those who say they are against it are not opposed on principle, but because they fear the cost this would add to the purchase price of the equipment.
There is no doubt that setting up a test bench or introducing a certification scheme would be complex, both technically and organisationally. Nevertheless, relevant precedents, such as engine power test benches and ISOBUS certification schemes, may provide a useful basis. These examples have demonstrated that test benches and certification schemes can create value while encouraging manufacturers to engage in a process of competitive emulation and continuous improvement.
Experience at ARVALIS shows that it is possible to recalibrate an unsatisfactory RTK autosteering system to deliver the target level of accuracy, with reliable and stable performance over time. Moreover, the process is less complex that might initially be expected: it can be achieved by adjusting a small number of dealer-accessible parameters and can be readily implemented for the most precision-demanding operation on a given farm.

A test bench and/or certification scheme would enable stakeholders in the agricultural equipment sector to rely on a standardised method for assessing accuracy. Such a method would be likely to:

- turn conjecture into empirical evidence regarding the factors explaining differences in accuracy between tractors of the same model;
- inform adjustments to parts manufacturing specifications;
- provide a standardised method for calibrating the parameters of autosteering systems, thereby eliminating vehicle-to-vehicle differences at the factory and ensuring that the quality of autosteered vehicles entering the market consistently meet higher quality standards;
- increase customer satisfaction and, consequently, the number of promoters of RTK autosteering, thereby generating additional revenue for dealers and manufacturers;
- reduce user complaints, thereby alleviating the workload and stress of dealership staff working in digital and precision farming departments, while also reducing the need for tractor returns and exchanges resulting from customer dissatisfaction;
- provide an objective basis for addressing user complaints arising from subjective experiences, by drawing on test results obtained through a standardised method applied across the agricultural equipment sector.

If implemented, a system for assessing RTK autosteering accuracy could contribute to renewed growth in the agricultural equipment market, while contributing to the sector's efforts to advance the agroecological transition. Growing societal pressure to reduce the use of synthetic inputs in agriculture, the discontinuation of regulatory or commercial support for older active ingredients, the continued emergence of resistance to pesticides, and a slowdown in the development of new active ingredients all point to precision farming as a reliable and promising means of meeting the needs of tomorrow's farmers. The shortcomings currently observed in RTK autosteering systems should not be allowed to hinder innovation, particularly as these systems already support sound and effective farming practices when properly configured and used.

References

- Agreste, 2025. Enquête sur la structure des exploitations agricoles 2023. Accessed 1 September 2026. https://agreste.agriculture.gouv.fr/agreste-web/methodon/S-ESEA2023/methodon/
- Desbourdes, Caroline, 2014. RTK : des corrections pour revenir au même endroit. Perspectives agricoles 409, pages 44–51.
- Piel, Gwendolan, 2026. Le guidage de précision en agriculture : enjeux, limites et leviers d'optimisation pour les exploitations. Agricultural engineering degree thesis, supervised by Gawain Jones (Institut Agro Dijon) and Régis Hélias (ARVALIS).

High-Fidelity 3D Reconstruction of Potato Tubers from Sparse Unposed RGB Images

Adrien Schockaert[a,b,c,*], Guillaume Dufaye[a], Mohammed Hachbouk[a], Vincent Magnier[b], Hazem Wannous[c], Jean-François Witz[b]

[a] Downs, 59670 Sainte-Marie-Cappel, France
[b] Univ. Lille, CNRS, Centrale Lille, UMR 9013 LaMCube, F-59000 Lille, France
[c] CERI SN, IMT Nord Europe, 59650 Villeneuve-d'Ascq, France
* Corresponding author. Email: aschockaert@groupedubrulle.com

Abstract

Geometrically representative models of agricultural products are difficult to obtain because their natural shapes cannot be captured adequately by generic primitives. This paper presents a learning-based method for reconstructing potato tubers from sparse, unordered, and unposed RGB images without depth measurements or camera parameters. A variational auto-decoder (VAD) first learns a continuous category-level shape space from the reference meshes of the 3DPotatoTwin dataset. Its decoder combines sinusoidal representation networks with feature-wise linear modulation to represent multiple tuber geometries through compact latent codes.

A view-factorized Transformer subsequently maps frozen self-supervised image features into this latent space. On the 51-tuber test split, the proposed method obtains a Chamfer-distance score of 0.15 in the CD $\times 10^3$ reporting convention, compared with 0.35 for DISN and 0.28 for CoRe++. These values correspond to reductions of 57.1% and 46.4% in average surface discrepancy, respectively. Qualitative results show that the method recovers the principal tuber shape and localized deformations, although some fine surface details remain smoothed. The reconstructed meshes provide geometrically representative assets that can be integrated into downstream simulation workflows.

KEYWORDS: 3D reconstruction; potato tubers; signed distance functions; sparse multi-view learning; implicit neural representations; simulation

Complexity level: 3

1/ INTRODUCTION

Agricultural production must respond to increasing demand while reducing resource use and product losses. Computer vision and machine learning support this transition toward precision agriculture in applications ranging from crop monitoring to post-harvest inspection. Their development, however, depends on representative annotated data [1], which are difficult to acquire in industrial agricultural environments because of rare defects, seasonal variability, dirt, and changing illumination conditions.

Synthetic data can complement physical acquisition by providing images together with exact object masks, depth maps, and pose labels without manual annotation [2]. Their usefulness depends on the fidelity of the virtual environment and its correspondence with the physical system. Digital twins link a physical system to a virtual representation capable of reproducing the states and behaviors required by a target application [3,22]. Such workflows require representative models of both the environment and the objects interacting within it. Potato tubers exhibit substantial variability in size and shape, and generic geometric primitives do not reproduce their local surface variations. Traditional 3D acquisitions can provide accurate models but often require costly sensors or controlled, object-specific procedures [23,24]. Implicit neural representations such as DeepSDF [10] provide continuous, resolution-independent geometry, whereas NeRF [9] and 3D Gaussian Splatting [25] primarily optimize appearance for novel-view synthesis. The required representation must therefore generalize across tubers and produce an explicit, geometrically accurate surface suitable for downstream simulation.

This work investigates whether a small, unordered set of unposed RGB images can recover a sufficiently precise tuber mesh. The method adapts a decoupled geometric-prior and image-to-latent strategy introduced by SDFFormer [16] from synthetic ShapeNet categories to potato geometry. The principal architectural change is the implicit decoder: a FiLM-modulated SIREN replaces the positional-encoding MLP used in SDFFormer. The image encoder receives neither camera parameters nor depth at inference and supports a variable number of views.

The contributions are:

[1] an adaptation of the SDFFormer framework to reconstruct potato tubers from sparse, unposed RGB images;
[2] a variational FiLM-modulated SIREN decoder designed to represent both global tuber shape and localized surface variations;
[3] an evaluation against DISN and CoRe++ on a tuber-disjoint test split using normalized Chamfer distance;
[4] a workflow for exporting reconstructed meshes as assets for downstream simulation.

2/ RELATED WORK

2.1 Representations

Classical image-based 3D reconstruction commonly combines Structure-from-Motion (SfM) and Multi-View Stereo (MVS). SfM estimates camera parameters and a sparse scene structure from image correspondences [6], whereas MVS uses the recovered camera geometry and overlapping views to estimate dense surface geometry [7]. These pipelines can produce detailed reconstructions when the images provide sufficient overlap, texture, and photometric consistency. Their performance degrades on weakly textured surfaces, occlusions, and illumination changes, while their acquisition and calibration requirements can limit their use in high-throughput industrial environments. High-resolution point clouds and meshes can also incur substantial memory and processing costs.

Implicit Neural Representations (INRs) instead describe geometry as the level set of a continuous function parameterized by a neural network. Occupancy Networks represent a surface as the decision boundary between occupied and free space [11], while DeepSDF represents it as the zero level set of a signed distance function (SDF) [10]. DeepSDF introduced an auto-decoder formulation in which a shared coordinate-based network and an instance-specific latent code are jointly optimized over a collection of shapes. Compared with discrete grids, such representations can be queried at arbitrary spatial resolutions and can model shapes with varying topology.

Standard multilayer perceptrons used in INRs exhibit a spectral bias toward low-frequency functions [17], which can limit their ability to reproduce fine surface variations. Fourier feature mappings [8] alleviate this limitation by projecting spatial coordinates into a higher-dimensional periodic space before applying the multilayer perceptron. SIREN [18] instead uses sinusoidal activation functions throughout the network, and an initialization scheme designed to represent complex signals and their spatial derivatives. Its performance nevertheless depends on appropriate initialization and frequency hyperparameters. Feature-wise Linear Modulation (FiLM) provides a complementary conditioning mechanism by applying latent-dependent scale and shift parameters to intermediate activations [19]. This makes it possible for a shared SIREN decoder to represent multiple object instances while preserving a coordinate pathway suited to fine geometric variations.

Neural Radiance Fields (NeRFs) [9] represent a scene using a continuous function that maps spatial positions and viewing directions to volume density and emitted radiance. More recently, 3D Gaussian Splatting (3DGS) [25] has represented scenes with optimized anisotropic Gaussian primitives and differentiable splatting, enabling high-quality real-time rendering. Both families have substantially advanced novel-view synthesis. However, their original formulations are optimized using image-space rendering losses; geometric accuracy, watertightness, and explicit surface validity are not their principal objectives. The present work therefore focuses on a representation trained directly from geometric supervision and capable of producing an explicit surface for downstream simulation.

2.2 Sparse-View Reconstruction

When only a few images are available, classical SfM and MVS become under-constrained because correspondences may cover only a small portion of the object. Learning-based methods address this ambiguity by acquiring structural priors from collections of complete training shapes. Instead of reconstructing each object solely from its observed image correspondences, these methods predict a plausible complete geometry consistent with the available views.

Early geometry-supervised approaches commonly represent the target shape using voxel occupancy. 3D-R2N2 [26] recurrently integrates features from one or more images and predicts a three-dimensional occupancy grid. Pix2Vox [27] independently generates a coarse volume from each image and uses context-aware fusion to combine the most informative regions across views. More recent attention-based architectures improve information exchange between unstructured input images. UMIFormer [13] separates intra-view feature extraction from inter-view token correlation, LRGT [14] groups tokens across views to model long-range dependencies efficiently, and GARNet [15] uses global-aware attention to estimate the contribution of each view. These approaches are supervised using ground-truth voxel occupancy and do not require camera extrinsics as network inputs. However, their commonly used output grids impose a spatial-resolution bottleneck that can suppress fine surface details.

Continuous occupancy and signed-distance fields provide an alternative to fixed-resolution voxel decoding. Rather than predicting every element of a dense grid, they learn the geometric value associated with an arbitrary spatial query. This makes them particularly relevant when the desired output is a smooth and geometrically precise surface. SDFFormer [16] maps a sparse, unordered set of unposed RGB images into the latent space of a pretrained signed-distance decoder. Its two-stage formulation first teaches a geometric prior from complete shapes and then trains an image encoder to predict the corresponding latent representation.

The present work follows this separation between geometric-prior learning and image-to-latent mapping. However, it replaces the positional-encoding multilayer perceptron used by SDFFormer with a FiLM-modulated SIREN and adapts the framework from normalized ShapeNet objects to potato-tuber geometry. The network receives neither depth measurements nor camera extrinsics at inference and reconstructs a continuous surface from an unordered, variable-size set of RGB observations.

2.3 3D Reconstruction of Potato Tubers

Three-dimensional reconstruction of potato tubers has principally been investigated for phenotyping, grading, and yield estimation. Su et al. [28] reconstructed potato models from depth images and used the resulting three-dimensional volume and shape information for mass estimation. Active acquisition systems have been employed when greater geometric precision is required. Cai et al. [23] combined a monocular camera with line-laser triangulation and reconstructed the potato surface after interpolating missing regions of the acquired point cloud. Their system produced accurate volume estimates under controlled conditions but required the tuber to be rotated through a complete scan. Liu et al. [24] used an SfM-MVS pipeline to reconstruct detailed tuber models for quantitative phenotyping, including measurements of volume, shape, eye number, and eye depth. Such systems produce detailed geometry but require controlled imaging, extensive viewpoint coverage, and per-object reconstruction.

To mitigate the limitations of previous work, Blok et al. introduced CoRe++ [4], a method that uses an implicit neural representation to reconstruct potato tubers. A convolutional encoder processes an RGB-D observation and predicts a latent code that conditions a DeepSDF decoder. The method reported an average completion error of 2.8 mm and an average reconstruction time of 10 ms per tuber, demonstrating the potential of learned implicit representations for high-throughput applications. Nevertheless, its input remains dependent on depth measurements, and the authors reported that volume accuracy varied with the tuber position in the image.

In contrast to CoRe++, the proposed method operates from multiple RGB observations without depth or camera poses and reconstructs a complete continuous surface from an unordered, variable-size set of observations.

2.4 Synthetic Data and Learned Shape Generation

Synthetic agricultural data can reduce collection and annotation costs because labels can be obtained directly from the virtual scene, although the gap between synthetic and real observations remains a major limitation [2]. Beyond reconstructing observed objects, learned shape representations can also support the creation of diverse geometric assets. In the proposed variational formulation, tuber geometries are encoded in a continuous latent space regularized toward a shared Gaussian prior. In principle, latent vectors can be sampled from this prior or interpolated between learned representations and decoded as continuous signed distance fields, providing a potential mechanism for generating novel candidate tuber geometries. Such generated shapes could complement reconstructed instances in downstream simulation and synthetic data workflows. However, this paper evaluates only the reconstruction of observed tubers from RGB images. The realism, diversity, and usefulness of geometries obtained through latent sampling or interpolation are not assessed here and remain subjects for future work.

3/ MATERIALS AND METHODS

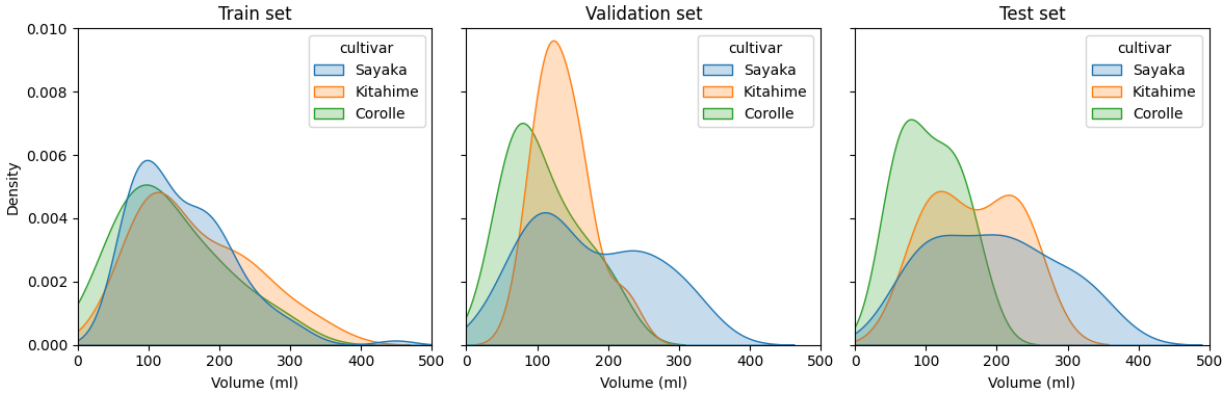


Figure 37: Distribution of tuber volumes by cultivar and dataset split, adapted from [5].

3.1 Dataset and Tuber Disjoint Split

Experiments are conducted on 3DPotatoTwin [5], which contains 339 tubers from three cultivars. Each tuber is associated with 20–30 RGB-D frames acquired on a harvester conveyor and a complete reference mesh reconstructed using a controlled three-camera turntable setup. In the proposed sparse-view setting, only the RGB channels are provided to the network; neither depth measurements nor camera poses are used. We retain the published tuber-disjoint 70/15/15 split, comprising 237 training, 51 validation, and 51 test tubers and designed to preserve cultivar and morphological diversity. All observations of a given tuber remain in the same subset, preventing information leakage through alternative views of a test instance.

Each RGB image is cropped around the tuber while preserving its aspect ratio and then resized to 224 × 224 pixels. At each training iteration, V views are sampled without replacement and randomly permuted. This randomization discourages the network from using the acquisition order as a proxy for camera pose and promotes robustness to unordered inputs.

The reference meshes are centered and scaled to the cube $[-0.5, 0.5]^3$, providing a common coordinate domain for network training. Following the SDFFormer [16] training protocol, 2,048 signed-distance queries are sampled per shape and epoch using a mixture of near-surface and uniformly distributed points. Near-surface samples concentrate supervision around the zero-level set from which the mesh is extracted, while uniform samples constrain the sign and global behavior of the field throughout the bounding volume.

3.2 Architecture Overview

The proposed architecture separates continuous shape representation from visual inference. A variational FiLM-modulated SIREN decoder represents each tuber as a signed distance function conditioned by a 256-dimensional latent code. A sparse multi-view encoder subsequently maps an unordered set of RGB images into the same latent space. At inference, the predicted code conditions the frozen decoder, which can then be queried at arbitrary spatial coordinates to reconstruct the tuber surface. The two components are described below before presenting their training procedure.

3.3 Variational FiLM-Modulated SIREN Decoder

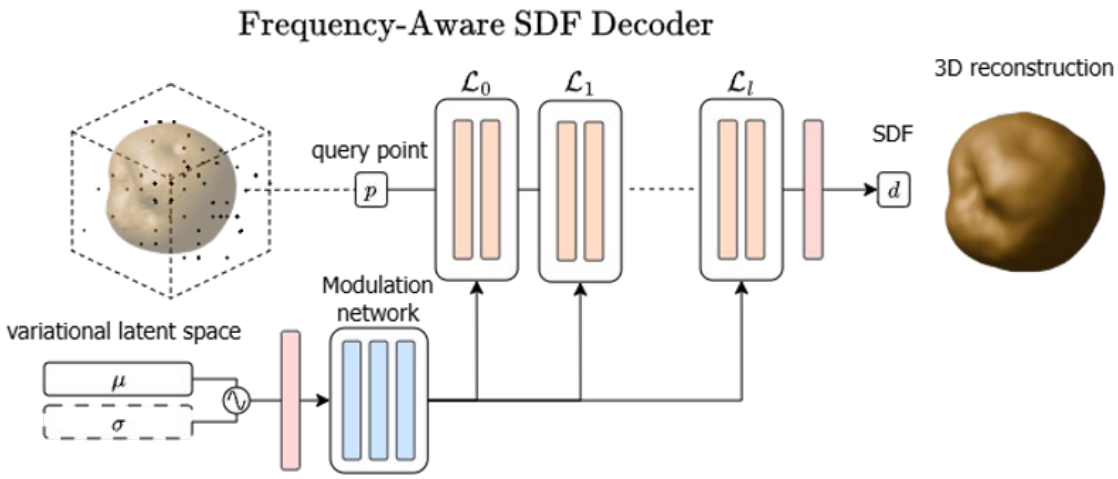


Figure 2: Architecture of the variational FiLM-modulated SIREN decoder.

The decoder represents the signed distance of a query point $\mathbf{p} \in \mathbb{R}^3$ as $\hat{d} = f_\theta(\mathbf{p}; \mathbf{z})$, where $\mathbf{z} \in \mathbb{R}^{256}$ represents the geometry of one tuber. The reconstructed surface is defined by the zero-level set

$$\mathcal{S}(\mathbf{z}) = \{\mathbf{p} \in \mathbb{R}^3 \mid f_\theta(\mathbf{p}; \mathbf{z}) = 0\}.$$

As illustrated in Figure 2, the decoder separates the coordinate and conditioning pathways. The spatial coordinate $\mathbf{p}$ is processed by an eight-layer SIREN of width 512 [18]. In parallel, the latent code $\mathbf{z}$ is passed through a mapping network that generates one pair of channel-wise scale and shift parameters, $(\boldsymbol{\gamma}^\ell, \boldsymbol{\beta}^\ell)$, for each hidden layer ℓ. These parameters modulate the corresponding sinusoidal features using FiLM [19]:

$$\mathrm{FiLM}(\mathbf{h}^\ell; \boldsymbol{\gamma}^\ell, \boldsymbol{\beta}^\ell) = \boldsymbol{\gamma}^\ell \odot \mathbf{h}^\ell + \boldsymbol{\beta}^\ell.$$

During geometric-prior learning, each training tuber i is associated with a diagonal Gaussian latent distribution $q_i(\mathbf{z}) = \mathcal{N}\left(\boldsymbol{\mu}_i, \mathrm{diag}(\boldsymbol{\sigma}_i^2)\right)$, rather than a single deterministic code. A latent vector is obtained using the reparameterization

$$\mathbf{z}_i = \boldsymbol{\mu}_i + \boldsymbol{\sigma}_i \odot \boldsymbol{\epsilon}, \qquad \boldsymbol{\epsilon} \sim \mathcal{N}(\mathbf{0}, \mathbf{I}).$$

The parameters $\boldsymbol{\mu}_i$ and $\boldsymbol{\sigma}_i$ are optimized directly for each training mesh; consequently, this component constitutes a variational auto-decoder rather than a conventional variational autoencoder.

3.4 Sparse Multi-View Encoder

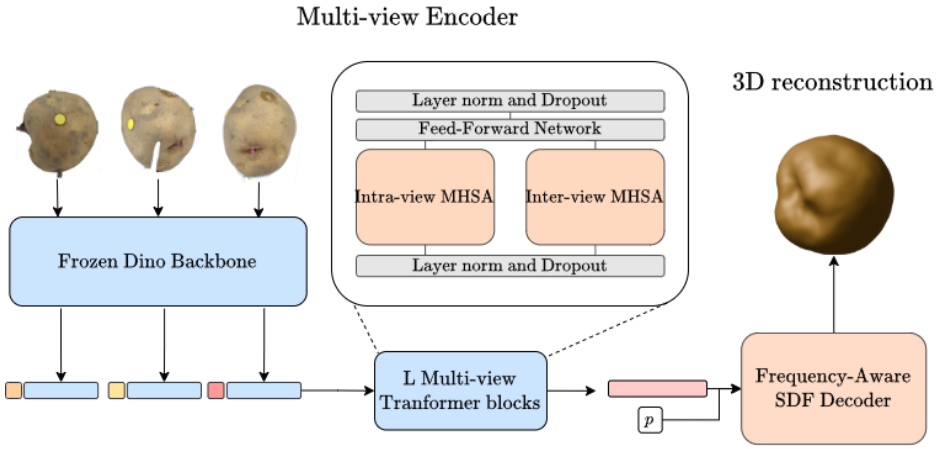


Figure 3: Architecture of our full pipeline

The multi-view encoder maps a variable-size set of RGB observations, $\mathcal{I}_i = \{I_i^1, \dots, I_i^V\}$, to a single latent estimate $\hat{\mathbf{z}}_i \in \mathbb{R}^{256}$. A frozen pretrained DINOv2 backbone [20] independently extracts patch-level features from each image. Freezing the backbone reduces the number of trainable parameters and preserves the general-purpose visual representation learned during self-supervised pretraining.

The resulting tokens are processed by four view-factorized Transformer blocks. Each block first models relationships between tokens belonging to the same image and then exchanges contextualized information across views. This factorization separates local image understanding from multi-view information fusion while avoiding the cost of applying unrestricted attention to all tokens simultaneously. Finally, a learnable latent query attends to the fused token sequence and produces the predicted shape code $\hat{\mathbf{z}}_i$.

The encoder receives neither depth measurements nor extrinsic camera parameters. In this work, “unposed” therefore means that camera poses are not provided to the reconstruction network; the architecture does not contain a separate pose-estimation module. Randomizing the input order during training discourages reliance on the conveyor acquisition sequence and promotes robustness to unordered observations.

3.5 Two-Stage Training Strategy

Training is divided into two principal stages. The first learns the variational geometric prior from complete tuber meshes, whereas the second maps sparse RGB observations into the resulting latent space. In Stage 1, the SIREN decoder, FiLM mapping network, and per-tuber variational parameters are optimized jointly. For each sampled latent code and set of spatial queries, the objective is

$$\mathcal{L}_{\text{prior}} = \mathcal{L}_{\text{SDF}} + \lambda_{\text{eik}}\mathcal{L}_{\text{eik}} + \beta_{\text{KL}} D_{\text{KL}}\big(q_i(\mathbf{z}) \parallel \mathcal{N}(\mathbf{0}, \mathbf{I})\big).$$

The signed-distance term $\mathcal{L}_{\text{SDF}}$ is the mean absolute error between predicted and reference distances. The Eikonal term penalizes deviations of the spatial-gradient norm from one, encouraging the predicted field to retain the properties of a signed distance function. The KL divergence regularizes the instance distributions toward a common Gaussian prior. It discourages

isolated and unbounded latent codes and thereby promotes a compact latent space in which neighboring representations tend to decode into smoothly varying tuber geometries. This regularization encourages, rather than formally guarantees, meaningful latent interpolation.

Once the geometric prior has been learned, the decoder and FiLM mapping network are frozen. Stage 2 follows the image-to-latent training strategy introduced by SDFFormer [16]. It begins with latent regression, in which the multi-view encoder predicts the optimized posterior mean $\boldsymbol{\mu}_i$ associated with each training tuber:

$$\mathcal{L}_{\text{latent}} = \|\hat{\mathbf{z}}_i - \boldsymbol{\mu}_i\|_2^2.$$

This initialization teaches the encoder to locate an observed tuber within the learned shape space. The encoder is then fine-tuned through the frozen decoder using direct signed-distance supervision:

$$\mathcal{L}_{\text{encoder}} = \mathcal{L}_{\text{latent}} + \lambda_{\text{SDF}}\mathcal{L}_{\text{SDF}}.$$

The second step makes the mapping geometry-aware: it corrects latent prediction errors that may be small in Euclidean latent distance but produce substantial displacements of the decoded surface.

3.6 Mesh Extraction and Simulation Interface

When an explicit geometric asset is required, the predicted SDF is evaluated on a regular three-dimensional grid, and its zero-level set is extracted using Marching Cubes [21]. The reconstructed surface can then be checked for disconnected components, self-intersections, and watertightness. A simplified collision mesh may also be generated to improve the stability and computational efficiency of contact simulation. Together, the surface and collision representations define an asset suitable for downstream simulation. Validation of simulated behavior against real-world observations is left for future work.

4/ EXPERIMENTAL PROTOCOL AND RESULTS

4.1 Evaluation Protocol

The evaluation is performed on the tuber-disjoint test subset of 3DPotatoTwin, comprising 51 tubers that are not observed during training. Surface accuracy is assessed using the symmetric Chamfer distance between point sets sampled from the reconstructed and reference meshes. The meshes are evaluated in the normalized coordinate system introduced during preprocessing, and the reported values are multiplied by 10^3. Lower values indicate closer agreement between the reconstructed and reference surfaces.

We compare the proposed method with DISN [12], which predicts an implicit surface from a single RGB image, and CoRe++ [4], which reconstructs potato geometry from an RGB-D observation. The methods differ in their input modalities and are therefore treated as application-level references rather than controlled architectural ablations. All values reported below use the same test split, normalization, surface-sampling procedure, and Chamfer-distance implementation.

4.2 Quantitative Results

Method	Input	CD $\times 10^3 \downarrow$
DISN [12]	Single RGB image	0.35
CoRe++ [4]	RGB-D observation	0.28
Ours	Sparse unposed RGB images	**0.15**

Table 1: Quantitative reconstruction results on the 51-tuber test set. Chamfer distance is reported in normalized units multiplied by 10^3; lower is better.

The proposed method obtains the lowest Chamfer distance, with a value of 0.15 compared with 0.28 for CoRe++ and 0.35 for DISN. These results correspond to relative reductions of 46.4% and 57.1%, respectively. The improvement indicates that the reconstructed point sets are, on average, more closely aligned with the reference tuber surfaces.

The comparison also highlights the benefit of combining information from multiple observations. DISN must infer the complete shape from a single RGB image, whereas CoRe++ supplements its color observation with depth. The proposed method instead aggregates complementary geometric evidence from several RGB views without requiring depth measurements or camera poses.

Because input modalities and view counts differ, the observed improvement cannot be attributed exclusively to the FiLM-modulated SIREN decoder. Controlled decoder and view-count ablations will be required to isolate the contribution of each component.

4.3 Qualitative Reconstruction Results

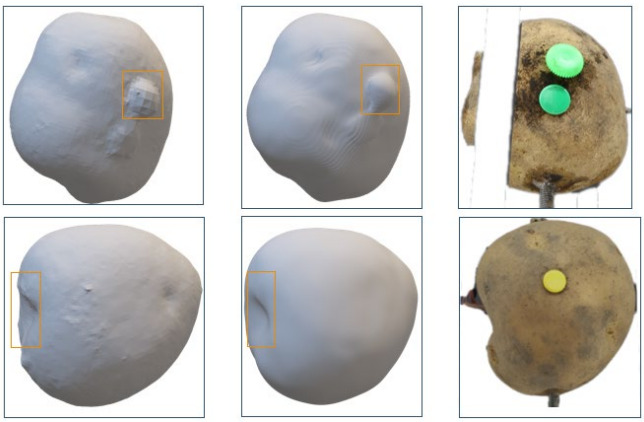


Figure 4: Qualitative comparison between reference potato meshes and reconstructions produced by the proposed method. From left to right: reference mesh, reconstructed mesh, and one of the six RGB images used as input. Orange boxes highlight challenging regions recovered by the method.

Figure 4 compares reference meshes with surfaces reconstructed by the proposed method. The reconstructions preserve the overall shape, elongation, and principal deformations of the tubers,

while the learned shape prior produces complete surfaces in regions that are only partially observed in the input images.
These qualitative results demonstrate the effectiveness of the reconstruction but also highlight a limitation: reconstructed tubers tend to be smoother than the reference meshes. This behavior is consistent with the regularizing effect of the learned latent shape space, which favors plausible surfaces but may suppress uncommon or weakly observed details. Future work could examine how the model hyperparameters influence this smoothing effect.

5/ DISCUSSION

The proposed method reduces the reported Chamfer-distance score from 0.35 for DISN and 0.28 for CoRe++ to 0.15. This represents an improvement of 57.1% over DISN and 46.4% over CoRe++, indicating a substantially closer average agreement between the reconstructed and reference surfaces. Complementary views and the learned shape prior plausibly contribute to this improvement. However, DISN uses one RGB image, CoRe++ uses RGB-D, and our method uses multiple RGB images; the comparison therefore evaluates complete systems rather than isolating the FiLM-modulated SIREN. Controlled decoder and view-count ablations remain necessary.

The dataset also covers only 339 tubers, three cultivars, and one acquisition system, while the pipeline assumes prior segmentation and cross-view association. Future evaluation should add per-tuber dispersion, F-score, normal-consistency, and mesh-validity measures and test new acquisition conditions. Isaac Sim import establishes asset compatibility, not physical fidelity: simulation parameters and resulting behavior must be validated through controlled experiments before claims about simulated dynamics or sim-to-real transfer can be made.

6/ CONCLUSION

This paper presented a method for reconstructing potato tubers from sparse, unordered, and unposed RGB images. A variational FiLM-modulated SIREN auto-decoder learns a continuous latent space of complete tuber geometries, while a view-factorized Transformer maps the available RGB observations into that space without depth measurements or camera extrinsics. The predicted signed distance field is converted into an explicit surface that can be exported for downstream simulation. On the 51-tuber test set, the method achieves 0.15 under the CD $\times 10^3$ reporting convention, compared with 0.35 for DISN and 0.28 for CoRe++. Future work will broaden the reconstruction evaluation and validate the generated assets within simulated and real-world environments.

ACKNOWLEDGEMENTS
This work was conducted as part of a CIFRE doctoral project involving Downs, IMT Nord Europe and LaMCube. The authors thank the 3DPotatoTwin team for making the paired potato dataset and associated reconstruction resources available. The authors also thank the technical staff who contributed to the acquisition and simulation platforms.

REFERENCES
[1] C. Wang and Z. Xiao, “Potato Surface Defect Detection Based on Deep Transfer Learning,” Agriculture, vol. 11, no. 9, art. 863, 2021. doi: 10.3390/agriculture11090863.
[2] M. Afonso and V. Giufrida, “Editorial: Synthetic Data for Computer Vision in Agriculture,” Frontiers in Plant Science, vol. 14, art. 1277073, 2023. doi: 10.3389/fpls.2023.1277073.
[3] C. Verdouw, B. Tekinerdogan, A. Beulens, and S. Wolfert, “Digital Twins in Smart Farming,” Agricultural Systems, vol. 189, art. 103046, 2021. doi: 10.1016/j.agsy.2020.103046.

[4] P. M. Blok, F. Magistri, C. Stachniss, H. Wang, J. Burridge, and W. Guo, “High-throughput 3D Shape Completion of Potato Tubers on a Harvester,” Computers and Electronics in Agriculture, vol. 228, art. 109673, 2025. doi: 10.1016/j.compag.2024.109673.
[5] H. Wang, P. M. Blok, J. Burridge, et al., “3DPotatoTwin: A Paired Potato Tuber Dataset for 3D Multi-sensory Fusion,” Plant Phenomics, vol. 7, no. 4, art. 100123, 2025. doi: 10.1016/j.plaphe.2025.100123.
[6] J. L. Schönberger and J.-M. Frahm, “Structure-from-Motion Revisited,” in Proc. IEEE CVPR, 2016, pp. 4104–4113.
[7] Y. Furukawa and C. Hernández, “Multi-View Stereo: A Tutorial,” Foundations and Trends in Computer Graphics and Vision, vol. 9, nos. 1–2, pp. 1–148, 2015. doi: 10.1561/0600000052.
[8] M. Tancik, P. P. Srinivasan, B. Mildenhall, et al., “Fourier Features Let Networks Learn High Frequency Functions in Low Dimensional Domains,” in Advances in Neural Information Processing Systems, vol. 33, 2020, pp. 7537–7547.
[9] B. Mildenhall, P. P. Srinivasan, M. Tancik, J. T. Barron, R. Ramamoorthi, and R. Ng, “NeRF: Representing Scenes as Neural Radiance Fields for View Synthesis,” in Proc. ECCV, 2020, pp. 405–421.
[10] J. J. Park, P. Florence, J. Straub, R. Newcombe, and S. Lovegrove, “DeepSDF: Learning Continuous Signed Distance Functions for Shape Representation,” in Proc. IEEE/CVF CVPR, 2019, pp. 165–174. doi: 10.1109/CVPR.2019.00025.
[11] L. Mescheder, M. Oechsle, M. Niemeyer, S. Nowozin, and A. Geiger, “Occupancy Networks: Learning 3D Reconstruction in Function Space,” in Proc. IEEE/CVF CVPR, 2019, pp. 4460–4470.
[12] Q. Xu, W. Wang, D. Ceylan, R. Mech, and U. Neumann, “DISN: Deep Implicit Surface Network for High-quality Single-view 3D Reconstruction,” in Advances in Neural Information Processing Systems, vol. 32, 2019, pp. 492–502.
[13] Z. Zhu, L. Yang, N. Li, C. Jiang, and Y. Liang, “UMIFormer: Mining the Correlations between Similar Tokens for Multi-View 3D Reconstruction,” in Proc. IEEE/CVF ICCV, 2023, pp. 18226–18235.
[14] L. Yang, Z. Zhu, X. Lin, J. Nong, and Y. Liang, “Long-Range Grouping Transformer for Multi-View 3D Reconstruction,” in Proc. IEEE/CVF ICCV, 2023, pp. 18257–18267.
[15] Z. Zhu, L. Yang, X. Lin, C. Jiang, N. Li, L. Yang, and Y. Liang, “GARNet: Global-Aware Multi-View 3D Reconstruction Network and the Cost-Performance Tradeoff,” Pattern Recognition, vol. 142, art. 109674, 2023. doi: 10.1016/j.patcog.2023.109674.
[16] A. Schockaert, H. Wannous, V. Magnier, J.-F. Witz, and G. Dufaye, “SDFFormer: Robust Continuous Surface Extraction from Sparse Unposed Images via Learned Geometric Priors,” manuscript submitted to the German Conference on Pattern Recognition (GCPR), 2026.
[17] N. Rahaman, A. Baratin, D. Arpit, et al., “On the Spectral Bias of Neural Networks,” in Proc. 36th ICML, PMLR 97, 2019, pp. 5301–5310.
[18] V. Sitzmann, J. N. P. Martel, A. W. Bergman, D. B. Lindell, and G. Wetzstein, “Implicit Neural Representations with Periodic Activation Functions,” in Advances in Neural Information Processing Systems, vol. 33, 2020, pp. 7462–7473.
[19] E. Perez, F. Strub, H. de Vries, V. Dumoulin, and A. Courville, “FiLM: Visual Reasoning with a General Conditioning Layer,” Proc. AAAI Conf. Artificial Intelligence, vol. 32, no. 1, 2018. doi: 10.1609/aaai.v32i1.11671.
[20] M. Oquab, T. Darcet, T. Moutakanni, et al., “DINOv2: Learning Robust Visual Features without Supervision,” Transactions on Machine Learning Research, 2024.
[21] W. E. Lorensen and H. E. Cline, “Marching Cubes: A High Resolution 3D Surface Construction Algorithm,” ACM SIGGRAPH Computer Graphics, vol. 21, no. 4, pp. 163–169, 1987. doi: 10.1145/37402.37422.
[22] A. Subeesh and N. Chauhan, “Agricultural Digital Twin for Smart Farming: A Review,” Green Technologies and Sustainability, vol. 4, no. 2, art. 100299, 2026. doi: 10.1016/j.grets.2025.100299.

[23] Z. Cai, C. Jin, J. Xu, and T. Yang, “Measurement of Potato Volume With Laser Triangulation and Three-Dimensional Reconstruction,” IEEE Access, vol. 8, pp. 176565–176574, 2020. DOI: 10.1109/ACCESS.2020.3027154.
[24] J. Liu et al., “Quantitative Potato Tuber Phenotyping by 3D Imaging,” Biosystems Engineering, vol. 210, pp. 48–59, 2021. DOI: 10.1016/j.biosystemseng.2021.08.001.
[25] B. Kerbl, G. Kopanas, T. Leimkühler, and G. Drettakis, “3D Gaussian Splatting for Real-Time Radiance Field Rendering,” ACM Transactions on Graphics, vol. 42, no. 4, art. 139, 2023. doi: 10.1145/3592433.
[26] C. B. Choy, D. Xu, J. Gwak, K. Chen, and S. Savarese, “3D-R2N2: A Unified Approach for Single and Multi-View 3D Object Reconstruction,” in Proc. ECCV, 2016, pp. 628–644.
[27] H. Xie, H. Yao, X. Sun, S. Zhou, and S. Zhang, “Pix2Vox: Context-Aware 3D Reconstruction From Single and Multi-View Images,” in Proc. IEEE/CVF ICCV, 2019, pp. 2690–2699.
[28] Q. Su, N. Kondo, M. Li, H. Sun, and D. F. Al Riza, “Potato Feature Prediction Based on Machine Vision and 3D Model Rebuilding,” Computers and Electronics in Agriculture, vol. 137, pp. 41–51, 2017. doi: 10.1016/j.compag.2017.03.020.
[29] NVIDIA Corporation, “NVIDIA Isaac Sim,” [Online]. Available: https://developer.nvidia.com/isaac/sim. Accessed: Sep. 14, 2026.

Scenario Generation and Autonomous Control for High-Precision Vineyard Operations in Virtual Environments

Claudio Maroni[a,*], Marco E. Pezzola[a], Elisabetta Leo[a], Farouk El Farji[b,*], Thomas Karasiewicz[b]

[a]Soluzioni Ingegneria, Lecco, Italy
[b]IPG Automotive France, Vélizy-Villacoublay, France
* Corresponding author. Email: claudio.maroni@si-ita.it, farouk.el.farji@ipg-automotive.com

Abstract

The increasing demand for agricultural automation requires efficient and reliable methods for developing and validating autonomous systems. In vineyards, traditional field testing is costly, time-consuming, and affected by safety constraints and environmental variability. This study presents a repeatable simulation-based methodology for autonomous tractor operations, combining realistic vineyard scenario generation with sensor-driven control strategies.

A high-fidelity digital vineyard is developed from geo-referenced data, reproducing terrain elevation, slope, camber, vine-row geometry, and surface irregularities. The simulation framework integrates IPG Automotive TruckMaker and the AgriSI platform developed by Soluzioni Ingegneria through a co-simulation approach, enabling realistic modelling of vehicle dynamics, tyre–soil interaction, and sensor behaviour.

An autonomous control architecture based on a state machine manages idle, in-row navigation, and U-turn phases. Model Predictive Control (MPC) is employed for lateral and longitudinal control, using ultrasonic sensors for in-row positioning and GNSS-IMU information for U-turn manoeuvres..

The framework enables systematic testing under different terrain conditions, plant maturity, soil roughness, sensor configurations, and localization errors. This controlled and repeatable environment supports the identification of performance limitations and optimization of autonomous driving strategies before field deployment.

The results demonstrate that combining high-fidelity virtual environments with MPC-based control provides a robust and scalable approach to autonomous vineyard navigation, reducing the need for extensive field testing while enabling realistic evaluation under complex operational conditions.

KEYWORDS: Precision Farming, Vineyards, Scenario Generation, Autonomous Driving, Simulation, Virtual Testing

Complexity level: 4

1/ INTRODUCTION

Throughout history, viticulturists have faced significant challenges inherent to grape cultivation. However, in recent decades, an agricultural revolution powered by technological advancements

has enabled faster, more precise, and safer management of plant health. This transformation has spurred research into new approaches to further accelerate progress in the field. The agricultural market is rapidly evolving to meet global demands, with Precision Farming (PF) leading the way. Specifically, PF focuses on maximizing output while minimizing input [1], addressing critical global issues such as population growth [2], environmental impact [3], and the effects of geopolitical events [4]. Furthermore, it tackles the urgent need to reduce energy consumption, labor requirements [5], and the use of chemicals, in line with modern regulatory guidelines [6]. In essence, PF is an agricultural approach aimed at increasing productivity while minimizing energy, labor, chemical inputs, land use, and overall resource consumption.

In this context, agricultural tractors play a pivotal role in inspecting vineyards and providing farmers with accurate crop status and yield estimations. Sensor systems are essential tools for achieving this goal. combiningance, the VinBot system employs 2D laser sensors and cameras [7], while the VineRobot combines ultrasound, fluorescence, and camera sensors with Artificial Intelligence [8]. Other examples include the integration of 3D vision, Light Detection and Ranging (LiDAR), and ultrasonic sensors for precision canopy management [9], as well as systems focused exclusively on LiDAR technology for geometric evaluation of vegetation [10].

The success of PF also hinges on the ability to autonomously navigate fields, reducing farmer intervention and improving application precision by minimizing the unpredictability of human behavior. Autonomous driving performance depends on the choice of controller algorithms and the feedback sensors. Various methods are proposed in the literature for row-following and headland turns.

Developing autonomous driving algorithms through field testing is risky, time-consuming, and costly. Consequently, simulation technology has emerged as a transformative tool in vineyard management, overcoming seasonal limitations and providing a safe environment for precise scenario testing [11]. Simulation offers researchers a powerful resource to refine vineyard strategies, enhance efficiency, experiment with new tools, and ensure the sustainability of the agricultural sector [12, 13, 14]. To achieve higher fidelity a co-simulation framework utilizing TruckMaker [15] and AgriSI [16] which provides robust vehicle dynamics modeling (18-DOF), customizable terrain scenarios, and efficient sensor integration can be used [17].

This paper introduces a repeatable simulation-based methodology for autonomous tractor operations in vineyards. The primary contributions of this work include:

- a systematic methodology for creating highly realistic 3D virtual simulation scenarios from actual geo-referenced data;
- an efficient state-machine-based control architecture utilizing Model Predictive Control (MPC) for both in-row straight-line navigation and end-row U-turn maneuvers;
- a detailed quantitative analysis evaluating the individual and combined impacts of micro- and macro-terrain irregularities on localization and path-following performance.

2/ MATERIALS AND METHODS

2.1 Scenario Creation for Simulation

The development of a realistic virtual simulation environment is designed to mimic the physical behavior of a real tractor equipped with sensors operating in a vineyard. The process begins with the selection of a geo-referenced field from a 2D map. Based on this input, the algorithm generates the elevation profile of the cultivated terrain by leveraging the GIS API, which provides

the altitude data for points within the selected field. Additionally, using the field's corner positions, the start and end points of the first vine row, and the nominal distance between rows as inputs, the algorithm automatically positions the individual vine plants. Figure 1 illustrates a comparison between the actual plant distribution and the computed plant placement generated by the algorithm.

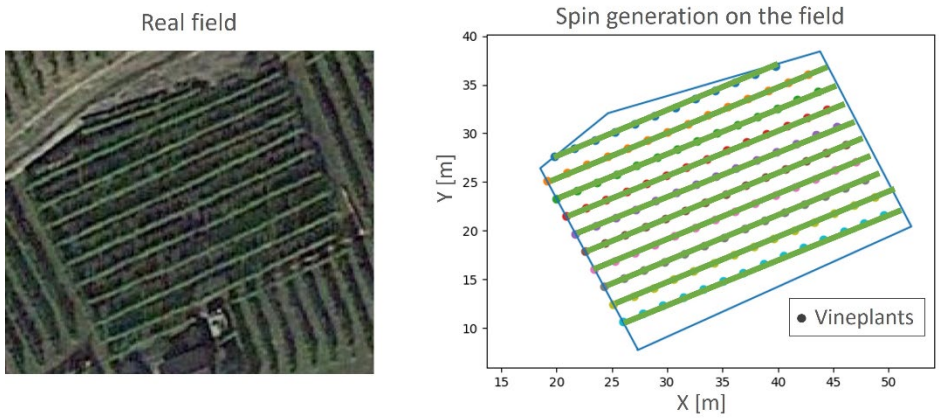


Figure 4 - Comparison of the real plant distribution with the spin generation.

Once the 2D plant positions are determined, their heights are assigned using the elevation data extracted from the GIS API. The digital twin of the vineyard is built inside AgriSI. This tool, in co-simulation with IPG TruckMaker, incorporate a highly realistic 18-DOF vehicle model, simulate detailed tire-soil interactions, and mimic virtual sensor behaviors. A perspective view of the generated digital twin is presented in Figure 3.

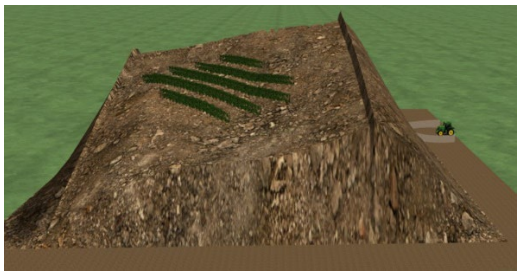


Figure 5 - Perspective view of the digital twin in AgriSI.

The virtual vineyard includes grapevine models representing three distinct vegetative maturity levels. As plants mature, their leaf density and canopy width increase, as depicted in Figure 4. The width of the vegetation directly impacts the distance measurements acquired by the virtual ultrasonic sensors integrated on both sides of the tractor.

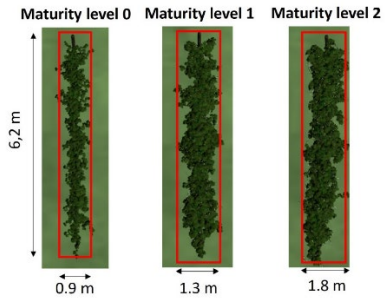


Figure 6 - Vine plant width as a function of the vegetative maturity level.

To evaluate the proposed control architecture under challenging conditions, the simulation scenario was configured to replicate a demanding vineyard layout. The vine rows are arranged following a parabolic distribution to introduce a curved reference trajectory. Additionally, the simulation incorporates plants with varying maturity levels randomly distributed throughout the field. Figure 5 illustrates the overall layout, highlighting the plant distribution and the optimal path that the tractor must follow. The reference trajectory accounts for local variations due to plant maturity, keeping the tractor centered between active rows, while the U-turns are automatically planned at the endpoints of each straight segment.

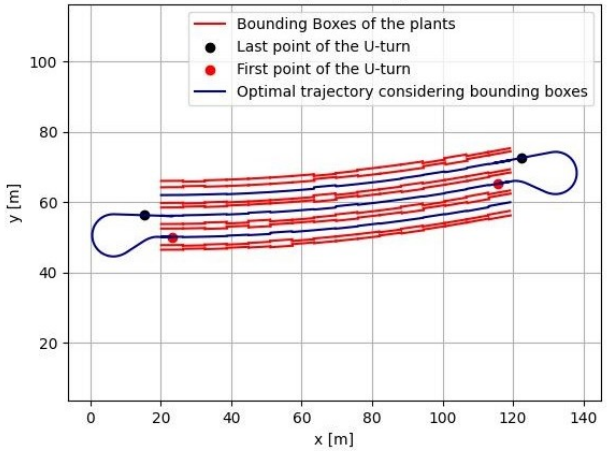


Figure 7 - Complete nominal trajectory to be followed in the testing scenario.

The 3D terrain morphology is generated by combining macro-irregularities: elevation, slope, and camber profiles. The elevation profile represents vertical height changes along the longitudinal axis (X), ranging from 0 to 10 m. The slope profile describes the gradient along the lateral axis (Y), starting from an initial elevation and modifying the terrain up to a maximum lateral slope of 0.05 m/m. The camber profile represents the transverse tilt of the terrain, simulating the inclination from the center-line to the edge, with a maximum value of 0.0005 m/m^2. Resulting complete 3D surface is shown in Figure 6.

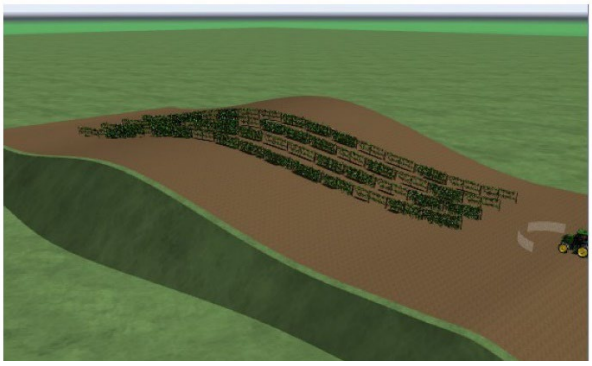


Figure 8 - Complete 3D trajectory of the tractor in the simulated vineyard scenario.

In addition to macro-profiles, variations in soil roughness were introduced to analyze the impact of micro-irregularities on control performance. These micro-irregularities are modeled as sinusoidal waves applied throughout the field, rotated by 60 degrees to generate continuous lateral forces on the vehicle. The wave period is set to 1 m, and the amplitude values range from 0.025 to 0.065 m. Table 1 summarizes the parameters of the sinusoidal wave roughness.

Table 6 - Parameters of the sinusoidal wave soil roughness.

Parameter	Value
Rotation around z-direction [deg]	60
Height in z-direction (amplitude) [m]	0.025 to 0.065
Wave period [m]	1.0

2.2 Model Predictive Control (MPC) Framework

The control framework is designed to autonomously navigate a tractor along vineyard rows and execute U-turn maneuvers to transition between rows, accounting for the impact of uneven terrain. The framework employs a Model Predictive Control (MPC) approach [18] implemented using MATLAB and Simulink, and validated through co-simulation with AgriSI and TruckMaker. To compute optimal control actions, the MPC leverages a linearized 3-DOF vehicle model, which is well-suited for vineyard navigation due to the tractor's low operational speeds. The physical reference vehicle is the John Deere 6R 120 tractor [19].

To manage the overall vineyard navigation, the decision-making algorithm is implemented as a state machine with three distinct operational states, as illustrated in Figure 7:

- **Idle State**: This phase lasts for the first few meters of simulation to ensure that the virtual environment is fully loaded and that the tractor is correctly positioned. During this state, the MPC is inactive, and the steering angle remains zero.
- **Straight State**: During this phase, the tractor autonomously navigates between the plant rows. It uses lateral feedback from local ultrasonic sensors to calculate lateral distances and adjust its steering to maintain an equal distance from both row walls.
- **U-Turn State**: Triggered at the end of a row, this state manages the out-of-field transition and execution of the U-turn to align the vehicle with the next row. It relies on absolute positioning sensors (GNSS-IMU) to follow a predefined trajectory.

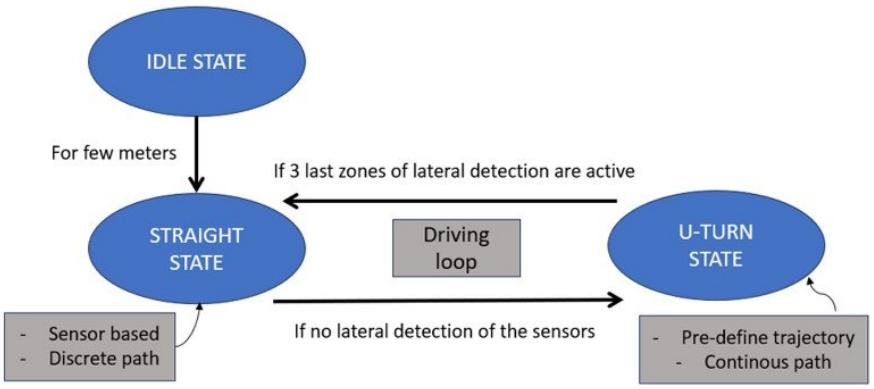


Figure 9 - State machine logic for autonomous vineyard navigation.

In the Straight State, the tractor's target speed is maintained constant at 15 km/h, and control is executed using the Simulink 'Lane Keeping Assist' (LKA) block [20]. To create a robust reference centerline path, the range of the ultrasonic sensors is divided into seven longitudinal detection zones on each side of the tractor. This allows the system to filter out individual plant gaps and calculate a smooth centerline. The controller continuously adjusts the steering angle to minimize

the lateral deviation (e1) and relative yaw angle (e2) with respect to this centerline. A schematic of this controller operation is shown in Figure 8.

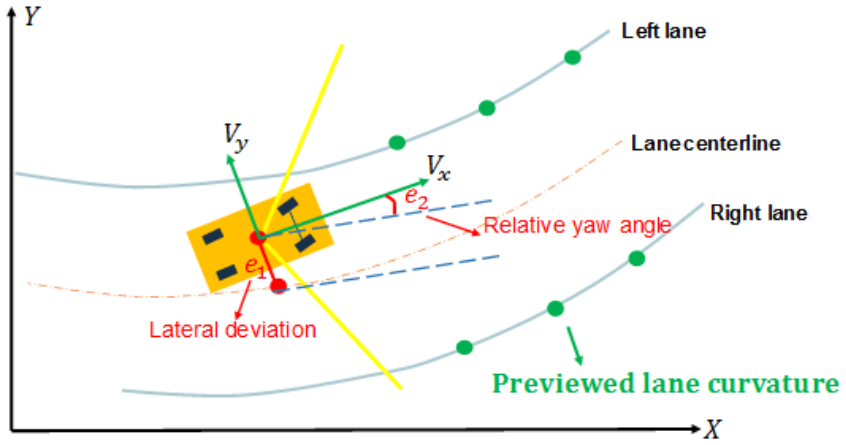


Figure 10 - Schematic of the centerline-following MPC controller in the Straight state.

The transition from the Straight to the U-Turn State is triggered when local sensors no longer detect vegetation on either side of the tractor, indicating that the end of the filare has been reached. During the U-turn, the tractor's speed is automatically reduced to 5 km/h to enable a tight turning radius. For this state, the 'Path Following Control System' block [21] is activated, combining lateral path following with longitudinal speed control. The predefined reference path is positioned and oriented according to the last valid coordinate of the straight state. The U-turn is considered complete, triggering a transition back to the Straight State, when the three furthest detection zones of the local sensors detect the start of the next row.

2.3 Sensor Systems and Localization

This section details the implementation of the sensors used for relative and global positioning. For relative in-row positioning (Straight State), virtual ultrasonic sensors based on the 'Free Space' model in AgriSI are employed. These sensors detect the bounding box of the nearest vine vegetation. A simulation of an ideal tractor driving perfectly along the row centerline was analyzed to evaluate sensor accuracy. Figure 9 compares the actual canopy widths with those detected by the Free Space sensors.

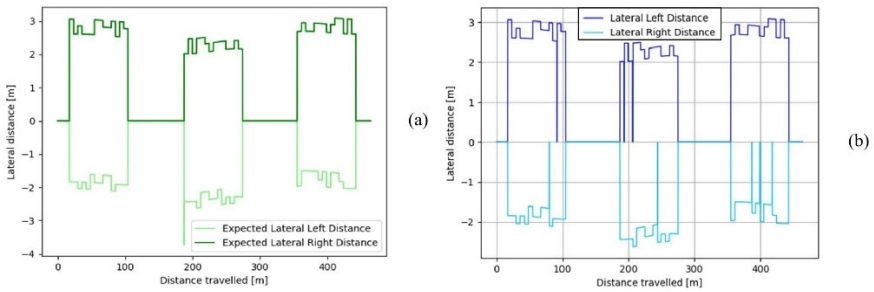


Figure 11 - Lateral distance measurements: expected (a) vs. virtual sensor detections (b).

By combining the sensor measurements with the vehicle's geo-referenced coordinates, the width and spatial density of the canopy can be recreated. The accuracy is evaluated using the percentage of correct width estimations (Pi) for each maturity level, where the actual plant width serves as the ground truth. The Free Space sensor achieved detection accuracies of 89%, 92%,

and 94% for vegetative maturity levels 1, 2, and 3, respectively, confirming its suitability for in-row lateral control.

For global localization (U-Turn State), three distinct estimation methodologies were investigated and compared:

- **Open-Loop Analytical Model**: This method integrates the 3-DOF equations of motion using the tractor's control inputs. Although highly accurate during initial phases, accumulated errors due to tire slip, terrain irregularities, and noise cause significant drift over time, making it unreliable for extended maneuvers.
- **GNSS-Only Estimation**: A standard GNSS model provides the absolute X-Y position of the vehicle. However, to determine the heading (yaw angle), a moving average filter must be applied to consecutive position coordinates to estimate the trajectory angle. While X-Y tracking is reasonably precise, the estimated heading is extremely noisy and biased.
- **GNSS-IMU Sensor Fusion**: An Inertial Measurement Unit (IMU) is added to measure the yaw rate, which is integrated over time to provide a smooth and accurate yaw angle. Since tractor operational speeds in vineyards are low, the integrated yaw rate provides an exceptionally stable heading, matching the real vehicle orientation with high precision.

Based on these results, the GNSS-IMU configuration was selected as the baseline global sensor setup for all subsequent closed-loop simulations.

3/ RESULTS AND DISCUSSION

To evaluate the tracking performance of the proposed control architecture under realistic operational conditions, the lateral deviation of the tractor from the reference centerline is calculated at each simulation step. The global performance of the trajectory-tracking algorithm is quantified using the Root Mean Square Error (RMS) calculated over the entire simulation duration.

3.1 Influence of Positioning Sensors

An initial set of simulations was conducted in a simplified virtual environment that excluded terrain slopes and soil roughness, comparing the closed-loop performance using the GNSS-IMU sensor configuration against an 'ideal' scenario with perfect state knowledge. The results are divided into the Straight and U-turn phases (Figure 10). The comparison revealed that localization errors and absolute state estimation delays have a significant impact on the U-turn phase, where the lateral error RMS increased. In contrast, the impact on straight-line performance is minimal, as straight-line guidance depends primarily on the relative measurements of the local ultrasonic sensors. However, a small increase in lateral error at the start of the straight rows is observed, caused by heading and lateral offsets inherited from the U-turn exit.

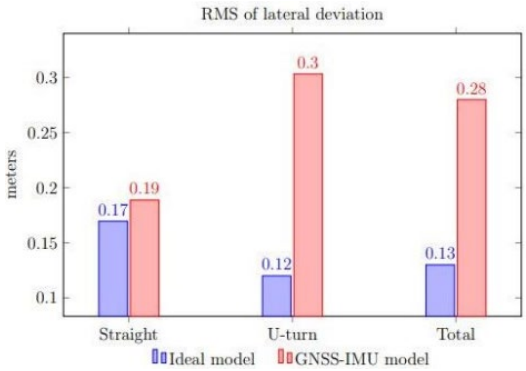


Figure 12 - Comparison between the ideal and the GNSS-IMU model performance in terms of RMS of lateral deviation

3.2 Influence of Soil Roughness

The second analysis examined the impact of micro-irregularities on a flat terrain, using the GNSS-IMU sensor configuration. As the roughness height (sinusoidal wave amplitude) increased from 0.025 to 0.065 m, path-following accuracy decreased, as shown in Figure 11

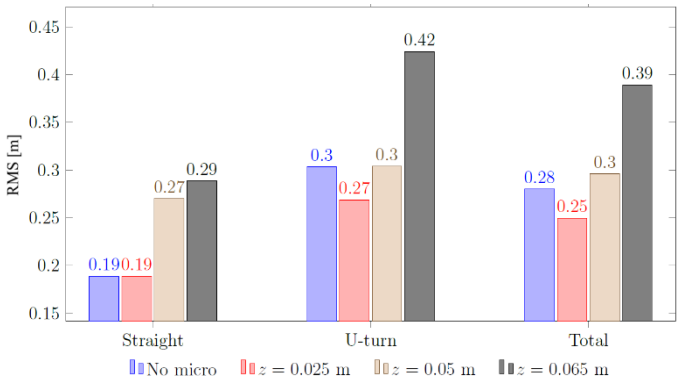


Figure 13 - Analysis of the effect of micro-irregularities, in the GNSS-IMU model, on the RMS of lateral deviation

3.3 Influence of 3D Terrain Profile

The third comparison incorporated macro-irregularities (elevation, slope, and camber profiles) while neglecting micro-roughness. The results showed a strong correlation between tracking errors and macro-terrain variations. The continuous lateral slopes (up to 0.05 m/m) and banking profiles introduce persistent lateral gravitational forces that pull the vehicle downhill. Unlike the localized disturbances caused by micro-roughness, macro-irregularities cause a uniform reduction in performance, degrading tracking precision similarly in both the Straight and U-turn phases (Figure 12).

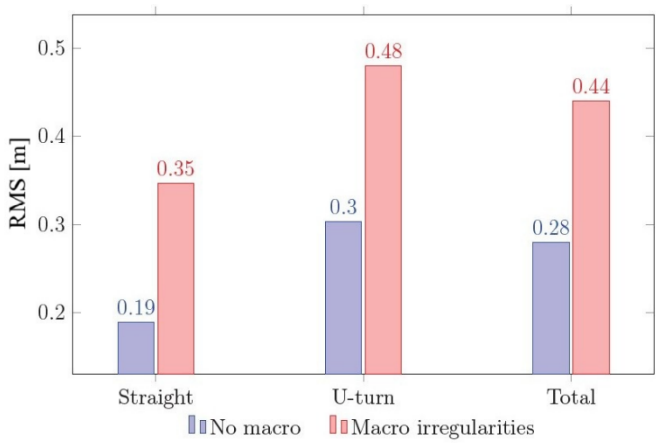


Figure 14 - Analysis of the effect of macro-irregularities, in the GNSS-IMU model, on the RMS of lateral deviation

3.4 Combined Influence of Micro- and Macro-Irregularities

To evaluate the MPC controller under fully realistic conditions, simulations were conducted in an environment combining both macro-slopes and micro-roughness. The tracking performance under four conditions (Combined 0.025 m roughness, Combined 0.05 m roughness, Macro-Only, and Flat Terrain) was compared. Interestingly, the introduction of low-level micro-roughness

(0.025 m amplitude) slightly improved tracking performance during both straight-line and turning maneuvers. This localized phenomenon is likely due to an increase in tire grip and lateral traction under the specific contact mechanics model of AgriSI. In contrast, when the roughness amplitude was increased to 0.05 m, significant trajectory deviations occurred during the U-turn phase, whereas the Straight phase remained highly robust. This difference arises because the Straight controller relies on real-time relative distance measurements to adjust to local conditions, while the U-turn controller relies on a predefined trajectory in the global frame, making it more sensitive to integrated sensor noise and mechanical disturbances.

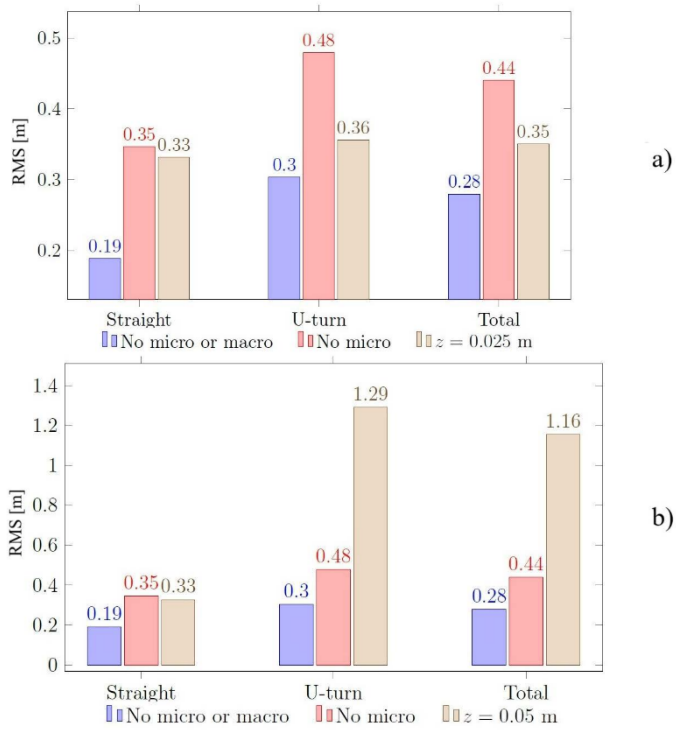


Figure 15 - Analysis of the combined effect of roughness and macro irregularities, in the GNSS-IMU model, on the RMS of lateral deviation. Considering low rougheness (a) and high roughness (b) levels

4/ CONCLUSIONS

This research establishes a comprehensive and repeatable methodology for the virtual prototyping and validation of autonomous agricultural tractors operating in high-precision vineyard environments. By leveraging advanced simulation software, specifically TruckMaker coupled with the AgriSI multi-physics suite, this study successfully designed a high-fidelity digital twin of a real vineyard. This virtual environment accurately reproduced critical three-dimensional topographical features including altitude profiles, banking, and camber, as well as the precise geometric positioning and varying maturity levels of the vine rows. Consequently, this framework provides a highly realistic, scalable, and safe platform for testing complex autonomous driving algorithms and sensor behaviors, effectively bypassing the seasonal constraints, logistical bottlenecks, and safety risks inherent to physical field trials.

A major contribution of this work is the development of an efficient control architecture based on a finite-state machine, utilizing a Model Predictive Control (MPC) algorithm to govern the optimal control actions. The navigation logic effectively divides the autonomous operation into distinct phases. For in-row navigation, the system relies on a cost-effective suite of virtual ultrasonic sensors to continuously evaluate lateral distances to the plant canopy. For out-of-field headland maneuvers, where local lateral references are absent, the architecture transitions to a global

positioning approach, employing a combination of GNSS and IMU measurements to estimate the vehicle's position and orientation during U-turns. This minimal-sensor configuration successfully balances high trajectory-following precision with economic viability.

Extensive simulation campaigns highlighted the system's robustness while revealing crucial insights into the impact of terrain irregularities. The performance of the control architecture is heavily dependent on the trajectory-following approach applied. In the straight-line phase, the ultrasonic-based reactive control exhibited high resilience to global localization errors and micro-irregularities (soil roughness), though it demonstrated a distinct sensitivity to severe lateral slopes. In contrast, the U-turn maneuvers which rely on executing a pre-defined continuous trajectory were found to be highly vulnerable to both state estimation drift and high-amplitude micro-irregularities. The accuracy of localization sensor data proved to be the most critical factor during these headland turns, underlining the limitations of open-loop path tracking in highly uneven agricultural environments.

Ultimately, this paper represents a significant foundational step toward developing a comprehensive, faster-than-real-time framework for simulating autonomous agricultural machinery. The ability to rapidly and automatically iterate through diverse operational scenarios offers immense value for the future of Precision Farming. Promising directions for future research include the exploration of advanced filtering techniques, such as Extended Kalman Filters, to better mitigate sensor noise and handle complex 3D dynamics. Furthermore, incorporating more sophisticated virtual perception systems, like simulated camera-based vision, and conducting extensive experimental field campaigns will be essential steps to bridge the gap between simulation and reality, fully validating the digital twin's realism and the controller's real-world applicability.

REFERENCES

1. Patil, S.S.; Bhalerao, S. A. Precision farming: The most scientific and modern approach to sustainable agriculture. Int. Res. J. Sci.Eng. 2013, 1, 21–30.
2. De Wrachien, D.; Schultz, B.; Goli, M. B. Impacts of population growth and climate change on food production and irrigation and drainage needs: A world-wide view. Irrig. Drain. 2021, 70, 981–995.
3. Pendrill, F.; Gardner, T. A.; Meyfroidt, P.; Persson, U. M.; Adams, J.; Azevedo, T.; Bastos Lima, M. G.; Baumann, M.; Curtis, P. G.; De Sy, V. Disentangling the numbers behind agriculture-driven tropical deforestation. Science 2022, 377, eabm9267.
4. Glauben, T.; Svanidze, M.; Götz, L.; Prehn, S.; Jamali Jaghdani, T.; Đuri´c, I.; Kuhn, L. The war in Ukraine, agricultural trade and risks to global food security. Intereconomics 2022, 57, 157–163.
5. Karahan, M.; Abay, C.; Ito, R. Determining Factors of Retaining Young Farmers in Agriculture: A Case study in Turkey and Japan. Agris -Line Pap. Econ. Inform. 2023, 15, 41–54.
6. European Commission. From Farm to Fork: New Regulations to Reduce Risk and Pesticide Use in the EU; European Commission—Questions and Answers; European Commission: Brussels, Belgium, 2022.
7. Lopes, C. M.; Torres, A.; Guzman, R.; Graça, J.; Reyes, M.; Vitorino, G.; Braga, R.; Monteiro, A.; Barriguinha, A. Using an unmanned ground vehicle to scout vineyards for non-intrusive estimation of canopy features and grape yield. In Proceedings of the GiESCO International Meeting, 20th, Sustainable Viticulture and Wine Making in Climate Change Scenarios, Mendoza, Argentina, 5–10 November 2017; GiESCO: Montpellier, France, 2017.
8. Diago, M. P.; Tardaguila, J. A new robot for vineyard monitoring. Wine Vitic. J. 2015, 30, 3. AgriEngineering 2025, 1, 0 21 of 21

9. Liu, H.; Yan, S.; Shen, Y.; Li, C.; Zhang, Y.; Hussain, F. Model predictive control system based on direct yaw moment control for 4WID self-steering agriculture vehicle. Int. J. Agric. Biol. Eng. 2021, 14, 175–181.
10. Bernad, P.; Lepej, P.; Rozman, ˇC.; Pažek, K.; Rakun, J. An evaluation of three different infield navigation algorithms. In Agricultural Robots-Fundamentals and Applications; IntechOpen: London, UK, 2019.
11. Rizzardo, C.; Katyara, S.; Fernandes, M.; Chen, F. The importance and the limitations of sim2real for robotic manipulation in precision agriculture. arXiv 2020, arXiv:2008.03983.
12. Luecke, G. R. Greenspace: Virtual reality interface for combine operator training. Presence 2012, 21, 245–253.
13. Shamshiri, R.; Hameed, I. A.; Pitonakova, L.; Weltzien, C.; Balasundram, S. K.; Yule, I. J.; Grift, T. E.; Chowdhary, G. Simulation software and virtual environments for acceleration of agricultural robotics: Features highlights and performance comparison. Chin. Soc. Agric. Eng. 2018, 11, 15–31.
14. Gutiérrez-Cejudo, J.; Lujak, M.; Fernández, A. Agrobots Architecture and Agrobots-Sim Simulator for Dynamic Agri-Robot Coordination. In Proceedings of the International Conference on Practical Applications of Agents and Multi-Agent Systems, Guimarães, Portugal, 12–14 July 2023; Springer: Berlin/Heidelberg, Germany, 2023; pp. 5–17.
15. IPG Automotive Group. TruckMaker. 2023. Available online: https://www.ipg-automotive.com/en/products-solutions/ software/carmaker/ (accessed on 21 May 2024).
16. Soluzioni Ingegneria. Available online: https://si-ita.it/products/agrisi (accessed on 1 January 2025).
17. Cheli, F.; Abdelaziz, A.K.M.; Arrigoni, S.; Paparazzo, F.; Pezzola, M. Precision Agriculture Applied to Harvesting Operations through the Exploitation of Numerical Simulation. Sensors 2024, 24, 1214. [CrossRef]
18. Yu, S.; Hirche, M.; Huang, Y.; Chen, H.; Allgöwer, F. Model predictive control for autonomous ground vehicles: A review. Auton. Intell. Syst. 2021, 1, 1–17.
19. John Deere 6120r, 2023. Available online: https://www.deere.com/en/tractors/utility-tractors/6-family-utility-tractors/6120r-utility-tractor/ (accessed on 1 June 2024).
20. MathWorks. Lane Keeping Assist System Using Model Predictive Control. Available online: https://it.mathworks.com/help/mpc/ug/lane-keeping-assist-system-using-model-predictive-control.html (accessed on 26 June 2024).
21. MathWorks. Path Following Control System. Available online: https://it.mathworks.com/help/mpc/ref/pathfollowingcontrolsystem.html (accessed on 26 June 2024).

Cyber Resilience for Connected Agricultural Machinery: From Digital Transformation to EU CRA Compliance

Luffy Lu[a,*]

[a] VicOne Inc., 11F, No. 198, Section 2, Tun Hwa South Road, Taipei, Taiwan (R.O.C.)
* Corresponding author. Email: luffy_lu@vicone.com

Abstract

Agricultural machinery is becoming increasingly software-driven, connected, and autonomous, expanding cybersecurity risks beyond individual machines to connected services, software supply chains, and long product lifecycles. This paper examines how this transformation affects agricultural machinery manufacturers under the Cyber Resilience Act (CRA; Regulation (EU) 2024/2847) and identifies the key cybersecurity and compliance challenges they face.
The analysis highlights three critical areas: maintaining visibility across complex component supply chains, managing evolving vulnerabilities throughout long machine lifecycles, and addressing CRA obligations alongside machinery safety requirements and emerging sector-specific cybersecurity standards. It finds that CRA compliance cannot be treated as a one-time, pre-market activity but requires continuous cybersecurity management across product development and post-market operations. The paper concludes that agricultural OEMs need an integrated lifecycle approach encompassing Secure by Design, Supply Chain Security, Risk Management, Continuous Monitoring, and Incident Reporting.

KEYWORDS: smart agriculture, autonomous systems, product cybersecurity, vulnerability management, software bill of materials, supply chain security

Complexity level: 3

1/ INTRODUCTION

Agricultural machinery is undergoing a technological shift from traditional mechanical equipment toward software-driven, connected, and increasingly autonomous systems. In the past, advances in agricultural machinery were driven primarily by improvements in mechanical design, power systems, and operational efficiency. Today, electronic controls, software, connectivity, sensors, and artificial intelligence are becoming increasingly important to how these machines operate and perform. As agricultural machinery becomes more software-driven, connected, and autonomous, its operation increasingly depends on the integrity and availability of software, data, and connectivity. [7]

This transformation builds on decades of development in precision agriculture. High-precision Global Navigation Satellite System (GNSS) and Real-Time Kinematic (RTK) positioning have enabled automated steering, path planning, and precision field operations. At the same time, telematics, cellular connectivity, and cloud platforms have transformed standalone machines into connected systems capable of continuous data exchange, remote monitoring, and fleet management. [7]

A pivotal development in recent years is the transition from technologies that primarily assist operators toward systems capable of perceiving their environment, making decisions, and executing tasks with greater autonomy. The convergence of computer vision, machine learning, and edge computing enables agricultural machinery to analyze sensor and camera data and make operational decisions in real time. John Deere describes this capability as “Sense & Act,” using cameras, edge computing, and machine learning to perceive the surrounding environment and respond accordingly. Its See & Spray technology, for example, uses onboard cameras to distinguish crops from weeds, determine where treatment is needed, and apply spray precisely. Processing takes place directly on the machine, enabling real-time decisions without complete dependence on cloud connectivity. [2]

These sensing and decision-making capabilities are becoming the foundation for higher levels of autonomous operation. AI, sensing, and control technologies are continuing to move agricultural machinery beyond operator assistance and automated functions toward semi-autonomous and autonomous field operations. [7] In 2026, this trajectory advanced further toward unmanned operation. Kubota introduced its next-generation Agri Robo Tractor MR Series, integrating GNSS/RTK-based autonomous operation, AI cameras, millimeter-wave radar, and cellular remote monitoring. The tractors can plan operating routes, detect people and obstacles, and perform field operations autonomously. Remote monitoring allows operators to leave the worksite while checking machine status and managing operations remotely. The series is scheduled for commercial release in Japan in 2027. [6]

As agricultural machinery becomes more dependent on software and connectivity, digital systems are also becoming increasingly involved in how machines perceive their environment, make operational decisions, and control physical actions. RTK positioning, cameras and sensors, electronic control units (ECUs), CAN/ISOBUS communications, and software-based control functions now form an interconnected architecture supporting critical field operations.

This deeper digital dependency changes the potential consequences of cybersecurity weaknesses and system disruptions. Positioning errors can cause machinery to deviate from intended routes or operating boundaries. Perception errors can affect how machinery identifies crops, people, or obstacles. Control disruptions can result in unintended machine behavior or interrupted operations. System unavailability can also lead to operational downtime, particularly during time-sensitive planting, spraying, or harvesting periods.

As more operational functions become software-controlled, the integrity and resilience of these digital systems become increasingly important to reliable and safe physical operation. Cybersecurity risk in agricultural machinery therefore needs to be considered at the system level, including which digital components support critical functions, how those components interact, and how weaknesses in one part of the system could affect the product as a whole.

At the same time, cybersecurity responsibilities are increasingly being formalized through regulation. The EU Cyber Resilience Act (CRA) establishes mandatory cybersecurity requirements for products with digital elements placed on the EU market and introduces lifecycle obligations covering secure design, vulnerability management, security updates, third-party components,

incident reporting, and post-market support. [4] For agricultural machinery manufacturers, these requirements intersect with increasingly complex product architectures, long machine lifecycles, and extensive reliance on third-party software and components.

The objective of this paper is to examine the cybersecurity challenges arising from the growing digital dependency of connected agricultural machinery and to analyze their implications under the EU Cyber Resilience Act. The analysis focuses on the expanding attack surface, third-party component and supply chain dependencies, long product lifecycles, and the practical challenges associated with implementing CRA requirements. Based on this analysis, the paper identifies five priorities for agricultural machinery manufacturers to strengthen lifecycle cyber resilience: Secure by Design, Supply Chain Security, Risk Management, Continuous Monitoring, and Incident Reporting.

2/ MATERIALS AND METHODS

This study applies a structured qualitative analysis to examine cybersecurity risks and regulatory requirements associated with connected and increasingly autonomous agricultural machinery. The analysis focuses on three areas: the evolving digital architecture and attack surface of agricultural machinery, cybersecurity challenges arising from third-party dependencies and long product lifecycles, and the implications of the EU Cyber Resilience Act (CRA) for agricultural machinery manufacturers.

2.1 Scope of Analysis

The analysis focuses on agricultural machinery that incorporates software, electronic control systems, connectivity, digital services, and increasingly autonomous functions. The scope includes onboard systems such as electronic control units (ECUs), embedded software, sensors, GNSS/RTK positioning, CAN/ISOBUS networks, and AI-enabled or autonomous functions, as well as external connectivity and supporting digital services.

Cybersecurity is considered from a product lifecycle perspective, covering product development, third-party component integration, market release, vulnerability management, security updates, and post-market support. Particular attention is given to the responsibilities of agricultural machinery manufacturers as product manufacturers and integrators of software and components supplied by third parties.

2.2 Technology and Attack Surface Analysis

The digital architecture of connected agricultural machinery is analyzed by grouping relevant technologies and interfaces into four attack surface areas:

- Onboard Systems: ECUs and embedded software, sensors and GNSS/RTK, CAN and ISOBUS networks, and AI and autonomous systems.
- Connectivity & Remote Interfaces: telematics, communication modules, and remote access.
- External Systems & Services: cloud services and APIs, farm management platforms, and remote monitoring and service platforms.
- Software & Update Channels: OTA updates and software and firmware distribution.

These areas are used to examine how increasing connectivity and software dependency extend the cybersecurity boundary beyond the physical machine. Interactions among onboard systems, remote interfaces, cloud services, and software distribution channels are considered to identify

where vulnerabilities or disruptions may affect machine operation and the broader product ecosystem.

2.3 Regulatory Analysis

The regulatory analysis focuses primarily on the EU Cyber Resilience Act and its requirements for products with digital elements. Relevant CRA provisions are examined in relation to the characteristics of connected agricultural machinery, including cybersecurity risk assessment, secure-by-design principles, component visibility and software bills of materials (SBOMs), third-party component due diligence, security testing, vulnerability management, security updates, support periods, vulnerability and incident reporting, technical documentation, and conformity assessment. [4]

The analysis also considers the broader regulatory and standardization landscape relevant to agricultural machinery, including the EU Machinery Regulation (EU) 2023/1230 [3] and ISO/DIS 24882 [5]. CEMA implementation guidance on the CRA is used to provide additional industry context regarding product scope, OEM–supplier relationships, vulnerability handling, and support periods. [1]

2.4 Analytical Framework

The analysis connects technological evolution with cybersecurity and regulatory implications through a lifecycle-oriented framework. First, the expanding digital architecture of agricultural machinery is examined to identify how software, connectivity, remote services, and update mechanisms broaden the cybersecurity attack surface. Second, third-party dependencies and long machine lifecycles are considered to assess challenges related to component visibility, vulnerability management, security updates, and ongoing support. Third, these challenges are mapped against relevant CRA requirements to identify practical implications for agricultural machinery manufacturers.

Based on this analysis, the resulting cybersecurity and compliance considerations are organized into five lifecycle priorities: Secure by Design, Supply Chain Security, Risk Management, Continuous Monitoring, and Incident Reporting.

3/ RESULTS AND DISCUSSION

3.1 Expanding Cybersecurity Attack Surface

The analysis shows that as agricultural machinery integrates more software, connectivity, and digital services, its attack surface increasingly extends beyond the machine itself. Onboard systems now interact with telematics, remote services, cloud platforms, and farm management applications, creating pathways through which data, commands, software, and updates move across the broader digital ecosystem.

The attack surface can be grouped into four areas:

Attack Surface Area	Examples
Onboard Systems	• ECUs & Embedded Software • Sensors & GNSS / RTK • CAN & ISOBUS Networks • AI & Autonomous Systems
Connectivity & Remote Interfaces	• Telematics • Communication Modules • Remote Access
External Systems & Services	• Cloud Services & APIs • Farm Management Platforms • Remote Monitoring & Service
Software & Update Channels	• OTA Updates • Software & Firmware Distribution

Table 1. Key Attack Surface Areas in Connected Agricultural Machinery

These systems are increasingly interconnected. Telematics connects field machinery with backend platforms for operational data exchange, monitoring, and remote services. Farm management platforms connect machine and operational data with cloud-based applications and external services. Over-the-Air (OTA) update mechanisms provide a pathway for distributing software and firmware to deployed systems.

As a result, the cybersecurity boundary of agricultural machinery can no longer be considered only at the level of individual onboard components. Security weaknesses affecting connectivity, backend services, remote access, or software distribution may also influence the cybersecurity of the final product. This broader attack surface increases the importance of understanding dependencies and interactions across the complete product architecture.

3.2 Supply Chain Cybersecurity Challenges

The attack surface extends further through the software and component supply chain. Agricultural machinery manufacturers integrate ECUs, controllers, firmware, open-source software, communication modules, and other technologies developed and maintained by third parties.

A vulnerability in any of these dependencies can introduce risk into the final product. An OEM may not develop every component in a machine, but it still needs sufficient visibility into third-party dependencies to understand and manage their impact on the cybersecurity of the final product.

This creates a particular challenge for agricultural machinery manufacturers because cybersecurity risk is not limited to software developed internally. Component information, vulnerability status, remediation activities, security updates, and support periods may depend on multiple suppliers. Product-level cybersecurity management therefore requires visibility across both internally developed and externally supplied components.

3.3 Long Machine Lifecycles and Fast-Moving Software Risks

Agricultural machinery may remain in operation for many years, while its software and digital components evolve much faster. New vulnerabilities can emerge, dependencies can become outdated, and third-party components can reach end of support long after market release.

As a result, a machine that is secure at release may not remain secure throughout its lifetime. Cybersecurity must therefore extend beyond pre-market testing to continuous vulnerability management, security updates, and lifecycle support.

These challenges are increasingly becoming regulatory responsibilities. CRA implementation guidance from the European Agricultural Machinery Association (CEMA) highlights many of the same issues, including product scope, OEM–supplier relationships, vulnerability handling, and support periods, underscoring the need to manage cybersecurity across both the supply chain and the product lifecycle. [1]

The combination of long machine lifecycles and continuously evolving software risks is particularly significant for agricultural machinery. Manufacturers need not only to identify vulnerabilities when products are developed, but also to determine how emerging risks will be assessed, remediated, and communicated after products have entered the market.

3.4 Implications of the EU Cyber Resilience Act

The EU Cyber Resilience Act establishes cybersecurity requirements for products with digital elements placed on the EU market. [4] For agricultural machinery manufacturers, this means determining whether and how the CRA applies to their products and, where applicable, managing cybersecurity throughout the product lifecycle.

These responsibilities extend from secure design and risk assessment to third-party component management, vulnerability handling, security updates, and post-market support. The findings above therefore have direct implications for how agricultural machinery manufacturers approach CRA compliance.

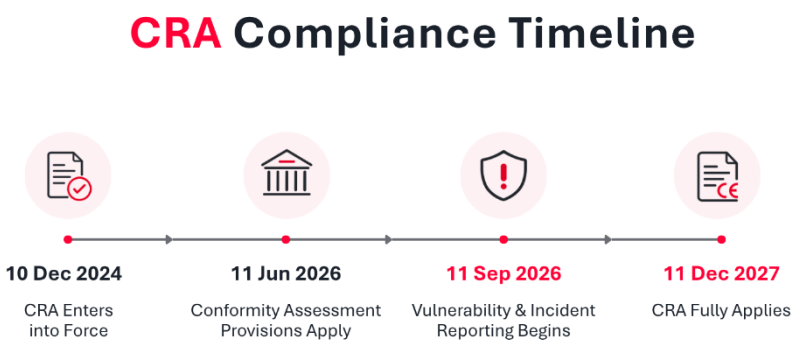


Figure 1. Timeline of key implementation milestones for the EU Cyber Resilience Act (CRA).

3.4.1 Key CRA Requirements for Agricultural Machinery Manufacturers

The CRA introduces cybersecurity requirements that extend across the product lifecycle, covering both the security properties of products and the processes manufacturers use to manage vulnerabilities. [4] For agricultural machinery manufacturers, the following requirements are particularly relevant given the growing use of software, connectivity, and third-party components in modern machines.

Key CRA Requirement	What It Means for Agricultural Machinery Manufacturers	CRA Reference
Cybersecurity Risk Assessment	Assess cybersecurity risks based on the product's intended purpose, reasonably foreseeable use, operating environment, and expected use, and use the assessment to guide design, development, production, delivery, and maintenance.	Art. 13(2)–(4)
Secure by Design & Default	Design and develop products with an appropriate level of cybersecurity, including secure configurations, access controls, data and command integrity, availability, attack-surface reduction, and appropriate mitigation mechanisms.	Art. 13(1)–(2); Annex I, Part I (1)–(2)
Component Visibility & SBOM	Identify and document product components and vulnerabilities, including an SBOM in a machine-readable format covering at least top-level software dependencies.	Annex I, Part II (1); Annex VII (2)(b)
Third-Party Component Due Diligence	Exercise due diligence when integrating supplier software, firmware, open-source software, and other third-party components, and address vulnerabilities affecting those components.	Art. 13(5)–(7)
Security Testing & Vulnerability Management	Regularly test and review product security and address and remediate identified vulnerabilities without delay based on the risks they pose.	Art. 13(8); Annex I, Part II (2)–(3)
Security Updates & Support Period	Ensure vulnerabilities are effectively handled throughout the support period and provide secure mechanisms for distributing security updates. The support period must generally be at least five years and should reflect the expected period of product use. For long-lived agricultural machinery, defining and maintaining an appropriate cybersecurity support period is therefore particularly important.	Art. 13(8)–(9); Annex I, Part I (2)(c); Part II (7)–(8)
Vulnerability & Incident Reporting	Establish processes to report actively exploited vulnerabilities and severe security incidents within the CRA's required reporting timelines, and inform affected users where required.	Art. 14(1)–(5)
Technical Documentation & Conformity	Maintain traceable evidence—including risk assessments, architecture, SBOM, vulnerability-handling processes, and security test results—and complete the applicable conformity assessment before issuing the EU Declaration of Conformity and CE marking.	Art. 13(12)–(13); Art. 28, 30–32; Annex VII–VIII

Table 2. Key CRA Requirements and Implications for Agricultural Machinery Manufacturers

For agricultural machinery manufacturers, these requirements extend beyond software developed in-house and continue after market release. CRA compliance therefore requires ongoing visibility into product components and supplier dependencies, together with processes for vulnerability handling, security updates, and compliance throughout the applicable support period.

3.4.2 Common Challenges in Achieving CRA Compliance

For agricultural machinery manufacturers, the challenge is not only understanding CRA requirements, but implementing them consistently across complex products, supplier ecosystems, and long operational lifecycles. Several practical challenges can make this particularly difficult.

- **Limited Software and Component Visibility**
  Maintaining an accurate view of software, firmware, dependencies, and versions across product variants is essential for SBOM management and vulnerability assessment.

  Key question: Can manufacturers identify what is deployed across their products?

- **Fragmented Supplier Security Information**
  Vulnerability, remediation, update, and support information may be distributed across multiple suppliers, making product-level impact assessment and remediation coordination more difficult.

  Key question: Can security information be consistently obtained and coordinated across suppliers?

- **Operational Constraints on Security Updates**
  Limited connectivity and time-critical agricultural operations can complicate the deployment of security updates without disrupting machine availability.

  Key question: Can updates be delivered securely without compromising operational continuity?

- **Operationalizing Vulnerability Handling and Reporting**
  CRA compliance requires manufacturers to coordinate vulnerability assessment, remediation, disclosure, and reporting across products and suppliers.

  Key question: Can vulnerabilities and incidents be handled within the required timelines?

Together, these challenges demonstrate that CRA compliance is not limited to implementing individual technical controls. It also requires manufacturers to establish processes that connect product architecture, supplier information, vulnerability management, update mechanisms, and regulatory reporting throughout the product lifecycle.

3.5 Cybersecurity in the Broader Agricultural Machinery Regulatory Landscape

CRA compliance does not exist in isolation. Agricultural machinery manufacturers also need to consider how product cybersecurity relates to machinery safety requirements and emerging sector-specific cybersecurity standards.

Regulation / Standard	Relevance to Agricultural Machinery
EU Cyber Resilience Act (CRA)	Establishes mandatory cybersecurity requirements for products with digital elements, covering secure design, vulnerability handling, security updates, reporting, and conformity throughout the product lifecycle.
EU Machinery Regulation (EU) 2023/1230	Establishes safety requirements for machinery, including protection against corruption or manipulation that could lead to hazardous situations or affect compliance with essential health and safety requirements.
ISO/DIS 24882	Addresses product cybersecurity engineering for agricultural machinery, tractors, and earth-moving machinery across the product lifecycle.

Table 3. Broader Regulatory and Standardization Landscape for Agricultural Machinery

Together, these developments reinforce the need to integrate cybersecurity with existing product development, safety, and compliance processes. For agricultural machinery manufacturers, cybersecurity is therefore becoming part of a broader product assurance framework rather than a standalone activity performed only before market release.

3.6 From CRA Requirements to Lifecycle Cyber Resilience: Five Key Priorities

The analysis indicates that CRA compliance for agricultural machinery requires a continuous approach connecting product development, supply chain security, risk management, and post-market operations. Based on the cybersecurity and regulatory challenges identified above, five priorities provide a lifecycle-oriented framework for strengthening cyber resilience.

3.6.1 Secure by Design

Integrate cybersecurity risk assessment and threat modeling into the product development lifecycle to identify potential attack paths, critical assets, and security requirements early in the design process. Security considerations should be reviewed as product architectures, software components, connectivity, and autonomous functions evolve.

Core question: Are cybersecurity risks addressed from the start?

3.6.2 Supply Chain Security

Establish automated Software Bill of Materials (SBOM) ingestion, vulnerability enrichment, and continuous component tracking across Tier-1 and Tier-2 suppliers. Maintain visibility into software versions, dependencies, known vulnerabilities, remediation status, and supplier support information throughout the product lifecycle.

Core question: Do we know what is inside our products?

3.6.3 Risk Management

Continuously assess identified vulnerabilities in the context of the actual product architecture, affected components, exposure, and potential operational impact. Prioritize remediation based on product-specific risk rather than vulnerability severity alone, enabling engineering teams to focus resources on vulnerabilities that pose meaningful risks to deployed products.

Core question: Which vulnerabilities pose real risks to our products?

3.6.4 Continuous Monitoring

Continuously monitor emerging vulnerabilities and changes affecting software and components used across deployed product variants. Maintain traceability between newly disclosed vulnerabilities and affected products so that manufacturers can reassess risk and initiate remediation or security updates when necessary.

Core question: How do we manage risks as they evolve over time?

3.6.5 Incident Reporting

Establish coordinated processes for vulnerability and incident assessment, remediation, disclosure, and regulatory reporting. Define clear responsibilities, escalation paths, and evidence collection procedures to support timely decisions and meet CRA reporting requirements when actively exploited vulnerabilities or severe security incidents are identified.

Core question: Can we respond and report within required timelines?

4/ CONCLUSIONS

Agricultural machinery is becoming increasingly dependent on software, connectivity, digital services, and third-party components. This transformation expands the cybersecurity boundary beyond the physical machine to include onboard systems, remote interfaces, cloud services, software distribution channels, and the broader component supply chain. At the same time, the long operational lifecycles of agricultural machinery create an ongoing challenge as software vulnerabilities, dependencies, and supplier support conditions continue to evolve after products enter the market.

The analysis shows that these characteristics have direct implications for compliance with the EU Cyber Resilience Act. CRA requirements extend cybersecurity responsibilities across the product lifecycle, including cybersecurity risk assessment, secure-by-design practices, component visibility and SBOM management, third-party component due diligence, vulnerability management, security updates, incident reporting, and technical documentation. For agricultural machinery manufacturers, meeting these requirements therefore depends not only on securing internally developed systems but also on maintaining sufficient visibility and coordination across suppliers and deployed products.

The findings identify five priorities for strengthening lifecycle cyber resilience: Secure by Design, Supply Chain Security, Risk Management, Continuous Monitoring, and Incident Reporting. Together, these priorities provide a structured approach for connecting product cybersecurity with CRA compliance across product development and post-market operations.

As agricultural machinery continues to become more connected, software-driven, and autonomous, cybersecurity can no longer be treated as a one-time activity performed before market release. It needs to become an integral part of how agricultural machinery is designed, developed, supported, and maintained throughout its lifecycle.

REFERENCES

[1] **CEMA**, CEMA Implementation Guidance on the EU Cyber Resilience Act (CRA 2024/2847), Version 1, December 2025.

[2] **Deere & Company**, "Sense & Act," John Deere.

[3] **European Parliament and Council of the European Union**, Regulation (EU) 2023/1230 of 14 June 2023 on machinery and repealing Directive 2006/42/EC of the European Parliament and of the Council and Council Directive 73/361/EEC, OJ L 165, 29 June 2023, p. 1.

[4] **European Parliament and Council of the European Union**, Regulation (EU) 2024/2847 of 23 October 2024 on horizontal cybersecurity requirements for products with digital elements and amending Regulations (EU) No 168/2013 and (EU) 2019/1020 and Directive (EU) 2020/1828 (Cyber Resilience Act), OJ L, 2024/2847, 20 November 2024.

[5] **International Organization for Standardization**, ISO/DIS 24882, Agricultural machinery, tractors, and earth-moving machinery — Product cybersecurity, Draft International Standard, Edition 1, under development.

[6] **Kubota Corporation**, "Kubota to Launch Unmanned Autonomous Tractors with Remote Monitoring Capabilities," 6 August 2026.

[7] **H. Prankl**, "Trends in Digital Systems and IT," DLG (German Agricultural Society), 22 September 2025.

Rollover Prevention Safety Device for Mobile Equipment

Bastien Laurent[a,*], Lama Al Bassit[a], Philippe Héritier[b], Roland Lenain[a]
[a] INRAE, UR TSCF, Université Clermont Auvergne, 63178 Aubière, France
[b] INRAE, UR TSCF, Université Clermont Auvergne, 03150 Montoldre, France
* Corresponding author. Email: bastien.laurent@inrae.fr

Abstract

In agriculture, rollover of mobile machines is one of the leading causes of work-related fatalities. For several years, the TSCF INRAE research unit has investigated the dynamic stability of off-road vehicles and developed algorithms for real-time estimation of metrics indicative of rollover risk. These algorithms have been validated through various projects. Building on previously obtained results, this paper presents a low-cost safety kit designed to assess rollover risk in real time. The kit combines inertial, GPS data with state-observer algorithms to reconstruct unmeasurable variables and computes lateral and longitudinal load-transfer ratio as indicators for rollover risk.

The estimated risk level is displayed to the operator via an onboard screen or, in autonomous systems, transmitted over a CAN bus to trigger corrective actions. Prototypes were field-tested on off-road vehicles, demonstrating the generality of the approach, its ability to estimate rollover risk without expensive instrumentation, and its ease of integration into vehicles. The proposed device provides a basis for a novel active-safety solution that can be fully integrated into vehicles, enabling autonomous corrective actions to mitigate rollover risk and help prevent accidents.

KEYWORDS: Mobile machine stability, Rollover risk reduction, Safety device, Risk estimation, active safety

Complexity level: 3

1/ INTRODUCTION

Among accidents involving agricultural and forestry tractors, rollover incidents are the most severe in terms of driver injuries and fatalities, accounting for approximately half of fatal accidents involving these types of machines (Abubakar et al., 2010), (Rondelli et al., 2018), (Wang et al., 2024).

Off-road vehicles rollover risk mitigation is currently based on rollover protective structure (ROPS) (Rondelli et al., 2010). These structures don't prevent accidents, but combined with seat belts, can reduce the damage on the driver and on the vehicle in case of accident. Many research and innovation work focusing on stability control of off-road vehicles to bring up new systems able to prevent, or reduce the occurrence, of rollover accidents.

Over the past several years, the TSCF research unit at INRAE has conducted extensive research on the dynamic stability of off-road vehicles and safety solutions aimed at mitigating rollover risks. (Bouton et al., 2007, 2008) proposed a dynamic modelling of wheeled all-terrain vehicles designed for dynamic stability analysis and an on-line rollover risk indicator dedicated to off-road vehicles considering the variation of tire/ground grip conditions. (Richier et al., 2011) proposed advanced observers and algorithms to estimate an on-line stability metric for all-terrain vehicles. The founding is applied to fast light vehicles (quad and mobile robots) navigating in environments with slopes and changing grip conditions. It allowed the development of strategies and solutions to manage vehicles' speeds to maintain its dynamic stability (Richier et al., 2012). Later on, Denis et al., 2016) adapted the previous approach and the developed algorithms to heavy reconfigurable vehicles having active suspensions. The same approach has then been validated on various types of off-road vehicles as part of several projects. Recently (Al Bassit et al., 2025) adapted the algorithms of on–line estimation of stability metrics on vehicles having mobile tools and so a complex internal dynamic. The rollover risk estimation algorithms developed by TSCF have been shown to be valid in several contexts at this stage. However, implementing these algorithms on mobile vehicles was complex. For testing and validation purposes, this integration was carried out as part of various projects using temporary instrumentation. This was relatively time-consuming to set up and had to be studied and adapted on a case-by-case basis. The present paper proposes a new stage in the development of safety solutions to mitigating rollover risks. It details the design of a new device of easy integration on different types of vehicles allowing an on-line monitoring of vehicle dynamics, estimation of rollover risk, and warning the driver in case of immediate risk.

Some stability monitoring and rollover warning devices have been already proposed and studied throw research work. (Nichol et al. 2005) proposed a low-cost device for rollover driver warning and (Casazza et al., 2016) evaluated a commercial device intended to calculate a stability index to inform driver. Both devices are based on simplified, static, or steady state, modeling of the vehicle. Where stability evaluation doesn’t take into consideration a prediction of vehicle dynamic, which reduces the ability of these devices to evaluate rollover risk. (Kise and Zhang, 2006) and (Zhu et al., 2019) propose stability monitoring systems integrating perception sensors, stereovision camera or Lidar, to detect the terrain in front in the vehicle and predict the rollover risk through the estimation of the future roll and pitch angles of the vehicle. Here also no dynamics modeling of the vehicle is considered; the risk is related mainly to the impact of uneven terrain on the vehicle's stability and not on its velocity, yaw rate, and other dynamic variables. Finally, (Liu and Koc, 2013) propose a system that can detect rollover after its occurrence and send accident report to emergency to allow ensuring driver safety.

The device presented in this paper is a low-cost device based on dynamic modeling of off-road vehicles. It is able to predict vehicle dynamic behavior, calculate metrics representative of lateral and longitudinal rollover risk, and provide an on-line estimation of risk level. This information is displayed, as an alert, on the driver screen to allow him to take suitable action to prevent the rollover accident. In case of an autonomous vehicle, the rollover risk estimation is sent through the robot CAN bus to be used as an input of rollover prevention safety functions.

In this paper, the materials and methods used to develop the new safety device are presented through a review of the theoretical approach and of the metric adopted for stability estimation (Section 2.1); a description of the algorithm architecture and data needed and measured by the device (Section 2.2); and a presentation of the sensors and electronic components constituting the proposed device (Section 2.3). The results obtained are presented through a detailed description of the device integration on two types of agricultural mobile machines (Section 3.1), followed by an overview of the field tests conducted with the equipped machines on terrain with

calibrated slopes and an analysis of the rollover risk assessment provided by the device during these tests (Section 3.2).

2/ MATERIALS AND METHODS

This section presents the hardware and software architecture of the novel low-cost safety device which is designed to estimate the rollover risk of mobile machines in real time and prevent it.
The main functionalities of the new safety device, for which specific technical solutions and design choices were developed, are related to: (i) its ability to acquire data, both online and offline, related to the vehicle and its motion; (ii) its ability to process these data in real time to estimate metrics representative of vehicle stability; and (iii) its ability to inform the operator of the associated risk or, in the case of an autonomous vehicle, to communicate control algorithms in order to mitigate or prevent the risk.

2.1 Quantifying vehicle stability metrics

The proposed system computes the risk of rollover based on stability metrics thanks to a model of vehicle dynamics. Such a representation is depicted in figure 1 and splitted in two frames. It permits to define the two main metrics that are used to estimate the risk, namely lateral and longitudinal load transfer rates (LTRLa and TRLLO) as metrics to characterize lateral and longitudinal stability, respectively. These rates are mathematically defined by the following equations:

$$LTR_{La} = \frac{F_{Le} - F_{Ri}}{F_{Le} + F_{Ri}}, \qquad LTR_{Lo} = \frac{F_{Fr} - F_{Re}}{F_{Re} + F_{Fr}}$$

F_{Le} and F_{Ri} are the normal components of the tyre/ground contact forces applied to the left and right sides of the vehicle.
F_{Fr} and F_{Re} are the normal components of the tyre/ground contact forces applied to the front and rear of the vehicle.

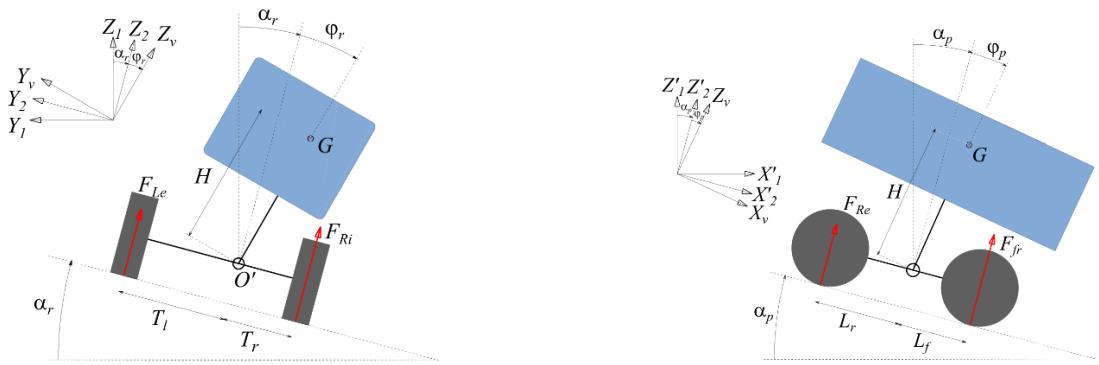


Figure 16. Vehicle roll model (a), Vehicle pitch model (b), and parameters

By definition, the values of load transfer rates vary between -1 and +1. Values at these extremes indicate that one side of the vehicle is raised off the ground. The nearer a vehicle's LTR gets to ±1, the more hazardous its condition becomes and, conversely, the closer the LTR is to 0, the safer the vehicle's situation.

The computation of these metrics requires knowledge of wheel–ground forces. These forces cannot be readily measured in real-time. Therefore, the algorithms at the core of the device are

based on state observers, using a dynamic model of the vehicle and online measurements of some motion variables. they reconstruct, in real time, the quantities required to compute the metrics representative of the vehicle's stability.

The dynamic model of off-road vehicles and the state observers adopted in the device algorithms are detailed in (Bouton et al., 2007), (Bouton et al., 2008) and (Richier et al., 2011).

The main considerations taken into account in this dynamic model can be summarized as follows:

- Off-road vehicles move on natural terrains and are exposed to variable grip conditions which influence their stability. To take this into account, the dynamic model incorporates sliding effects by introducing slip angles and the corresponding lateral forces acting on the wheels into the mathematical formulation.
- A linear tire model is considered to allow a simple formulation and a real-time calculation. This linear modeling is expressed by linear relations between wheels' lateral forces and wheels' slip angles and by introducing a coefficient representing tires' cornering stiffness. This coefficient is adaptable on-line to reflect variation of grip conditions
- Tyre cornering stiffness and slip angles are estimated online using state observers that infer these variables from a limited set of measured quantities, namely vehicle longitudinal velocity, yaw rate and steering angle.

The employed dynamic models and observers make it possible to obtain variables necessary to estimate lateral load transfer rate. Estimation of longitudinal load transfer rate is detailed in (Al Bassit et al., 2025) where a steady-state pitch assumption is considered for its calculation.

2.2 Data for stability estimation algorithms

Two types of data are required to calculate the metrics characterizing rollover risk: parameters of the vehicle's design and variables describing the vehicle's instantaneous motion.

The vehicle parameters are the track width, wheel-base, mass, mass-inertia matrix, centre-of-gravity location, roll stiffness, roll damping coefficient and pitch stiffness. In this study they are treated as constant, although the developed device can be adapted for vehicles whose parameters vary. Some of these values are obtained from preliminary tests performed on the vehicle during device integration (see section 3.1.); the remaining values are estimated from empirical feedback. These parameters are implemented in the device software during its integration onto the vehicle.

The vehicle-motion variables are measured in real time by the device sensors (as described in section 2.3). They comprise vehicle speed, vehicle acceleration, yaw rate and ground-bank angle, among other quantities.

The stability estimation process is summarized in Figure 2. Vehicle motion variables allow the observer to estimate grip conditions by estimating global tire cornering stiffness. These variables are then employed to extrapolate the vehicle's velocity and steering angle for the next step. With these predicted quantities, the future slip angle and yaw rate are computed, and the future lateral load transfer ratio LTR_{La} is obtained. The longitudinal load transfer ratio LTR_{Lo} is calculated directly from the measured vehicle-motion variables.

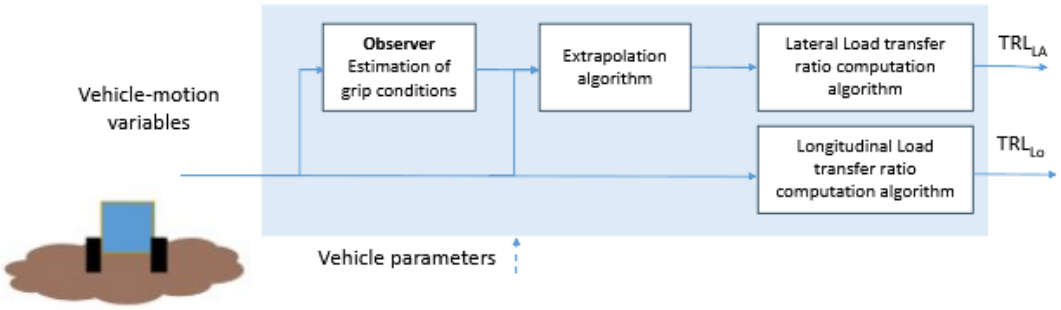


Figure 17. Stability estimation process

2.3 Device hardware

As the objective is to develop an antirollover kit that could be deployed on a broad spectrum of machines operating in natural environments while remaining affordable for farmers, a trade-off between the device's cost and the robustness required for operation under harsh conditions (extreme temperatures, dust, rain, etc.) is made.

The dynamic variables required as a minimum input for the algorithm are longitudinal acceleration, forward speed, and yaw rate. To obtain these quantities, an inertial measurement unit (IMU) and a GNSS receiver are selected. The GNSS module is coupled to a datalogging board; although this additional component is not strictly necessary, the ability to record raw measurements considerably simplifies development and validation. Both sensors communicate via a CAN bus and have been demonstrated to be sufficiently robust for agricultural use.

Based on experience with embedded controllers on robotic platforms, a similar controller is chosen and optimized in two respects: the number of I/O ports was reduced to the strict minimum required, and the physical envelope was minimized so that the unit can be easily installed within a tractor cab. Controllers of this family are already employed in numerous industrial applications and are known for their reliability, durability, and reasonable price.

The controller is programmed with the CODESYS 3.5 development environment, which provides native support for real-time acquisition of all sensor data and for the execution of the embedded stability-estimation calculations.

The kit is also designed to be fully compatible with the ISOBUS standard, which is implemented in most modern agricultural machines. This compatibility contributes to the low-cost target because the rollover-risk warning can be displayed directly on an existing tractor screen via a simple gateway that translates the on-board code into ISOBUS-compatible messages.

Since ISOBUS is based on the CAN-bus protocol, all sensors are selected to be CAN-bus compliant. This choice greatly simplifies data acquisition and leaves open to the possibility of adding additional sensors later without requiring extra I/O ports on the controller. The CAN-bus architecture is straightforward: it consists of a two-wire differential data bus terminated at each end with a 120 Ω resistor. Each sensor (referred to as a node) is connected to these two wires and is assigned a unique address for each of its measured variables (Figure 3)

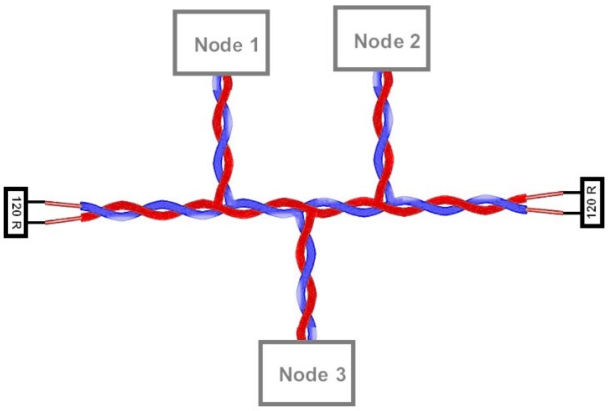


Figure 18. CAN bus architecture

The kit is conceived to minimize the cable lengths required for operation; a CAN-bus splitter is therefore employed. The wiring diagram for integration on a tractor is shown in Figure 4.

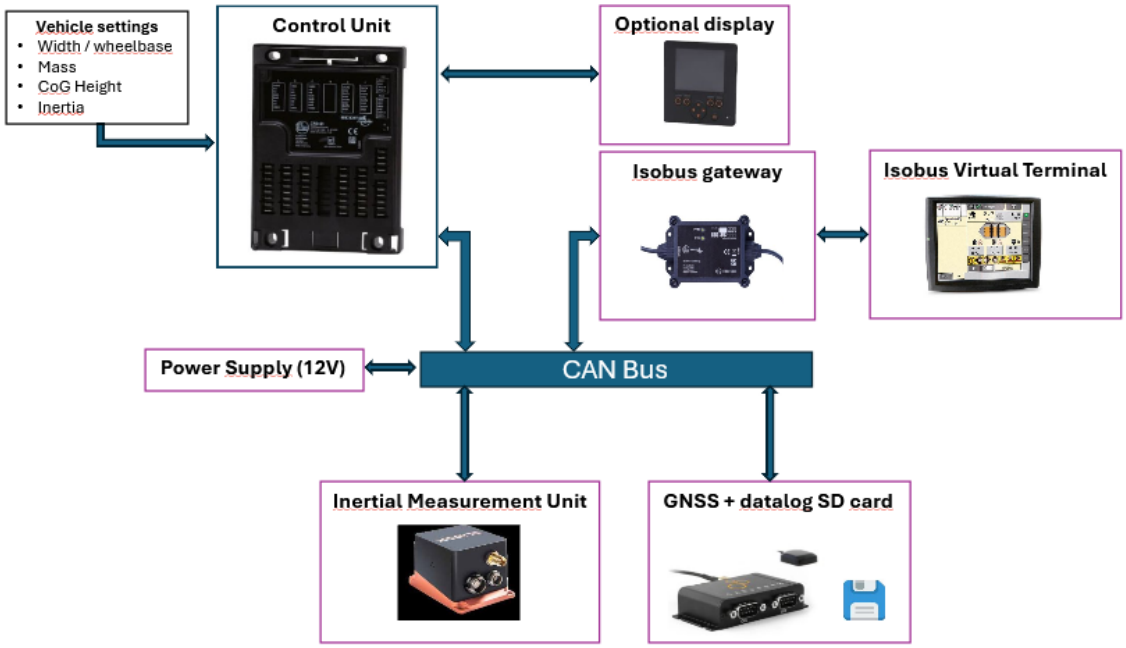


Figure 19.Prototype architecture

3/ RESULTS AND DISCUSSION

Two prototypes of the proposed safety device were developed and integrated into both autonomous and manually operated vehicles to validate their operation and assess their ease of integration. Several experimental campaigns were conducted on different types of vehicles. These experiments aimed to assess the generality of the approach across a range of off-road vehicle types, applications, and operating conditions, and to validate the device's ability to estimate rollover risk without relying on expensive instrumentation. They also aimed to assess its potential for preventive intervention by providing risk information to the operator or, in the case of autonomous vehicles, by enabling corrective actions to be triggered.

3.1 Device integration into mobile machinery

The first vehicle used for the experimental evaluation was a John Deere 6R110 tractor. This machine is equipped with the ISOBUS protocol and is operated daily on our experimental farm site.
The integration of the device into the tractor was relatively straightforward, with all components installed inside the tractor cab (Figure 5), except for the inertial measurement unit (IMU) and the GNSS antenna. Particular attention must be paid to the positioning of the IMU, which should preferably be mounted as close as possible to the center of the rear axle. The GNSS antenna was mounted on the tractor roof to ensure reliable signal reception. Finally, the power supply connector and the ISOBUS In-Cab connector were connected to their respective interfaces inside the cab. The device can then be switched on or off using the dedicated switch.



Figure 20. Tractor's kit integration

The tractor's ISOBUS interface recognizes the newly connected device. The user can then navigate through the available menus to access the software interface.
The way information is presented on the display is an important consideration for rollover risk management. The driver should not be overwhelmed by excessive information, as the risk estimation must remain clear and easy to interpret during operation. In this prototype, the graphical representation is constrained by the gateway, which only supports display slots for numerical values and a limited number of simple graphical formats.
However, the gateway also allows information to be organized into tabs, making additional data available to the driver without overloading the main display. The rollover risk estimation is the only information presented graphically, while all other parameters are displayed as numerical values (Figure 6).

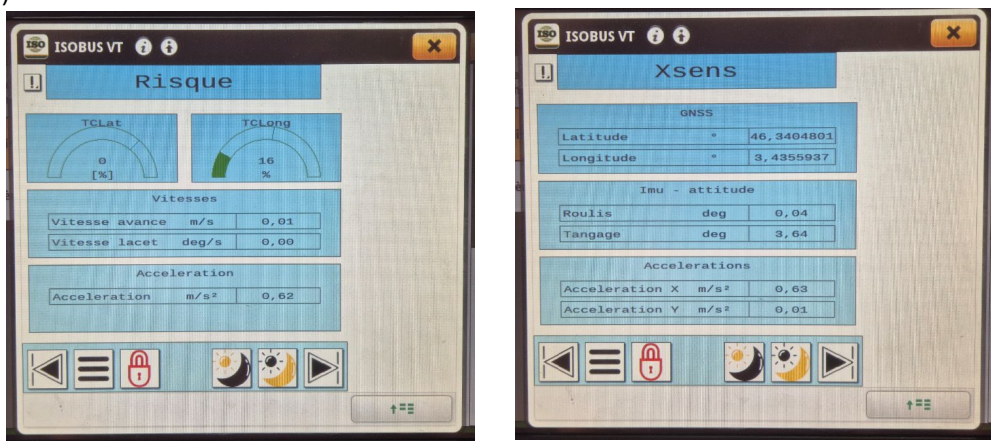


Figure 21. ISOBUS kit display, risk on the left, and another tab on the right

The second vehicle equipped with the prototype is an agricultural robot from SabiAgri (Figure 7). As the vehicle is equipped with a driver's seat and rollover protection structure (ROPS), it can be used either as a classic electric tractor or as an autonomous agricultural robot. The integration of the device into the robot is also straightforward, although it differs slightly from the tractor implementation due to the absence of the ISOBUS protocol. In this configuration, the optional display is used instead of the ISOBUS gateway. A USB-to-CAN interface is employed to enable communication between the robot's onboard computer and the prototype.

Unlike the tractor implementation, the robot configuration allows the prototype to modify the vehicle's speed setpoint. Consequently, the risk management strategy is simplified, as vehicle speed plays a key role in rollover risk.



Figure 22. Agricultural robot (left) and integrated device (right)

As mentioned in section 2.2, the control unit needs some vehicle parameters to estimate the risk. A part of those parameters can be readily obtained through direct measurements, such as the track width, wheelbase, and vehicle mass. However, the other parameters, namely the inertia matrix and the position of centre of gravity (CoG), require dedicated static experiments for their determination. The recommended procedure for conducting these experiments is based on the protocol described in ISO 789-6:2019. This standard specifies a method for determining the CoG height using a weighbridge and appropriate lifting equipment. These measurements only need to be performed once for a given vehicle and may alternatively be obtained from the vehicle manufacturer when available. Since suitable lifting equipment was not available for the present experiments, an approximation of the ISO 789-6:2019 procedure was implemented. The experimental setup was designed to remain as close as possible to the standardized protocol, while replacing the lifting equipment with ramps and using portable weighing devices positioned beneath the rear wheels (Figure 8).



Figure 23. Static experiments conducted with the robot (left) and the tractor (right)

3.2 Field tests

The experimental tests of the prototype were conducted at an INRAE experimental site located in Montoldre (03), France. The site provides several dedicated test areas for experiments involving agricultural machinery and robotic platforms. Among these facilities are a series of earth mounds with calibrated and well-characterized slopes. Four different slope inclinations are available: 15%, 20%, 25%, and 30%.



Figure 24. Robot (left) and tractor (right) trajectories used for our experiments in sloped areas.

Figure 9 shows the robot while following its planned trajectory and traversing slopes of 20% and 25%. These slopes generate different levels of lateral load transfer (LTR_{La}), resulting in two distinct baseline values. Turns are introduced along the trajectory to investigate the influence of yaw rate on lateral load transfer.

As the vehicle oscillates during motion, variations in LTR_{La} can be observed. These variations are attributed to changes in yaw rate, which can either increase or reduce the lateral load transfer induced by the slope. The two regions of lower LTR_{La} observed in the graph (Figure 10) correspond to the U-turns performed by the robot on even ground to transition from one slope to the other.

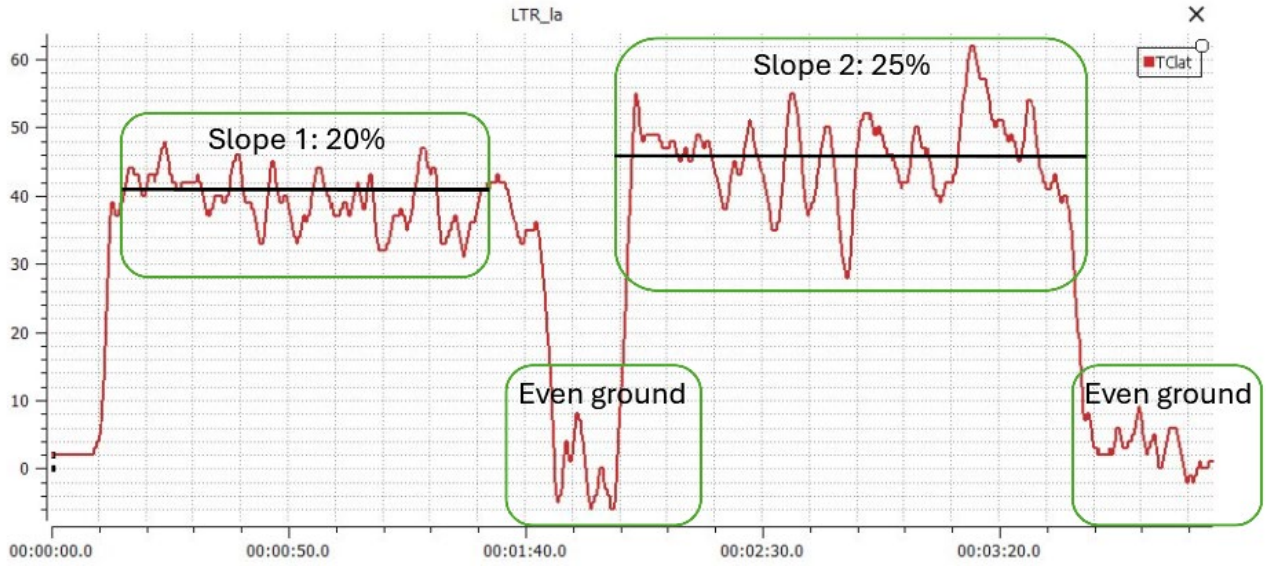


Figure 25. Lateral load transfer variation of the robot along its trajectory.

The same experimental environment was used to evaluate the device integrated into the tractor, as shown in Figure 11. The tractor was driven across all available slopes, resulting in a different average LTR_{La} value for each slope. Depending on the direction of the vehicle tilt, the LTR_{La} can be either positive or negative.

Compared with the robot, the same slope gradient results in a different LTR_{La} value for the tractor. This difference is due to the different vehicle parameters, particularly the center-of-gravity position, track width, and other geometric and inertial characteristics.

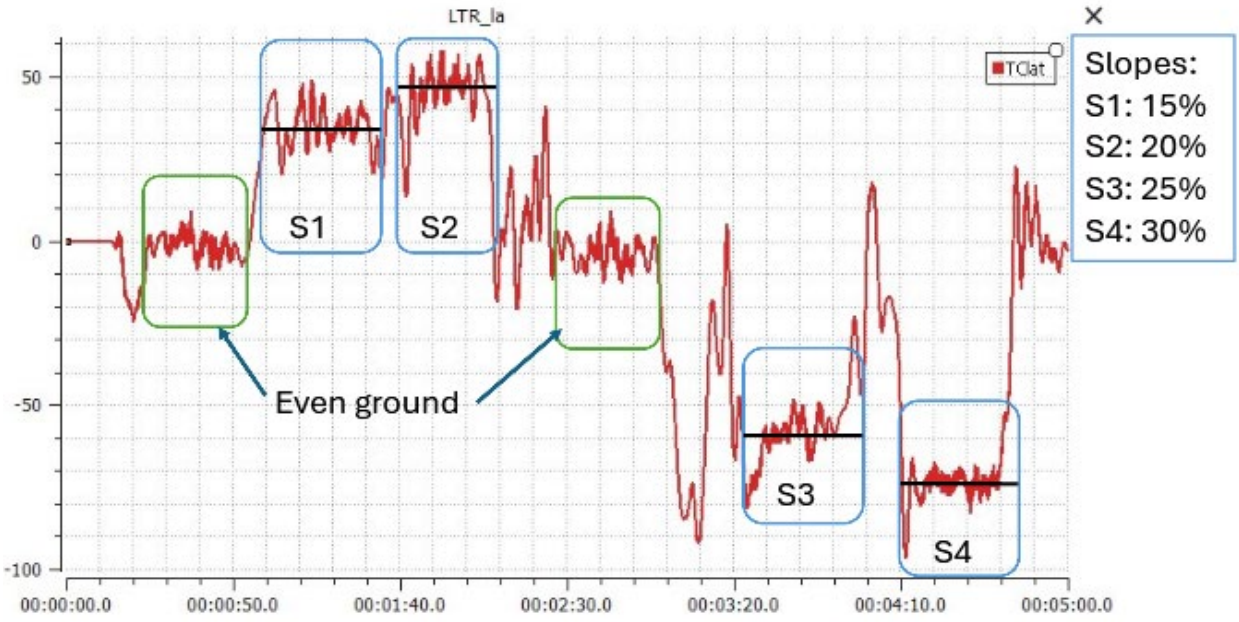


Figure 26. lateral load transfer variation of the tractor along its trajectory.

4/ CONCLUSIONS

TSCF work has led to the development of algorithms capable of estimating, in real time, metrics that empirically characterize the rollover risk of vehicles operating on natural terrain. Such algorithms provide a strong foundation for the development of active safety systems that can be integrated into mobile machinery. These systems are capable of either warning the operator or directly intervening in vehicle control functions to prevent rollover events, thereby enhancing operational safety in off-road environments.

This paper presents a safety device designed to assess the risk of rollover of mobile machines, developed based on the results of research on dynamic stability. The device, built using low-cost hardware and sensors, forms a safety kit that can be integrated into mobile machines, either autonomous or manually operated, to estimate the level of rollover risk and provide this information to the operator through a graphical interface, enabling the operator to anticipate and mitigate hazardous situations. In the case of autonomous machines, the device can provide direct feedback to the machine control system, enabling corrective actions such as speed reduction and/or steering adjustment to mitigate rollover risk.

The new low-cost device, through its installation on two types of machinery (an agricultural tractor from the brand John Deere and an agricultural robot from SabiAgri) and tests on terrains with known, calibrated slopes, demonstrated the ease of its integration and its effectiveness in estimating metrics that characterize its stability level.

Beyond its potential as a retrofit solution that provides rollover-risk warnings for existing machines, the kit was also developed as a demonstrator to show that rollover risk can be estimated with simple, low-cost sensors. This safety concept could later be incorporated into new mobile machines as part of a fully integrated active-safety system, enabling automated corrective

actions to be taken when a critical rollover risk is detected, thereby preventing a rollover and offering a level of protection that far exceeds that provided by the rollover-protective structures (ROPS) required by safety standards.

ACKNOWLEDGEMENTS

This work has been granted by Plant2Pro® Carnot Institute in the frame of its 2024 call for projects. Plant2Pro® is supported by ANR (agreement #24 CARN 0024-01).

REFERENCES

- L. Al-Bassit, B. Laurent, P. Heritier, R. Duval, V. Sulis and R. Lenain, “Instrumentation and field tests to evaluate a rollover risk estimator for mobile machinery with mobile tools”, AGRITECHDAY, AXEMA, Oct 2025, Clermont-Ferrand, France, pp.198. DOI: 10.48550/arXiv.2607.09188
- N. Bouton, R. Lenain, B. Thuilot and J. C. Fauroux, “A rollover indicator based on the prediction of the load transfer in presence of sliding: application to an all-terrain vehicle”. In : Proceedings 2007 IEEE International Conference on Robotics and Automation. IEEE, 2007. p. 1158-1163. DOI: 10.1109/ROBOT.2007.363141
- N. Bouton, R. Lenain, B., Thuilot, & P. Martinet. “A rollover indicator based on a tire stiffness backstepping observer: Application to an all-terrain vehicle”. In 2008 IEEE/RSJ International Conference on Intelligent Robots and Systems (pp. 2726-2731). DOI: 10.1109/IROS.2008.4650648
- C. Casazza, R. Martelli, V. Rondelli, “Evaluation of a Commercial Tractor Safety Monitoring System Using a Reverse Engineering Procedure”. J Agric Saf Health. 2016 Oct 17;22(4):215-225. DOI: 10.13031/jash.22.11667
- D. Denis, B. Thuilot, R. Lenain, “Online adaptive observer for rollover avoidance of reconfigurable agricultural vehicles”, Computers and Electronics in Agriculture, Volume 126, 2016, Pages 32-43, DOI: 10.1016/j.compag.2016.04.030
- ISO 789-6:2019, Agricultural tractors — Test procedures — Part 6: Centre of gravity
- B. Liu, A. B. Koc, “SafeDriving: A mobile application for tractor rollover detection and emergency reporting”, Computers and Electronics in Agriculture, Volume 98, 2013, Pages 117-120, DOI: 10.1016/j.compag.2013.08.002 .
- C.I. Nichol, H. J. 3rd Sommer, D. J. Murphy, “Simplified overturn stability monitoring of agricultural tractors”, J Agric Saf Health. 2005 Feb;11(1):99-108. DOI: 10.13031/2013.17900
- M. Kise, Q. Zhang, “Sensor-in-the-loop tractor stability control: Look-ahead attitude prediction and field tests”, Computers and Electronics in Agriculture, Volume 52, Issues 1–2, 2006, Pages 107-118, DOI: 10.1016/j.compag.2006.02.003.
- M. Richier, R. Lenain, B. Thuilot and C. Debain, "On-line estimation of a stability metric including grip conditions and slope: Application to rollover prevention for All-Terrain Vehicles," 2011 IEEE/RSJ International Conference on Intelligent Robots and Systems, San Francisco, CA, USA, 2011, pp. 4569-4574, DOI: 10.1109/IROS.2011.6094450
- M. Richier, R. Lenain, B. Thuilot and C. Debain, “Preservation of stability of automated off-road robots: Application to adaptive and predictive speed management”, International Conference on Agricultural Engineering, Valencia Conference Centre. France. 2012.
- V. Rondelli, C. Casazza, R. Martelli, "Tractor rollover fatalities, analyzing accident scenario", Journal of Safety Research, Volume 67, 2018, Pages 99-106, DOI: 10.1016/j.jsr.2018.09.015.
- V. Rondelli and A. L. Guzzomi, “Selecting ROPS safety margins for wheeled agricultural tractors based on tractor mass”, Biosystems Engineering, Volume 105, Issue 3, 2010, Pages 402-410, DOI: 10.1016/j.biosystemseng.2009.12.013.

- L. Wang, F. Liu, Z. Song, Y. Ni, Z. He, Z. Zhai, Z. Zhu, Q. Zhou, Z. Song, Z. Li, Advances in tractor rollover and stability control: Implications for off-road driving safety, Computers and Electronics in Agriculture, Volume 226, 2024, DOI: 10.1016/j.compag.2024.109483.
- Q. Zhu, W. Chen, H. Hu, X. Wu, C. Xiao and X. Song, "Multi-sensor based attitude prediction for agricultural vehicles", Computers and Electronics in Agriculture, Volume 156, 2019, Pages 24-32, DOI: 10.1016/j.compag.2018.11.008.

THANKS

We would like to extend our warmest thanks to all the authors, speakers and participants who contributed to the success of AGRITECH DAY 2026.

Your presence and commitment were essential in making this event a rich and not-to-be-missed event.

We are also grateful for the time and effort devoted by the members of the scientific committee to evaluating the paper proposals. Their expertise once again enabled us to offer a top-quality programme.

We would also like to thank MASSEY FERGUSON, CETIM and UNILASALLE for opening their doors to us for exceptional and unprecedented visits. Your generosity and hospitality were greatly appreciated.

The AXEMA organisation team looks forward to seeing you all in 2027 for the 10th AGRITECH DAY.

MORE INFORMATION?

TECHNICAL DEPARTMENT CONTACTS:

Guillaume BOCQUET
DIRECTOR OF REGULATORY AFFAIRS
g.bocquet@axema.fr

Juliette CANTALOUBE
TECHNICAL ADVISER
j.cantaloube@axema.fr

Cathy SWALEHE
TECHNICAL ADVISER
c.swalehe@axema.fr

COMMUNICATION DEPARTMENT CONTACTS:

Adina GILL
COMMUNICATION MANAGER
a.gill@axema.fr

Made with the support of:

Graphic design by:
Laetitia BARDOUL

OUR SPONSOR – BKT



BKT
GROWING TOGETHER

Balkrishna Industries Limited (BKT) is a leading manufacturer in the Off-Highway tyre market and a global specialist in the agricultural, industrial, construction and earthmoving sectors. Thanks to BKT's strong commitment to Research & Development, the company creates high-performance tyres meeting the rigorous demands of the industry, working closely with suppliers to ensure sustainable growth, in compliance with the stringent environmental and social standards.

This is how BKT has become a benchmark in the design and production of safe, innovative, and high-quality tires, with distribution partners in over 160 countries across five continents.

As a dedicated partner to the agricultural sector, BKT supports numerous initiatives and proudly shares the values of innovation, proximity, and performance that drive AGRITECH DAY

VISIT THE BKT WEBSITE:

https://companyprofile.bkt-tires.com/portrait/

OUR SPONSOR – AMS SOLTECH



AMS
SAFETY, COMFORT & EFFICIENCY

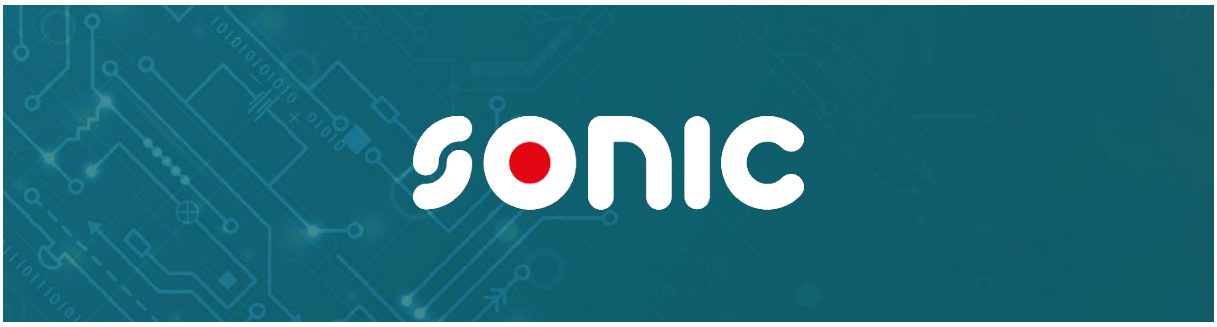
AMS, onboard electronics serving agricultural safety, comfort, and performance.
For more than 50 years, AMS has placed innovation, quality, and customer satisfaction at the heart of its development. A specialist in onboard electronics since 1969, the company designs high-performance, durable, and innovative audio and video solutions tailored to meet the operational needs of agricultural professionals.

Located in the heart of northern France, AMS leverages its field experience and technical expertise to develop equipment suited to the most demanding environments. Its solutions help improve the safety, comfort, and efficiency of end users in their day-to-day work.

VISIT THE AMS SOLTECH WEBSITE:

https://ams-soltech.com/en/

OUR SPONSOR – SONIC EQUIPMENT



SONIC

Sonic Equipment is a global specialist in professional hand tools, fully equipped toolboxes and premium storage solutions. Founded in 2004, the company supports professionals across a wide range of sectors, including agriculture, automotive, heavy-duty and industry.

Sonic's approach is built around a simple objective: helping professionals work more efficiently, safely and productively. Its solutions combine high-quality tools with smart storage systems designed to keep workshops organised and ensure that the right tool is always within reach.

From complete toolsets and modular storage solutions to individual hand tools, Sonic develops equipment tailored to the demanding environments faced by technicians every day. With a strong focus on quality, ergonomics and efficient workspace organisation, the company helps optimise maintenance and repair operations.

With an international presence and a growing network of partners, Sonic Equipment continues to develop solutions designed to meet the evolving needs of professional workshops and technicians.

VISIT THE SONIC EQUIPMENT WEBSITE:

https://www.sonic-equipment.com/fr-fr

OUR SPONSOR – MMT MOVING MAGNET



MMT (Moving Magnet Technologies) is a technology company specialising in the design and development of innovative electromagnetic and mechatronic solutions for mobility applications.

Innovation lies at the heart of MMT's expertise. The company develops high-value-added technologies for electric motors, actuators and sensors, helping manufacturers address complex technical challenges and develop smarter, more efficient solutions.

With 250 international patents and 100 licence agreements worldwide, MMT has built a strong model based on technological innovation, intellectual property and the transfer of its technologies to industrial partners around the world.

By combining expertise in electromagnetism, mechanics, electronics and mechatronics, MMT supports the development of new solutions for the future of mobility, from the initial concept through to technology transfer and industrialisation.

VISIT THE MMT WEBSITE:

https://www.movingmagnet.com/en